

**REGIOSELECTIVITY OF THE PHOTOISOMERIZATION OF ACYCLIC  
1,3-DIENES AND STABLE TRANS CYCLOHEPTENES**

by

Veselin Y Ruychev

A dissertation submitted to the Graduate Faculty of  
Auburn University  
in partial fulfillment of the  
requirements for the Degree of  
Doctor of Philosophy

Auburn, Alabama  
December 8 2012

Keywords: retinal, diene, photolysis, conical intersection, zwitterion, stable  
cycloheptenes

Copyright 2012 by Veselin Y Ruychev

Approved by

Michael E. Squillacote, Chair, Associate Professor  
Peter Livant, Associate Professor, Chemistry  
Anne Gorden, Associate Professor, Chemistry  
German Mills, Associate Professor  
James Witte, Associate Professor

## ABSTRACT

There is still no complete understanding of how the visual system controls the regioselectivity of the photoisomerization of the C<sub>11</sub>=C<sub>12</sub> double bond in the visual chromophore retinal. In this work we used a series of acyclic 1,3-dienes, as models of the visual system. We investigated effects of substituents on the dienes photochemistry. The substituents were chosen to reveal the relative importance of inertial mass, charge stabilizing capability and steric size in controlling which of the two bonds of the diene preferentially photoisomerized. The photochemical experiments were conducted in solvents of different polarity to examine the extent of charge development in the excited state pathways that were traversed. The dienes that were chosen, synthesized and purified were isomers of 6,6-dimethyl-2,4-heptadiene (DMH), 2,4-nonadiene (ND) and 1,1,1-trifluoro-2,4-hexadiene (TFHD). In addition, we attempted to synthesize 1,2-dideutero-1,3-pentadiene (DDPD). To explain the observed substituent effects, a hybrid mechanism was proposed, where the charge stabilizing capability of the substituents determined which specific conical intersection was preferred and thus which double bond was preferentially photoisomerized.

Previously in our group it was determined that the decay of *trans*-cycloheptene to its *cis* isomer does not occur via “direct twisting” about the double bond. Rather it occurs through a dimerization of two *trans* molecules to produce a 1,4-biradical which quickly geometrically

relaxes and cleaves to form two *cis*-cycloheptene molecules. If this bimolecular mechanism could be inhibited sterically, there is a possibility that one could produce room temperature stable *trans*-cycloheptenes. To test this possibility, we chose to examine the stability of three allylically substituted *trans*-cycloheptenes, 3,3,7,7-tetramethyl (TMCHP) and *syn* and *anti* 3,7-di-*t*-butyl (DTBCHP) *trans*-cycloheptene. Using a variety of NMR techniques and high level *ab initio* calculations, we were able to prove that we could photochemically produce these stable *trans*-cycloheptenes which should now be considered the smallest *trans* cycloalkenes to be persistent at room temperature.

## ACKNOWLEDGMENTS

I would like to thank my mentor, Dr. Michael E. Squillacote, for his guidance and encouragement over the past six years. All the experimental and analytical skills, knowledge and confidence I gained for that period of time, are product of his dedication to my beginner's steps in graduate education and research. I sincerely apologize for all the endless sleepless nights, Dr. Squillacote. I would also like to thank my graduate committee for the support and help they have given me throughout my years at Auburn.

To all my friends Allan, Krissy, Dan, Pascal, Christine, Caroline, Mallory and Alex and whoever you are I do not mention, thank you for giving me so many good times, correcting and improving my English, for the memories and great friendships we have created.

Last, but by no means least, I am very thankful to my family. Especially to my beautiful wife, who supported me at every step and hard time I went through and for giving birth to our beautiful, and oh-so-curious, daughters Ellie and Lydia.

## TABLE OF CONTENTS

ABSTRACT .....	ii
ACKNOWLEDGMENTS .....	iv
LIST OF TABLES .....	x
LIST OF FIGURES .....	xii
LIST OF ABBREVIATIONS .....	xxii
CHAPTER I .....	1
1. Regioselectivity of the photoisomerization of acyclic 1,3-dienes .....	1
1.1. Introduction .....	1
1.1.1. Lowest excited states of acyclic polyenes .....	5
1.1.2. Photochemically induced geometry isomerization in acyclic polyenes ...	6
1.1.2.1. Cyclopropyl biradical mechanism .....	7
1.1.2.2. Hula Twist .....	9
1.1.2.3. Bicycle Pedal mechanism .....	12
1.1.2.4. Zwitterionic intermediate mechanism and related net charge effects .....	13
1.1.3. Conical intersection .....	21
1.1.3.1. Avoided crossings, i.e. wells .....	21
1.1.3.2. Surface crossing, i.e. slides .....	23
1.1.3.3. The intermediary conical intersection .....	24
1.1.3.4. Competitive conical intersections .....	33
1.1.4. Dynamic effects .....	34
1.1.5. Substituent effects .....	37
1.1.6. Molecules of past and current interest .....	38
1.1.7. This work .....	46
1.2. Experimental .....	48
1.2.1. Instrumentation and equipment used .....	48
1.2.2. Materials Used: purification and preparation .....	48
1.2.2.1. Purification of solvents and reagents .....	48
1.2.2.1.1. Preparation and Conditioning of Drying Agents .....	48
1.2.2.1.2. Purification of Propionitrile .....	48

1.2.2.1.3. Purification of HPLC grade hexane	49
1.2.2.1.4. Purification of Acetonitrile	50
1.2.2.1.5. Purification of Chloroform-d <sub>3</sub>	50
1.2.2.1.6. Purification of Tetrahydrofuran (THF)	50
1.2.2.1.7. Purification of Methylene Chloride and Ether	50
1.2.2.1.8. Purification of Pyridine	50
1.2.2.1.9. Purification of p-toluenesulfonyl chloride (p-TosCl)	50
1.2.4. Synthesis and Purification of 6,6-Dimethyl-2,4-heptadiene (DMH)	51
1.2.4.1. Procedure A	51
1.2.4.1.1. Preparation of Phenyl Lithium	51
1.2.4.1.2. Neopentyl Phosphonium Iodide	52
1.2.4.1.3. Preparation of 6,6-Dimethyl-2,4-heptadiene	53
1.2.4.2. Preparation of 6,6-Dimethyl-2,4-heptadiene (DMH) via Wittig Reaction with Schlosser modification	53
1.2.4.3. Purification and Storage of Isomers	55
1.2.4.4. Photolysis of DMH Isomers	55
1.2.4.4.1. Analytical Gas Chromatography Conditions	55
1.2.4.4.2. Sample Preparation	56
1.2.4.4.3. Photolysis Conditions and setup	56
1.2.5. 2,4-Nonadiene (ND)	57
1.2.5.1. Synthesis and Purification	57
1.2.5.1.1. Preparation of Pentyltriphenylphosphonium Bromide	57
1.2.5.1.2. Titration of n-Butyllithium	57
1.2.5.1.3. Preparation of 2,4-Nonadiene (Wittig Reaction Method)	58
1.2.5.1.4. Equilibration of 2,4-Nonadiene with Iodine	58
1.2.5.1.5. Purification and Storage of Isomers	59
1.2.5.2. Photolysis of ND isomers	59
1.2.5.2.1. Analytical Gas Chromatography Conditions	59
1.2.5.2.2. Sample Preparation	59
1.2.5.2.3. Photolysis conditions and setup	60
1.2.6. 1,1,1-trifluoro-2,4-hexadiene (TFHD)	60
1.2.6.1. Synthesis of 1,1,1-trifluoro-2,4-hexadiene	60
1.2.6.1.1. Synthesis of 1,1,1-trifluoro-4-hexene-2-ol	60
1.2.6.1.2. Preparation of Tosylate of 1,1,1-trifluoro-4-hexene-2-ol	61
1.2.6.1.3. Preparation of TFHD	62
1.2.6.2. Purification and Storage of Isomers	62

1.2.6.3. Photolysis of TFHD	62
1.2.6.3.1. Analytical Gas Chromatography Conditions	62
1.2.6.3.2. Sample Preparation	63
1.2.6.3.3. Photolysis conditions and setup	63
1.2.7. Synthesis of <i>cis</i> -1,2-dideutero- <i>trans</i> -1,3-pentadiene (DDPD)	63
1.2.7.1. Preparation of 2-tosyl-4-yne-pentane ( <b>tosylate</b> )	64
1.2.7.2. Preparation of 3-ene-1-pentyne (ene-yne)	64
1.2.7.3. Synthesis of <i>cis</i> -1,2-dideutero- <i>trans</i> -1,3-pentadiene (DDPD)	65
1.2.7.4. Synthesis of DDP in quinoline solution	65
1.2.7.5. Synthesis of DDPD - Dry run without base	66
1.2.7.6. Synthesis of DDPD - Lindlar reaction	66
1.2.7.7. Synthesis of DDPD in propionitrile	67
1.3. Results and discussion	68
1.3.1. DMH Results and discussion	70
1.3.1.1. Synthesis and purification	70
1.3.1.2. Analysis and photochemistry	78
1.3.2. 1,3-nonadiene (ND) results and discussion	85
1.3.2.1. Synthesis and purification of ND	86
1.3.2.2. Analysis of photochemistry of ND	94
1.3.3. 1,1,1-trifluoro-2,4-hexadiene (TFHD) results and discussion	100
1.4. Conclusions	113
1.5. Future research	118
CHAPTER II	125
2. Stable trans cycloheptenes	125
2.1. Introduction	125
2.1.1. Double bonds History	125
2.1.2. Trying to understand character of double bond	126
2.1.3. Strain in double bonds	127
2.2. Understanding the formation of strained geometries of cyclic alkenes	128
2.2.1. Pyramidalization angle	128
2.2.1.1. Borden's definition	129
2.2.1.2. Winkler definition	129
2.2.2. Twisting and pyramidalization	130
2.2.3. POAV analysis	133
2.2.4. Early recognition of trans more stable than cis in acyclic vs. cyclic	135
2.3. Conformations of strained cyclic alkenes	136
2.3.1. Geometry of <i>trans</i> -cyclooctene	136

2.3.2. Geometry of <i>trans</i> -molosila-cycloheptene	137
2.3.3. Geometry of <i>trans</i> -trisilacycloheptene	138
2.4. Thermal Isomerization of cycloalkenes	138
2.4.1. Determination of the isomerization barrier by Gano and Doering	138
2.4.2. Isomerization of <i>trans</i> -cyclooctene and cyclohexene	139
2.5. Excited states	141
2.5.1. The most simple cis-trans isomerization - Ethylene	141
2.5.2. Potential Energy Surfaces of cyclic alkenes	142
2.5.2.1. Absorption - direct photolysis	144
2.5.2.2. Energy transfer excitation	144
2.5.3. Strained Cycloheptenes produced photochemically	148
2.5.3.1. Barrier of trans to cis transition determination in cycloheptenes	154
2.5.4. Previous computational investigations and results	155
2.5.5. Winkler and POAV analysis of <i>trans</i> -CHP	159
2.5.6. Biradical mechanism for trans to cis decay	161
2.6. Experimental	167
2.6.1. Equipment and techniques used	167
2.6.1.1. Materials	167
2.6.1.2. Analytical data collection	167
2.6.1.3. Sample purification	167
2.6.1.4. Glassware and equipment	167
2.6.1.5. Photolysis equipment	168
2.6.1.6. Purification of substituted cycloheptenes	168
2.6.1.7. Bromination to assign syn and anti DTBCHP isomers	169
2.6.3. Low temperature photolysis experiments - sample preparation and conditions	171
2.6.4. TMCHP room temperature decay experiments	171
2.6.5. Computational experiments - methods and basis sets	172
2.7. Results and discussion	173
2.7.1. Dynamic NMR	173
2.7.2. <i>Trans</i> -TMCHP	177
2.7.3. <i>Trans</i> -anti-DTBCHP	179
2.7.4. <i>Trans</i> -syn-DTBCHP	182
2.7.5. Stability	185
2.8 Conclusions	189
REFERENCES	191





## LIST OF TABLES

<b>Table 1.1:</b> Distribution of cis isomers during the direct irradiation of all- <i>trans</i> -retinal and related compounds . . . . .	2
<b>Table 1.2:</b> S- <i>trans</i> -1,3-butadiene vertical excitation energies (ev) . . . . .	6
<b>Table 1.3:</b> Product Quantum yields from 1,3-pentadiene . . . . .	7
<b>Table 1.4:</b> Quantum yields of direct 2,4-hexadiene isomerization . . . . .	8
<b>Table 1.5:</b> <sup>1</sup> H NMR, <sup>13</sup> C NMR and coupling constants on identified DMH isomers. . .	77
<b>Table 1.6:</b> 1H and 13C NMR shifts of EE, EZ, ZE and ZZ-ND . . . . .	89
<b>Table 1.8:</b> Relative percentages of all TFHD isomers before and after I <sub>2</sub> equilibration .	101
<b>Table 1.8:</b> <sup>1</sup> H NMR, <sup>13</sup> C NMR and coupling constants of the four isomers of 1,1,1-trifluoro-2,4-hexadiene (TFHD). . . . .	103
<b>Table 1.9:</b> Determination of solvent polarity of propionitrile-hexane system using Reichardt's dye at RT. . . . .	111
<b>Table 2.1:</b> Degree of twist available to cycloalkene $\pi, \pi^*$ excited states as estimated from dreiding models. . . . .	142
<b>Table 2.2:</b> Some benzene derivatives triplet energies. . . . .	147
<b>Table 2.3:</b> Characterization of <i>trans</i> -cycloheptene via <sup>13</sup> C NMR and force field simulations. . . . .	152
<b>Table 2.4:</b> Calculated <i>trans-cis</i> cycloheptene energy differences. . . . .	154
<b>Table 2.5:</b> Experimental and calculated <sup>13</sup> C chemical shifts of <i>cis</i> and <i>trans</i> -CHP. . . .	156

<b>Table 2.6:</b> Calculated <i>cis</i> - <i>trans</i> CHP energy difference at various levels. All <i>ab initio</i> energies are corrected for zero-point energy. ....	157
<b>Table 2.7:</b> Distortion Angles (deg) of some trans-cycloalkenes. ....	159
<b>Table 2.8:</b> POAV1/3D-HMO analysis of some strained cyclic alkenes. ....	160
<b>Table 2.9:</b> POAV2/3D-HMO analysis of some strained cyclic alkenes. ....	160
<b>Table 2.10:</b> Identification of <i>trans</i> -TMCHP via experimental vs. calculated <sup>13</sup> C NMR shifts. ....	179
<b>Table 2.11:</b> Identification of <i>trans</i> -anti-DTBCHP via experimental vs. calculated <sup>13</sup> C NMR chemical shifts. ....	182
<b>Table 2.12:</b> Identification of <i>trans</i> -syn-DTBCHP via experimental vs. calculated <sup>13</sup> C NMR chemical shifts. ....	184
<b>Table 2.13:</b> Results of DTBCHP rate studies. ....	186

## LIST OF FIGURES

<b>Figure 1.1</b> Photoisomerization of Rhodopsin .....	1
<b>Figure 1.2</b> 11- <i>cis</i> retinal bound to Lys and enveloped in opsin protein fold. ....	3
<b>Figure 1.3</b> The two lowest excited states of short polyene molecules. ....	5
<b>Figure 1.4</b> Photochemistry of 1,3-pentadiene. ....	7
<b>Figure 1.5</b> Mechanism for the formation of 1,3-dimethylcyclopropene from 1,3-pentadienes. ....	8
<b>Figure 1.6</b> Allyl-methylene biradical intermediate. ....	9
<b>Figure 1.7</b> Cyclopropylmethylene mechanism for the <i>cis-trans</i> isomerization of 2,4-hexadiene. ....	9
<b>Figure 1.8</b> Proposed Hula Twist mechanism (upper) and one bond flip(lower). ....	10
<b>Figure 1.9</b> Photoproducts produced through HT mechanism from pre-vitamin D. ....	11
<b>Figure 1.10</b> Photochemical isomerization of OT .....	11
<b>Figure 1.11</b> Proposed mechanisms for polyene photoisomerization. ....	12
<b>Figure 1.12</b> Photochemistry of <i>cis-</i> and <i>trans-</i> 3-ethyldienecyclooctene .....	14
<b>Figure 1.13</b> Photochemical development of zwitterionic intermediate in hexatriene suggested by Duben .....	15
<b>Figure 1.14</b> Electronic states of ethylene and <i>s-cis-s-trans</i> -diallyl. ....	16
<b>Figure 1.15</b> Charge separation $\Delta q$ in $Z_1$ excited singlet state of $90^\circ$ -twisted ethylene as a function of the pyramidalization angle $\Phi$ . ....	16
<b>Figure 1.16</b> Charge separation in $Z_1$ excited state of DHT as a function of $\theta$ . Note the	

unsymmetric nature of the curve at $\sim 90^\circ$ . . . . .	17
<b>Figure 1.17</b> Potential energy surfaces of the lowest S states as a function of pyramidalization angle. . . . .	17
<b>Figure 1.18</b> Photochemical isomerization of <i>cis</i> -1-deutero- <i>trans</i> -1,3-pentadiene . . . . .	18
<b>Figure 1.19</b> Four possible zwitterionic forms of 1,3-pentadiene . . . . .	18
<b>Figure 1.20</b> Suggested reaction path for the isomerization of 1,3-pentadiene. . . . .	19
<b>Figure 1.21</b> Methanol trapping study of an acyclic 1,3-diene. . . . .	20
<b>Figure 1.22</b> State correlation diagram showing the disrotatory closure of 1,3-butadiene. . . . .	21
<b>Figure 1.23</b> The 2-in-2 model for surface touching. The two planes shown correspond to the homosymmetric and heterosymmetric case. . . . .	24
<b>Figure 1.24</b> <b>Left:</b> two potential energy surfaces form the double cone if plotted against $X_1$ and $X_2$ ; <b>Right:</b> $X_1$ and $X_2$ span the “branching space”, while the “intersection space” is a (F-2)-dimensional hyperline. . . . .	25
<b>Figure 1.25</b> Surface connection patterns for conical intersections. . . . .	26
<b>Figure 1.26</b> Schematic representation of different reaction path topologies and positions of the conical intersection region along a reaction coordinate. . . . .	27
<b>Figure 1.27</b> The skeletal movement of excited 1,3-butadiene and minima on the conical intersection surface. . . . .	29
<b>Figure 1.28</b> Disrotatory (D) and conrotatory (C) computed minimal energy paths from Frank-Condon region to the $2A_1/1A_1$ conical intersection involved in the photochemistry of 1,3-butadiene. . . . .	30
<b>Figure 1.29</b> The photoisomerization of t-HTE. . . . .	33
<b>Figure 1.30</b> Energy profiles along the MEPs describing the competing excited isomerization paths from the Franck-Condon point to the decay points $S_1/S_0$ CI <sub>C2-C3</sub> and $S_1/S_0$ CI <sub>C4-C5</sub> of	

t-HTE. ....	34
<b>Figure 1.31</b> Three classes of barrierless reaction pathways characterized by different excited state dynamics. (a) 2-cis-C <sub>5</sub> H <sub>6</sub> NH <sub>2</sub> <sup>+</sup> (b) all-trans-HT (c) CHD. ....	36
<b>Figure 1.32</b> Comparison of the molecular structures, energy gradient, and S <sub>1</sub> initial MEPs for cis-C <sub>5</sub> H <sub>6</sub> NH <sub>2</sub> <sup>+</sup> (open squares) and α-methyl cis-C <sub>5</sub> H <sub>6</sub> NH <sub>2</sub> <sup>+</sup> (open diamonds). The structures at 1.5 au from the Franck-Condon point are indicated by the label HM. .	38
<b>Figure 1.33</b> Acyclic 1,3-dienes as models for the photoisomerization of retinal. ....	39
<b>Figure 1.34</b> 250-MHz <sup>1</sup> H NMR of a 1% solution in diethylether of (A) <i>cis</i> -1-deutero- <i>trans</i> -1,3-pentadiene; (B) after 2 min of photolysis with a 1000W Hg(Xe) arc lamp at 0°C; (C) after 30 min and (D) after 8 h of photolysis. ....	40
<b>Figure 1.35</b> Photoisomerization of a 3.2M pentane solution of EE-FHD a) before irradiation b)after 60 sec of irradiation with 245nm light and at RT. ....	42
<b>Figure 1.36</b> Solvent effect on the photoregioselectivity. ....	43
<b>Figure 1.37</b> Solvent effect studies of the photoisomerization of 1-fluoro-2,4-hexadiene	44
<b>Figure 1.38</b> Proposed pathway from 1 <sup>1</sup> Bu state showing differing polarizations and leading to two different conical intersections. ....	45
<b>Figure 1.39</b> Molecules of interest in this work. ....	46
<b>Figure 1.40</b> UV-VIS spectrum of propionitrile before and after purification ....	49
<b>Figure 1.41</b> Micro Mary-go-round apparatus ....	56
<b>Figure 1.42</b> Synthetic route for preparation of <i>cis</i> -1,2-dideutero- <i>trans</i> -1,3-pentadiene.	64
<b>Figure 1.43</b> Molecules of interest in this work. ....	68
<b>Figure 1.44</b> Wittig mechanism used for synthesis of DMH and ND ....	70
<b>Figure 1.45</b> Wittig mechanism with Schlosser modification. ....	71

<b>Figure 1.46</b> Wittig reaction with Schlosser modification used to prepare DMH. . . . .	72
<b>Figure 1.47</b> Comparison of <sup>1</sup> H NMR of DMH prepared via Wittig reaction (top) and Wittig reaction with Schlosser modification (bottom) . . . . .	73
<b>Figure 1.48</b> Prep GC of DMH isomers. . . . .	74
<b>Figure 1.49</b> <sup>1</sup> H NMR of EE DMH . . . . .	75
<b>Figure 1.50</b> <sup>1</sup> H NMR of EZ DMH . . . . .	76
<b>Figure 1.51</b> Efficiency curve dependence on carrier gas. . . . .	79
<b>Figure 1.52</b> Progression of the photochemical isomerization of EE-DMH in hexane obtained using analytical GC. . . . .	79
<b>Figure 1.53</b> Photoisomerization of EE-DMH to photostationary state (hexane; 254nm; 0°C) . . . . .	80
<b>Figure 1.54</b> Formation of ZE, EZ and ZZ DMH at less than 1% conversion of EE-DMH (hexane; 254nm; 0°C) . . . . .	81
<b>Figure 1.55</b> Photoisomerization of EE-DMH in hexane . . . . .	81
<b>Figure 1.56</b> Formation of ZE, EZ and ZZ DMH at less than 1% conversion of EE-DMH (propionitrile; 254nm; 0°C) . . . . .	82
<b>Figure 1.57</b> Photoisomerization of EE-DMH in propionitrile . . . . .	82
<b>Figure 1.58</b> Triplet photochemistry of EE-DMH sensitized with benzophenone (hexane; 254nm; 0°C) . . . . .	83
<b>Figure 1.59</b> Formation of EE, ZZ, and ZE DMH at less than 3% conversion of EZ-DMH (hexane, 254 nm, 0 °C). . . . .	84
<b>Figure 1.60</b> Photolysis of EZ-DMH in hexane. . . . .	84
<b>Figure 1.61</b> Triplet photochemistry of EZ-DMH with benzophenone (hexane; 254nm; 0°C) . . . . .	85

<b>Figure 1.62</b> Equilibration of ND with I <sub>2</sub> .....	86
<b>Figure 1.63</b> Preparative GC of 2,4-nonadiene top: crude ND after equilibration middle: 2 <sup>nd</sup> prep of EE/EZ peak bottom: 2 <sup>nd</sup> prep of ZE peak. ....	88
<b>Figure 1.64</b> EE and EZ isomers of 2,4-nonadiene. ....	90
<b>Figure 1.65</b> EZ and EE isomers of 2,4-nonadiene. ....	91
<b>Figure 1.66</b> ZE and ZZ isomers of 2,4-nonadiene. ....	92
<b>Figure 1.67</b> ZZ isomer of 2,4-nonadiene. ....	93
<b>Figure 1.68</b> Photolysis setup for ND with “golf tee shaped” tube. ....	94
<b>Figure 1.69</b> Analytical GC of the Photolysis of 2,4-Nonadiene .....	94
<b>Figure 1.70</b> Photoisomerization of EE-ND in propionitrile until photostationary state. ....	95
<b>Figure 1.71</b> Low percent photochemical conversion of EE-ND in hexane. ....	96
<b>Figure 1.72</b> Photoproducts from EE-ND irradiation in hexane and their relative ratio. .	96
<b>Figure 1.73</b> Low percent photochemical isomerization of EE-ND in propionitrile. ...	97
<b>Figure 1.74</b> Photoproducts from EE-ND irradiation in propionitrile and their relative ratio. ....	97
<b>Figure 1.75</b> Low percent of photochemical conversion of ZE-ND in hexane. ....	98
<b>Figure 1.76</b> Photoproducts of ZE-ND in hexane and their relative ratio. ....	98
<b>Figure 1.77</b> Low percent of photochemical conversion of ZE-ND in propionitrile. ...	99
<b>Figure 1.78</b> Photoproducts of ZE-ND in propionitrile and their relative ratio. ....	99
<b>Figure 1.79</b> Synthesis path for the preparation of 1,1,1-trifluoro-2,4-hexadiene .....	100



<b>Figure 1.80</b> Preparative GC of 1,1,1-trifluoro-2,4-hexadiene: (A) removing ZZ and impurities; (B) separation of EE from EZ and ZZ; (C) purification of B washed in propionitrile. ....	102
<b>Figure 1.81</b> <sup>1</sup> H NMR spectrum of EE-TFHD. ....	104
<b>Figure 1.82</b> <sup>1</sup> H NMR spectrum of ZE-TFHD. ....	105
<b>Figure 1.83</b> Analytical GC of the photolysis of 1,1,1-trifluoro-2,4-hexadiene .....	106
<b>Figure 1.84</b> Photoisomerization of EE-TFHD to ZE, EZ and ZZ isomers until photostationary state. ....	107
<b>Figure 1.85</b> Less than 5% conversion of EE-TFHD to ZE and EZ isomers (hexane; 254nm; 0°) .....	107
<b>Figure 1.86</b> Photoisomerization of pure EE-TFHD in 100% hexane solution. ....	108
<b>Figure 1.87</b> Triplet photochemistry of EE-TFHD to ZE, EZ and ZZ (hexane; 254 nm; 0° C) .....	109
<b>Figure 1.88</b> Possible TFHD triplet states .....	109
<b>Figure 1.89</b> Initial delay of ZZ-TFHD formation from EE-TFHD in degassed and sensitizer-free solution (100% hexane; 254 nm; 0° C). ....	110
<b>Figure 1.90</b> Less than 2% conversion of EE-TFHD to ZE and EZ isomers (propionitrile; 254 nm; 0°). ....	110
<b>Figure 1.91</b> Photoisomerization of EE-TFHD in propionitrile .....	111
<b>Figure 1.92</b> Photoregioselectivity of EE-TFHD (254nm; 0° C) and E <sub>t</sub> value of a mixed propionitrile-hexane solvent system. ....	112
<b>Figure 1.93</b> Possible routes of photochemical isomerization of EE-DMH and EE-ND	115

<b>Figure 1.94</b> Possible route for the photoisomerization of EE-TFHD .....	117
<b>Figure 1.95</b> Photoregioselectivity of 1-deutero-1,3-pentadiene in low temperature conditions. ....	118
<b>Figure 1.96</b> Expected charge stabilizing effect on the energy gap between $Z_{1B}$ and $Z_{2B}$ . ....	118
<b>Figure 1.97</b> 250-MHz $^1\text{H}$ NMR of a 1% solution in diethylether of (A) <i>cis</i> -1-deutero- <i>trans</i> -1,3-pentadiene; (B) after 2 min of photolysis with a 1000W Hg(Xe) arc lamp at $0^\circ\text{C}$ ; (C) after 30 min and (D) after 8 h of photolysis. ....	119
<b>Figure 1.98</b> Incomplete deuteration of the hydrazine leads to partially protonated product. Also the presence of <i>trans</i> -deuteration is detected. ....	121
<b>Figure 1.99</b> Deuterium exchange and isomerization problems in the synthesis of 1,2-dideutero-1,3-pentadiene. ....	123
<b>Figure 2.1</b> Double bond formation between two carbons, following Van't Hoff's idea of connecting two tetrahedral valencies of each atom, all laying in the plane of the paper. ....	125
<b>Figure 2.2</b> Hückel's trigonal representation of double bond formation between two carbon atoms in the molecule of ethylene. The unhybridized $p_z$ orbitals of both carbons overlap above and below the single sigma bond. ....	126
<b>Figure 2.3</b> Pauling's bent bonds representation of the double bond, formed in the molecule of ethylene. ....	127
<b>Figure 2.4</b> Van't Hoff's structures of <i>cis</i> -Maleic and <i>trans</i> -Fumaric acids .....	127
<b>Figure 2.5</b> Twisting ( <b>A</b> ) and bending ( <b>B</b> ) distortions in a double bond. With <b>T</b> is marked the angle of twisting; angle <b>P</b> denotes the angle of pyramidalization (bending). ....	128
<b>Figure 2.6</b> Scheme representation of a pyramidalized alkene by Borden. ....	129
<b>Figure 2.7</b> Model to explain Winkler's definition of pyramidalization angle. ....	129

<b>Figure 2.8</b> Modes of distortion of strained alkenes. ....	130
<b>Figure 2.9</b> Definition of angles around a distorted C=C bond. ....	131
<b>Figure 2.10</b> Flat, concave and convex deformations of a strained alkene. ....	133
<b>Figure 2.11</b> a) Anthracene derivative with all substituents bent toward one side of the ethylene skeleton; b) Twisted double bonds in twistene ....	134
<b>Figure 2.12</b> Anti-Bredt's bridged trans-cyclo alkenes. ....	134
<b>Figure 2.13</b> Twisted cyclooctene ....	135
<b>Figure 2.14</b> (a) Conformation of <i>trans</i> -cyclooctene; (b) Projection of cyclooctene structure along the C=C bond. ....	136
<b>Figure 2.15</b> X-ray structure of <i>trans</i> -1,1,3,3,6,6-hexamethyl-1-sila-4-cycloheptene with comparison to HF/6-31** calculation (italics) bond lengths (Å). The hydrogens have been omitted. ....	137
<b>Figure 2.16</b> Synthesis of trisilyl <i>trans</i> -cycloheptene. ....	138
<b>Figure 2.17</b> Structures and relative energies (kcal/mol) for <i>trans</i> -cyclohexene conformers and transition states. ....	140
<b>Figure 2.18</b> Potential Energy surfaces of the ground and lower excited states of ethylene. ....	142
<b>Figure 2.19</b> Three possible situations for energy transfer between sensitizer (Sens) and Acceptor (A) ....	145
<b>Figure 2.20</b> Sensitization by Schenck mechanism ....	147
<b>Figure 2.21</b> Proposed direct photolysis mechanism for CHP. ....	150
<b>Figure 2.22</b> <i>Cis-trans</i> photosensitization of CHP. ....	150
<b>Figure 2.23</b> Inoue's mechanism for production of <i>trans</i> -CHP via a singlet exciplex. .	151

<b>Figure 2.24</b> Characterization of <i>trans</i> -cycloheptene via experimental (right) and simulated (left) dynamic <sup>1</sup> H NMR. . . . .	153
<b>Figure 2.25</b> Calculated transition energies for <i>cis</i> to <i>trans</i> cycloheptene's transition . . . . .	154
<b>Figure 2.26</b> Geometries optimized by CASSCF/6-31G(d) (a) pseudorotation transition state of <i>trans</i> -CHP. (b) <i>trans</i> -to- <i>cis</i> transition state of CHP (bond lengths in Å, torsion angles given for each C-C bond and CCC valence angle for each C atom). . . . .	156
<b>Figure 2.27</b> The double bond torsional potential energy profile of CHP. . . . .	158
<b>Figure 2.28</b> Some <i>trans</i> -cycloalkenes . . . . .	159
<b>Figure 2.29</b> 1,4-biradical mechanism of <i>trans</i> -CHP isomerization. . . . .	161
<b>Figure 2.30</b> Reaction scheme of tetramethylene biradical. . . . .	161
<b>Figure 2.31</b> Reaction scheme of tetramethylene biradical. . . . .	162
<b>Figure 2.32</b> Michl's proposed formation of <i>trans</i> tetramethylene to explain high ratio between cleavage and closure. . . . .	163
<b>Figure 2.33</b> Photolysis of 2,3,4,5-tetraphenylcyclopentanone. . . . .	163
<b>Figure 2.34</b> Bimolecular mechanism for <i>trans</i> to <i>cis</i> isomerization of CHP, $k_a \gg k_g, k_c \gg k_{rg}$ . . . . .	164
<b>Figure 2.35</b> CHP dimerization. The cleavage of <i>gauche</i> biradicals to two <i>trans</i> -CHP as well as the cleavage of all biradicals to <i>trans</i> - and <i>cis</i> -CHP are not depicted. . . . .	165
<b>Figure 2.36</b> Sterically blocked substituted <i>trans</i> -cycloheptenes of interest. . . . .	166
<b>Figure 2.37</b> Modified low temperature photolysis apparatus. . . . .	170
<b>Figure 2.38</b> Synthesis of substituted cycloheptenes. . . . .	173
<b>Figure 2.39</b> Identification of substituted cycloheptenes through bromination. . . . .	174

<b>Figure 2.40</b> Conformational MMX calculations of minimum energies (kcal/mol) of different cis and trans substituted cycloheptenes. ....	176
<b>Figure 2.41</b> Ring flip barrier for <i>trans</i> -TMCHP .....	177
<b>Figure 2.42</b> Identification of <i>trans</i> -TMCHP through dynamic <sup>1</sup> H NMR and coupling constant. ....	178
<b>Figure 2.43</b> Ring flip barrier calculation for <i>trans</i> -anti-DTBCHP .....	180
<b>Figure 2.44</b> Identification of <i>trans</i> -anti-DTBCHP through dynamic <sup>1</sup> H NMR .....	181
<b>Figure 2.45</b> Room temperature <sup>1</sup> H NMR spectra of <i>cis</i> - and <i>trans</i> -syn-DTBCHP. ...	183
<b>Figure 2.46</b> Room temperature decay studies of <i>trans</i> -TMCHP. ....	185
<b>Figure 2.47</b> Plot of the thermal decay at 133 °C for <i>trans</i> -anti-DTBCHP using methyl benzoate and dodecane standards. ....	187
<b>Figure 2.48</b> Plot of the thermal decay at 133 °C for <i>trans</i> -syn-DTBCHP using methyl benzoate and dodecane standards. ....	188

## LIST OF ABBREVIATIONS

**CI** - conical intersection

**HT** - Hula twist

**DMH** - 6,6-dimethyl-2,4-heptadiene

**ND** - 2,4-nonadiene

**TFHD** - 1,1,1-trifluoro-2,4-hexadiene

**DDPD** - 1,2-dideutero-1,3-pentadiene

**CHP** - cycloheptene

**DTBCHP** - 3,7-ditert-butyl-1,2-cycloheptene

**TMCHP** - 3,3,7,7-tetramethyl-1,2-cycloheptene

## CHAPTER I

### 1. Regioselectivity of the photoisomerization of acyclic 1,3-dienes

#### 1.1. Introduction

The visual pigment, found in both rod and cone cells in the human eye, is called rhodopsin (**Figure 1.1**). The pigment is made of two bound entities - a molecule of 11-*cis* retinal and the protein opsin. They are linked together via a protonated Schiff base at the terminal amino group of a lysine of the protein.

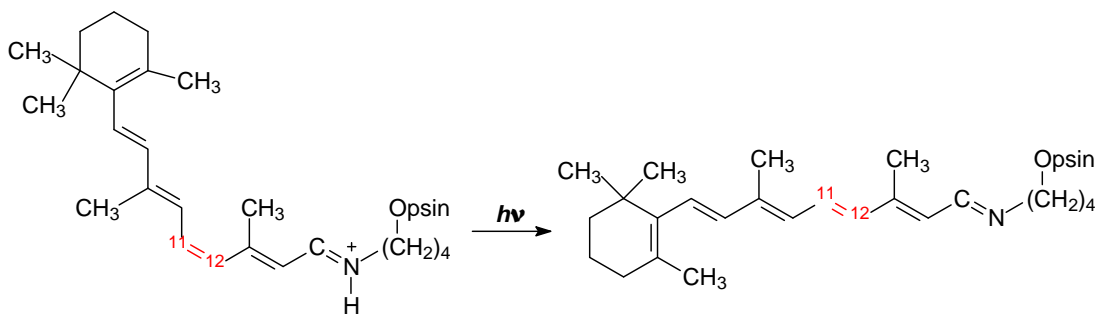


**Figure 1.1** Photoisomerization of Rhodopsin

When photolyzed, the 11-12 *cis*-retinal changes its geometrical conformation to all-*trans*-retinal in 200 fs with about 65% efficiency.<sup>1,2</sup> During the isomerization, a proton transfer occurs setting off a G-protein cascade which disturbs the resting membrane potential, thus leading to the induction of optic nerve impulse. The regiospecificity of this system is remarkable. For unbound retinal 85% of the photoisomerization is around the 11-12 C=C double bond with the remaining 15% “non-specific” isomerizations occurring at the remaining double bonds of retinal. When bound in the rhodopsin complex however, the

retinal exhibits 100% preferential rotation around the 11-12 double bond. How the protein opsin controls and improves the regiospecificity of the retinal's photoisomerization is still unknown and hence of great interest.

In his work, G. Wald,<sup>3</sup> speculated that steric hindrance, especially that produced by the methyl group at C<sub>13</sub>, was an important factor for the high regiospecificity of the double bond photoisomerization. In the following years, his proposal was thoroughly investigated and supported through different photochemical studies on various all-*trans*-retinal molecules (**Table 1.1**).<sup>4,5,6</sup>

**Table 1.1:** Distribution of *cis* isomers during the direct irradiation of all-*trans*-retinal and related compounds

Compound	Solvent	Photostationary states, %				
		7c,	9c,	11c,	13c,	other
Retinal	Hexane	0,	5,	0,	24,	1 <sup>2</sup>
	Ethanol	0.5,	7,	19.5,	24.5,	1 <sup>2</sup>
	Acetonitrile	4.5,	23,	29,	9.2,	3 <sup>4</sup>
9-Demethylretinal	Hexane	1.3,	1.2,	0,	37,	0 <sup>5</sup>
	Acetonitrile	7.2,	8.1,	20,	21,	0 <sup>5</sup>
13-Demethylretinal	Hexane	0,	9.7,	2.6,	6.8,	0 <sup>5</sup>
	Ethanol	3,	21,	23,	0,	0 <sup>6</sup>
	Acetonitrile	6,	24,	25,	0,	0 <sup>6</sup>

As seen in **Table 1.1**, all species were photoisomerized in very nonpolar and very polar solvents. When comparing the results obtained in the same solvent environment, it was concluded that the position of the methyl group on the carbon chain, had a noticeable effect on the regioselectivity. This observation suggested the presence of steric effects. From the collected data it was also concluded that there was not only a steric, but also a solvent effect,



affecting the regioselectivity of the double bond rotation. Thus these results seem to support some charge separation during the photoisomerization process.

The opsin's protein envelope (**Figure 1.2**), however, not only was determined to increase the regioselectivity of the photoisomerization of retinal, but was also mitigating the absorption

wavelength. The maximal wavelength at which 11-*cis* retinal absorbs in ether is 380nm. However, rhodopsin complexes in the rod cells in human eye, i.e. RH1 rhodopsins, absorb light wavelengths at about 500nm. They are responsible for the human's monochromatic vision in low light. Other opsin proteins, found in the cone cells in the human eye, such as SWS1 and SWS2, are responsible for the absorption of light in both the violet/UV and blue ( $\lambda=425\text{nm}$ ) regions respectively; the middle (RH2  $\lambda=530\text{nm}$ ) and long (LWS  $\lambda=560\text{nm}$ ) wavelength sensitive opsins are responsible for the green and red color recognition. In their work, published in 2006, Goddard et al<sup>7</sup> reported their computational results on the role of human red, green and blue opsins. What they proposed was that the green to blue opsin shift is caused in part by the conformational twisting of the 11-*cis*-retinal protonated Schiff base. Another additional mechanism for red-shifting the blue opsin was the influence of polar side chains of opsin.

One of the most amazing facts is that 11-*cis* retinal is employed in the vision of all vertebrates. The only difference is the nature of the opsin enveloping it. A perfect example

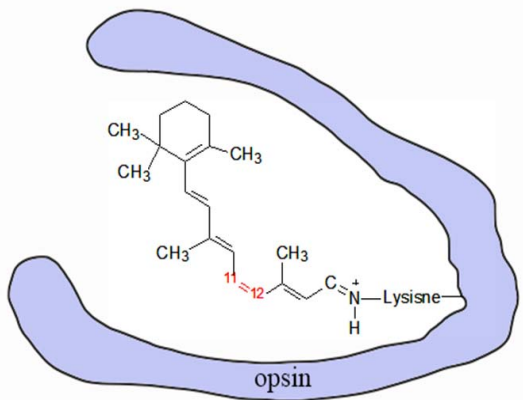


**Figure 1.2** 11-*cis* retinal bound to Lys and enveloped in opsin protein fold.

is the coelacanth *Latimeria chalumnae*, a fish from the Devonian period, found at in the Indian Ocean as deep as 200m near the Comoros Archipelago. This fish, uses the photochemical visual RH1 and RH2 pigments and is an amazing example because the species has not significantly changed morphologically in the past 400 million years.

There are other examples, such as the bacteriorhodopsin, where the retinal exists as all *trans*-retinal. When photolyzed, it was found to produce the 13-*cis*-retinal in approximately 500 fs<sup>8</sup> with a quantum yield in the range of 0.64 to 0.67.<sup>9,10,11,12,13,14</sup> In the case of archaeobacterium, *Halobacterium halobium*, the bacteriorhodopsin is employed as a proton pump, i.e. absorbing light and transferring protons through the cell membrane. Another known molecule with common structure to bacteriorhodopsin is halorhodopsin, which acts as a light-driven chloride pump, while channelrhodopsin, i.e. light-activated channel, is found in *Chlamydomonas reinhardtii*.

In order to understand the way the different opsins influence the retinal's absorptivity, several questions must be asked:

1. How are the high speeds at which the rhodopsin complex isomerizes accomplished;
2. How is the very high ~65% quantum yield established, especially considering that initial theoretical approximations predicted that no more than 50% photoisomerization quantum yield was possible;
3. How is the high photoregioselectivity accomplished? The answer to this question would include how the opsin protein controls/improves the retinal's regioselectivity of photoisomerization as well as an explanation for the high photo regioselectivity shown by 11-*cis*-retinal itself.

In the past several decades multiple mechanisms explaining the photochemical path of polyene isomerization through possible excited states have been proposed. These include the Hula Twist,<sup>15,16</sup> the Bicycle Pedal,<sup>17</sup> Zwitterionic intermediates,<sup>18</sup> and Conical Intersections.<sup>19</sup> Before discussing those mechanisms, the formation and nature of the two lowest excited states in polyenes must be discussed.

### 1.1.1. Lowest excited states of acyclic polyenes

A molecular excited state is reached when an electron absorbs photonic energy and promotes itself to a higher energy level. Spectroscopic data showed the symmetry of the lowest excited states for polyenes to be  $1^1\text{Bu}$  and  $2^1\text{Ag}$ . The  $1^1\text{Bu}$  excited state is reached when a single electron is promoted from the highest occupied molecular orbital (HOMO) to the lowest unoccupied molecular orbital (LUMO). Due to the electron excitation and the orbital occupancy change, the electron density may shift, consequently leading to charge separation. Because of that, this type of excited state is considered “ionic like.” It has been determined that relaxation of  $1^1\text{Bu}$  state occurs by rotation around a double bond.

The  $2^1\text{Ag}$  excited state is achieved by mixing three doubly excited electron configurations and, unlike the  $1^1\text{Bu}$  excited state, here charge separation is not possible. This state is referred to as “covalent.”<sup>20,21,22</sup> The relaxation route for  $2^1\text{Ag}$  was determined to be more comprehensive, involving coincident rotation of both the double and single bonds.<sup>23,24,25</sup> The first semiempirical

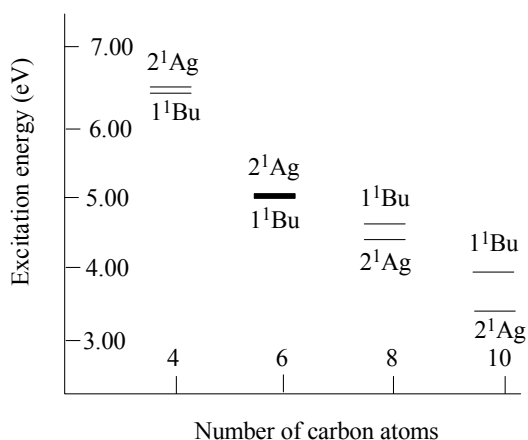


**Figure 1.3** The two lowest excited states of short polyene molecules.

and low level *ab-initio* calculations<sup>26,27,28</sup> generalized the order of the excited states for short polyenes finding the 2<sup>1</sup>A<sub>g</sub> state to be the lower one. It was assumed this is true for long polyenes as well.<sup>29,30,31,32,33,34,35</sup> More recent experimental results<sup>20,45</sup> and advanced calculations<sup>36,37,38,39,40,41,42,43,44,45</sup> show that in short polyenes the order is reversed. The energy differences between the two states are plotted in **Figure 1.3**<sup>37</sup> against the number of carbon atoms found in the polyene molecule main. The experimentally observed and recently calculated energies of *s-trans*-1,3-butadiene are listed in **Table 1.2**.

**Table 1.2:** *S-trans*-1,3-butadiene vertical excitation energies (ev)

State	CI <sub>4</sub> <sup>38,3</sup>	SACCI <sub>36</sub>	Hv <sup>40</sup>	MRCI <sub>41</sub>	MRCI1 <sup>4</sup>	CASPT2 <sup>4</sup>	MRMP <sub>44</sub>	VESH <sup>40</sup>	GVBCI <sup>4</sup>	EXP
1 <sup>1</sup> B <sub>u</sub>	6.23	6.39	6.1	6.48	7.07	6.23	6.21	6.14	6.9	6.25 <sup>45</sup>
2 <sup>1</sup> A <sub>g</sub>	6.67	7	6.2	6.53	8.67	6.27	6.31	6.19	7.06	7.411 <sup>20</sup>
1 <sup>3</sup> B <sub>u</sub>		3.48	3.2	3.18	3.6	3.2	3.2	3.23	3.35	3.22 <sup>45</sup>
1 <sup>3</sup> A <sub>g</sub>		5.15	4.8	4.9		6.27	6.31			

### 1.1.2. Photochemically induced geometry isomerization in acyclic polyenes

The photochemistry of 1,3-pentadiene, as the example of the most simple mono-substituted acyclic 1,3-diene, has been studied extensively.<sup>46,47,48,49,50,51,52</sup> Upon photolysis, all *trans*-1,3-pentadiene was determined to produce variety of photoproducts: the *cis-trans* product, the *s-cis*- *s-trans* product, cyclobutenes and bi-cyclobutanes.

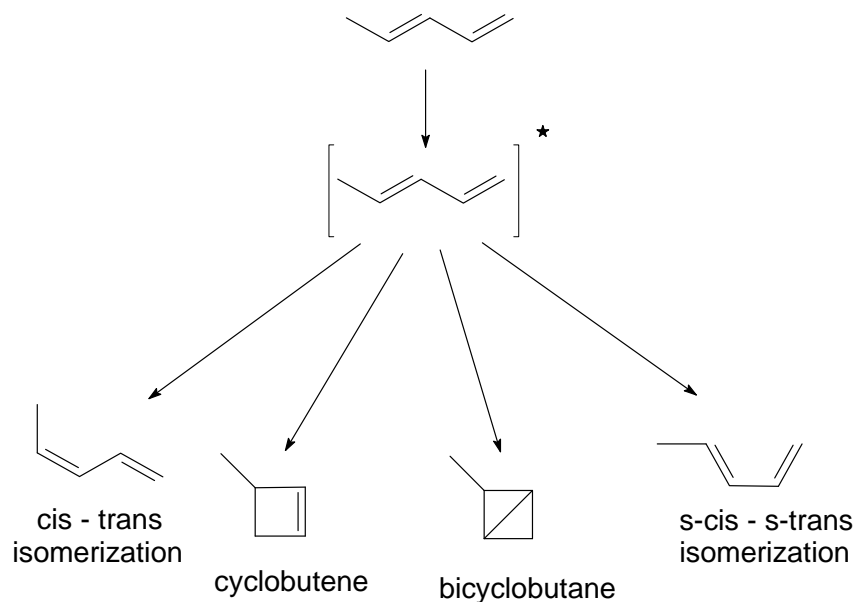


**Figure 1.4** Photochemistry of 1,3-pentadiene.

#### 1.1.2.1. Cyclopropyl biradical mechanism

In their work, Boue and Srinivasan<sup>47</sup> photolyzed the two geometric isomers of 1,3-pentadiene and reported the experimentally obtained quantum yields of the photoproducts (**Table 1.3**). When comparing the quantum yields of 1,3-dimethyl-cyclopropene, they discovered the cis precursor gave almost two times higher yield than the trans. In an effort to fit these results, they proposed a mechanism (**Figure 1.5**)

**Table 1.3:** Product Quantum yields from 1,3-pentadiene

	Product quantum yields from 1,3-pentadiene		
	3-methylcyclobutene	isomeric 1,3-pentadiene	1,3-dimethylcyclopropane
Cis	0.0034	0.1	0.00088
Trans	0.03	0.083	0.0019

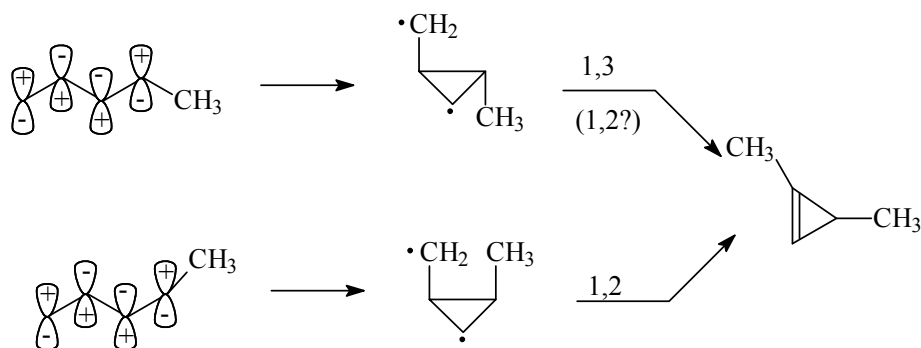


**Figure 1.5** Mechanism for the formation of 1,3-dimethylcyclopropene from 1,3-pentadienes.

of isomerization involving the formation of a cyclopropyl carbinyl biradical intermediate.

It was noted that the cyclopropene could be produced from the *cis*-1,3-pentadiene via 1,2 hydrogen shift only. Alternatively, a biradical formed from the *trans*-1,3-pentadiene, could go either through 1,2 or 1,3 hydrogen shift, explaining the doubling of the quantum yield.

In his studies of hexadienes, Saltiel et al.<sup>48</sup> reported the quantum yields of photoproducts after direct 2,4-hexadiene irradiation (**Table 1.4**).

**Table 1.4:** Quantum yields of direct 2,4-hexadiene isomerization

$\Phi_{EE-ZE}$	$\Phi_{ZZ-ZE}$	$\Phi_{ZE-EE}$	$\Phi_{ZZ-EE}$	$\Phi_{ZE-ZZ}$	$\Phi_{EE-ZZ}$	$\sum\Phi$
0.37	0.41	0.17	<0.03	0.29	<0.03	1.31

These results showed that upon direct irradiation, for each photon absorbed, at best only one of the double bonds rotates. This compares to triplet photochemistry experiments with 2,4-hexadiene, where it was determined that simultaneous rotation of the two double bonds occurs upon absorption of one photon, meaning with different multiplicities, different

reaction paths are taken. From the small  $\Phi_{ZZ-EE}$  and  $\Phi_{EE-ZZ}$  numbers in **Table 1.4**, one could also conclude that the  $S_1 \rightarrow T_1$  intersystem crossing is inefficient.

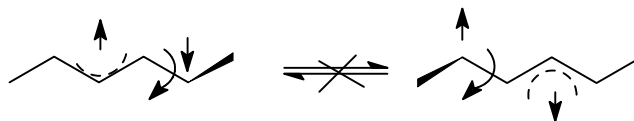


**Figure 1.6** Allyl-methylene biradical intermediate.

As a result, Saltiel suggested two pathways to explain the observations: a biradical mechanism involving the formation of cyclopropylmethylene species (**Figure 1.7**), but he also suggested the formation of an allylmethylene biradical intermediate (**Figure 1.6**).<sup>48</sup>

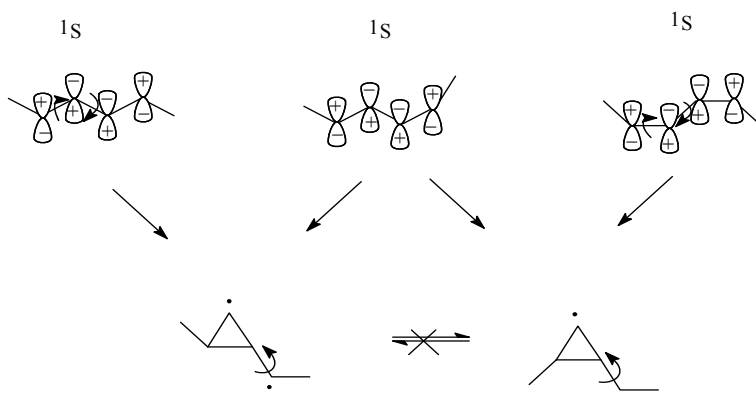


**Figure 1.7** Cyclopropylmethylene mechanism for the *cis-trans* isomerization of 2,4-hexadiene.

### 1.1.2.2. Hula-twist mechanism (HT)

In effort to explain the space and time conserving isomerization of retinal in the tight protein envelop of opsin, in 1985 Lui and Asato<sup>15,16</sup> proposed the Hula Twist mechanism. Inspired by the Hawaiian traditional dance Hula, in this mechanism there is a simultaneous

twist around about a double bond and neighboring single bond. Rather than just rotating the terminal units, the molecule is involved in a “kink” of a single C-H between the double and single bonds. The small geometry change involved in the Hula Twist and bond flip are shown in **Figure 1.8**.

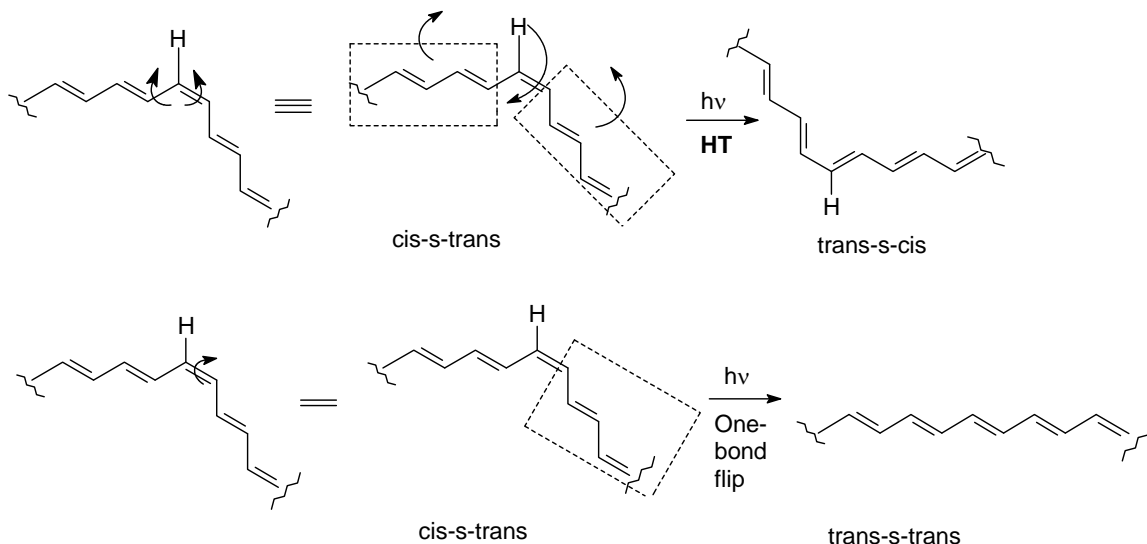


**Figure 1.8** Proposed Hula Twist mechanism (upper) and one bond flip(lower).

Liu and Asato suggested that their mechanism could describe the geometrical changes experienced not only by protein bound chromophores but by small organic molecules as well.<sup>53,54,55</sup> The main idea supported in their work was that in solution the mechanism of a simple double bond rotation dominates (OBF in **Figure 1.11**), whereas in solid/frozen media, with a protein envelop as a perfect example with its high space strain, the mechanism of choice would be the HT. They accumulated a number of experiments which could have been explained by a HT<sup>50,56,57,58,59,60</sup> mechanism however, Fuss et al.<sup>61</sup> was the first to report experimental evidence in 1998.



In their studies of pre-vitamin D, isomers using photochemical spectroscopic techniques, they observed the exclusive formation of T and T<sub>0</sub> photoproducts via simultaneous rotation around double and single bonds (**Figure 1.9**).<sup>61</sup>

It was later determined that the all *trans*-octa-1,3,5,7-tetraene (OT) photoisomerizes via the HT mechanism as well.<sup>62</sup> In cryogenic photochemical experiments at 4.3K with n-

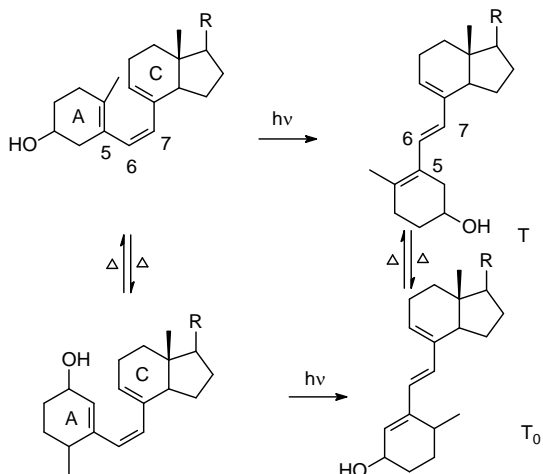


**Figure 1.9** Photoproducts produced through HT mechanism from pre-vitamin D.

octane as a matrix, photolysis of OT produced the 2-*s-cis*-conformation. The reason for the regioselectivity of this molecule in this particular experiment could be explained with the nature of the solid matrix, i.e. linear-shape of space available for the necessary rotation. Had a HT occurred at any other ene center, including the C3-C4 double bond isomerization which predominates in fluid solution,<sup>63</sup> it would have lead to a very bent structure, which would be difficult to establish in the solid n-octane matrix (**Figure 1.10**).<sup>53,54,55</sup> Thus the photoisomerization that could be best accomplished by this matrix was an HT isomerization of the terminal double bond.

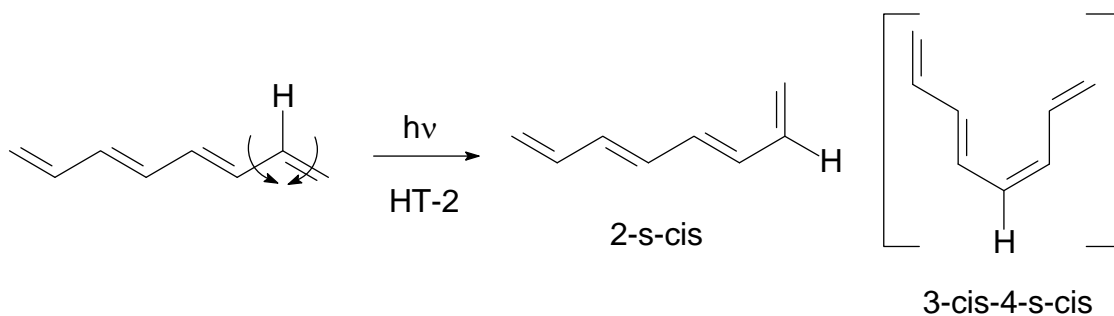


**Figure 1.10** Photochemical isomerization of OT

In their work Garavelli et al.<sup>64</sup> used the tZt-penta-3,5-dieniminium cation as a model of the protonated Schiff base in rhodopsin. Based on calculations, they found that the isomerization of the cation went through a non-HT mechanism. However, when another model for rhodopsin was examined, i.e. all *trans*-1,3,5-hexatriene, their results indicated a HT like mechanism.<sup>64</sup> Because the radiationless decay was very fast, the conclusion was that the photochemical pathway involved molecular distortion to arrive at a  $S_1/S_0$  conical intersection from which rapid decay to the ground state could occur.

### 1.1.2.3. Bicycle Pedal mechanism

The Bicycle Pedal mechanism was introduced as an alternative explanation for the space conserving photoisomerization of rhodopsin (**Figure 1.11**). The concept of this process was introduced in 1976 by Warshel<sup>17</sup> as a joint rotation about parallel C=C double bonds. With rhodopsin this process causes the cis conformation of the  $C^{11}=C^{12}$  bond to become trans

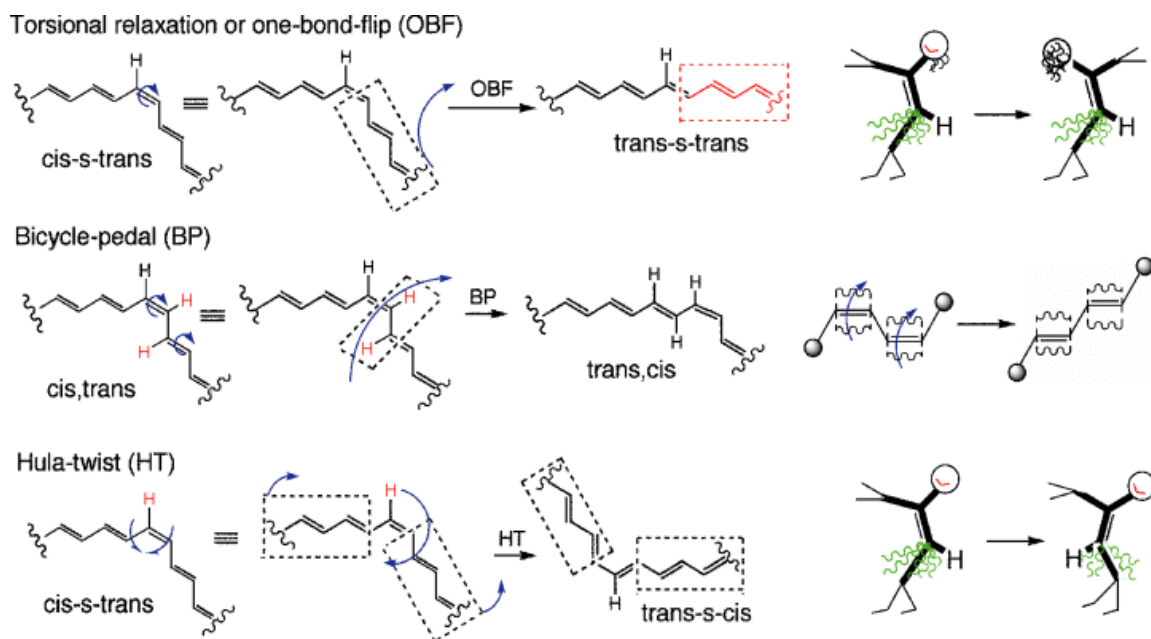


**Figure 1.11** Proposed mechanisms for polyene photoisomerization.

while the terminal C=N bond simultaneously isomerizes. In 2008, Weingart et al.<sup>2</sup> stated that the new mechanism doesn't explain the extreme twisting observed in the all-trans conformer of the primary rhodopsin intermediate.

Contrary to Weingart, Olivucci et al.<sup>65</sup> suggested that in rhodopsin, the bicycle pedal mechanism does take place and occurs as clockwise rotation about the C<sup>9</sup>=C<sup>10</sup> double bond and counterclockwise rotation about the C<sup>11</sup>=C<sup>12</sup> double bond. In the same year, 2010, Olivucci reported the possibility of another space conserving rotation mechanism during bacteriorhodopsin's photoisomerization, called aborted double bicycle pedal. With it, Olivucci and his group asserted that the N-H bond breakage was the primary event for the proton pumping with three adjacent double bonds' rotations. They reported that C<sup>11</sup>=C<sup>12</sup>, C<sup>13</sup>=C<sup>14</sup> and C<sup>15</sup>=N rotated counterclockwise, clockwise and counterclockwise respectively, with a conical intersection occurring when the C<sup>13</sup>=C<sup>14</sup> double bond has twisted -60°. At the conical intersection they calculated the degree of twisting around the C<sup>11</sup>=C<sup>12</sup> and C<sup>15</sup>=N to be 27° and 21° respectively. Combined, those angles do not counterbalance entirely for the -60° twist at C<sup>13</sup>=C<sup>14</sup>, but the angle variations almost completely compensate for the molecule's global geometry change in space. Additionally, the N-H-402 (W402) hydrogen bond was determined to stretch along the excited state pathway, leading to its probable breakage, while remaining adjacent to the bound to the complex counter-ion.

#### **1.1.2.4. Zwitterionic intermediate mechanism and related net charge effects**

In 1970 Dauben and Ritscher<sup>66</sup> published the results from their studies on bicyclobutanes, photochemically prepared from *cis*- and *trans*-3-ethylidenecyclooctene. Orbital symmetry suggests that the ring-closure should have proceeded in a joint cycloaddition of the two

double bonds via an antarafacial-antarafacial or suprafacial-suprafacial (2+2) cyclization. Such process should lead to the formation of *endo-trans* (a-a) and *exo-cis* (s-s) from the *cis* diene and *exo-trans* (a-a) and *endo-cis* (s-s) from *trans* diene respectively. What they found however, was that the bicyclobutane photochemically produced from *cis*-diene, is epimeric at only one center, i.e. an (s-a) cyclization (**Figure 1.12**).

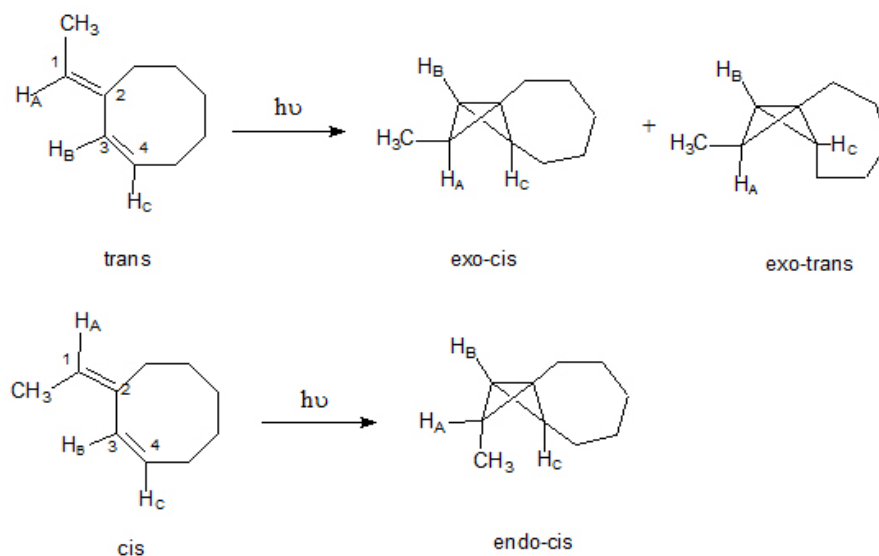


**Figure 1.12** Photochemistry of *cis*- and *trans*-3-ethyldienecyclooctene

They proposed three possible electronic configurations of a singlet excited state, formed by the rotation of the C<sup>3</sup>=C<sup>4</sup> double bond. The first electronic configuration, an allyl cation-methylene anion, was rejected because of its high energy of formation. It also did not fit the stereochemistry of cyclopropene formation, as well as methanol trapping products. Being a biradical, the second configuration was also discarded as a possibility due to its high activation energy for closure. It also did not explain the results from the methanol additions. The third one however, fit perfectly with the stereochemistry of cyclopropene formation as

well as with the methanol addition products. The third electronic configuration was the allyl anion-methylene cation.

The ingenuity of his finding, is that Dauben's would-be intermediate, derived from the neutral and nonpolar hydrocarbon, had very strong ionic character. In their later work, Dauben et al. proposed the involvement of a similar zwitterionic intermediate<sup>67</sup> in the stereospecific<sup>68</sup> photoproduction of bicyclo[3,1,0]hexane from hexatriene (**Figure 1.13**).

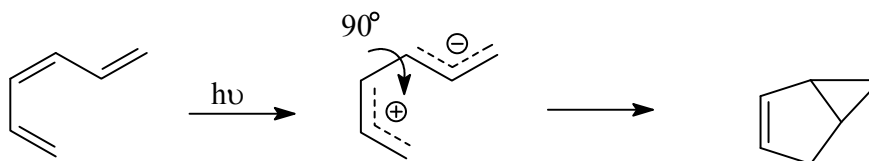


**Figure 1.13** Photochemical development of zwitterionic intermediate in hexatriene suggested by Dauben

Dauben et al.<sup>68</sup> suggested that when the central double bond is twisted, this could produce several electronic states. Two of them would be biradical states, a triplet ( $^3D$ ) and a singlet ( $^1D$ ) states and two zwitterionic states, i.e.  $Z_1$  and  $Z_2$ . Based on later unpublished methanol trapping work, the biradical states were discarded as a possibility.

In their work in the early 1970s Wulfman and Kumei published data,<sup>69</sup> which suggested that an excited, twisted alkene would have a  $Z_1$  or  $Z_2$  character, or in other words - the two lowest excited states would be ionic.<sup>70,71,72</sup> The two states were assumed to be symmetrically-amalgamated two resonating ionic entities, where the out-of-phase combination is the lowest (**Figure 1.14**). Unsymmetrical substitution of the alkene would lead to interruption of the energy equivalence of the  $+ \leftrightarrow -$ ,  $- \leftrightarrow +$ . This led Wulfman and Kumei to the conclusion that

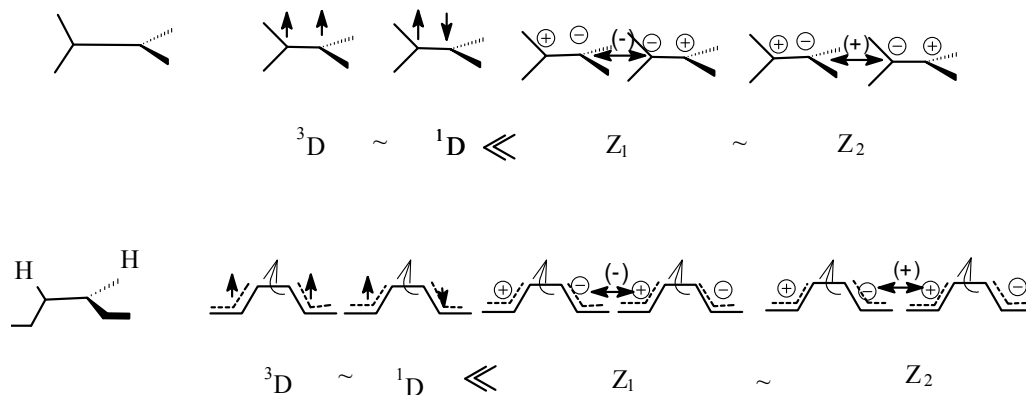


**Figure 1.14** Electronic states of ethylene and *s-cis-s-trans*-diallyl.

100% of one of the two ionic structures could be produced, when a small perturbation mixed  $Z_1$  and  $Z_2$ .<sup>73</sup>

Bonacic-Koutecky<sup>74</sup> et al. theoretically studied excited ethylene (**Figure 1.15**<sup>74</sup>) where charge separation,  $\Delta q$ , has occurred between the two carbons in the excited state. Using *ab-initio* approximation at the 4-31G level, the charge separation was calculated as a function of the pyramidalization angle  $\Phi$ . At a pyramidalization angle of  $15^\circ$ , the charge separation was calculated to be  $0.72e$ . It was also found that  $\Delta q = 0.87e$  when the C atom is fully  $sp^3$  hybridized.

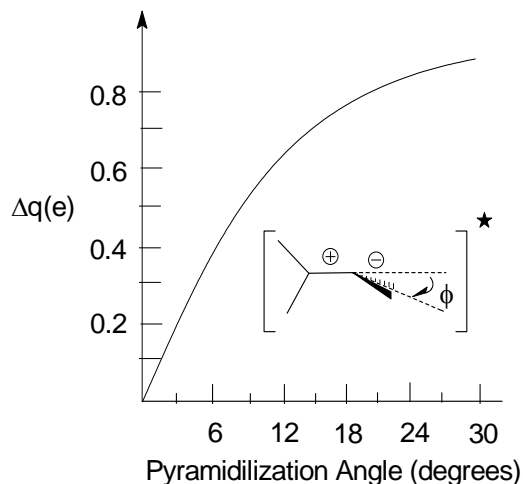


**Figure 1.15** Charge separation  $\Delta q$  in  $Z_1$  excited singlet state of  $90^\circ$ -twisted ethylene as a function of the pyramidalization angle  $\Phi$ .

The pyramidalization angle can be increased through a simple chemical substitution. For example, when twisted to  $90^\circ$  the propene molecule was calculated to exhibit a large charge separation without sign of pyramidalization ( $\Delta q = 0.84e$ ).

Calculations for the  $Z_1$  state of *s-cis-s-trans*-diallyl (1,3,5-hexatriene), or **DHT**, were also performed. When the central twist angle,  $\theta$ , was varied from  $0^\circ$  to  $180^\circ$  it was found that, at almost all values, the charge was equally distributed. A large charge separation was “observed” only at the nearly perpendicular conformation with  $\theta = 91^\circ \geq \theta \geq 89^\circ$  (**Figure 1.16**).

However, later calculations, did not exhibit this type of “sudden polarization” effect. Instead, it was determined that polarization occurs gradually over a broad range of twisting angles and not just in a narrow region.<sup>75,76</sup>

Only half a decade after Bonacic-Koutecky, Bruckmann and Salem<sup>77</sup> reported their studies of the two lowest excited state surfaces for the 1,3-butadiene (**Figure 1.17**). In their work, they proposed the existence of two minima at the

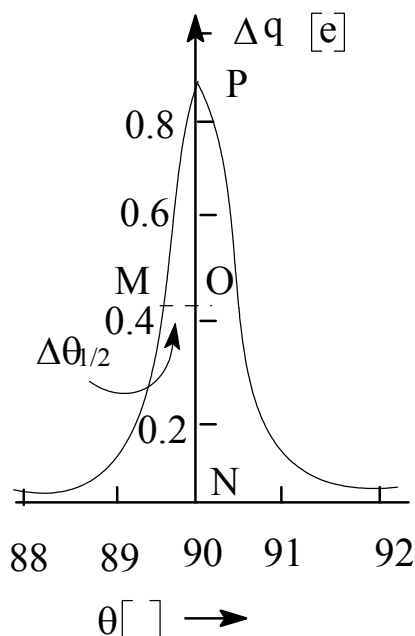


**Figure 1.16** Charge separation in  $Z_1$  excited state of DHT as a function of  $\theta$ . Note the unsymmetric nature of the curve at  $\sim 90^\circ$ .

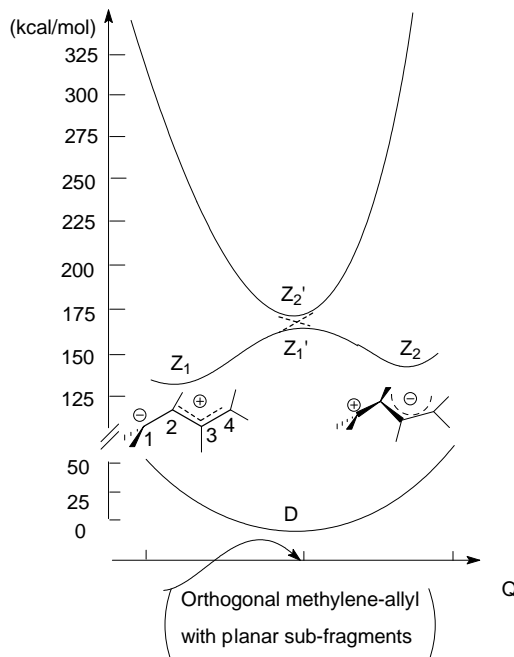


**Figure 1.17** Potential energy surfaces of the lowest S states as a function of pyramidalization angle.

lowest potential energy surfaces of the lowest excited singlet state. These consisted of an allyl cation - methylene anion zwitterion  $Z_1$  which was calculated to be 9.2 kcal/mol lower in energy than an allyl anion - methylene cation zwitterion species,  $Z_2$ . These zwitterions were separated by a barrier of 6.6 Kcal/mol.

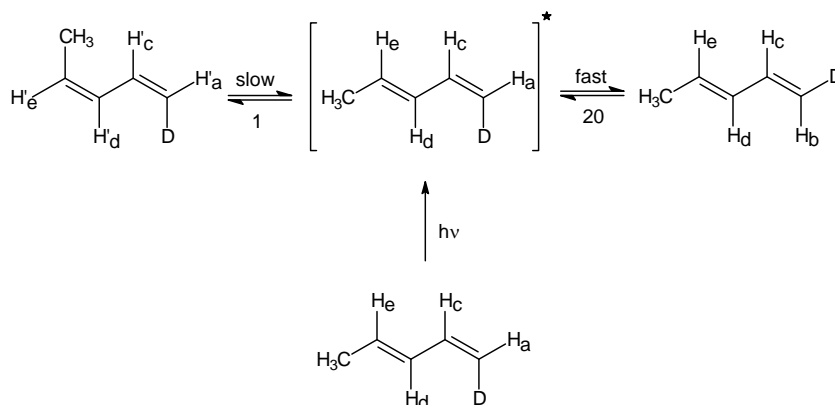


**Figure 1.18** Photochemical isomerization of *cis*-1-deutero-*trans*-1,3-pentadiene

In their experimental work on *cis*-1-deutero-*trans*-1,3-pentadiene, Squillacote and Semple<sup>49</sup> photolyzed the diene at 254nm and found a 20 times higher isomerization about the C=C double bond substituted with deuterium, compared to the methyl substituted double bond (**Figure 1.18**).

The difference in the preferences of rotation of the two double bonds in the mono-deutero pentadiene was explained by the development of zwitterionic-like species during the isomerization process. Squillacote and Semple

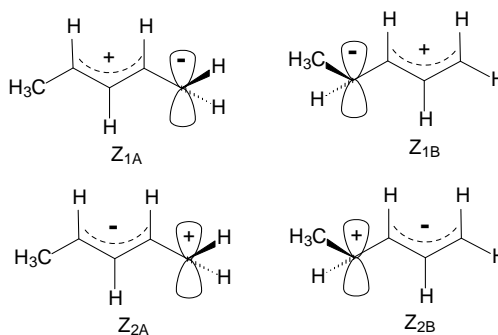


**Figure 1.19** Four possible zwitterionic forms of 1,3-pentadiene



noted that there were four possible orthogonal allylmethylene zwitterionic states (**Figure 1.19**) for this unsymmetrical diene.

Only two of the four would allow the methyl group to stabilize a positive charge, i.e.  $Z_{1A}$  and  $Z_{1B}$ . The observed photoregioselectivity suggested that the allyl cation-methylene anion species,  $Z_{1A}$ , was the preferred pathway, in agreement with the calculations<sup>35,76</sup> (**Figure 1.20**).<sup>49</sup>

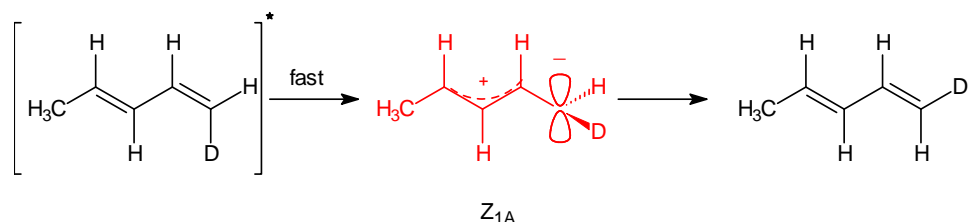


**Figure 1.20** Suggested reaction path for the isomerization of 1,3-pentadiene.

In later studies, using the methanol trapping technique, numerous  $\alpha,\beta$  unsaturated carbonyl species were photolyzed and provided an unambiguous library of data, confirming the existence of zwitterionic forms developed during the photochemically induced isomerization.<sup>78,79,80,81,82,83</sup> Schuster et al.<sup>79</sup> reported his results from photolysis of cyclohexa-2,5-dienone in methanol solutions as evidence of reaction going through zwitterionic fragmentation. Afterwards many more examples of such photochemical reactions were reported such as for thiazepines,<sup>82</sup> epoxides,<sup>83</sup> and 2-(hydroxyalkyl) pyran-4-ones.<sup>81</sup>

Proving zwitterions formed from non-polar molecules, however, proved to be very challenging. When methanol was photochemically added to phenylallenes<sup>84</sup> and arylbutadienes,<sup>85,86</sup> the mechanism's path was defined as addition to zwitterions almost

unequivocally. When stilbenes were photolyzed in methanol, however,<sup>87,88</sup> the results showed methanol inclusion by a carbene formed from a 1,2-hydride shift, rather than a zwitterion.

Unfortunately, there is no concrete trapping evidence that zwitterions are made from 1,3-dienes. Dauben<sup>66</sup> excluded the participation of a biradical excited state, based on an unpublished methanol trapping experimental data. In their work in the late 1960's, Baltrop and Browing<sup>89</sup> published data about the addition of methanol to a series of acyclic 1,3-dienes (**Figure 1.21**).

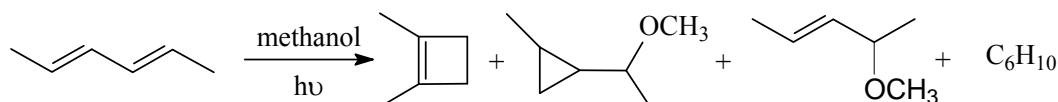


**Figure 1.21** Methanol trapping study of an acyclic 1,3-diene.

Here, the existence of the methanol adducts could have been viewed as the evidence for the formation of charge separation in the excited states, especially considering the nonpolar properties at the ground state. However, in 1969, Dauben<sup>90</sup> proposed that these adducts were product of a thermal addition to the bicyclobutanes produced photochemically. In their experiment, no methanol addition products were produced upon the direct photolysis of butadiene in acid free methanol. However, if acid was added, the production of almost equal amounts of cyclobutane methyl ether and cyclopropylcarbinyl methyl ether was detected. Methyl ethers appeared after the addition of 0.1M hydrochloric acid to the acid free photolyzed reaction mixture, preceded by the immediate disappearance of the initial bicyclobutane product. However some of Baltrop's methyl ethers were not produced from bicyclobutanes, so the question remains open.

### 1.1.3. Conical intersection

#### 1.1.3.1. Avoided crossings, i.e. wells

In the late 1960's and early 1970's Van der Lugt and Oosterhoff<sup>91</sup> were among the first to postulate the importance of avoided crossings as possible pathways for relaxation from an excited to the ground state. The concept of avoided crossing, as postulated by them, described the changes happening on potential energy surfaces when two states with the same multiplicity and symmetry approach each other. The interaction between those two states would be described as a mix of “phase in” and “phase out” combinations, and thus no crossing of these states would be possible. A crossing would be allowed only if the two electronic states had different symmetries and could not mix.

Woodward and Hoffman<sup>92,93</sup> were the first to propose that orbital symmetry plays a major role in reactions. A very good example would be the disrotatory electrocyclic formation of cyclobutene from 1,3-butadiene. There, only the reactant's and product's orbital symmetries, with respect to the mirror plane, would be considered.

The avoided crossing rule, together with the symmetry element of this reaction, would give the state correlation diagram shown in

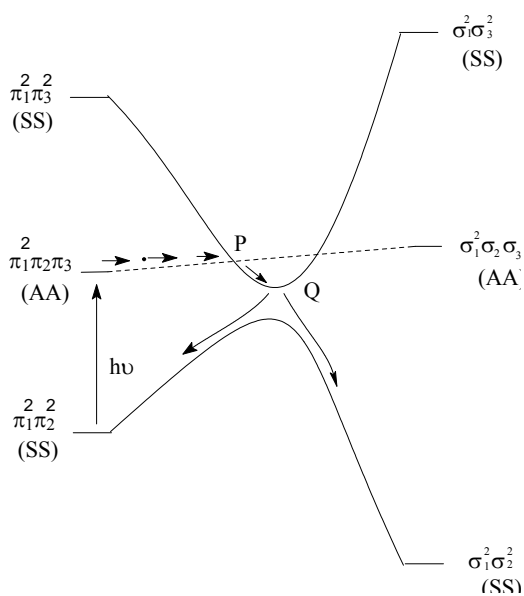


**Figure 1.22** State correlation diagram showing the disrotatory closure of 1,3-butadiene.

**Figure 1.22.**

Lugt and Oosterhoff<sup>94</sup> described the avoided crossing in a molecule as an excited state energy minimum, as from this point the molecule could “jump down” to the ground state. This idea was used to explain the absence of fluorescence and phosphorescence of dienes, photochemically excited in liquid solutions. The reasoning was that the antisymmetric excited state would “drop” into the well of the symmetric excited state so quickly, that interconversion to ground state with emission of light would not take place.

This picture of how photochemistry works was nearly universally accepted, but some scientists argued that there were several problems with it.<sup>95</sup> Desouter-Lecomte and Lorquet discussed the probability (P) for radiationless decay between two electronic states,<sup>95</sup> employing the Landau-Zener model<sup>96</sup> as:

$$P = \exp [-(\pi/4)\xi]$$

It is important to mention that in their representation, the two states were calculated to have different energies, represented as  $\Delta E(q)$ . In this equation the Massey parameter is  $\xi$  and is described as:

$$\xi = [\Delta E(q) / (|q| \cdot g(q))]$$

Where  $|q|$  is vector of nuclear displacement and  $g(q)$  is non-adiabatic coupling matrix element. They found that unless  $\Delta E$  has a value of 2 kcal/mol or less, the calculated decay probability would be very small. So small in fact, that the van der Lugt and Oosterhoff's postulate that photochemical reactions proceed via excited state minima produced by avoided crossings would not be consistent with the speed of the most photochemical reactions. This reasoning was nevertheless ignored by the large majority of photochemists.

### 1.1.3.2. Surface crossing, i.e. slides

As was described previously, two overall symmetric excited states do not cross each other, but rather form minima on potential energy surfaces. However, if the excited molecule distorts asymmetrically, the previously repelled states can adopt a common point on their potential energy surfaces. Michl et al. used the simple 2 electron-2orbital model to investigate the effects of such a system.<sup>97,98</sup>

It was determined that with this model, four different species would be produced: one biradical triplet (T) and three biradicaloid singlets (G, S, D). Biradicals and biradicaloids were defined as two degenerate, approximately non bonding orbitals, populated with a pair of electrons.

A homosymmetric biradical was described as two non-interacting orbitals, equal, or very close, in energy. Both fully dissociated H<sub>2</sub> and 90°twisted ethylene could be considered as quintessential homosymmetrical biradical.

There are three types of biradicaloids:

- Homosymmetric biradicaloids - the localized orbitals  $\chi_a$  and  $\chi_b$  are equal in energy and interact (partially twisted ethylene);
- Heterosymmetric biradicaloid - the localized orbitals  $\chi_a$  and  $\chi_b$  do not interact but are degenerate in energy ( 90° twisted ethylene);
- Nonsymmetrical biradicaloids - the localized orbitals  $\chi_a$  and  $\chi_b$  are both different in energy and interact (propene partially twisted about its double bond).

“Covalent perturbation” was determined to be the only possible perturbation of the two most localized interacting orbitals in a homosymmetric biradicaloid. The magnitude,  $\gamma$ , of

the covalent perturbation was represented as a double Hückel resonance integral between the two most localized orbitals.

The only viable perturbation in a heterosymmetric biradicaloid was the electronegativity difference between the two localized orbitals, resulting in their energy difference. This difference was called a polarizing perturbation and abbreviated as  $\delta$ . It is the existence of  $\delta$  that makes structures to mix.

In **Figure 1.23**<sup>99</sup> is shown the general representation of nonsymmetrical biradicaloids, where the  $\gamma \neq 0$ ,  $\delta \neq 0$ ; and the plane defined by  $E$  and  $\gamma$  depicts the Oosterhoff's diagram for avoided crossing between the ground state and the

doubly excited (D) state. However, a geometry change along the  $\delta$  coordinate would allow a  $S_1$ - $S_0$  intersection, leading to the formation of biradicaloids and create a surface crossing. This meant that even a small change in the symmetry of the two states could allow them to become degenerate and touch. This crossing point was called a conical intersection.

### 1.1.3.3. The intermediary conical intersections in photochemical reactions

The reaction mechanism of a non-adiabatic photochemical reaction is started with the absorption of light, creating an excited molecule in the Franck-Condon region on the potential energy surface of the first excited state  $S_1$ . The reaction is complete when the zero point energy level of the ground state  $S_0$  of the final product is reached. As described above

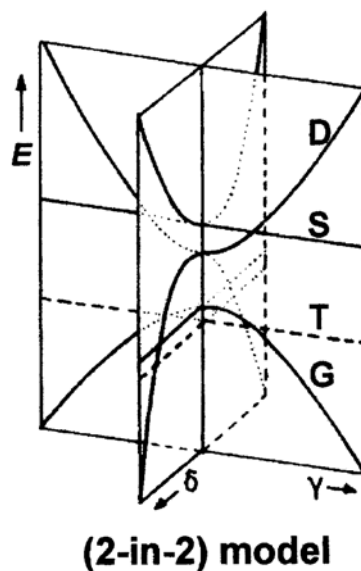


**Figure 1.23** The 2-in-2 model for surface touching. The two planes shown correspond to the homosymmetric and heterosymmetric case.

with Michl's 2-electron-2-orbital model, appropriate distortion of the system's symmetry could lead the two states  $S_1$  and  $S_0$  to cross at a common point. When the two potential energy surfaces of the excited and ground states are plotted against two special internal geometric coordinates, they form a double cone geometry, with common area at the tips of the cones (**Figure 1.24**)<sup>100,101</sup> and hence name "conical intersection". The two special internal geometric coordinates are  $X_1$ , i.e. the energy gradient difference vector and  $X_2$ , the nonadiabatic coupling vector (**Figure 1.24**). The gradient difference vector is formulated as:

$$X_1 = \partial(E_0 - E_1) / \partial q$$

The largest deviations in surface-slope are expected to occur in this direction. The nonadiabatic coupling vector  $X_2$  is formulated as:

$$X_2 = \langle \Psi_0 | \partial \Psi_1 / \partial q \rangle$$

This vector was created to describe the nuclear displacement responsible for the highest degree of mixing of the two adiabatic wave functions crossing at the tip of the cones. In

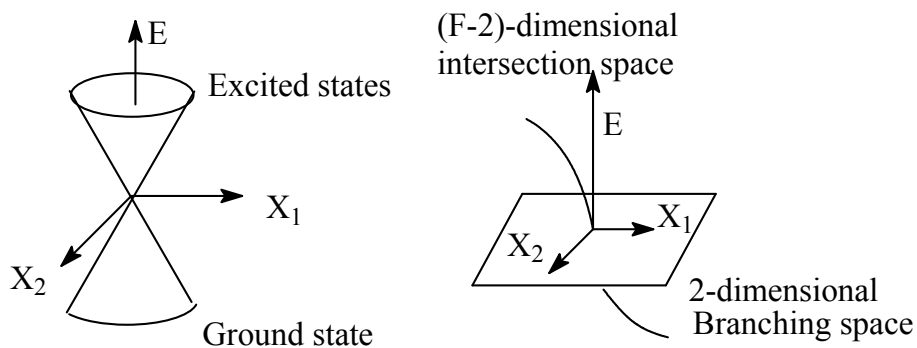


**Figure 1.24 Left:** two potential energy surfaces form the double cone if plotted against  $X_1$  and  $X_2$ ; **Right:**  $X_1$  and  $X_2$  span the "branching space", while the "intersection space" is a (F-2)-dimensional hyperline.

other words,  $X_2$  is the symmetry –lowering coordinate permitting the otherwise symmetric  $\Psi_0$  and  $\Psi_1$  to mix at the common point, the  $\delta$  in the 2-in-2 model.

The definition of conical intersection could be put as:<sup>101</sup> “Two states, even if they have the same symmetry, intersect along an (F-2)-dimensional hyperline as the energy is plotted against the F nuclear coordinates (F=3N-6), while for any point of the (F-2)-dimensional intersection space, the energies of the two states are the same.” The energy E and the energy gradient  $\partial E/\partial x$  (x = direction of nuclear displacement) must be the same for both states. The “branching space” is formed by the remaining  $X_1$  and  $X_2$  dimensions. Hence the conical intersections are determined to be 3N-8 dimensional potential energy surfaces.

Conical intersections offer a very good route of relaxation from the excited state to the ground state in a non-radiative fashion,<sup>102,103,104,105</sup> and so explain the very short, non radiative,

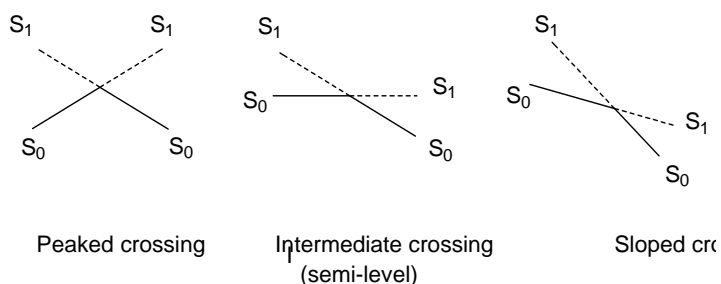


**Figure 1.25** Surface connection patterns for conical intersections.

lifetime of some excited states.<sup>46,106,107,108,109,110,111,112,113,114</sup> Further computational studies determined that the two conical potential energy surfaces could cross in three possible ways: “peaked”, “semilevel” and “sloped” pattern (**Figure 1.25**).<sup>115</sup>

It was also determined that development of the excited state would largely depend on the topology of the top cone, the “funnel”, which is the excited state’s potential energy surface. This meant that the dynamics of the photochemical reaction would depend on the form of conical intersection (**Figure 1.26**<sup>115</sup>).



If there is no energy barrier developed, the relaxation from the excited state to the ground state via the conical intersection could be “ultra fast” (**Figure 1.26**<sup>115</sup> **b, d, e, f**). However, if barrier is developed, then one could expect the photochemical reaction to “experience” temperature and wavelength dependence. In **Figure 1.26**<sup>115</sup> **c** is depicted a case where the excited molecule could go to either its relaxed form at ground state, or swing back to the lowest energy level of the excited state. In that case, the experimental reaction rate would be expected to be slowed. In **Figure 1.26f**<sup>115</sup> is shown another special case, where the shape of the common energy surface between the excited and ground states, creates the possible paths of relaxation to multiple photoproducts.

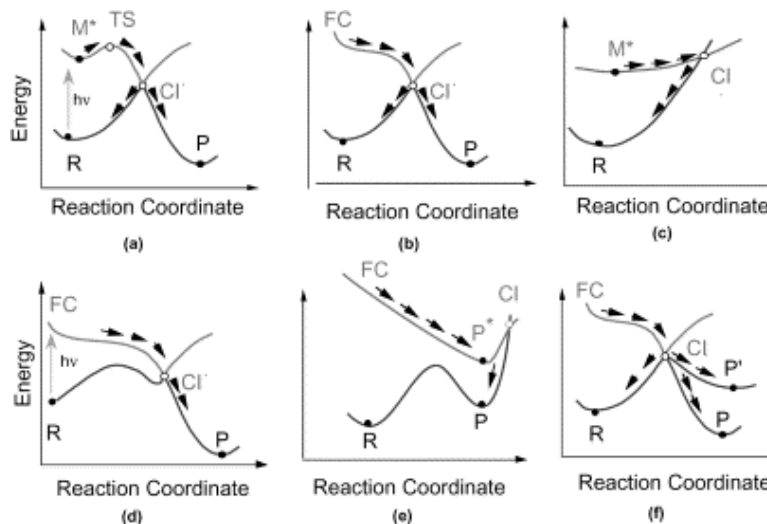


**Figure 1.26** Schematic representation of different reaction path topologies and positions of the conical intersection region along a reaction coordinate.

In his studies of potential energy surface intersections for polyatomic molecules, Longuet-Higgins<sup>116</sup> proposed a phase change theory stating that if the wave function of a given electronic state changed its sign when transported adiabatically around a loop in

nuclear configuration space, then the state must have been degenerate with another energy surface at some point within the loop. If described in simple words, in a photochemical reaction, the conical intersection must come from a region framed by a loop, where the total electronic wave function changes sign. The concept was demonstrated with a doublet  $H_3$  system. To define a loop they created three anchor points. Two of the points were designated for the reactant and the product. The third anchor point was determined in more intuitive way, i.e. it could define either a stable molecule or a meta-stable intermediate. The connections between the three points, however, had to be defined by elementary reactions, creating a single barrier between them.<sup>117,118</sup>

When applied to  $H_4$  system, the phase change rule was found to produce a perfect tetrahedral conical intersection located at the center. The tetrahedral geometry of the crossing  $S_0$  and  $S_1$  in the  $H_4$  system was predicted by Michl in 1977, and then correlated<sup>119</sup> to the 1,3-butadiene's photochemistry. The non-interacting  $\sigma$  framework was found very strained when the four butadiene  $p^\pi$  orbitals were centered on the tetrahedron's vertices pointing towards the center. However, as mentioned before, a conical intersection is spread within an entire  $3N-8$  dimensional space, meaning the framework could be distorted and twisted until a less strained form is found.

In their MC—SCF study,<sup>120</sup> Olivucci and coworkers proposed a distortion mode for the 1,3-butadiene molecule when photolyzed directly. They calculated a central C-C rotation in unison with a non-synchronous rotation of the two terminal  $CH_2$ . This rotation of one of the central CH groups up and out of the plane of the diene unit, a geometrical change that was later termed the “3-carbon kink”.<sup>120,121</sup> While not stated by the authors explicitly, this motion

has strong resemblance to the Hula Twist mechanism. The molecule of 1,3-butadiene had three different routes for relaxation through the conical intersection of the shared ground and excited state minima depending on the initial diene geometry (s-transoid or s-cisoid) and on the relative direction of rotation (conrotatory or disrotatory). The three entry paths, i.e. “s-transoid”, “s-cisoid” and “centraloid” are shown in **Figure 1.27**.<sup>120</sup> The first of these

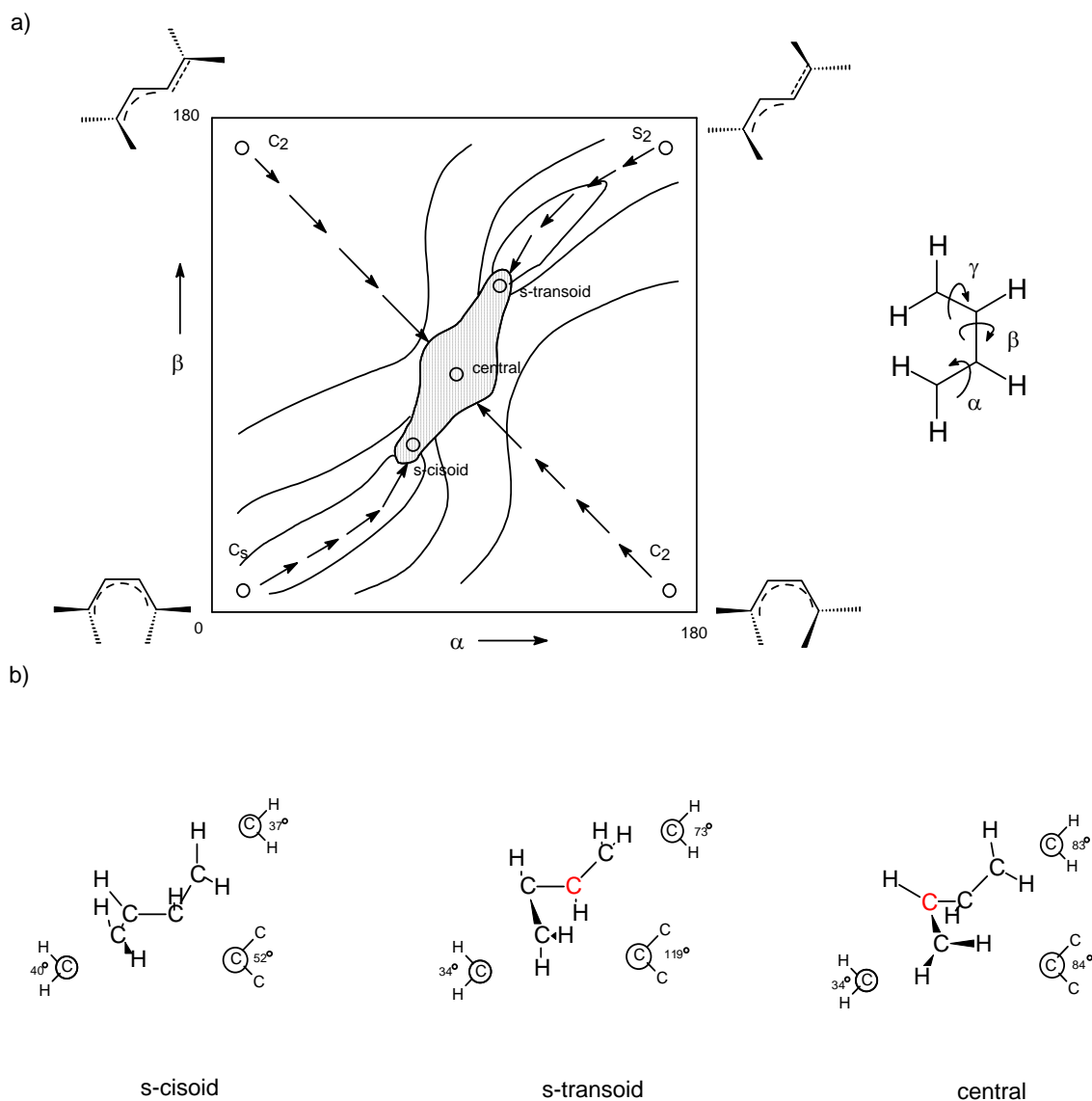


**Figure 1.27** The skeletal movement of excited 1,3-butadiene and minima on the conical intersection surface.

routes travels through an s-transoid minimum, laying only 3.2 kcal/mol below the B state's s-trans minimum. It is reached immediately after a disrotatory rotation of the terminal methylenes accompanied by central bond rotation of the s-trans conformer.

The s-cisoid minimum, laying 3.7 kcal/mol above the excited minimum, was reached in a fashion similar to that of the s-transoid, i.e. via a disrotatory motion of the s-cis conformer.

The centraloid point, laying 6 kcal/mol above the minimum, was reached by a conrotatory motion of either of the conformers, with  $\sim 90^\circ$  rotation around the double bonds.

The changes of the 1,3-butadiene's skeleton during the "three carbon kink" involved the development of a triangular substructure, where the behavior of the central C atom was consistent with that in the HT mechanism observed in the photolysis of pre-vitamin D<sup>61</sup> and all-trans-1,3,5,7-tetraene (OT).<sup>62</sup>

The potential energy surface was computed for the 1,3-butadiene's photochemistry (Figure 1.28).<sup>122</sup> The plot showed that the disrotatory path was barrierless, while the conrotatory path had a barrier of 7 kcal/mol. From here, it was concluded that the system would relax through the conical intersection along the disrotatory coordinate. This was in perfect agreement with the experimentally preferred disrotatory electrocyclic closure.

The efficiency of a photochemical

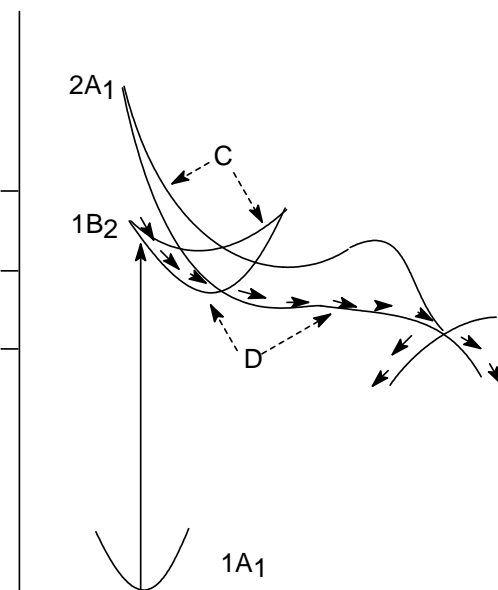


**Figure 1.28** Disrotatory (D) and conrotatory (C) computed minimal energy paths from Frank-Condon region to the  $2A_1/1A_1$  conical intersection involved in the photochemistry of 1,3-butadiene.

reaction<sup>123</sup> could be affected by the likelihood of different trajectories on the excited state surface, creating a path that is near the energetically preferred ground state. Steric effects could also block or alter certain pathways to the ground state, making other reaction routes more energy efficient, and thus favored.

Computational calculations showed that the butadiene's electronic structure of the conical intersection is that of a quasi-tetraradical<sup>124,125,126</sup> where four unpaired electrons are virtually isolated on the four carbon atoms of the molecule's framework. When the decay occurs, the four  $\pi$  electrons would be unpaired. From there, the moving force, leading the system along the ground state valleys, will be provided by the different electron recoupling and bond forming.

Robb and Olivucci extended their work on the involvement of conical intersections in diene photochemistry by addressing the photochemistry of several acyclic 1,3-dienes. In particular they focused their efforts on two experimental results from our group. The first of these involved the photochemistry of matrix isolated 2,3-dimethyl-1,3-butadiene. We were able to observe the relative rates of electrocyclic closure and double bond isomerization of the *s-cis* conformer of this molecule and also to compare the relative efficiencies of double bond isomerization of both the *s-cis* and the *s-trans* conformers.<sup>57,138</sup> We were able to observe these photochemical events because, unlike 1,3-butadiene, 2-methyl-1,3-butadiene or *cis* and *trans* 1,3-pentadiene, the photochemical conversion of the single bond conformers was very slow. It was mostly this issue that was addressed by Robb and Olivucci. They found that rotation of the central bond of 2,3-dimethyl-1,3-butadiene was unlikely to occur on the pathway to or within the conical intersection because the moment

of inertia of this bond had been increased by the methyl substituents. This inertia argument also explained why the per deuterio-2,3-dimethyl-1,3-butadiene had almost a negligible photochemical *s-cis* - *s-trans* isomerization.

The second set of experimental results from our group that was examined computationally by Robb and Olivucci has been previously mentioned. It involves the high photoregioselectivity of double bond isomerization of 1,3-pentadiene. Squillacote and Semple observed a greater than twenty to one preference for photoisomerization of the unsubstituted bond of *cis*-1-deutero-*trans*-1,3-pentadiene and explained this selectivity by an excited state pathway involving allyl cation-methylene anion zwitterions.<sup>ref</sup> Robb and Olivucci explained this photoregioselectivity on the basis of a difference in the moment of inertia of rotating about the methyl vs deuterium substituted double bond. Their calculations suggested that the heavier methyl group caused a moment of inertia for double bond rotation 35 times larger than that of the unsubstituted double bond. As in their explanation for the slow *s-cis* - *s-trans* photoisomerization of 2,3-dimethyl-1,3-butadiene, they believe mass effects were the controlling factor in the regioselectivity of the photochemical double bond isomerization of *trans*-1,3-pentadiene.

It needs to be noted here, that the computed minima within the conical intersections of dienes were asymmetrical, since the “carbon kink” could occur on either carbon 2 or 3. This meant that the isomerization would occur via two non-identical conical intersections with unsymmetrical dienes, such as 1,3-pentadiene.<sup>127,128,129,130,131,132</sup> The possibility of competing conical intersections was not commented on in these papers, but was discussed in this group’s later publications.

#### 1.1.3.4. Competitive conical intersections

Competing conical intersections could explain the preferential photoregioselectivity in some photoisomerization reactions. For example, calculations of the photochemistry of 2-cyano-1,3-butadiene, indicated a conical intersection with center of the kink at the C atom substituted with the CN group, instead of the unsubstituted carbon.<sup>121</sup> The high quantum yield of bicyclobutane in this molecule was explained by these calculations.

In 1997, Olivucci et al. calculated the mechanism of photochemical isomerization of all-*trans*-hepta-2,4,6-trienium cation (*t*-HTE). Their calculations indicated a possible trans-cis isomerization at the double bond in positions 2 or 4 (**Figure 1.29**).<sup>133</sup>

The presence of two minimum energy paths (MEPs), accounting for the photochemical isomerization, were reported. The MEPs started with a decay along a symmetric C=C double bond stretching mode (region I). Then an asymmetric twisting mode (region II) followed, which eventually ended in a “slide” into a conical intersection. The calculations suggested that the C<sub>2</sub>-C<sub>3</sub> and C<sub>4</sub>-C<sub>5</sub> isomerizations occurred in a barrierless fashion, with slightly different energy differences along the plateau region. However, because the C<sub>2</sub>-C<sub>3</sub> conical intersection was calculated with a lower energy, they concluded the photochemical isomerization around this bond to be favorable. (**Figure 1.30**)<sup>133</sup>

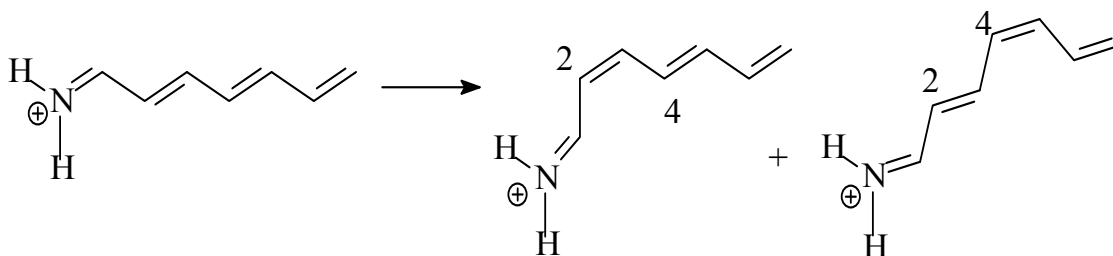


**Figure 1.29** The photoisomerization of *t*-HTE.

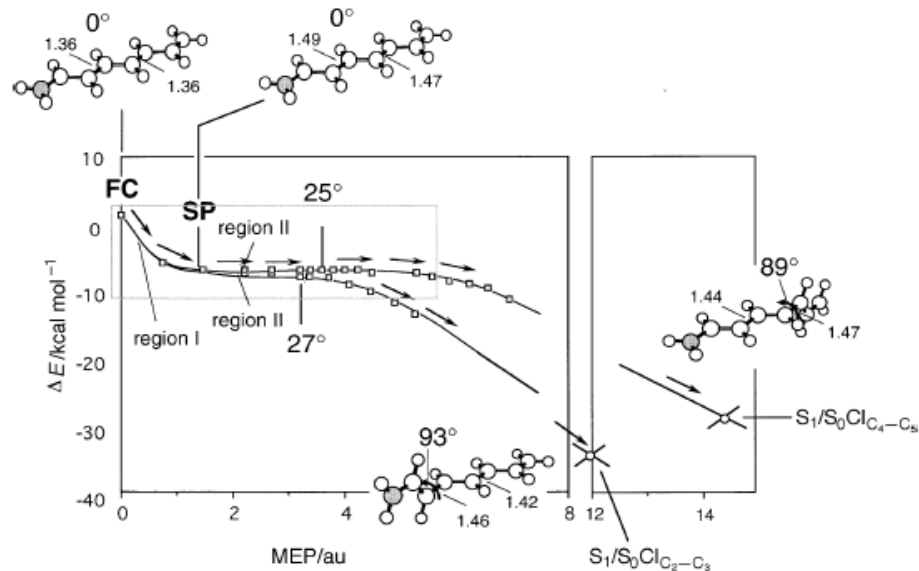


**Figure 1.30** Energy profiles along the MEPs describing the competing excited isomerization paths from the Franck-Condon point to the decay points  $S_1/S_0$  CI<sub>C<sub>2</sub>-C<sub>3</sub></sub> and  $S_1/S_0$  CI<sub>C<sub>4</sub>-C<sub>5</sub></sub> of t-HTE.

#### 1.1.4. Dynamic effects

All-*trans*-octa-1,3,5,7-tetraene and longer polyenes have been found to fluoresce from their first excited state ( $S_1$ ) with a lifetime of several nanoseconds. The short polyenes 1,3-butadiene and 1,3,5-hexatriene were found to have little to no fluorescence yield,<sup>102,105</sup> with very diffused absorption spectra even at low temperatures.<sup>113,114</sup> This longer lifetime of the  $S_1$  state for big all-*trans* polyene molecules (8 carbon atom skeleton or larger), is controlled by barriers on the excited states surfaces.<sup>134</sup> In 1993, Kohler and coworkers were the first to experimentally record the fluorescence lifetime of all-*trans* OT as a function of temperature.<sup>103</sup> They determined that at temperatures above 200K, there is a drastic shortening of the fluorescence lifetime. This was explained by the opening of a thermally



activated, very efficient and radiationless decay channel, with an energy barrier of approximately 4.3 kcal/mol. Later, Petek<sup>104</sup> reported the results of his studies for octatetraene. He measured the fluorescence decay rate of  $S_1$  in free jet expansion, as a function of the excitation energy. They determined that the radiationless decay channel was opened up at approximately 6 kcal/mol. In 1997, Garavelli<sup>134</sup> et al. reported the results of their studies of all-*trans*-1,3,5-hexatriene. They found that the excited state route has negligibly small barrier which leads to a very fast (sub picosecond) decay down to the ground state. For 1,3-butadiene, the barrier was calculated to disappear completely,<sup>135</sup> making the lifetime of the excited states even shorter.

In Raman studies on isoprene<sup>106</sup> it was found that the ionic like  $1^1B_u$  state is depopulated in a very short amount of time - around 10fs, probably because of a fast internal conversion to the nearby  $2^1A_g$  state.<sup>52</sup> This short lifetime is consistent with the diffuse absorption, observed in low-temperature experiments of not only the parent, but also the substituted butadienes.<sup>46,102,113,114</sup>

Observing photoinduced relaxation<sup>136</sup> experiments became possible with the development of ultrashort laser pulses. Farmanra et al.<sup>110</sup> reported the  $S_1$  lifetime of ethylene as less than 30fs. Later,<sup>104</sup> it was published that for *s-trans*-butadiene, the time for internal conversion was approximately 110fs. This result was very consistent with the time-dependent wave-packet results,<sup>112</sup> where it was determined that *s-trans*-1,3-butadiene underwent an ultrafast (30fs), radiationless decay from optically bright  $1B_u$  state into dark  $2A_g$  state.

The surface state dynamics could be affected not only by barriers but also by the surface's own shape. In their work Robb and coworkers reported three classes of ultrafast

reactions. Characterized and plotted using different excited-state dynamics, they were represented by the 2-*cis*-penta-2,4-dieniminium cation (2-*cis*-C<sub>5</sub>H<sub>6</sub>NH<sub>2</sub><sup>+</sup>), all *trans*-hexa-1,3,5-triene (all-*trans*-HT)<sup>134</sup> and cyclohexa-1,3-diene (CHD)<sup>137</sup> (**Figure 1.31**).

As seen in **Figure 1.31**, Robb and coworkers characterized the S<sub>1</sub> energy's surface with two domains, called region I and region II. Region I controlled the acceleration from the initially populated excited state, while region II would control the pathway leading to fast and efficient decay to the ground state through a conical intersection. During the acceleration, **Figure 1.31a** and **b**, a symmetric S<sub>1</sub> transient was developed, which then, after a symmetry distortion, led to a S<sub>1</sub>/S<sub>0</sub> conical intersection. As seen in **Figure 1.31c**, however,

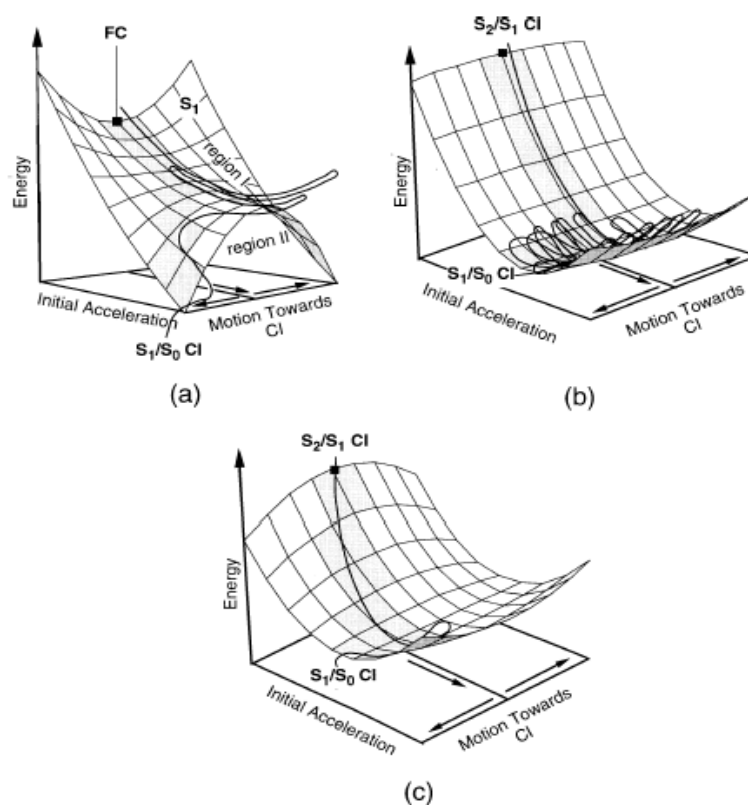


**Figure 1.31** Three classes of barrierless reaction pathways characterized by different excited state dynamics. (a) 2-*cis*-C<sub>5</sub>H<sub>6</sub>NH<sub>2</sub><sup>+</sup> (b) all-*trans*-HT (c) CHD.

the initial relaxation of CHD led towards an asymmetric  $S_1/S_0$  conical intersection in more direct fashion.

### 1.1.5. Substituent effects

As mentioned earlier, Wald<sup>3</sup> was the first to talk about the importance of steric effects in the retinal's photochemistry. Later, this was confirmed by a large amount of experimentally obtained data.<sup>4,74,5,6</sup> In their studies, Robb and coworkers were interested in the non-bonded interaction between  $\alpha$ -methyl group and spatially close  $\delta$  hydrogen of 2-*cis*- $C_5H_6NH_2^+$  and  $\alpha$ -methyl-2-*cis*- $C_5H_6NH_2^+$  (**Figure 1.32**).<sup>64</sup> What he observed was a sharp descent (up to 1.5 a.u.) in the  $S_1$  energy surface' region of the  $\alpha$ -methyl-derivative of

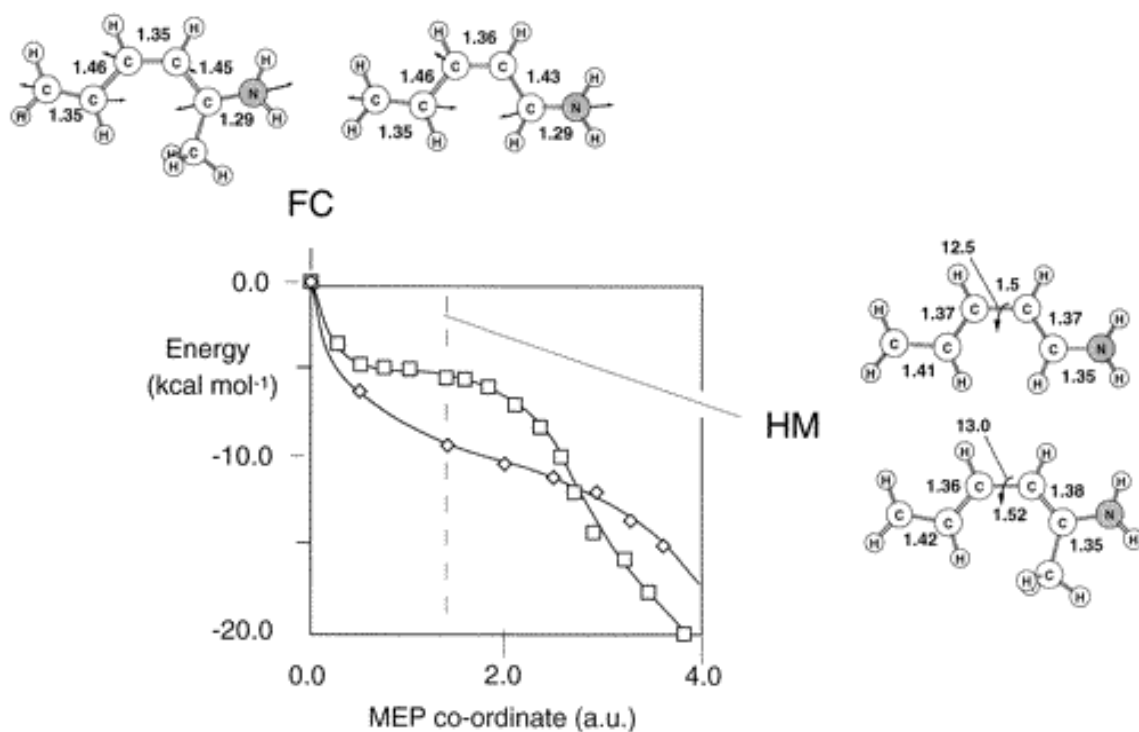


**Figure 1.32** Comparison of the molecular structures, energy gradient, and  $S_1$  initial MEPs for *cis*- $C_5H_6NH_2^+$  (open squares) and  $\alpha$ -methyl *cis*- $C_5H_6NH_2^+$  (open diamonds). The structures at 1.5 au from the Franck-Condon point are indicated by the label HM.

2-*cis*-C<sub>5</sub>H<sub>6</sub>NH<sub>2</sub><sup>+</sup>. This result meant that the methyl group played a major role in the acceleration of the initial double-bond expansion mode.

### 1.1.6. Molecules of past and current interest

What plays the most significant role in determining the photoregioselectivity in the isomerization of an 1,3-acyclic diene? If the pathway goes through a zwitterionic type of intermediate, with some charge separation occurring, then charge stabilizing effects from the substituents attached to the double bonds would be significant. As seen from **Figure 1.33**, if X stabilizes + and Y stabilizes - charges, and if, as calculations suggest, that the allyl cation- methylene anion type of zwitterion is favored, then photoisomerization should occur about the double bond with the Y substituent.

In conical intersections, however, there is no charge separation occurring, raising the question of what would control the photoregioselectivity if this pathway is traversed? It has been suggested that the regioselectivity is controlled simply by the mass of X and Y. The heavier the X, the harder it would be to rotate the bond it is attached to, so isomerization around the double bond bearing the lighter Y substituent would be expected.

So there are two very different ideas about what controls the photoregioselectivity of dienes:

1. During a photoisomerization of an asymmetric acyclic 1,3-dienes through a zwitterionic like species, a charge separation will occur and the charge stabilizing properties of the substituents will play a significant role in determining the regioselectivity.
2. During a photoisomerization of an asymmetric acyclic 1,3-dienes through a conical intersection, the mass of the substituents will control the regioselectivity of isomerization.

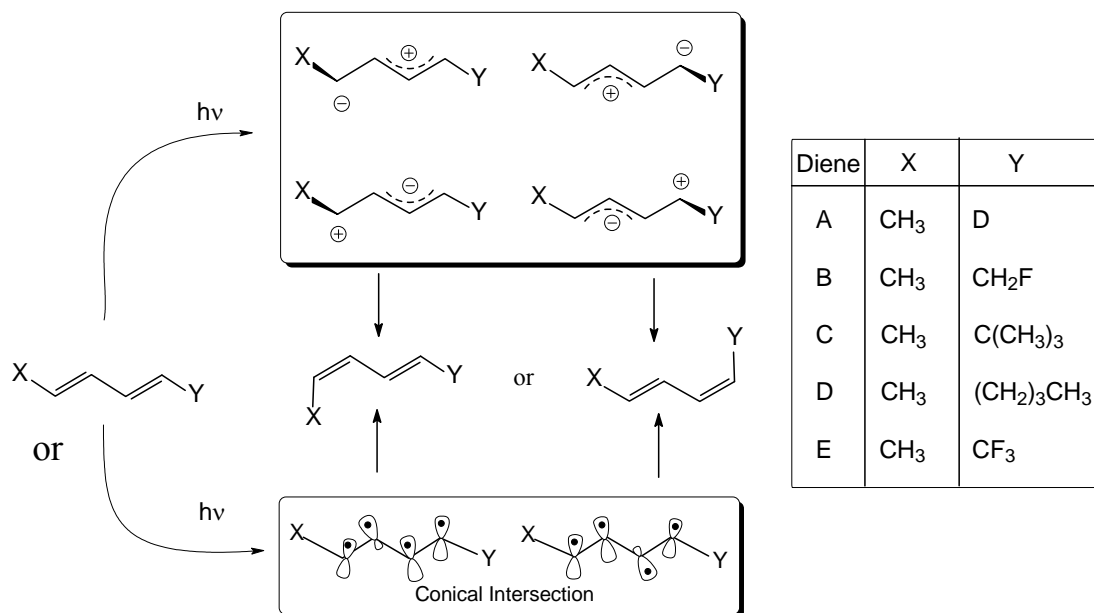


**Figure 1.33** Acyclic 1,3-dienes as models for the photoisomerization of retinal.

As noted before, in previous studies in our lab, Squillacote and Semple<sup>138</sup> investigated the photochemistry of *cis*-1-deuterio-*trans*-1,3-pentadiene (**Figure 1.33** diene A), to search for a rationale behind the regioselectivity of double bond photoisomerization in polyenes.

As seen from the NMR spectrum (**Figure 1.34**), after 2 minutes of irradiation time, about 25% of the deuterium substituted double bond has isomerized, while the double bond bearing the methyl group does not show any signs of rotation, i.e. lack of H<sub>c</sub>' peak formation. Given the signal to noise ratio of this spectrum, a preference for photoisomerization of the deuterium substituted double bond of at least 20-fold could be estimated. However, it is important to note that due to the overlap of H<sub>b</sub> peak of *trans*-1,3-pentadiene and the H<sub>a</sub>' peak of *cis*-1,3-pentadiene an accurate integration could not be obtained. After 30 minutes of irradiation at 0°C, the appearance of a triplet of triplets band for H<sub>c</sub>' of the *cis* isomer becomes apparent, as well as a complete photon equilibration of the deuterium substituted

bond. After 8h of photolysis, the photostationary state was reached.

If the *trans*-1,3-pentadiene went through a zwitterion photochemical isomerization, the  $Z_{1A}$  form (**Figure 1.19**) would be expected to be the lowest in energy, because the methyl group will stabilize the development of a positive charge, through a positive inductive effect, compared to the deuterium. This means that the double bearing the deuterium will rotate preferentially.

However this result has also been explained using a conical intersection mechanism.<sup>138,</sup>

<sup>158</sup> As mentioned previously, the calculation predicted preferential rotation around the double

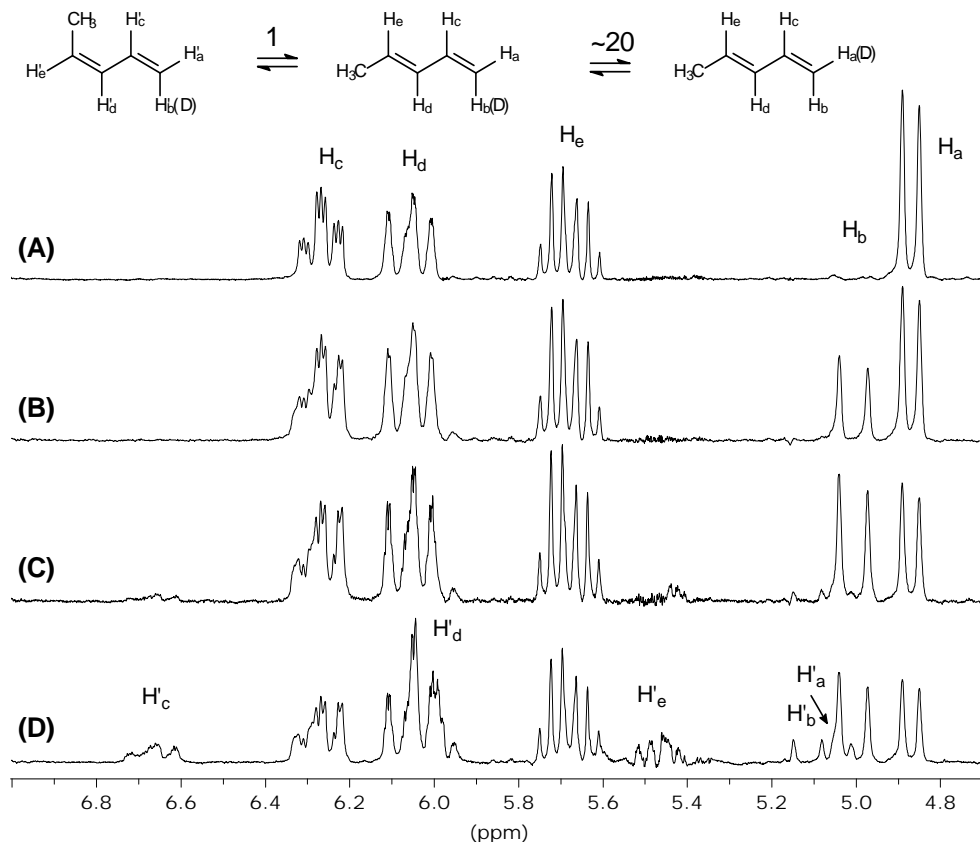


**Figure 1.34** 250-MHz <sup>1</sup>H NMR of a 1% solution in diethylether of (A) *cis*-1-deutero-*trans*-1,3-pentadiene; (B) after 2 min of photolysis with a 1000W Hg(Xe) arc lamp at 0°C; (C) after 30 min and (D) after 8 h of photolysis.

bond bearing the lighter of the two substituents. Therefore *cis*-1-deuterio-*trans*-1,3-pentadiene does not delineate between the two mechanisms. This required the employment of a substituted, unsymmetrical and acyclic 1,3-diene with two substituents which vary in both mass and charge stabilizing effects.

Squillacote et. al.<sup>139</sup> turned their attention (**Figure 1.35**) the photochemistry of the mono-fluoro methyl substituted EE-1-fluoro-2,4-hexadiene (EE-FHD) (Diene B in **Figure 1.33**).<sup>139</sup>

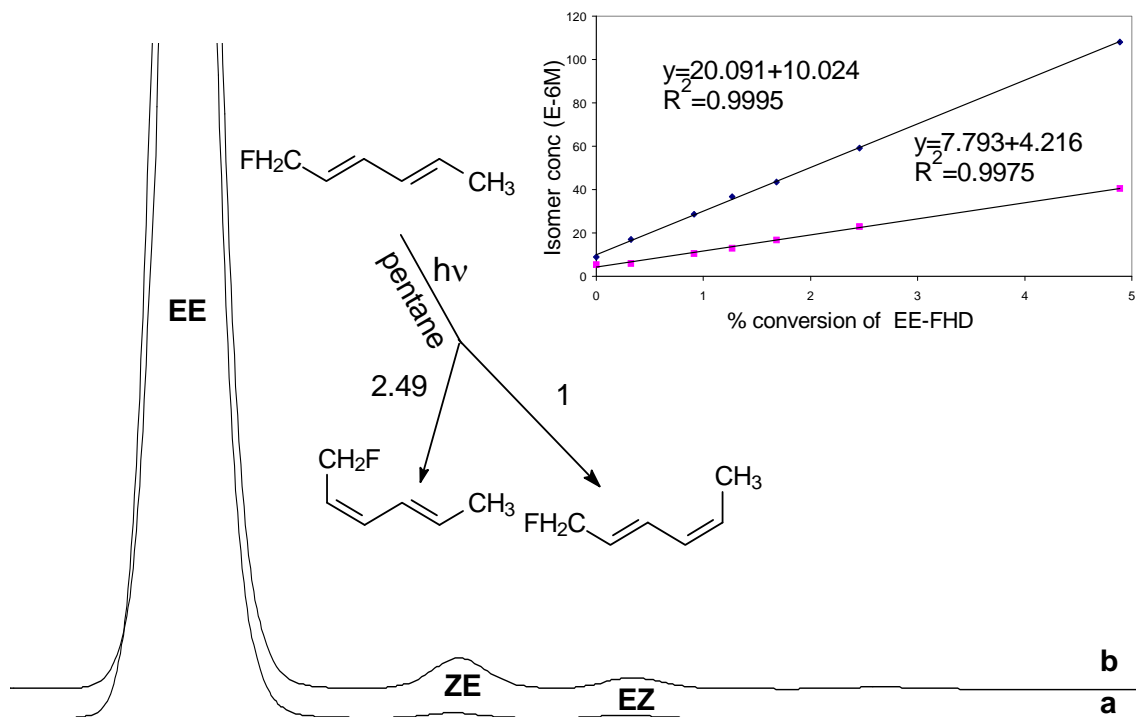


**Figure 1.35** Photoisomerization of a 3.2M pentane solution of EE-FHD a) before irradiation b) after 60 sec of irradiation with 245nm light and at RT.

When photolyzed in 100% pentane, a non polar solvent, the EE-1-fluoro-2,4-hexadiene exhibited a 2.5:1 preferential rotation around the monofluoromethyl substituted double bond. Thus the observed preferential rotation fit the zwitterionic mechanism for isomerization. As the monofluoromethyl group was also the heavier group, this result did not fit a simple conical intersection pathway, i.e. the charge stabilizing effect of the substituent had a greater effect on the photoregioselectivity of isomerization than the substituent's mass.

However, there are two other aspects of importance in the photoisomerization of the EE-FHD. The initial experiment was conducted in the non polar solvent pentane, and two isomers are produced upon photoisomerization in a nonpolar solvent, the regioselectivity of isomerization should depend on the energy difference of the excited states. For instance the two allyl cation methylene anion zwitterionic states shown at the top in **Figure 1.33** would be expected to have different energies based on the different charge stabilizing characteristics of substituents X and Y. Presumably the ratio of the photoproducts would reflect the charge stabilizing characteristics. If a more polar solvent is used for the photochemistry it would mitigate the importance of the charge stabilizing effects of the substituents. So if a zwitterionic pathway is followed, the two zwitterions will be closer in energy in a more polar solvent and the photoregioselectivity should decrease (**Figure 1.36 top**). To investigate the solvent effect on this molecule, Squillacote et al.<sup>157</sup> conducted a series of experiments where the polarity of the solvent was gradually increased by mixing nonpolar hexane and polar propionitrile.



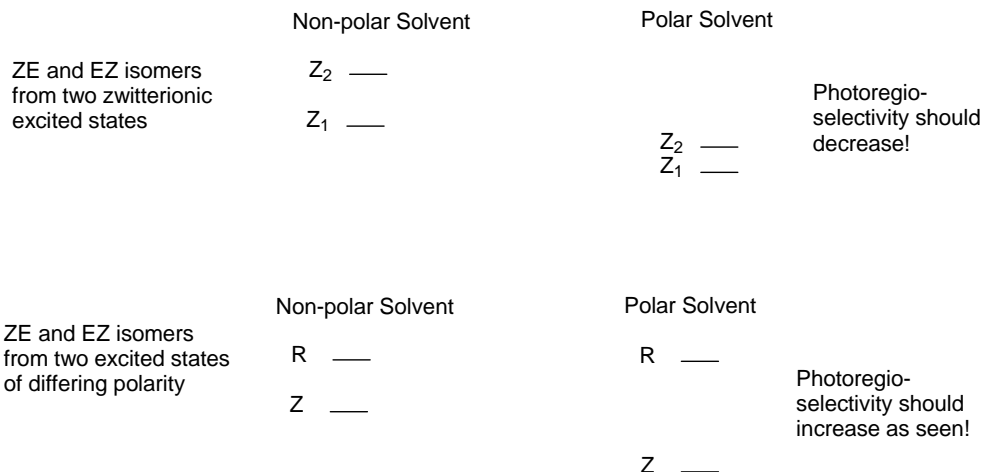


**Figure 1.36** Solvent effect on the photoregioselectivity.

The experimental results showed that with increasing polarity of the solvent, the regioselectivity of the photoisomerization increased rather than decreased. Further, this increase exactly mirrors (**Figure 1.37**) the change in polarity of the solvent mixture as measured by the solvent's  $E_t$  value.<sup>156</sup> It therefore seems unlikely that a competition between two pathways involving two different fully developed zwitterions is occurring.

The observed solvent effect on the photoregioselectivity of FHD is consistent with a computation between two pathways which differ in the amount of charge developed. If the two pathways have different polarities, the more polar pathway represented by Z in

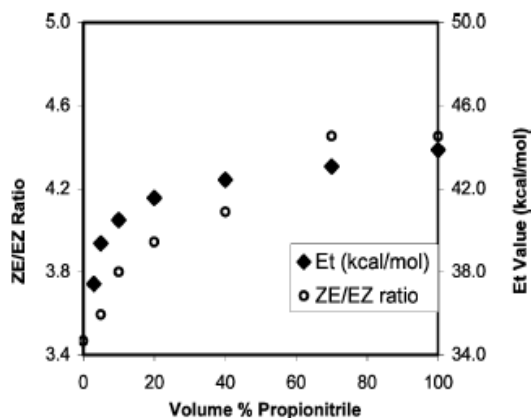


**Figure 1.37** Solvent effect studies of the photoisomerization of 1-fluoro-2,4-hexadiene

**Figure 1.36** will be more stabilized by a polar solvent than the less polar pathway, R, and the photoregioselectivity would be expected to increase. However, this system certainly shows a charge effect that is not consistent with a simple conical intersection picture. An amalgam of the two mechanism seems necessary, one that can explain the observed short lifetimes of the dienes'  $S_1$  state as well as the observed solvent effect on the photoregioselectivity (**Figure 1.38**).

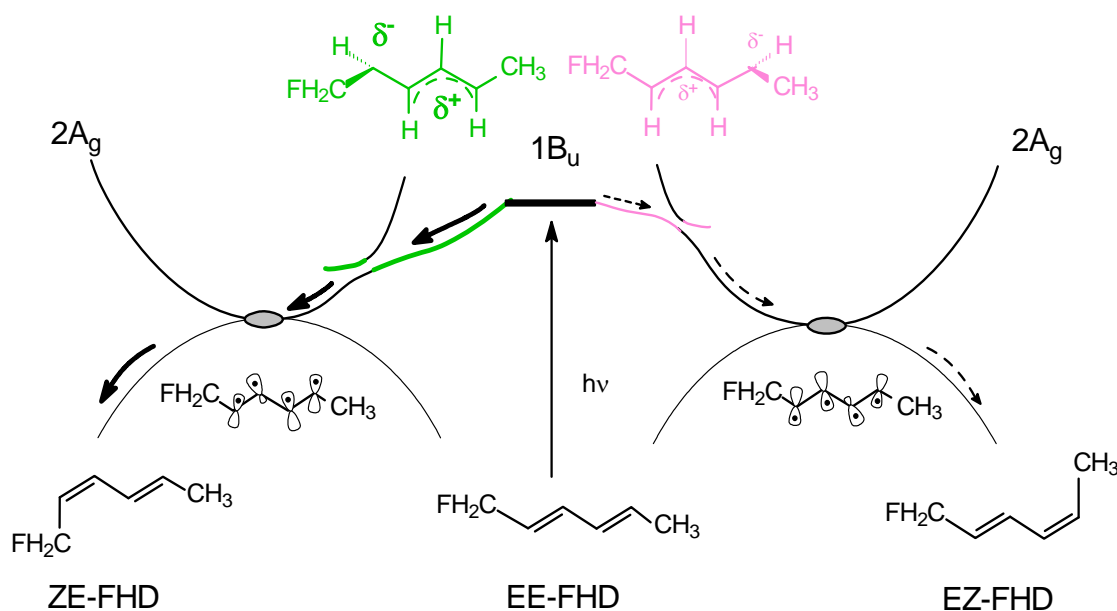


**Figure 1.38** Proposed pathway from  $1^1B_u$  state showing differing polarizations and leading to two different conical intersections.

As mentioned earlier the lack of symmetry of the conical intersections demands that two separate conical intersections would exist for unsymmetrical 1,3-dienes. Thus from the Franck-Condon region of the initially obtained  $1^1B_u$  state a bifurcation into two pathways leading to the two conical intersections must occur. It is known that the  $1^1B_u$  state has ionic

character<sup>140</sup> as well as a short life time<sup>111,112,141,142</sup> but the two pathways, leading from the Frank-Condon area of the  $1^1B_u$  state, would not be expected to have the same polarization. A pathway leading to the ZE-FHD conical intersection is expected to be more polarized because of the matching of the polarization and the charge stabilization properties of the substituents. On the other hand a mismatch of the charge stabilizing effects of the substituents and the character of an allyl cation - methylene anion polarization would create a pathway to the EZ-FHD conical intersection that is less polarized. In a polar solvent the more polarized pathway would be more stabilized and an increase in photoregioselectivity would result. Thus an interplay of charge effects and dynamics on the potential surface controls the rotational preference. This hybrid model explains the short diene excitation state lifetimes as well as the observed solvent effects. This model may also explain the relative small value of the EE-FHD photoregioselectivity (3:1), especially when compared to the 20:1 ratio observed with the mono-deutero substituted diene.

#### **1.1.7. This work**

In this work we decided to investigate the steric, inertia and charge stabilizing effects on the photoisomerization of series of acyclic 1,3-dienes (**Figure 1.39**) in different polarity environments.

We will examine the photochemistry of 6,6-dimethyl-2,4-heptadiene (DMH) and 2,4-nonadiene (ND). Both molecules are unsymmetrically substituted with groups which exhibit almost the same charge stabilizing effect, yet have substantially different masses. The molecule ND will be investigated as the n-butyl group may “experience” a higher resistance from the solvents due to its increased length as compared to the t-butyl group in the DMH.

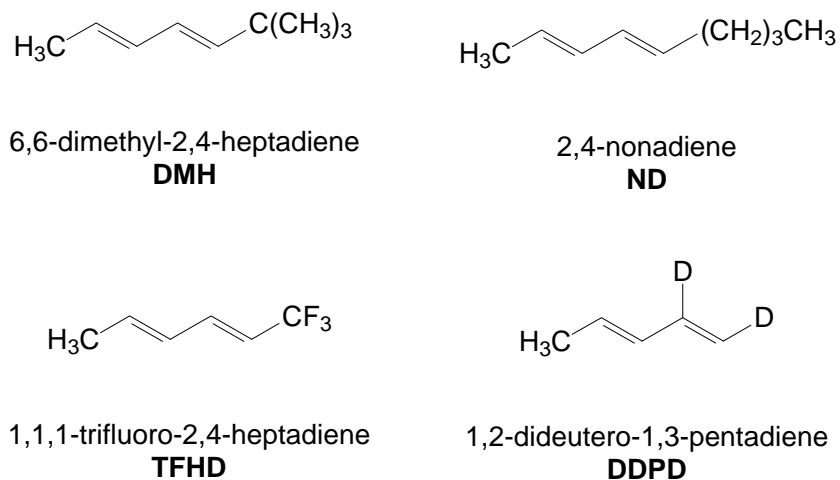


**Figure 1.39** Molecules of interest in this work.

We will synthesize and photoisomerize a trifluoromethyl substituted diene, i.e the 1,1,1-trifluoro-2,4-hexadiene, TFHD. This molecule is of interest because of the increased negative charge stabilizing effects and mass of the trifluoro group as compared to the monofluoro substituent of FHD. The solvent effect of all of these dienes will be investigated to examine the polarity differences of the pathways leading to the two diene isomers initially produced.

In addition, we will describe efforts to synthesize 1,2-dideutero-1,3-pentadiene (DDPD). Reinvestigating this system is necessary in order to more accurately determine the photochemistry of 1,3-pentadiene and to examine the solvent effect on the photoisomerization of this molecule.

## **1.2. Experimental**

### **1.2.1. Instrumentation and equipment used**

All spectral and chromatographic data were collected with the following unmodified instruments: Bruker Avance-250 NMR, Bruker Avance-400 NMR, Shimadzu GC-14A gas chromatograph equipped with a FID detector and Shimadzu Ezchrom software, GOW-MAC series 580 and series 350 gas chromatographs with TCD for preparative GC.

### **1.2.2. Materials Used: purification and preparation**

#### **1.2.2.1. Purification of solvents and reagents**

All reagents and solvents employed were of research, analytical or higher grade. They were obtained from SigmaAldrich, Wiley Organic, Fisher (Acros), VWR or Cambridge Isotope Laboratory and used without further purification, unless otherwise noted. For photochemical and spectroscopic studies, HPLC grade solvents, including hexane, were purchased from Aldrich and Fisher and showed no absorbance above 210 nm. Propionitrile of analytical grade was purchased from Aldrich and further purified as described in 2.2.1.2.

##### **1.2.2.1.1. Preparation and Conditioning of Drying Agents**

Molecular sieves (3A) were baked in ceramic oven at 220° C. Magnesium sulfate, sodium sulfate, sodium bicarbonate were dried in a vacuum oven at 120°C for at least 24 hours prior to use.

##### **1.2.2.1.2. Purification of Propionitrile<sup>143,144</sup>**

Propionitrile was refluxed over 1.5g (for every 100 mL of solvent) of anhydrous AlCl<sub>3</sub> for one hour. After a rapid distillation, the solvent was then refluxed for an hour over a mix of 1g of K<sub>2</sub>MnO<sub>4</sub> and 1g Li<sub>2</sub>CO<sub>3</sub> per 100 mL. After another rapid distillation, the

propionitrile was refluxed over  $\text{NaHSO}_4$  for additional hour. It was then distilled again. The collected solvent was then dried over  $\text{CaH}_2$  and refluxed for one more hour. A fractional distillation using a Vigreux column was performed and the propionitrile distilled. After every purification, a UV-VIS spectrum was obtained to determine the presence of any impurity leftovers, absorbing above the 245nm mark (**Figure 1.40**).

In the processes of multiple distillations, about 20% of the solvent was lost. The final fraction was stored under dry 3 Å molecular sieves. Prior every use, each amount of propionitrile was passed through  $\text{CaH}_2$  to quench both residual water and possible

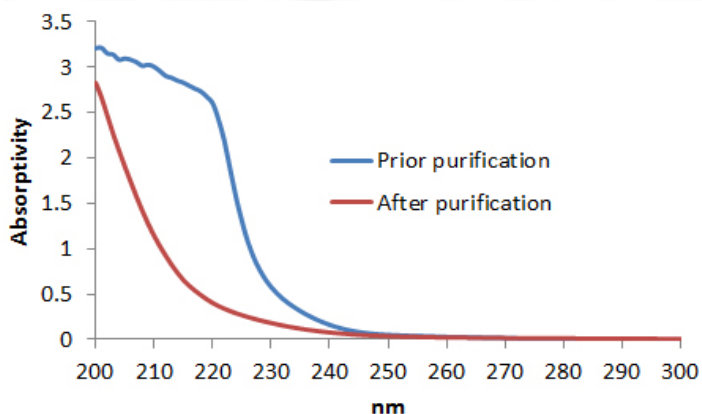


**Figure 1.40** UV-VIS spectrum of propionitrile before and after purification

acidic traces coming from the sieves. The UV/VIS spectrum of propionitrile stored under these conditions for many months showed no change in absorption.

#### 1.2.2.1.3. Purification of HPLC grade hexane

Small impurities in the HPLC grade hexane were removed by preparatory GC on Gow Mac 350 Series using an Alltech 30'×1/4" column packed with Chromosorb NAW coated with 30% OV-17 column using the following settings: Injector= 120; Detector= 120 and Column=100 with flow of  $\text{N}_2$  gas carrier of 60 ml/min. A fresh batch of solvent was purified via multiple 45  $\mu\text{L}$  injections prior to every photolysis.

#### **1.2.2.1.4. Purification of Acetonitrile<sup>145</sup>**

Acetonitrile was purified by sequential reflux and distillation from phosphoric oxide. It was then distilled from potassium carbonate and stored over 3 Å molecular sieves.

#### **1.2.2.1.5. Purification of Chloroform-d<sub>3</sub>**

Chloroform-d<sub>3</sub> was stored in its original container but over 3 Å molecular sieves for dryness.

#### **1.2.2.1.6. Purification of Tetrahydrofuran (THF)**

Pieces were freshly cut from bulk sodium metal, stored under oil, and rinsed with dry THF. The pieces were then added to the flask with THF, along with ~60 mg benzophenone. The solvent was then refluxed overnight until the appearance of the blue benzophenone ketylradical. Dry THF was freshly distilled from this solution prior to every synthesis.

#### **1.2.2.1.7. Purification of Methylene Chloride and Ether**

Dry di-ethyl ether and methylene chloride were obtained by employing an M-Brown solvent purification system.

#### **1.2.2.1.8. Purification of Pyridine**

Stock pyridine was refluxed over molecule sieves and KOH pellets for two hours, followed by fractional distillation and then stored over NaOH pellets for at least 48 hours before use.

#### **1.2.2.1.9. Purification of p-toluenesulfonyl chloride (p-TosCl)**

P-toluenesulfonyl chloride (10g) was dissolved in minimum amount of chloroform in a flask. The solution was then rinsed with a 1/1 mixture of pentane and hexane to precipitate the impurities. The precipitate was then removed with filtration. The solution of pure p-

toluenesulfonyl chloride was clarified with Norit and the solvent was removed under vacuum. Approximately 8g of pure p-TosCl was obtained for every initial 10g.

#### **1.2.4. Synthesis and Purification of 6,6-Dimethyl-2,4-heptadiene (DMH)**

##### **1.2.4.1. Procedure A**

###### **1.2.4.1.1. Preparation of Phenyl Lithium**

A solution of 0.1 mol of PhBr (15.847g) in 50ml of dry ether was prepared and transferred with cannula into a flame-dried 3 neck round bottom flask. The flask was equipped with a magnetic stir bar, reflux condenser topped with a oil bubbler and two rubber septa. The apparatus was continuously purged with Ar gas (UHP 300 Ar – Airgas UN1006). A two molar excess of Li (6.941 g; ~30 cm of lithium wire with 45 mg/cm) was rinsed with dry diethyl ether to remove the oil it was stored in. After cutting it into small pieces and exposing fresh metallic surface, the Li was transferred into the PhBr solution.

If the experiment setup was maintained moisture free, the reaction would start immediately. Because it is exothermic, the reaction caused the ether to reflux. After the ether reflux diminished, the reaction was stirred for an additional 30 minutes.

If the experiment setup was not maintained moisture free, an oxide layer is formed on the metal's surface, which hinders the reaction's initiation. To fix the problem the following steps were taken:

1. A long needle attached to an airtight syringe was used to puncture fresh cuts in the metal's surface. If this did not help a more invasive approach was used;
2. The Argon gas flow was increased and one of the necks of the round-bottomed flasks opened. The oil bubbler was stoppered, ensuring the only exit for the purging gas would be



the opened neck of the round bottom flask.

3. Using clean spatula, fresh cuts of the Li wire were made. Then the neck was then sealed back with new rubber septum, the bubbler was un-stoppered and the Ar flow decreased back to normal.

After the reaction was complete, the organo-metallic product was transferred into a clean dry round bottomed flask with cannula and then sealed with two overlapping septa. The non-reacted Li pieces remaining in the reaction pot, were slowly quenched with isopropanol.

To determine the exact concentration, the phenyl lithium was titrated using 1-pyreneacetic acid (0.2 g) as indicator. The acid was dissolved, in a previously flame-dried round-bottom flask, in 10 ml of dry THF to make 0.02 M solution. An air-tight syringe, equipped with a 220 mm 18 gauge stainless steel needle, was used to measure 1 ml of our freshly made PhLi. In single-drop additions the PhLi is injected into the 1-pyreneacetic acid solution until a red coloration is stable for ~30 seconds. The molarity of the PhLi was then determined and used in the subsequent experiments.

#### **1.2.4.1.2. Neopentyl Phosphonium Iodide<sup>146,147</sup>**

A mixture of 0.058 mol neopentyl iodide (6.63 ml), 0.050 mol triphenyl phosphine (13.11g) and sulfolane (6.805ml) was prepared in flame-dried 100ml round bottom flask, equipped with a reflux magnetic stir barr, condenser and a nitrogen bubbler. The mix was then heated with oil bath to 160 °C under nitrogen atmosphere. After 24 hours the oil bath was taken away and the reaction mixture allowed to cool to room temperature. The sulfolane was vacuum distilled away using a short path distillation column. The hard white solid that formed was then broken up and ground with a mortar pestle under ethyl acetate. The

resulting powder was washed with 50 additional mL of ethyl acetate and filtered. The powder was spread in a Petrie dish and dried in a vacuum oven overnight.

#### **1.2.4.1.3. Preparation of 6,6-Dimethyl-2,4-heptadiene (DMH) via Wittig Reaction**

A three necked 100 mL round bottom flask equipped with a pressure equalizing funnel was flame dried under Argon gas atmosphere. In the round bottom flask, a slurry of neopentyl triphenyl phosphonium iodide (10 mmol) in 30 mL dry THF was prepared. A solution of phenyl lithium (10 mmol) in ether was syringed into the addition funnel and flask.

After the whole amount of phenyl lithium was added very slowly to the contents of the round bottom flask, the mixture was stirred for ten minutes and then cooled to -70 °C. The solution turned a clear red. Using air tight syringe, crotonaldehyde (20 mmol) in 10 mL dry THF was added dropwise and stirred vigorously. The temperature was raised to -40 °C over a period of five minutes. The reaction was then brought to room temperature and stirred at room temperature for 0.5 h. It was then quenched with 30 mL of a mixture of water and ice. The solution was extracted with ether (3 times 30 mL). The solution was dried with MgSO<sub>4</sub> and filtered. The solvent was carefully removed with rotary evaporator. The crude product was purified by bulb to bulb distillation giving yield of ~15%.

#### **1.2.4.2. Preparation of 6,6-Dimethyl-2,4-heptadiene (DMH) via Wittig Reaction with Schlosser modification**

A setup of three neck 100ml round bottom flask, with a reflux condenser and addition funnel was flame-dried under purging Ar gas. To ensure positive flow and prevent moisture

accumulation, an oil bubbler was attached to the reflux condenser. A slurry of neopentyl triphenyl phosphonium iodide (10mmol, 4.6034 g) in 30 ml of dry THF was prepared in the 100ml round bottom flask. To the slurry was added a 10 mmol solution of phenyl lithium in 10 ml dry THF. After stirring for 10 minutes the red solution was cooled to ~ -78 °C in dry ice/acetone bath. The crotonaldehyde (10 mmol, 0.8286 ml), dissolved in 10 ml of dry THF was added dropwise and the solution was stirred vigorously for 10-15 additional minutes. After the solution decolorized, additional 11 mmol of phenyl lithium was added through the addition funnel and the temperature was brought down to -45 °C to -35 °C. A Gilman test was conducted and the solution was kept at these conditions until the test became negative. This took several hours.

**Gilman test:** Half a milliliter of a solution of 2 mg 1-pyreneacetic acid in dry THF is prepared in a flame dried round bottom flask. Using an airtight syringe, a small sample was pulled out of the reaction mixture and a single drop was suspended over the acid. If any red color appears at drop – the test is positive, indicating phenyl lithium is present in the reaction mixture.

The reaction mixture was then treated with 11 mmol (5.5 ml) solution of HCl in ether, which had been previously titrated. Then potassium tert-butoxide (15 mmol, 1.6833 g) was added. The reaction mixture was then poured over 12 ml of water and extracted two times with 15 ml of di-ethyl ether. The extract was stirred at room temperature for two hours, centrifuged, and the clear supernatant liquid was washed with water until the aqueous layer showed a neutral pH. The ether was carefully removed in vaquo and the resulted brown-yellow liquid was purified via bulb-to-bulb distillation at ~ 140 °C (yield ~ 30%).

### **1.2.4.3. Purification and Storage of Isomers**

DMH was purified using GOW-MAC series 580 preparatory gas chromatograph. The GC was equipped with Alltech 30'×1/4" column packed with Chromosorb NAW 100/120 mesh coated with 30% OV-17. The GC was set as follows: injector= 167°C; detector =168°C; column= 24°C with the lid of the oven propped open a half inch. Because of the radiant temperature from the injector port and the detector, the column indicator read 39°C. The flow was set to 50 ml/min. The retention time of the DMH (40 µL/injection) was approximately 1000 minutes. Due to the long retention time however, any small changes in the conditions, especially the temperature of the room, caused large deviations. The retention times of the dienes increased in the order: EE, ZE, EZ, ZZ. To collect, a 6mm tube, fitted with a spiral made of 2mm tubing, was submerged in liquid nitrogen and connected to the collection duct via latex tubing. After only one injection and collection, we were able to collect 95% pure EE isomer. A 99.95% purity of the desired EE-DMH was usually achieved after one additional purification of the first collection. Due to the small quantities in which the EZ was made, as well as due to the overlap with the rest of the isomers, this isomer proved more difficult to separate. It required between 4 to 5 consecutive injections in order to achieve 99.8% purity. We were never able to collect enough sample to purify ZE-DMH and investigate its photochemical isomerization.

### **1.2.4.4. Photolysis of DMH Isomers**

#### **1.2.4.4.1. Analytical Gas Chromatography Conditions**

The analytical gas chromatograph using a 30 m x .25mm column coated with a .25µm film of RTX-65 (65% diphenyl/ 35% dimethyl polysiloxane) was used to monitor the

photoisomerization, with the detector, injector, and oven temperatures at 320, 300, and 65 °C, respectively, and with a nitrogen gas (UHP300 from Airgas) carrier flow of ~10 cm/s. The four isomers of DMH were well separated. The retention times for the EE, ZE, EZ and ZZ isomers were 10.4, 11.2, 11.4, and 12.45 minutes respectively.

#### 1.2.4.4.2. Sample Preparation

The 99.5% isomerically pure diene was collected from preparative GC and was diluted with 100  $\mu$ L HPLC grade hexane or purified propionitrile. The sample was degassed with N<sub>2</sub> gas for 10-15 minutes. Then 7  $\mu$ L of the solution was transferred using an air tight syringe into each of a series of quartz capillaries, previously washed in basic solution and deionized water. The capillaries were quickly sealed using a torch and put in a micro merry-go-round-apparatus (Figure 1.43).

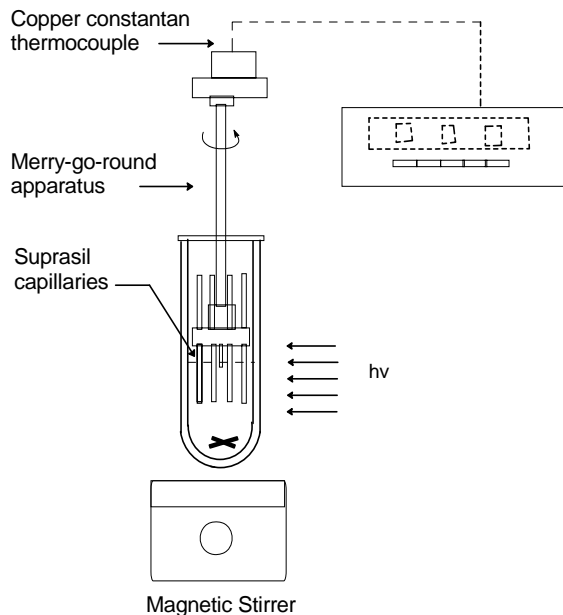


**Figure 1.41** Micro Merry-go-round apparatus

#### 1.2.4.4.3. Photolysis Conditions and setup

The micro merry-go-round-apparatus revolves at 120 rpm so that all samples were equally photolyzed. Samples were immersed in a quartz dewar in ice water (0-4 °C), making sure that the ice was not allowed to shield the samples. More ice was added every time the temperature exceeded 4° C. The irradiation source was a home-made Rayonet reactor with

six 25 Watt mercury vapor bulbs (GE-G2578). This emits light at wavelength 254 nm. At appropriate time intervals, the samples are taken out and injected into analytical GC in order to observe the photoconversion to the other isomers.

### **1.2.5. 2,4-Nonadiene (ND)**

#### **1.2.5.1. Synthesis and Purification**

##### **1.2.5.1.1. Preparation of Pentyltriphenylphosphonium Bromide**

A 500mL round bottom flask, equipped with a magnetic stir bar, reflux condenser and an oil bubbler, was flame dried under Nitrogen atmosphere. After triphenylphosphine (6 mmol; 1.574g) was dissolved in 250mL of toluene, pentylbromide (3.16 mmol; 0.477g) was added and the reaction mixture was left stirring for four days. The salt was then separated by vacuum filtration and then vacuum dried in a vacuum oven at room temperature overnight. The total yield was 100%, 2.48g, of pentyltriphenylphosphonium bromide.

##### **1.2.5.1.2. Titration of n-Butyllithium**

Before usage, the exact concentration of n-butyllithium, obtained from Aldrich-Acros, was determined through titration with pyreneacetic acid. A 50mL round bottom flask was flame-dried under nitrogen atmosphere, a magnetic stir bar was inserted and reflux condenser and an oil bubbler were attached. The pyreneacetic acid was dissolved in 5mL of dry THF and was added to the round bottom flask. The n-butyllithium was added dropwise to the solution using an air-tight syringe equipped with a 220 mm 18 gauge stainless steel needle. The addition continued until a red color persisted for ~30 sec. A total of 52 $\mu$ L of n-butyllithium was added to the solution. The calculated molarity of n-butyllithium was found to be 1.88mol/L, showing some decomposition of the original

2.17 M solution had occurred.

#### **1.2.5.1.3. Preparation of 2,4-Nonadiene (Wittig Reaction Method)<sup>148</sup>**

A three-neck round bottom flask equipped with a magnetic stir bar, reflux condenser topped with an oil bubbler, was flame-dried under nitrogen purge. After the glassware cooled to room temperature, pentyltriphenylphosphonium bromide (3.16 mmol; 0.477g) in 30mL of dry THF was added and stirred. The slurry was then cooled to 0°C with an ice bath. Using an air tight syringe, a solution of 1.88M n-butyllithium in hexanes (15.95mL) was added over a period of ten minutes. The reaction continued with the addition of crotonaldehyde (3.05 mmol) solution in 30mL of dry THF using a cannula. The reaction was refluxed for three hours, cooled to room temperature and then quenched with 10mL of ice water.

After quenching, the organic layers were extracted with three 30mL portions of di-ethyl ether washes. The organic fractions were combined and then dried over magnesium sulfate for 20 minutes. The drying agent was then filtered off and the solvent removed carefully with rotary evaporator. The residual oily product was purified by bulb-to-bulb distillation (yield 37%).

#### **1.2.5.1.4. Equilibration of 2,4-Nonadiene with Iodine<sup>149</sup>**

In order to improve the yield of the EE isomer, an equilibration was done on the crude using iodine. This equilibration decreased the amount of EZ and ZE isomers, while increasing the amount of the EE isomer. The crude was syringed into an ampule, along with one small crystal of iodine. The solution was stirred violently for several minutes vortexed and then placed in the sunlight for 24 hours. The crude was then quenched with a saturated solution of sodium thiosulfate and the organic layer was extracted from the water layer.

#### **1.2.5.1.5. Purification and Storage of Isomers**

2,4-Nonadiene was purified via preparative gas chromatography using Alltech 20' × 1/4" column packed with Chromosorb P-NAW 100/120 meshcoated with 20% OV-25. The conditions on the GC were set up as follows: detector and injector were set to 150 °C and the column to 50 °C and carrier gas flow to 50 mL/min. The retention time of the ND isomers under these conditions was approximately 800 minutes. Small changes in the conditions however could cause large changes in such long retention times. The retention times of the different ND conformers increased in the order: EE, EZ, ZE, ZZ. To collect the sample, a collection tube fitted with a spiral condenser was submerged in liquid nitrogen and connected to the detector output with silicon tubing. After two prep runs, EE and ZE-ND isomers could be obtained with a purity of 99.5% or higher.

#### **1.2.5.2. Photolysis of ND isomers**

##### **1.2.5.2.1. Analytical Gas Chromatography Conditions**

Shimadzu 14A analytical gas chromatograph equipped with a 30 m x .25mm column coated with a .25µm film of RTX-65 (65% diphenyl/ 35% dimethyl polysiloxane) was used to monitor the photoisomerization. The detector, injector, and oven temperatures were set at 320, 300, and 65 °C, respectively. The gas carrier was nitrogen gas (UHP300 from Airgas) with flow of ~10cm/s. The EE, EZ, ZE and ZZ isomers of 2,4-nonadiene were well separated showing retention times of 9.5, 9.8, 10.1 and 10.5 minutes respectively.

##### **1.2.5.2.2. Sample Preparation**

The 99.5% isomerically pure diene was collected from preparative GC and was diluted with 70 µL HPLC grade hexane or purified propionitrile. Each of the samples were placed



in a quartz tube with a silicon septum and degassed for fifteen minutes prior to photolysis. During photolysis an Ar filled balloon, sealed to a needle, was inserted through the septum into the quartz vessel to prevent the introduction of oxygen.

#### **1.2.5.2.3. Photolysis conditions and setup**

Samples were immersed in a quartz dewar in ice water (0-4 °C), while making sure that no ice shielded the samples. The irradiation source was a home-made Rayonet reactor with six 25 Watt mercury vapor bulbs (GE-G2578). This emits light at wavelength 254 nm. At appropriate time intervals, the samples are taken out and injected into analytical GC in order to observe the photoconversion to the other isomers.

#### **1.2.6. 1,1,1-trifluoro-2,4-hexadiene (TFHD)**

##### **1.2.6.1. Synthesis of 1,1,1-trifluoro-2,4-hexadiene**

###### **1.2.6.1.1. Synthesis of 1,1,1-trifluoro-4-hexene-2-ol**

Before the reaction, a pressure-round bottom flask was flame dried while being purged with Ar gas. All *O* – rings were greased for better seal. As a pressure breaker we used a balloon tied up to a needle and inserted into the system.

0.0269 mol (~1.55g) of 1-butene was condensed into a pressure-round bottom flask, cooled in dry ice bath, via cannula, after which 50 ml dry CH<sub>2</sub>Cl<sub>2</sub> were injected. After the solvent addition, 0.0269 mol (3.8 g) trifluoroacetaldehyde ethyl hemiacetal are injected very slowly with a syringe pump. While still being cooled in the dry ice bath, 0.0384 mol (11.35 g) of BF<sub>3</sub>·Et<sub>2</sub>O were added slowly. The reaction mixture was allowed to warm up to room temperature and stirred for 24 hours.

The reaction mixture is poured into a separatory funnel half full with ice chips. An additional 10-15 ml of  $\text{CH}_2\text{Cl}_2$  was used to rinse the the pressure round bottom flask and were added to the separatory funnel. The organic (bottom) layer is separated and then is washed 3 times with ice cold 15% HCl, followed by two washes with distilled water. The separated organic layer is then dried with  $\text{MgSO}_4$ . The dry solution was then vacuum filtered and the solvent distilled under low pressure to result in 76% yield, or 3.151g yellow oil of pure 1,1,1-trifluoro-4-hexene-2-ol.

#### **1.2.6.1.2. Preparation of Tosylate of 1,1,1-trifluoro-4-hexene-2-ol**

Before the reaction, the pyridine was dried for at least 24 hours over NaOH.

In a flame dried and  $\text{N}_2$  purged erlenmeyer flask, 0.07655 mol of TosCl (13.48g) was dissolved in approximately 50 ml ice cold pyridine followed by the slow injection of equimolar amount of the alcohol. The flask was then capped and left in the fridge overnight. The reaction was allowed to continue until no more crystallization occurred.

Once the reaction was complete, the mixture was quenched by pouring it into a beaker filled with a scoop of ice chips and the content transferred to a separatory funnel. Approximately 50 ml of  $\text{CH}_2\text{Cl}_2$  were added and the organic layer was separated. The remaining aqueous solution was rinsed four more times with additional 50 ml of  $\text{CH}_2\text{Cl}_2$  each time.

The combined organic solution was then washed twice with ice cold 15% HCl to wash away any residual pyridine, and then several times with distilled water until the remaining aqueous solutions did not show acidic litmus tests.

The resulting organic solution is then dried over  $\text{MgSO}_4$  and  $\text{Na}_2\text{SO}_4$  for 30 min. After

vacuum filtration, the  $\text{CH}_2\text{Cl}_2$  was distilled away under vacuum. The final product was produced in 60% yield, or 14.161g brown/yellow oil.

### **1.2.6.1.3. Preparation of TFHD**

The tosylate of 1,1,1-trifluoro-4-hexene-2-ol (2g; 0.006469 mol) was mixed with 40 mL of 1,8-diazabicyclo[5.4.0]-7-undecene (DBU). Immediately after the DBU addition, the round bottom flask is attached to three traps and the traps are attached to a rotary pump. The trap nearest to the pump is under liquid nitrogen while the last two were cooled in dry ice baths. After heating the mix to 60° C for 6 hrs, TFHD as a clear liquid is collected.

### **1.2.6.2. Purification and Storage of Isomers**

TFHD was prepped on the GOW-MAC series 580 and 350 GC using a 20'x1/4" 30% Alltech OV-17 non acid washed and 20'x1/4" Alltech 20% OV-210 columns. TFHD was first prepped on the OV-17 to eliminate the ZE and ZZ isomers. Using the OV-17, the injector and detector were set to 120 °C and the column was set to 32 °C . The flow was 50 +/- 1. Under these conditions we were able to collect the ZE and ZZ isomers with retention times of 52 and 58 minutes respectively. Then the OV-210 column was used to eliminate the EZ to give 99.8% pure EE. Using the OV-210, the detector and injector were set to 171 °C and the column was set to 24°C. The flow was 30 +/-1 ml/min, giving us EE peak with a retention time at approximately 186min.

### **1.2.6.3. Photolysis of TFHD**

#### **1.2.6.3.1. Analytical Gas Chromatography Conditions**

A Shimadzu 14A analytical gas chromatograph equipped with a 30 m x .25mm column coated with a .25µm film of DB-210 (50% - Trifluoropropyl) methyl polysiloxane was used

to monitor the photoisomerization. The detector, injector, and oven temperatures were set to 320, 300, and 35 °C, respectively. The gas carrier was nitrogen gas (UHP300 from Airgas) with flow of ~10cm/s. The ZE, EZ, EE and ZZ isomers of 2,4-nonadiene were well separated with retention times of 8.5, 8.75, 9.1 and 9.3 min respectively.

#### **1.2.6.3.2. Sample Preparation**

The 99.8% isomerically pure diene was collected from preparative GC and was diluted with the appropriate mixture of HPLC grade hexane and purified propionitrile. A sample of the pure diene in 100% propionitrile was prepared as well. Each of the samples were placed in a quartz tube with a silicon septum and degassed for fifteen minutes prior to photolysis. During photolysis an Ar filled balloon, sealed to a needle, was inserted in the quartz vessel to prevent the introduction of oxygen, by maintaining positive pressure.

#### **1.2.6.3.3. Photolysis conditions and setup**

Samples were immersed in a quartz dewar filled with ice water (0-4 °C), while making sure that no ice shielded the samples. The irradiation source was a home-made Rayonet reactor with six 25 Watt mercury vapor bulbs (GE-G2578). This emits light at wavelength of 254 nm. At appropriate time intervals, the samples are taken out and injected into analytical GC in order to observe the photoconversion to the other isomers.

#### **1.2.7. Synthesis of *cis*-1,2-dideuterio-*trans*-1,3-pentadiene (DDPD)**

To prepare the di-deutero substituted pentadiene, we decided to use the relatively short pathway depicted in **Figure 1.42**. All chemicals were purchased from Fisher (Acros), VWR or Cambridge Isotope Laboratory and used as is unless otherwise specified.

### 1.2.7.1. Preparation of 2-tosyl-4-yne-pentane (tosylate)

In a 200mL Erlenmeyer flask were dissolved 0.232 mol of p-TosCl (44.228g) in 50-75mL of ice cold and dry pyridine.

With a syringe 0.116mol of 4-pentyn-2-ol (10g) were then added and the solution left in the refrigerator overnight. The flask must not be agitated and the reaction is considered finished when no more crystals

are formed at the bottom of the flask.

The pyridine solution is then quenched with ice and the entire solution is then transferred in a separatory funnel. The solution is continuously kept cold with ice chips. The solution is extracted three times with methylene chloride washes. The organic solution is washed twice with 25mL of 1:1 ice-cold HCl to remove any remaining traces of pyridine. The solution is then washed with deionized water until the washes are neutral. The organic fraction is then dried for ~20 min with  $K_2CO_3$  and  $Na_2SO_4$ . Once filtered, the solvent is removed with rotary evaporator and the oily yellow tosylate stored in refrigerator. The yield for this reaction varied between 65% and 80%.

### 1.2.7.2. Preparation of 3-ene-1-pentyne (ene-yne)

In a two neck round bottom flask, equipped with stirring bar and a reflux with traps, are dissolved 0.0321 mol KOH with one spatula of Tide detergent in 10mL deionized water. Once the solution is heated to ~65°C, 0.1926mol of the tosylate were injected very slowly

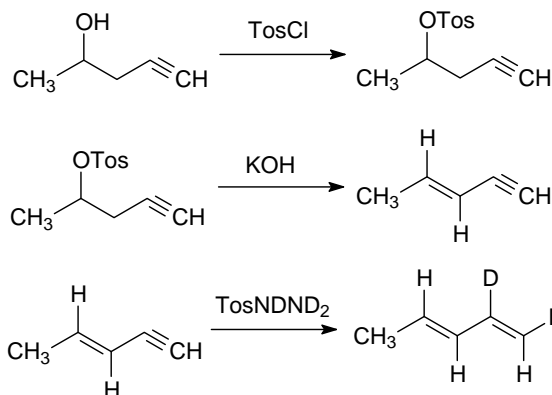


**Figure 1.42** Synthetic route for preparation of *cis*-1,2-dideutero-*trans*-1,3-pentadiene.

through the septum on the second neck of the round bottom flask. Fast addition of the tosylate resulted in the formation of large volume of soap bubbles so the tosylate was added for over an hour using a syringe pump. A teflon cannula was submerged in the reaction mixture at all times and nitrogen gas was passed through ensuring positive flow towards the trapping system, which consisted of 1<sup>st</sup> trap ice-water bath, 2<sup>nd</sup> and 3<sup>rd</sup> traps were in dry-ice bath. After the full addition of the tosylate, the reaction was allowed to proceed for several hours, until no more product was collected. The average yield for this reaction was ~80-85%.

#### **1.2.7.3. Synthesis of *cis*-1,2-dideutero-*trans*-1,3-pentadiene (DDPD)**

Prior to every synthesis, the hydrogen atoms of the hydrazide group in *p*-toluenesulfonylhydrazide (mp 108-110°C) had to be exchanged with deuterium. To accomplish this, 0.01 mol of the hydrazide were sealed in a pressure flask connected to a series of traps. Then it was washed five times with 99.9% D<sub>2</sub>O and then 2 times with 99.996%D<sub>2</sub>O. After each wash the water was pumped out. The hydrazide is barely soluble in D<sub>2</sub>O, so the exchange was facilitated by heating the slurry to 65° C. This also helped pumping out the deuterio/protio water. After all exchanges were done 0.0088mol NaAc were dissolved in 3mL D<sub>2</sub>O and syringed in, followed by 0.01mol of 3-ene-1-pentyne. The reaction was heated to 75°C overnight. The sample was then distilled out with gentle purge of nitrogen ensuring positive flow towards the collection vials. The average yield varied based on the conditions and length of the experiment 6-13%.

#### **1.2.7.4. Synthesis of DDP in quinoline solution**

The optimum conditions for this reaction were determined by reacting protio tosylhydrazide and ene-yne (1:1.1 molar ratio) in small scale reactions in NMR tubes and

monitoring the reaction progress by taking periodic  $^1\text{H}$  NMR spectra. It was determined that 72h was the optimum reaction time.

In flamed pressure flask purged with nitrogen are dissolved 0.0115 mol of tosylhydrazide (1.49g) in a minimum amount of quinoline (~7ml). The tube was sealed with a septum and topped with a balloon filled with nitrogen. The quinoline solution is then rinsed with 5 washes of 99.9%  $\text{D}_2\text{O}$  and three washes with 99.96%  $\text{D}_2\text{O}$ . After each addition of  $\text{D}_2\text{O}$ , the solution was stirred for 5 min and then centrifuged. The bottom organic layer was transferred to another pressure bottle to be further treated with  $\text{D}_2\text{O}$ . After the exchanges, 3-ene-1-pentyne (0.006082mol; 0.402g) was added with a syringe and the tube was immediately sealed. The reaction was heated overnight (~15h) at 65-70°C. The sample was then trapped and stored in an ampule.

#### **1.2.7.5. Synthesis of DDPD - Dry run without base**

In a pressure round-bottom flask were mixed tosylhydrazide (0.0115mol; 1.49g) with enough  $\text{D}_2\text{O}$  (99.9% pure) to make a slurry. After stirring for 15min, the 3-ene-1-pentyne (0.0046mol; 0.304g) was added and left in an oil bath overnight at 69°C. The tosylhydrazide was used as it's own base in a molar ratio to the 3-ene-1-pentyne in 1.8:1.

#### **1.2.7.6. Synthesis of DDPD - Lindlar reaction**

3-ene-1-pentyne (0.0031mol) is dissolved in 0.0206mL of quinoline. Lindlar catalyst (Palladium on Calcium carbonate, poisoned with lead) 0.02g is then added. The reaction is then sealed in a 10 ml round bottom flask with septum and a stir bar. Through the septa is attached a balloon sealed with a needle and filled with ~75mL of  $\text{D}_2$ . The volume of  $\text{D}_2$  is “eyeballed” by comparing the size of the inflated balloon with the size of a 100 mL round

bottom flask. The reaction is stirred overnight for 15hrs. The sample is then distilled and stored in an ampule.

#### **1.2.7.7. Synthesis of DDPD in propionitrile**

Tosylhydrazide (0.01604 mol; 2.987g) is dissolved in minimal amount of propionitrile (~31mL). The solution is then washed 5 times with 99.9% D<sub>2</sub>O and three times with 99.96% D<sub>2</sub>O, followed by 3-ene-1-pentyne addition (0.4358g; 0.00659mol) and heated to 65° C overnight. The sample is then distilled and stored in an ampule.



### 1.3. Results and discussion

In this work we conducted studies on a series of substituted acyclic 1,3-dienes (**Figure 1.43**). The substituents were chosen to reveal the relative importance of inertial mass, charge stabilizing capability and steric size in controlling which of the two bonds of the diene preferentially photoisomerized. The photochemical experiments were conducted in solvents of different polarity to examine the extent of charge development in the excited state pathways that were traversed.

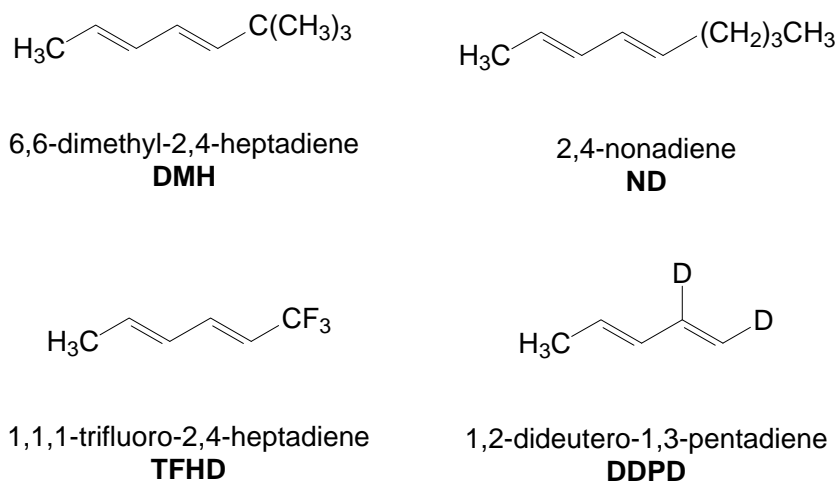


**Figure 1.43** Molecules of interest in this work.

EE-DMH and EE-ND were chosen to investigate the importance of the inertial mass of the substituent and viscosity effects caused by the shape of the substituent. The importance of steric effect on diene photochemistry was examined by investigating the photoisomerizations of EZ-DMH and ZE-ND.

The importance of the substituents' ability to stabilize charge was investigated by determining the photochemistry EE-TFHD. In all cases the photochemistry was examined

in either pure hexane, pure propionitrile or mixtures of these two solvents. Further, triplet photosensitization experiments were carried out to prove that the observed photochemistry was occurring on the singlet state surface.

We will also describe our efforts to synthesize 1,2-dideutero-1,3-pentadiene. Reinvestigating this system is necessary in order to more accurately determine the its photochemistry which previously showed a very high photoregioselectivity. To determine the cause of this high selectivity the solvent effect on the photoisomerization of this molecule must be determined.

### 1.3.1. DMH Results and discussion

#### 1.3.1.1. Synthesis and purification

The compounds EE and EZ 6,6-dimethyl-2,4-heptadiene (DMH) were prepared with the purpose of determining the importance of inertial effects in the control of the photochemistry in the visual system. The EE isomer had no important steric interaction and so was the ideal candidate to show the importance of inertial effects on the photoregioselectivity. On the other hand the EZ isomer has significant steric strain and so its photochemistry would reveal the importance of steric hindrance in determining which diene double bond isomerized preferentially. To obtain the stereospecific species, a synthetic route giving high yields as well as isomeric purity was needed. The reason for these requirements is that the photochemical data must be collected at very low conversion rates so as to avoid photochemistry from the products interfering with the results. Previous attempts to synthesize DMH in our lab were conducted by elimination or Suzuki mechanism. However, the attempts gave low product yields and inconsistent isomeric ratios so were not satisfactory. This is why the synthetic route based on Wittig reaction was attempted.

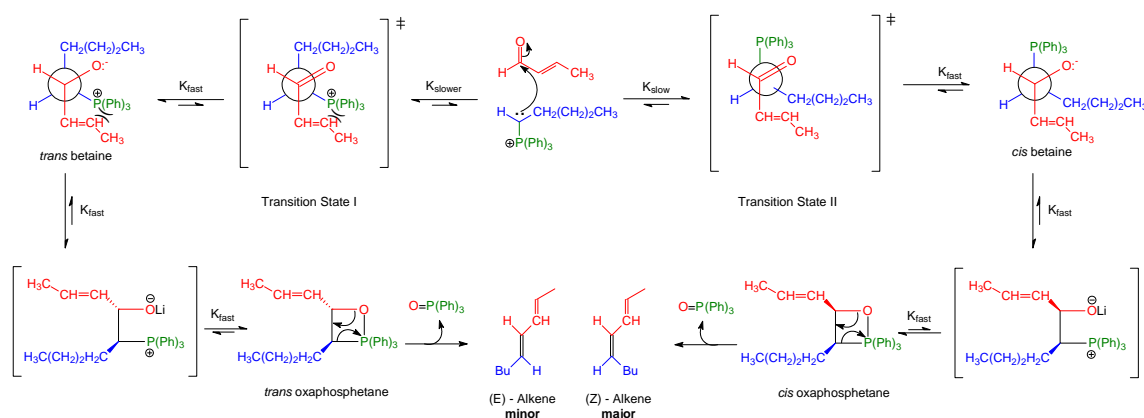
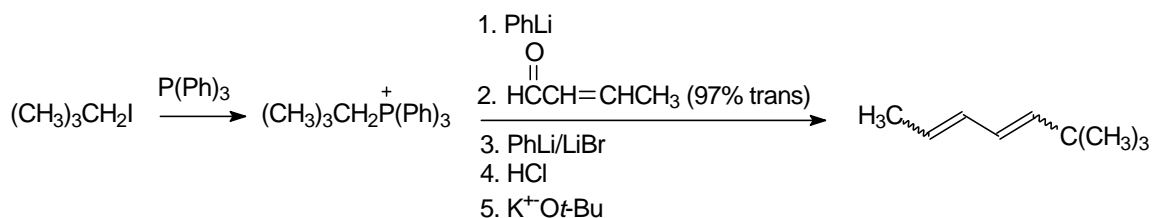


Figure 1.44 Wittig mechanism used for synthesis of DMH and ND

A typical Wittig reaction (**Figure 1.44**) gave DMH in fairly high yields (~80%). In the reaction, deprotonation of the phosphonium salt of the neopentyl iodide led to the formation of phosphonium ylide. When the ylide is reacted with crotonaldehyde, two different transition states are formed. The bulky triphenyl phosphorous group in transition state **I** is very close to the substituent on the aldehyde, causing steric hindrance. In transition state **II**, however, the allyl group of crotonaldehyde and triphenyl phosphorous are away from each other. The decreased steric hindrance makes this transition state favored. The resulting *cis* betain then closes to the *cis* oxaphosphetane. After losing triphenyl phosphine oxide, the *cis*-diene is produced as the major product, which in this case is the *EZ* isomer. The experimental results indicated that with straight Wittig reaction we achieved *EE:EZ:ZE:ZZ* ratio of 51:26:17:6 (**Figure 1.46 top**). The larger than usual amounts of the trans product, the *EE* isomer, is considered a consequence of the steric hindrance between the bulky *t*-butyl group and the allylic portion of croton aldehyde in transition state **II**.

To improve the stereospecificity of the reaction, i.e. increase the amount of the desired *EE*-DMH isomer, the Wittig mechanism with a Schlosser modification (**Figures 1.45 and 1.46**) was attempted.



**Figure 1.45** Wittig mechanism with Schlosser modification.

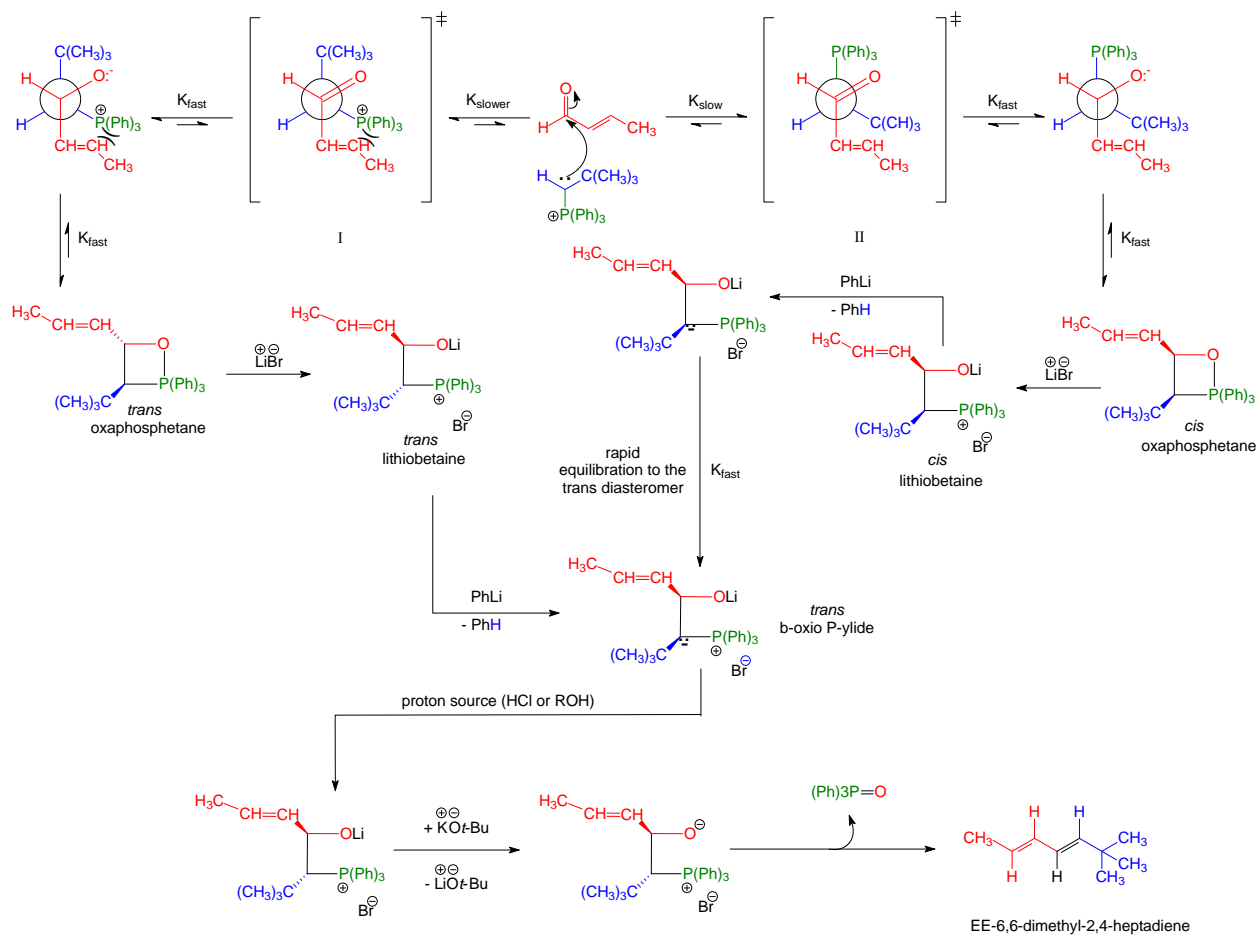


**Figure 1.46** Wittig reaction with Schlosser modification used to prepare DMH.

The second addition of alkyl lithium to the reaction initiates an equilibration of the *cis*- $\beta$ -oxio phosphorous ylide to the more stable *trans* isomer, followed by protonation with HCl. The lithium is displaced with potassium by treatment with potassium tert-butoxide so the resulting free *trans*-betaine will lose triphenyl phosphorous oxide and form the desired E-alkene.

The deprotonation of the lithiobetaine took approximately 10 hours. The reason was probably the insufficient amounts of LiBr needed to open the oxophosphatane. Nevertheless, after a negative Gilman test was obtained we produced DMH with isomeric mixture containing ~97% EE-DMH, ~3% EZ-DMH and less than 1% of the ZE and ZZ isomers (**Figure 1.47** bottom).

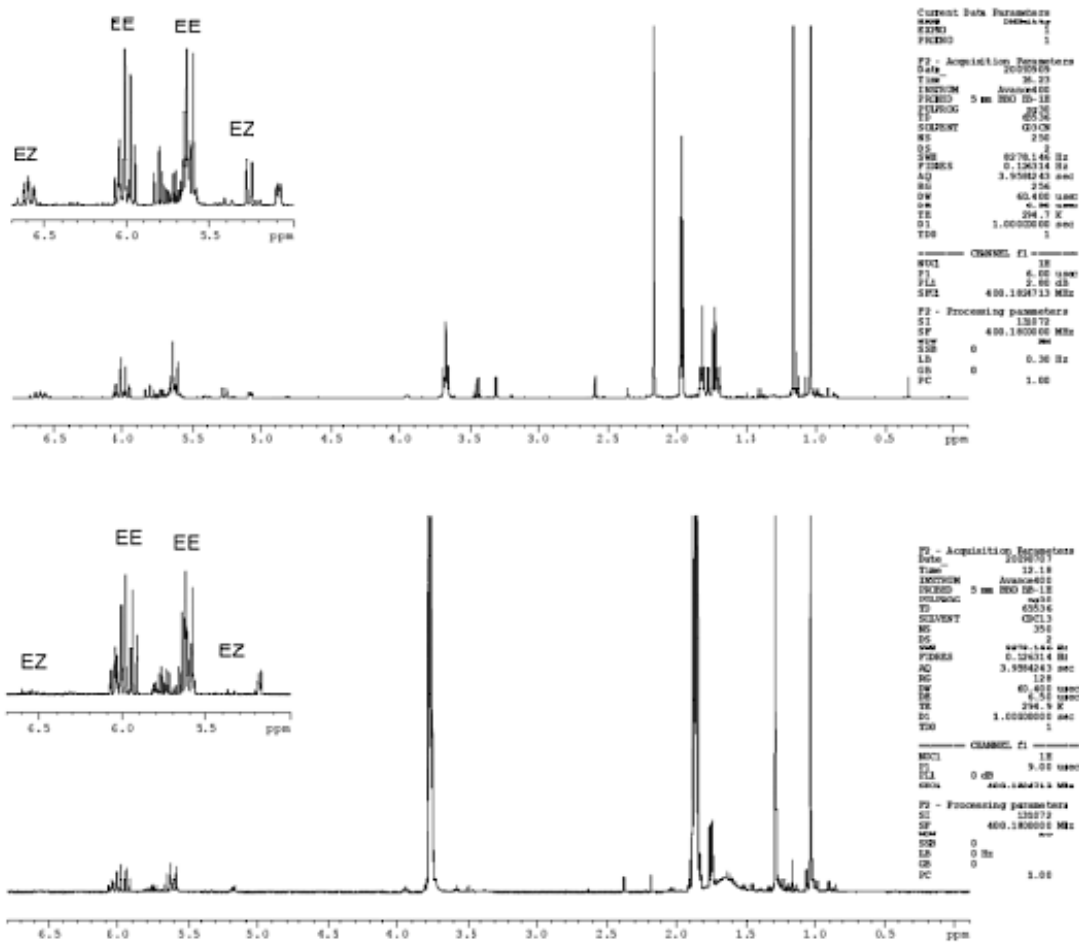


**Figure 1.47** Comparison of <sup>1</sup>H NMR of DMH prepared via Wittig reaction (top) and Wittig reaction with Schlosser modification (bottom)

To purify the EE-DMH from the rest of the isomers, preparative gas chromatography was employed. The purification proved to be very challenging as separating the EE from the small amount (~3%) of the ZE isomer was difficult (**Figure 1.47** bottom).

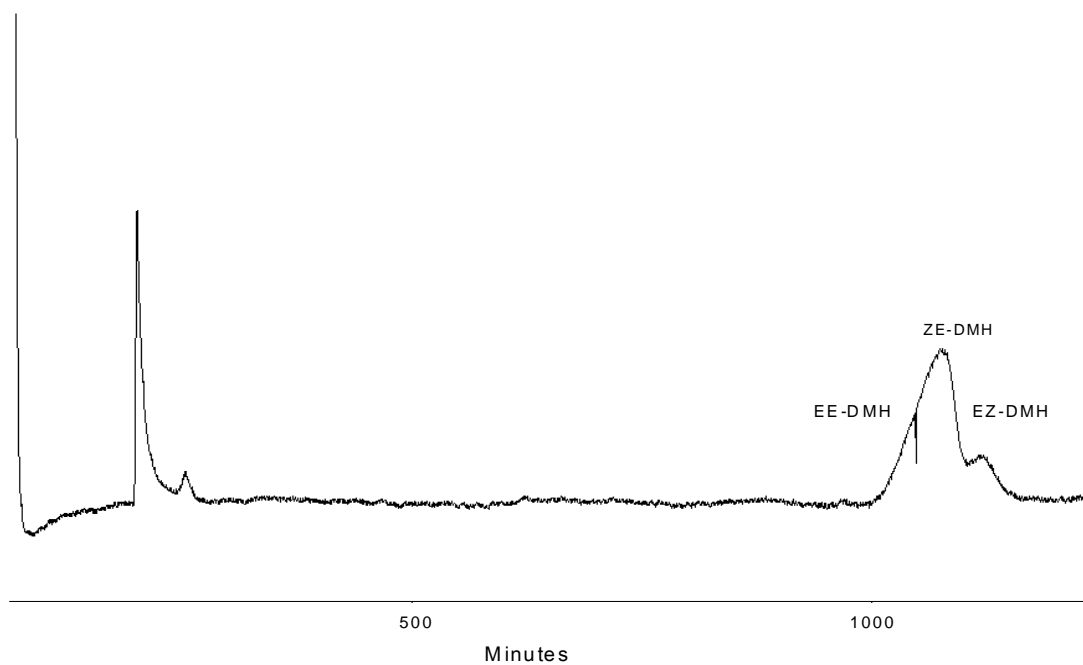


**Figure 1.48** Prep GC of DMH isomers.

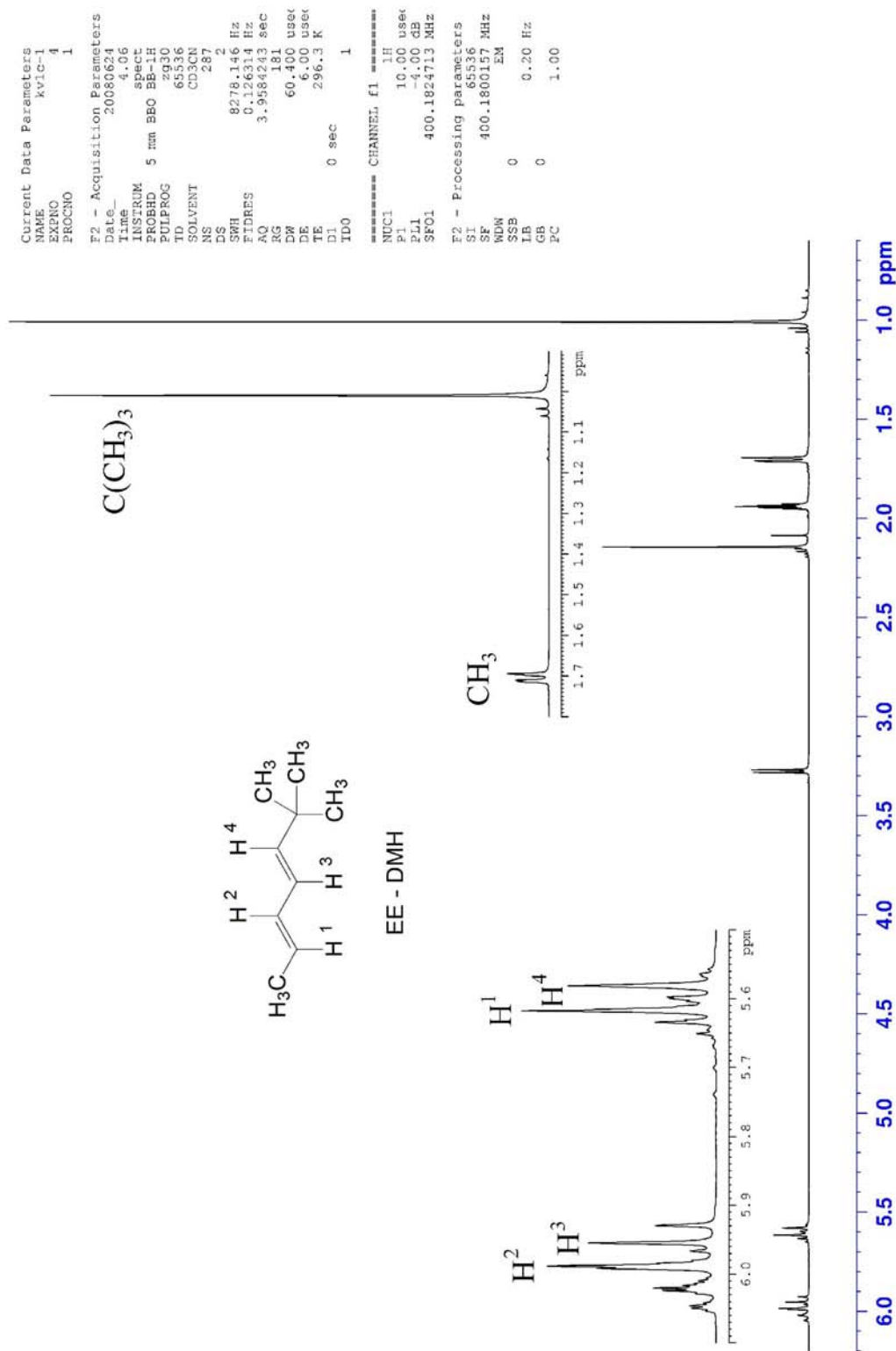


Figure 1.49 <sup>1</sup>H NMR of EE DMH



```

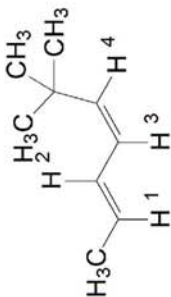
Current Data Parameters
NAME      XVIC-1
EXPNO    5
PROCNO   1

F2 - Acquisition Parameters
Date_    20080624
Time     4.40
INSTRUM  spect
PROBHD   5 mm BBO BB-1.
PULPROG  zg30
GAMMA    90
SOLVENT  CDCl3
NS       320
DS       2
SWH      8278.146 Hz
FIDRES   0.1246314 Hz
AQ       3.9584245 sec
RG       287.4
DE       60.000 usec
TE       300.2
D1       0.00 usec
T1G      1
----- CHANNEL f1 -----
NUC1     13C
P1       10.00 usec
PL1     -4.00 dB
SFO1     400.1824713 MHz

F2 - Processing Parameters
SI       32768
SF       400.1899388 MHz
WDW      EM
SSB      0
LR       0
GB       0
PC       1.00

```

C(CH<sub>3</sub>)<sub>3</sub>



EZ - DMH

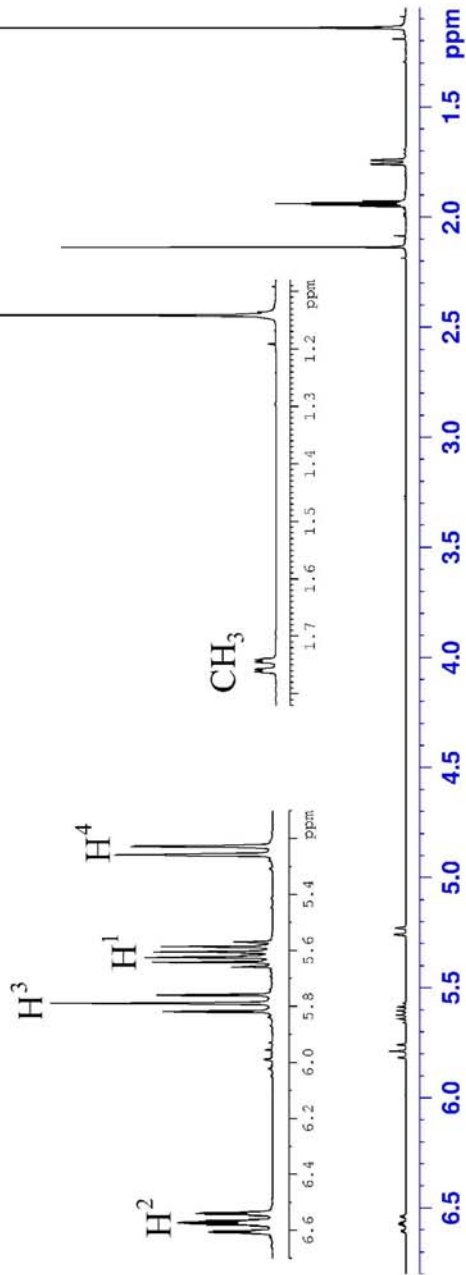
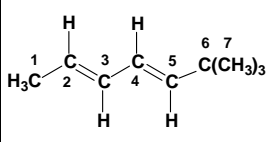
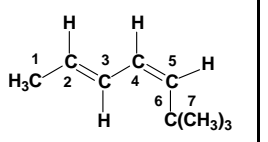
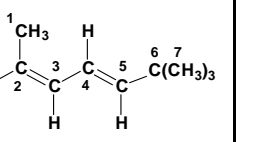
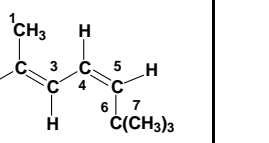


Figure 1.50 <sup>1</sup>H NMR of EZ DMH

**Table 1.5:**  $^1\text{H}$  NMR,  $^{13}\text{C}$  NMR and coupling constants on identified DMH isomers.

 EE-DMH			 EZ-DMH			 ZE-DMH			 ZZ-DMH		
ppm	Hz	Asgn	ppm	Hz	Asgn	ppm	Hz	Asgn	ppm	Hz	Asgn
6.010	$J_{2,3}=14.67$ $J_{3,4}=10.17$ $J_{1,3}=1.46$	H3	6.541	$J_{3,4}=11.59$ $J_{2,3}=14.88$	H3	6.30	$J_{4,5}=15.46$ $J_{3,4}=10.76$ $J_{2,4}=1.17$	H4	5.5	$J_{1,2}=5.85$ $J_{2,3}=11.05$	H2
5.960	$J_{4,5}=14.67$ $J_{3,4}=10.17$	H4	5.792	$J_{3,4}=11.59$ $J_{4,5}=11.88$	H4	5.96	$J_{2,3}=10.76$ $J_{1,3}=1.76$ $J_{3,5}=0.98$	H3	6.46	$J_{2,3}=11.05$ $J_{3,4}=10.98$	H3
5.610	$J_{2,3}=14.67$ $J_{1,2}=6.65$	H2	5.609	$J_{1,2}=6.75$ $J_{2,3}=14.88$	H2	5.72	$J_{4,5}=15.46$ $J_{3,5}=0.98$	H5	6.12	$J_{3,4}=10.98$ $J_{4,5}=12.04$	H4
5.600	$J_{4,5}=14.67$	H5	5.251	$J_{4,5}=11.88$	H5	5.38	$J_{2,3}=10.76$ $J_{1,2}=7.04$ $J_{2,4}=1.17$	H2	5.42	$J_{4,5}=12.04$	H5
1.700	$J_{1,2}=6.65$ $J_{1,3}=1.46$	H1	1.780	$J_{1,2}=6.75$	H1	1.72	$J_{1,2}=7.04$ $J_{1,3}=1.76$	H1	1.69	$J_{1,2}=5.85$	H1
1.010		H7	1.164		H7	1.04		H7	1.142		H7
143.900			139.499		C5	33.9			35.1		
133.100			130.161		C2	31.8			31.7		
127.900			128.180		C3	18.4			12.8		
126.300			127.213		C4						
33.600			33.848		C6						
30.000			31.678		C7						
18.200			18.540		C1						

The presence of this ZE impurity was unfortunately unavoidable because of crotonaldehyde's rapid cis-trans equilibration giving 97:3 trans: cis mixture. After numerous attempts however, we found preparative GC conditions that would allow us to prepare solutions of virtually pure EE and EZ-DMH. For this purpose we used a 30'×1/4" column, packed with Chromosorbp NAW 100-120 mesh coated with 30% OV-17 at room temperature. The order of elution of the isomers was EE, ZE, EZ, and ZZ (**Figure 1.48**). The retention time of the ZE isomer was just slightly lower than that of the EE isomer. To obtain the required minimum of 99.5% purity of EE for photolysis, we injected 40  $\mu$ L of the crude DMH mix and collected only the first third of the combined EE-ZE peak. Collections of several injections were necessary to obtain the required amount of the EE isomer. **Figure 1.49** shows the  $^1\text{H}$  NMR of the pure isomer. The EZ isomer was much better separated and could be obtained in 99.8% purity (**Figure 1.50**) with a single injection. Complete  $^1\text{H}$  NMR and partial  $^{13}\text{C}$  NMR spectra allowed identification of the four DMH isomers (**Table 1.5**).

### 1.3.1.2. Analysis and photochemistry

The microscale photolysis was performed using the merry-go-round apparatus shown in **Figure 1.43**. The isomerically pure EE-DMH (99.94%) was diluted with 100  $\mu$ L hexane or propionitrile. In each experiment decane (7  $\mu$ L) was used as a reference. The solution was degassed with nitrogen gas for at least 10 minutes and then 11 portions of 7  $\mu$ L of the solution were transferred to individual quartz capillaries. The capillaries were sealed and then placed in the micro-merry-go-round. The spinning of the apparatus ensured equal irradiation over all the capillary tubes. At appropriate time intervals, the samples are

removed and their isomeric ratios examined via analytical GC.

The separation efficiency of an analytical capillary column changes with different carrier gases at different flow rates (**Figure 1.52**). It's been determined that the best efficiency (minimum HETP) can be obtained using N<sub>2</sub>. The difficulty of using nitrogen as a gas carrier arises from fact that the minimum value occurs over a very narrow range of carrier gas linear velocities. The nitrogen's efficiency would sharply decrease when even a small change in

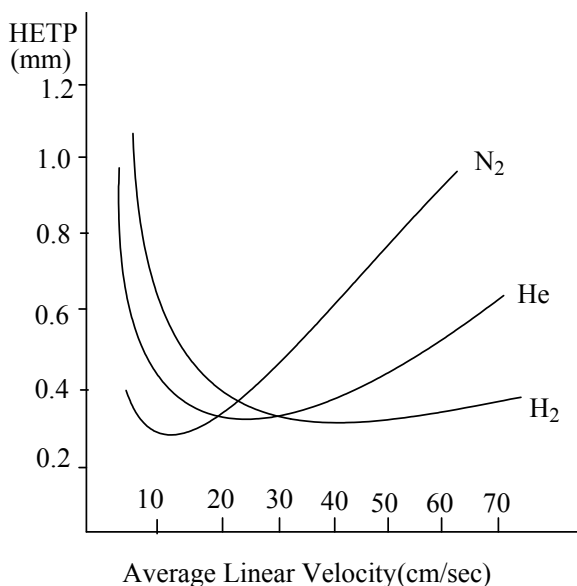


**Figure 1.51** Efficiency curve dependence on carrier gas.

the average linear velocity is made. By using methane as a reference, we adjusted the flow

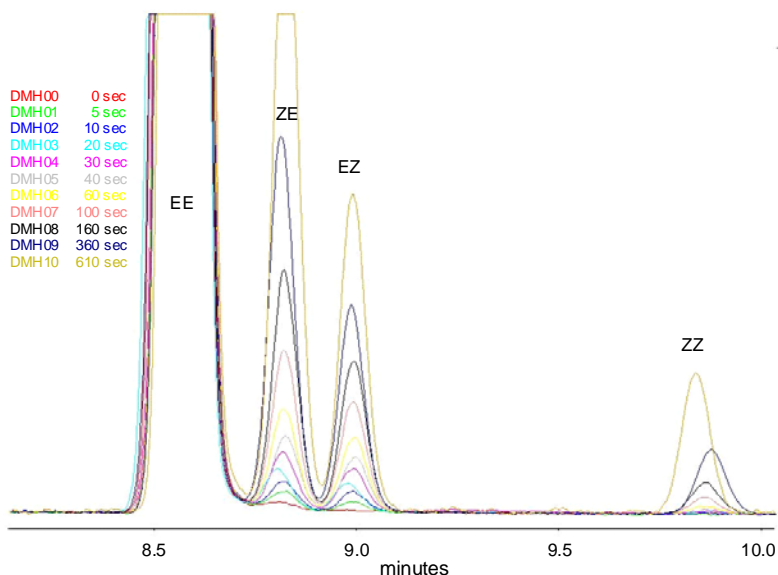


**Figure 1.52** Progression of the photochemical isomerization of EE-DMH in hexane obtained using analytical GC.

rate of the carrier gas on a 30 m x .25mm column coated with a .25 $\mu$ m film of RTX-65 (65% diphenyl/ 35% dimethyl polysiloxane), giving methane a retention time of 4.2 min. At this flow rate we achieved the best separation of the different DMH isomers (**Figure 15.2**). The identification of the GC peaks was accomplished by comparing NMR integrations and the integrations of the analytical GC peaks. The close match in areas allowed us to identify which peak corresponded to which isomer and to show that, as expected, the response factors of all four isomers was identical.

The sensitivity of analytical GC gave us the opportunity to monitor the photoisomerization of 99.9% pure EE-DMH even at the very low conversions, which is required in order to avoid significant back photoisomerization of the ZE:EZ isomers produced during the initial photolysis of EE-DMH.

**Figure 1.53** shows the plot of the photolysis data for EE-DMH in hexane. The sample is photolyzed completely to the photostationary state. The initial EE-DMH isomer conversions are shown in

**Figure 1.54**. The plotted almost parallel lines show that the double bond substituted by the lighter methyl group has a preferential isomerization of only 1.24 times more than the double bond bearing the t-butyl group which weighs almost four times as much. This result shows

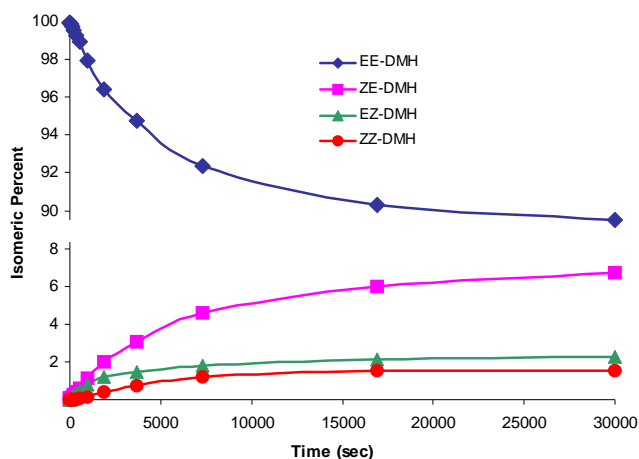


**Figure 1.53** Photoisomerization of EE-DMH to photostationary state (hexane; 254nm; 0°C)

that the mass of the substituent of the double bond has very little effect on determining the regioselectivity of polyene isomerization. Thus a photoisomerization pathway where the regioselectivity is determined simply by passage through a conical intersection cannot be correct.

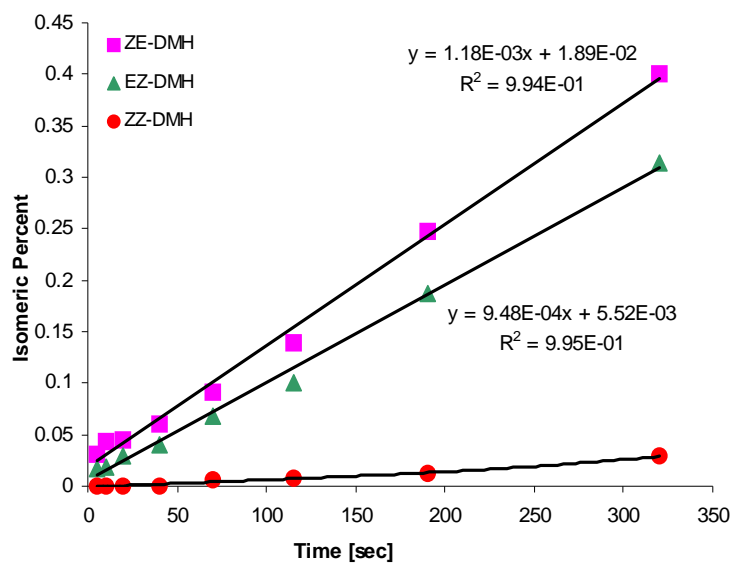


**Figure 1.54** Formation of ZE, EZ and ZZ DMH at less than 1% conversion of EE-DMH (hexane; 254nm; 0°C)

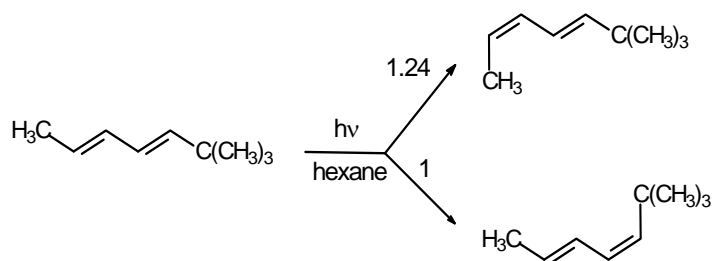


**Figure 1.55** Photoisomerization of EE-DMH in hexane

The photoisomerization of EE-DMH in the very polar solvent was investigated as well. As seen from the results plotted in **Figures 1.56** and **Figure 1.57**, there is virtually no change in the photoregioselectivity as compared to the nonpolar hexane solvent.

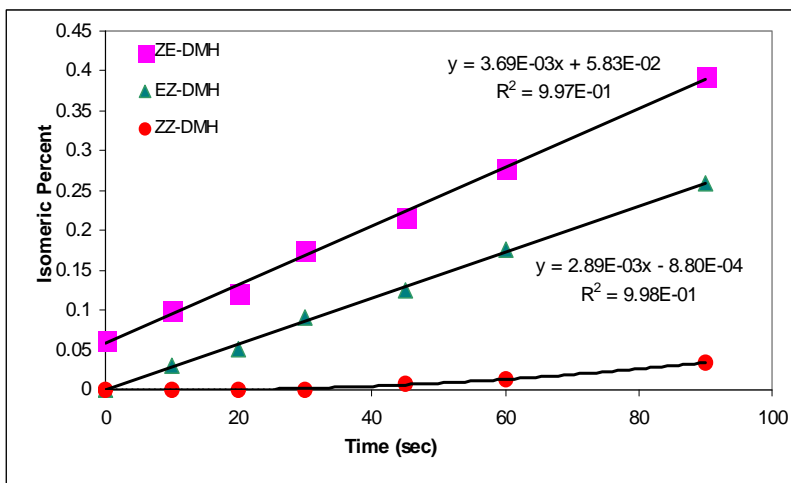


**Figure 1.56** Formation of ZE, EZ and ZZ DMH at less than 1% conversion of EE-DMH (propionitrile; 254nm; 0°C)

It has been speculated that in solution a methyl group may have a better charge stabilizing effect than a t-butyl group,<sup>150</sup> which could explain the ~25% preference for isomerization about the double

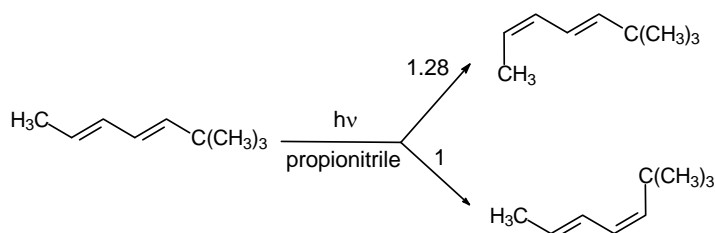


**Figure 1.57** Photoisomerization of EE-DMH in propionitrile

bond substituted with the methyl group. However, at best the difference in the charge

stabilizing effect of the two alkyl groups is small. This means that if our proposed picture of potential energy surface pathways is correct (**Figure 1.38**), there should be almost no difference in the polarization of the diene unit along the two isomerization pathways of EE-DMH. Thus very little (if any) solvent effect would be expected.

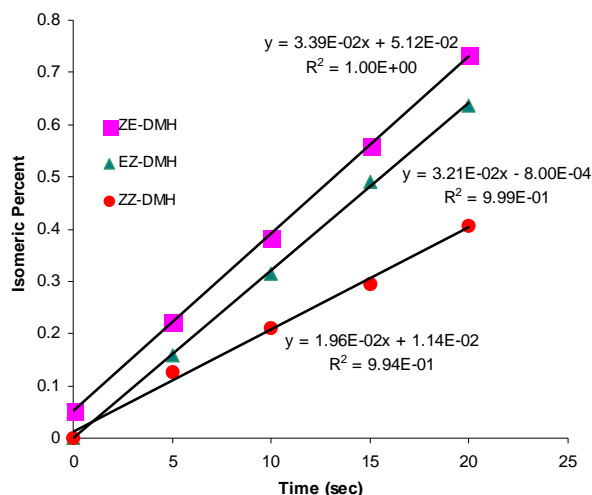


**Figure 1.58** Triplet photochemistry of EE-DMH sensitized with benzophenone (hexane; 254nm; 0°C)

To eliminate the possibility that our photochemical experiments involved a triplet, rather than singlet photochemistry, a separate photolysis of EE-DMH was conducted using benzophenone as a triplet sensitizer. When photolyzed in the presence of benzophenone, EE-DMH exhibited very different photochemistry (**Figure 1.58**). Because the triplet diene is essentially a 1,4-biradical, simultaneous rotation around both double bonds, is expected and our results showed exactly that.

This simultaneous photoisomerization of both diene double bonds results in the rapid formation of the ZZ isomer. It is obvious from the experiments without sensitizer that there is a period of induction for the ZZ isomer (**Figure 1.54 and 1.56**) because on the singlet surface it is formed by secondary photolysis of the EZ and/or ZE isomers. This induction period however, is completely eliminated when benzophenone is added to the solution. The ZZ isomer can be this rapidly produced from the initial structure only if a simultaneous



rotation around the two double bonds occurs.

The results described for EE-DMH clearly show that inertial effects are not particularly important in determining the regioselectivity of polyene photoisomerization. The importance of steric effects was investigated by examining the photoisomerization of EZ-DMH.

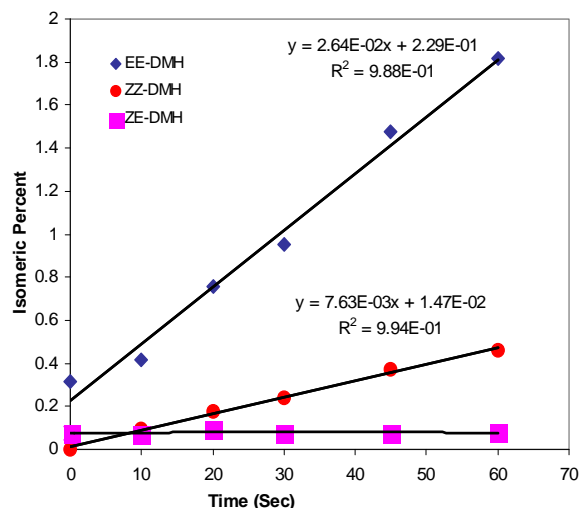


**Figure 1.59** Formation of EE, ZZ, and ZE DMH at less than 3% conversion of EZ-DMH (hexane, 254 nm, 0 °C).

The singlet photochemistry of pure EZ-DMH was examined in hexane

(**Figure 1.59**). It was surprising to find that there is only a three fold preference of isomerization about the double bond substituted with the bulky t-butyl group, even though there is severe steric hindrance between this group and the hydrogen linked to C<sub>3</sub>. This result suggests that steric interaction of the methyl group on C12 of retinal cannot be the proximal cause of the very high selectivity of isomerization about retinal's C11-C12 double bond.<sup>151</sup>

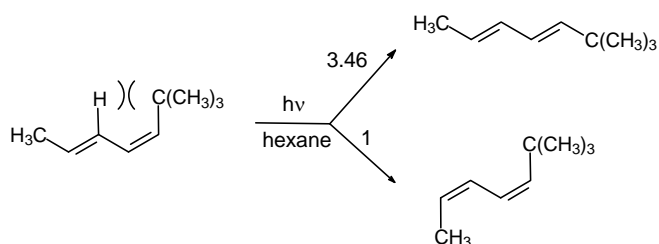


**Figure 1.60** Photolysis of EZ-DMH in hexane.

To again show that the chemistry we observe for this isomer is indeed singlet photochemistry we also examined the triplet sensitized photochemistry of EZ-DMH. Again the difference in singlet and triplet photochemistry was substantial (Figure 1.61). As with the EE isomer, rapid production of the “double” double bond isomerized product (in this case ZE-DMH) upon triplet sensitization showed that our previous photochemical results were delineating photochemical pathways on the singlet excited state potential energy surface.

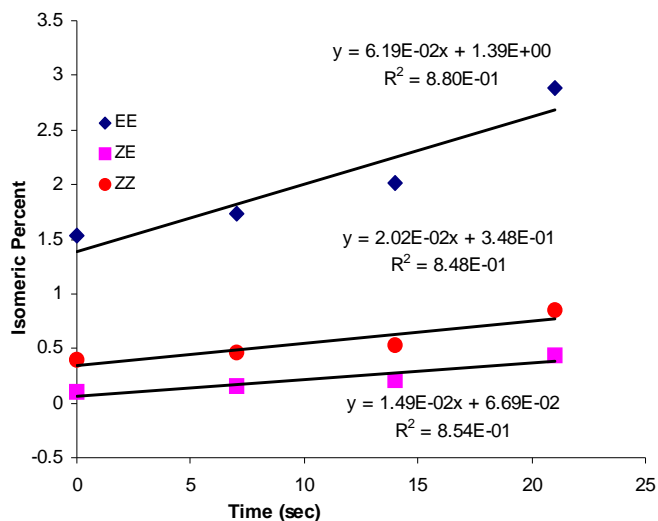


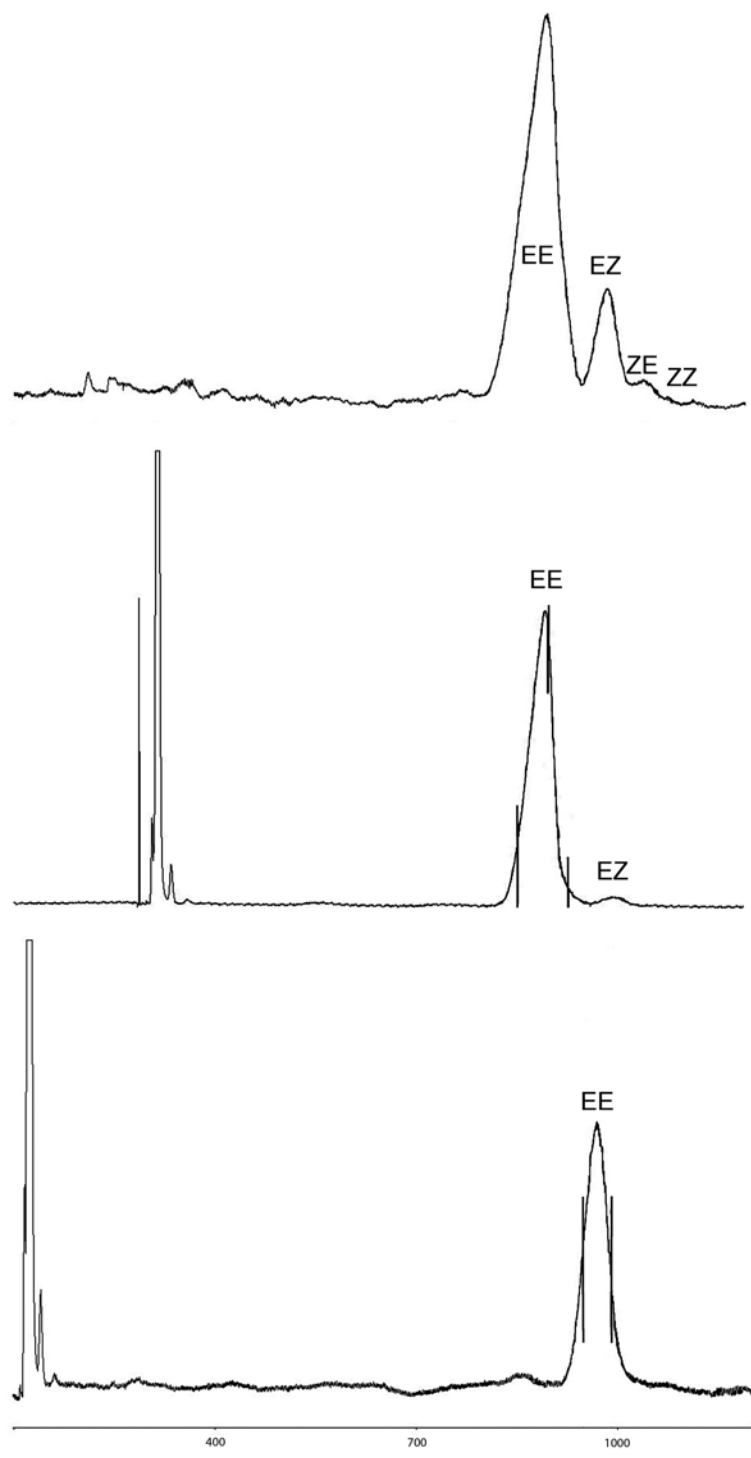
**Figure 1.61** Triplet photochemistry of EZ-DMH with benzophenone (hexane; 254nm; 0°C)

### 1.3.2. 1,3-nonadiene (ND) results and discussion

To determine whether the 20% difference in the isomerization efficiencies of the two double bonds in EE-DMH is caused by a difference in the electron donating ability of C-H vs C-C bonds, the very similar EE-ND and ZE-ND were synthesized to further examine the inertial, solvent and steric effects. The methyl and n-butyl groups of ND should have much more similar charge stabilizing effects, compared to the methyl and t-butyl groups of DMH. While mass effects should remain essentially the same, the four carbons of the n-butyl group exist as an extended chain, as opposed to the compact mass of the t-butyl group of DMH. If movement of the four carbon group is impeded by the solvent, the effect should be greater

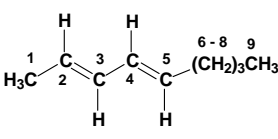
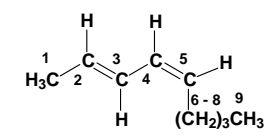
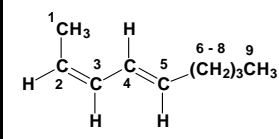
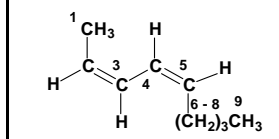


The order of elution of the isomers on a 20'×1/4" column, packed with Chromosorb P-AW 100/120 mesh and coated with 20% OV-25 at 50°C, was EE, EZ, ZE, and ZZ. The isomers were identified by a combination of different NMR techniques (**Table 1.6**), though the vinyl coupling constants were the primary means of identification. In order to obtain the necessary 99.5% purity of EE for photolysis, four successive 20uL injections of equilibrated crude were performed. Only the first half of the combined EE-EZ peak was collected (**Figure 1.64**). This collection was then prepped a second time using the same conditions, and again, the first half of the peak was collected. For the ZE isomer, we collected all of the peak except for the initial incline and final decline to avoid collecting any of the EZ or ZZ isomers (**Figure 1.66**). This was also prepped a second time, using the same collection cuts. While this procedure for purification allowed us to collect only very small amounts of the desired isomer, the photolysis and subsequent analysis could be successfully performed on a microscale.



**Figure 1.63** Preparative GC of 2,4-nonadiene top: crude ND after equilibration middle: 2<sup>nd</sup> prep of EE/EZ peak bottom: 2<sup>nd</sup> prep of ZE peak.

**Table 1.6:**  $^1\text{H}$  and  $^{13}\text{C}$  NMR shifts of EE, EZ, ZE and ZZ-ND

 EE-ND			 EZ-ND			 ZE-ND			 ZZ-ND		
ppm	Hz	Asgn	ppm	Hz	Asgn	ppm	Hz	Asgn	ppm	Hz	Asgn
6.002	$J_{1,3}=1.47$ $J_{3,4}=10.3$ $J_{2,3}=14.52$	H3	6.370	$J_{2,7}=1.15$ $J_{1,3}=1.72$ $J_{3,4}=11.01$ $J_{2,3}=15.07$	H3	6.364	$J=1.31$ 10.95 $J_{4,5}=15.11$	H4	6.306	$J_{1,3}=1.65$	H3
5.996	$J_{4,6}=1.27$ $J_{3,4}=10.3$ $J_{4,5}=14.42$	H4	5.935	$J_{2,7}=0.46$ $J_{2,7}=0.65$ $J_{4,6}=1.61$ $J_{3,4}=11.01$ $J_{4,5}=11.20$	H4	5.960	0.40 1.81 $J_{2,3}=10.79$	H3	6.273	$J_{4,6}=1.43$	H4
5.574	$J_{2,7}=0.76$ $J_{1,2}=6.7$ $J_{2,3}=14.52$	H2	5.675	$J_{2,7}=0.45$ $J_{1,2}=6.81$ $J_{2,3}=15.07$	H2	5.675	$J_{5,6}=7.07$ $J_{4,5}=15.11$	H5	5.517	$J_{2,6}=0.61$ $J_{2,7}=1.69$ $J_{1,2}=7.22$ $J_{2,3}=9.81$	H2
5.557	$J_{2,7}=0.97$ $J_{5,6}=6.98$ $J_{4,5}=14.42$	H5	5.290	$J_{5,6}=7.65$ $J_{4,5}=11.20$	H5	5.361	0.58 7.06 $J_{2,3}=10.84$	H2	5.473	$J_{1,5}=0.66$ $J_{2,7}=1.74$ $J_{5,6}=7.25$ $J_{4,5}=9.86$	H5
2.044	$J_{5,6}=6.98$ $J_{6,7}=7.06$	H6	2.156	$J_{5,6}=7.65$	H6	2.107	$J_{5,6}=6.88$	H6	2.170	$J_{5,6}=7.25$	H6
1.699	$J_{2,7}=0.73$ $J_{1,2}=6.7$	H1	1.746	$J_{1,3}=1.72$ $J_{1,2}=6.81$	H1	1.706	$J_{1,4}=0.56$ $J_{1,3}=1.82$ $J_{1,2}=7.08$	H1	1.719	$J_{1,3}=1.65$ $J_{1,2}=7.22$	H1
1.349		H7	1.335		H7	1.376		H7	1.352		H7
1.312		H8	1.305		H8	1.326		H8	1.325		H8
0.890	$J_{8,9}=7.23$	H9	0.900	$J_{8,9}=7.16$	H9	0.901	$J_{8,9}=7.15$	H9	0.897	$J_{8,9}=7.19$	H9
133.04		C5	130.68		C5	135.55		C5	132.87		C5
132.770		C3	130.04		C2	130.58		C3	126.87		C2
131.380		C4	129.62		C4	126.42		C4	125.54		C3
127.630		C2	128.09		C3	124.75		C2	124.30		C4
32.920		C6	32.74		C8?	33.19		C6	32.61		C7
32.410		C7	28.02		C6	32.39		C7	27.840		C6
22.990		C8	23.06		C7?	23.03		C8	23.07		C8
18.180		C1	18.42		C1	14.26		C9	14.27		C9
14.250		C9	14.29		C9	13.44		C1	13.31		C1

<sup>1</sup>H of 2,4-nonadiene, I<sub>2</sub> equilibrated, 1<sup>st</sup> prep on OV-25,  
2<sup>nd</sup> peak (ZE and EZ)

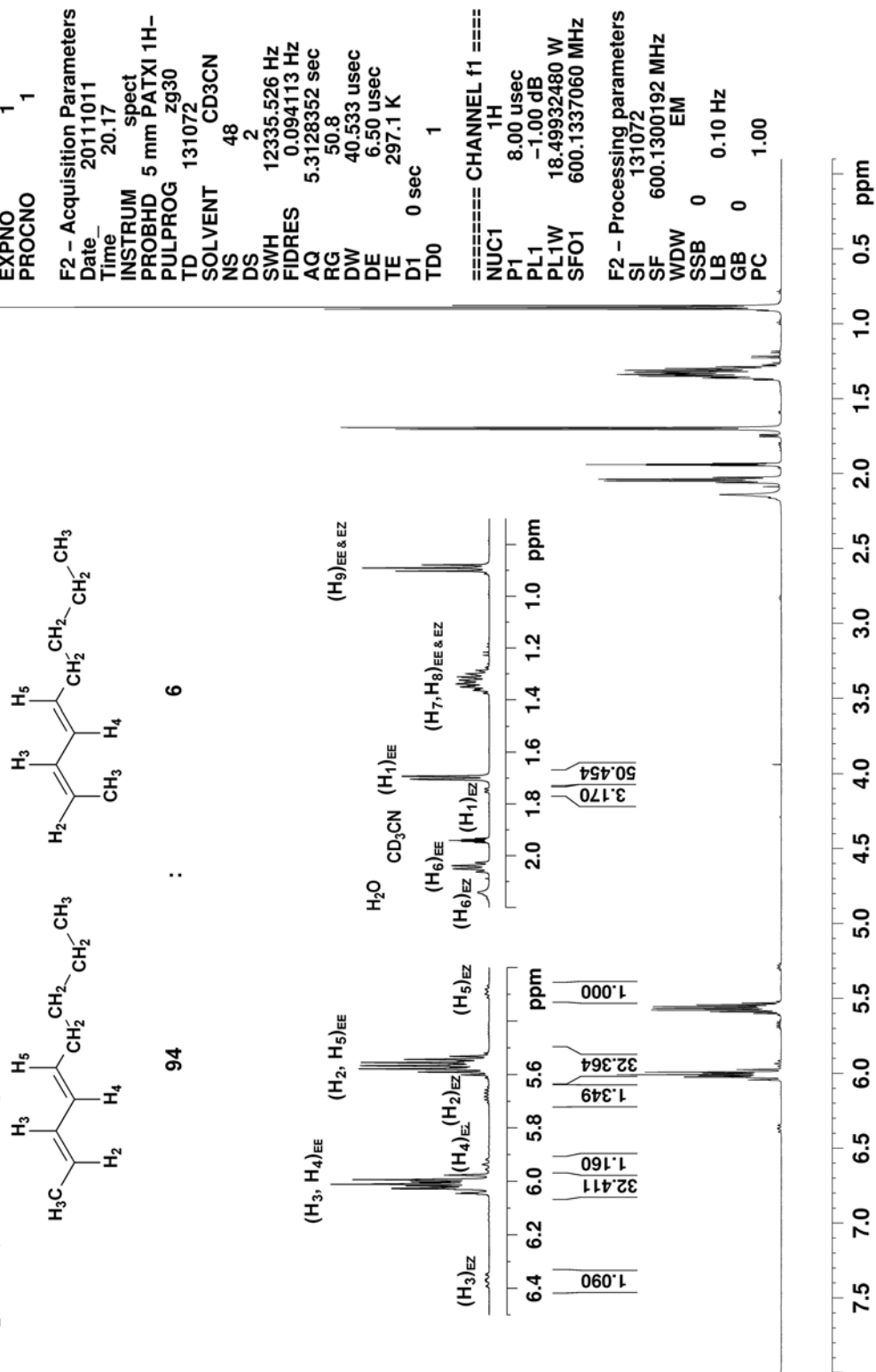
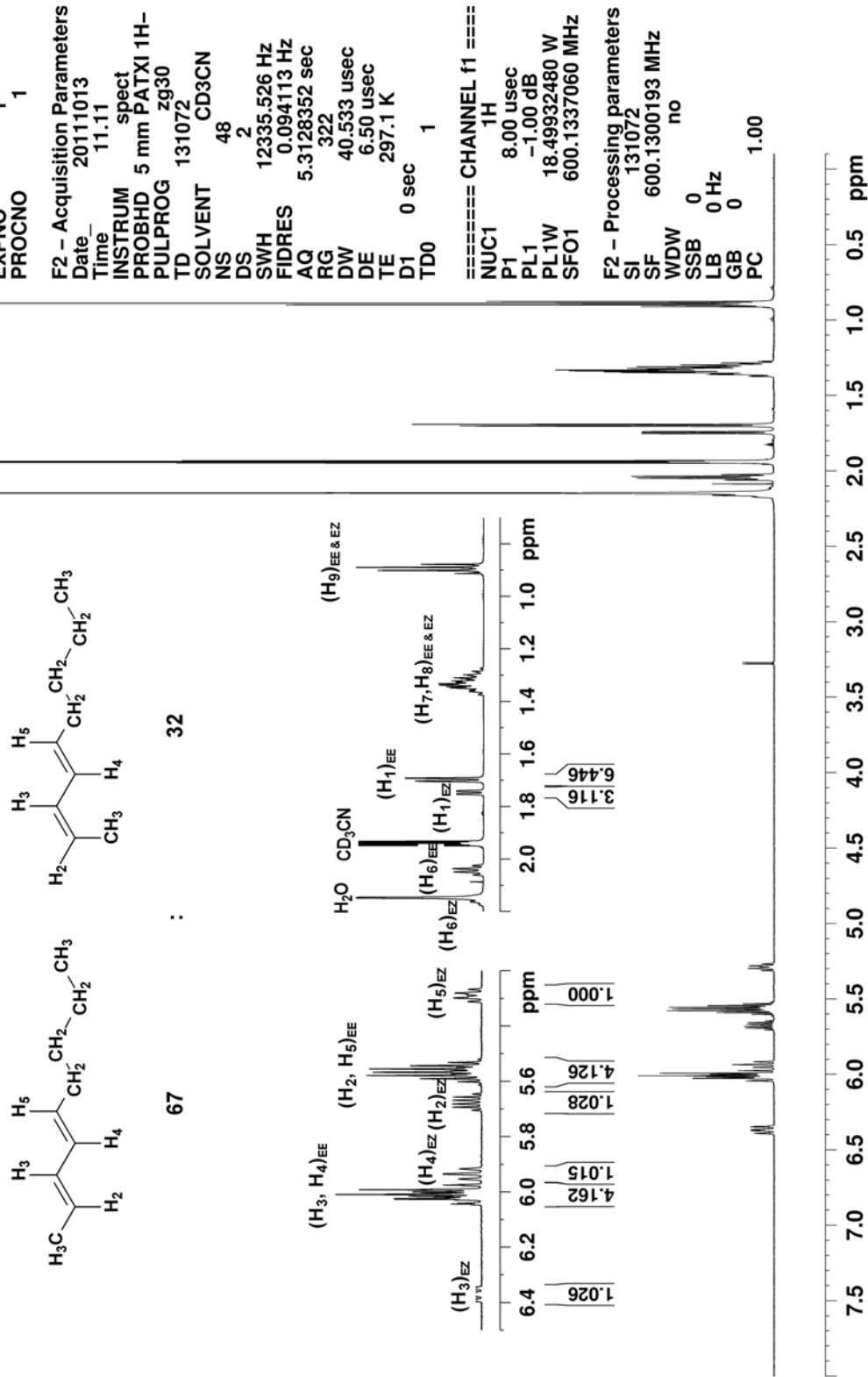


Figure 1.64 EE and EZ isomers of 2,4-nonadiene.





<sup>1</sup>H of 2,4-nonadiene, I<sub>2</sub> equilibrated, 1<sup>st</sup> prep OV-25  
 2<sup>nd</sup> half of first peak (EZ and ZE)



**Figure 1.65** EZ and EE isomers of 2,4-nonadiene.



<sup>1</sup>H of 2,4-nonadiene, I<sub>2</sub> equilibrated, 1<sup>st</sup> prep on OV-25  
 first half of third peak (ZE and ZZ)

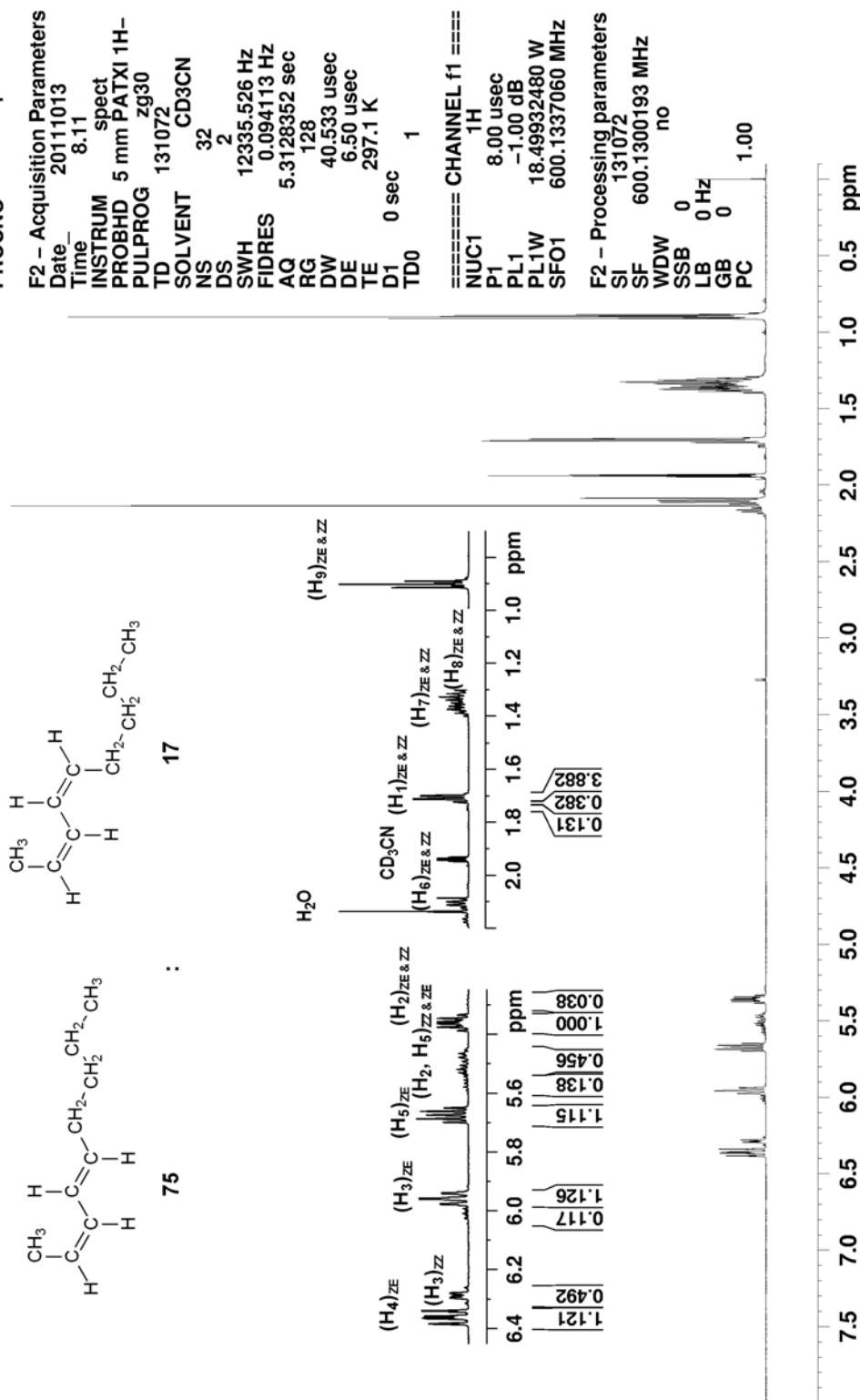


Figure 1.66 ZE and ZZ isomers of 2,4-nonadiene.



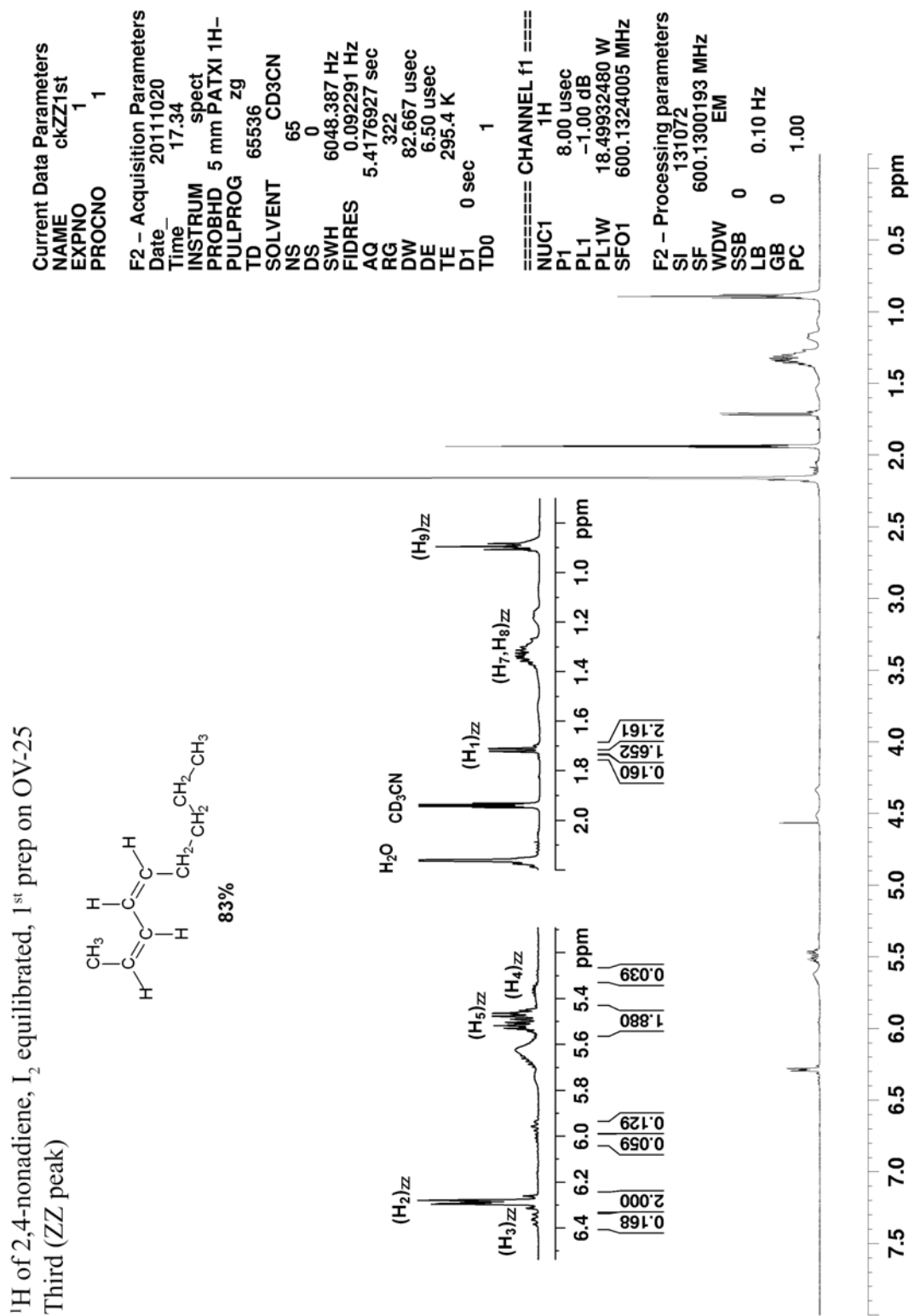


Figure 1.67 ZZ isomer of 2,4-nonadiene.

### 1.3.2.2. Analysis of photochemistry of ND

For the photolysis experiments, 99.5% isomerically pure EE-ND is diluted up to 100  $\mu\text{L}$  hexane or propionitrile with  $\sim 7$   $\mu\text{L}$  of decane as a reference. The solution is mixed in a specially designed “golf tee shaped” quartz tube (Figure 1.68). The wide portion of the tube is sealed with a silicone septum and degassed for fifteen

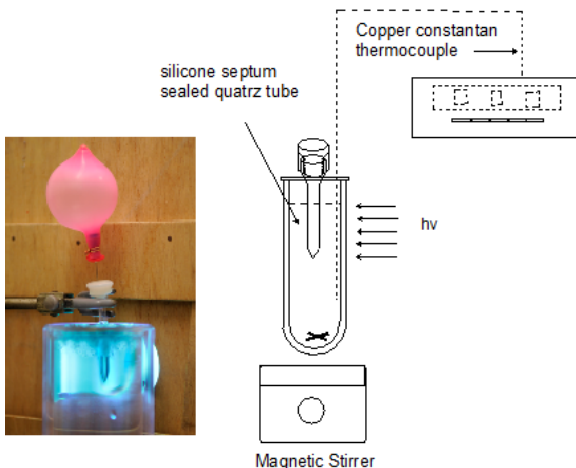


Figure 1.68 Photolysis setup for ND with “golf tee shaped” tube.

minutes. Before photolysis the sample was placed in a quartz dewar and cooled to  $0^\circ\text{C}$ . The sample was then irradiated for appropriate time intervals (Figure 1.69). Three or four  $1\ \mu\text{L}$

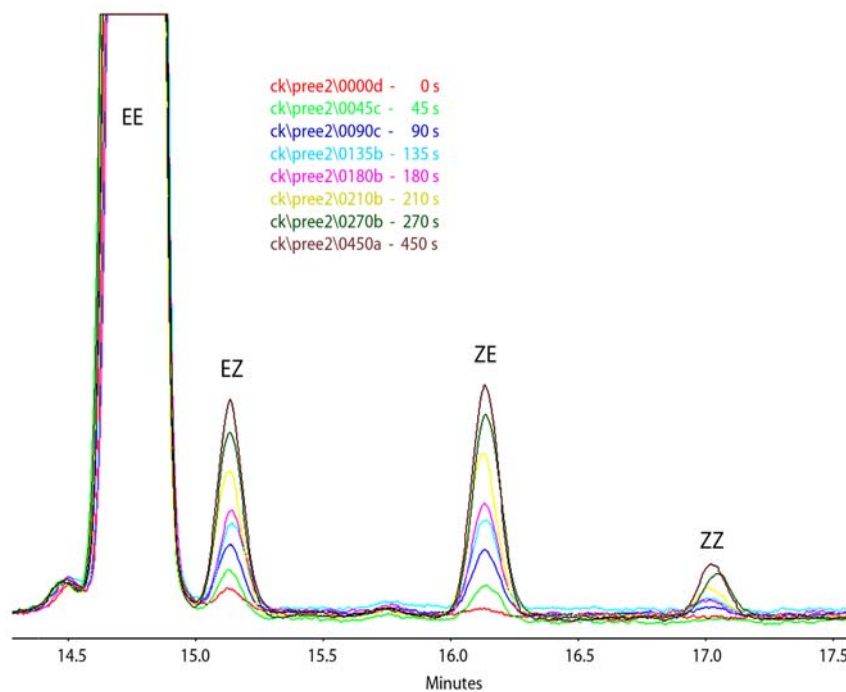


Figure 1.69 Analytical GC of the Photolysis of 2,4-Nonadiene

samples are removed via a microliter syringe and examined via analytical GC for each time interval. This process was repeated for the ZE isomer in hexane and in propionitrile as well.

**Table 1.8:** Comparison of the NMR and GC Isomeric Integrations.

ND Isomer	Crude		Crude I <sub>2</sub> equ.		EEEEZ 1st		EZEE 1st		ZEZZ 1st		ZZZE 1st	
	NMR	GC	NMR	GC	NMR	GC	NMR	GC	NMR	GC	NMR	GC
EE	35.28	34.98	67.50	67.44	94.03	93.56	67.25	67.25	4.51	9.83	2.42	3.22
EZ	57.60	60.14	11.97	12.45	5.97	5.56	32.75	31.91	2.90	3.73	3.81	3.35
ZE	3.20	1.39	17.44	17.22		0.78		0.61	74.81	71.39	10.55	11.16
ZZ	3.93	3.50	3.09	2.89		0.11		0.23	17.77	15.06	83.22	82.28

We were able to separate all ND isomers (**Figure 1.69**) on a 30 meter RTX-65 analytical GC column using nitrogen gas as the carrier. In **Table 1.8** each of the four analytical GC peaks could be assigned to a ND isomer by matching the NMR integrations of ND isomers (**Figures 1.64, 1.65, 1.66, 1.67**)

and the GC integrations of these mixtures. The close match of these integrations also showed that, as expected, the response factors of the ND isomers were essentially identical. **Figure 1.70** shows the photolysis of EE-ND in propionitrile until photoequilibrium is reached.

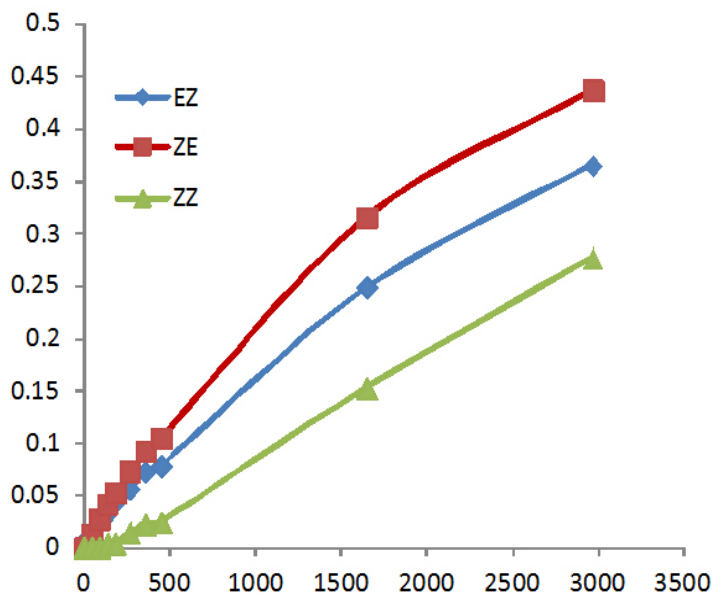


**Figure 1.70** Photoisomerization of EE-ND in propionitrile until photostationary state.

**Figure 1.71** shows the increase in the EZ and ZE isomers of ND at very low conversions of the starting EE. At these small conversions no back photolysis occurs. The results indicate that in hexane the double bond bearing the lighter methyl isomerizes 1.4 times more often than the double bond substituted with the heavier n-butyl group.

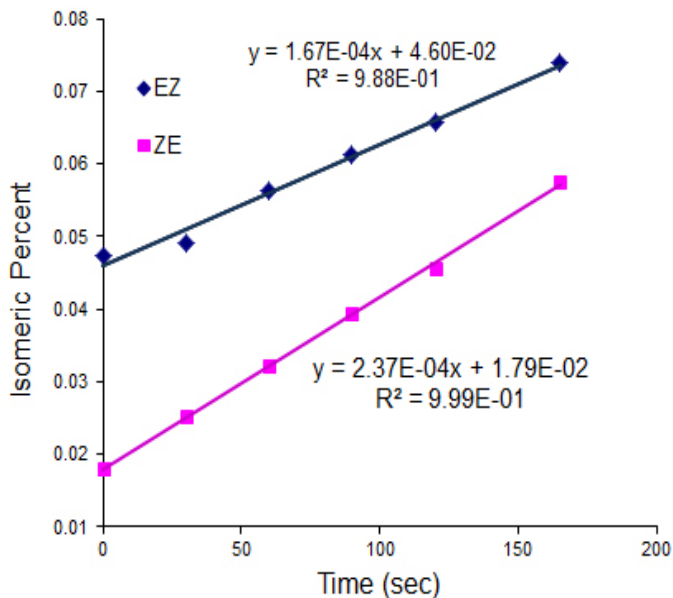


**Figure 1.71** Low percent photochemical conversion of EE-ND in hexane.

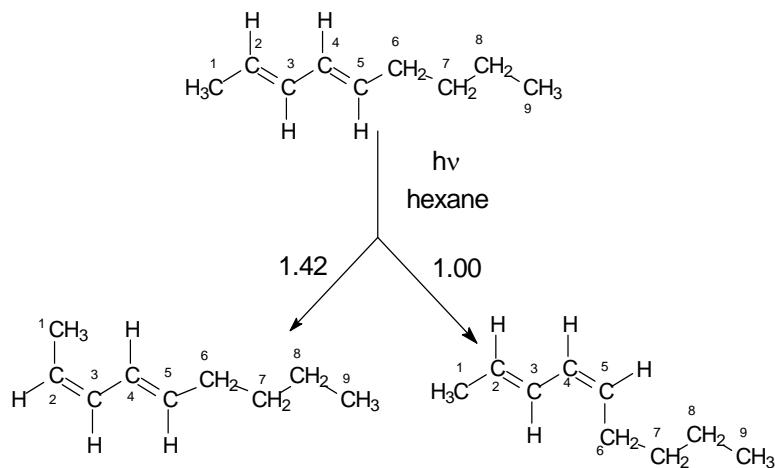


**Figure 1.72** Photoproducts from EE-ND irradiation in hexane and their relative ratio.



We also examined the photochemical conversion of EE-ND to EZ- and ZE-ND in propionitrile (**Figure 1.73**). The photoregioselectivity observed in this solvent ( $1.39/1 = \text{ZE}/\text{EZ}$ ) remained virtually the same as that seen with the nonpolar hexane. The absence of any change in regioselectivity of the

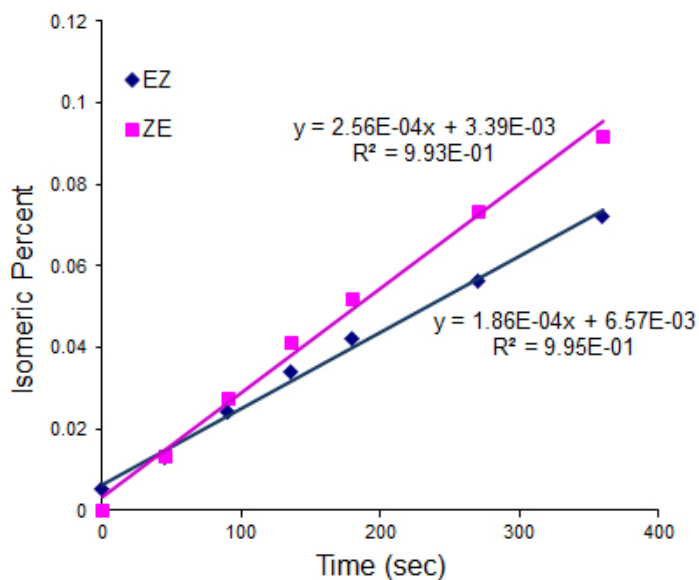


**Figure 1.73** Low percent photochemical isomerization of EE-ND in propionitrile.

photoisomerization of this molecule, in polar and non-polar solvents, suggests that there are no major charge effects determining which bond preferentially photoisomerizes. Supporting this conclusion is the observed photoregioselectivity of EE-ND (1.4), which is higher than

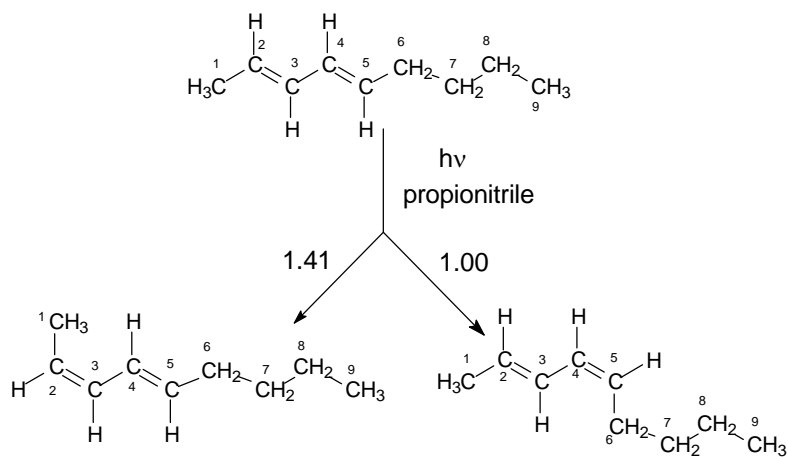


**Figure 1.74** Photoproducts from EE-ND irradiation in propionitrile and their relative ratio.

that seen for EE-DMH (1.2), regardless of the fact that the relative charge-stabilizing effects of the methyl and n-butyl groups of ND should be much closer than those of the methyl and t-butyl groups of DMH. This similarity should give a lower, rather than higher, photoregioselectivity in ND as compared to DMH. The slightly higher photoregioselectivity of EE-ND as compared to EE-DMH may simply be due to solvent restricting motion involving the long n-butyl group.

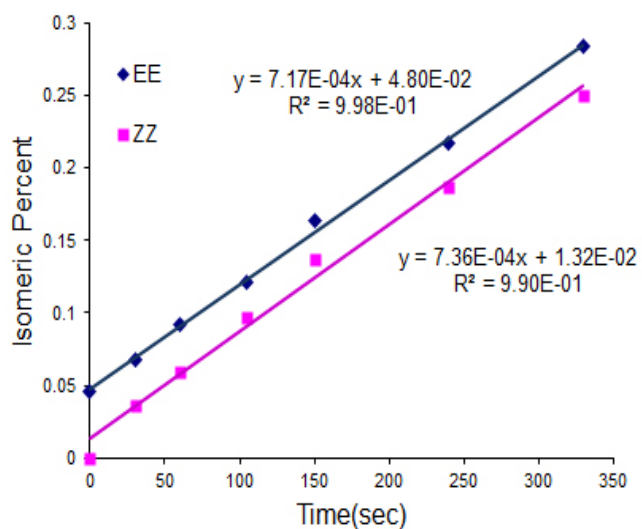


**Figure 1.75** Low percent of photochemical conversion of ZE-ND in hexane.

The ZE isomer of ND has a cis 2,3 double bond which of course is more sterically hindered than this bond in the EE isomer. Yet, in hexane the regioselectivity of ZE-ND is essentially 1 to 1 with no preference given for the isomerization of the more sterically hindered double bond.

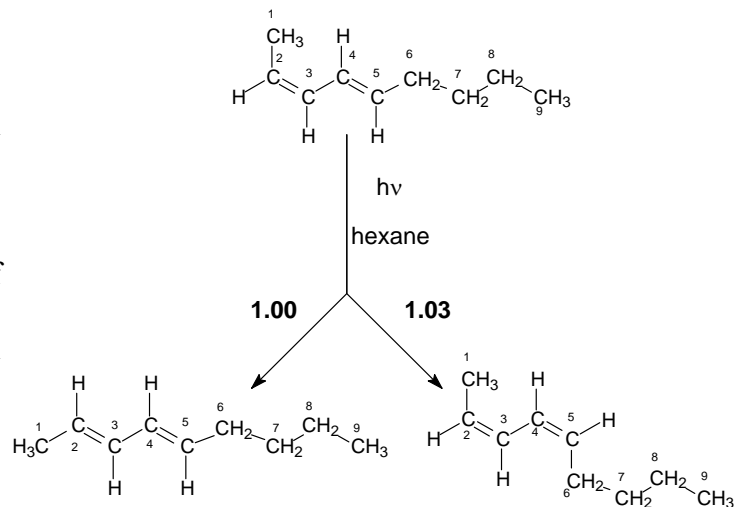


**Figure 1.76** Photoproducts of ZE-ND in hexane and their relative ratio.

The results from the photoisomerization of ZE-ND in propionitrile were similar to those in hexane in showing very little photoregioselectivity (**Figure 1.77**). We actually saw a slight preference (1.3) for rotation about the trans bond substituted with the n-butyl group.

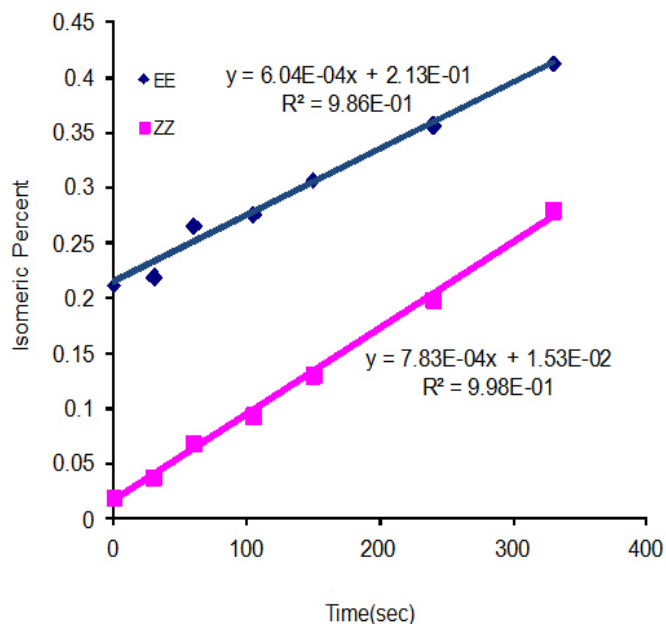


**Figure 1.77** Low percent of photochemical conversion of ZE-ND in propionitrile.

Unfortunately our data on this run shows significantly higher statistical error and so the uncertainty in this number is high. Nevertheless, the fact that there is little selectivity in this molecule suggests again that steric effects are not a dominant controlling factor in the photochemistry of dienes.

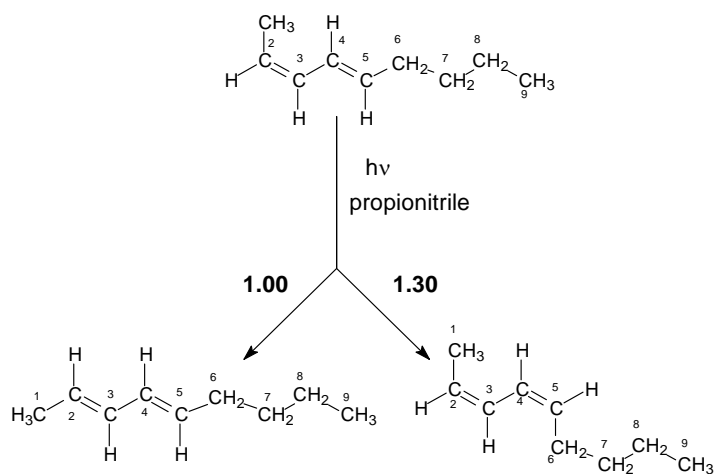


**Figure 1.78** Photoproducts of ZE-ND in propionitrile and their relative ratio.

### 1.3.3. 1,1,1-trifluoro-2,4-hexadiene (TFHD) results and discussion.

In previous studies in our group it was determined that the photoregioselectivity of photoisomerization for EE-FHD varied between 2 to 4 for the ZE/EZ ratio, depending on the polarity of the solvents used, at 25 °C.<sup>139</sup> At lower temperature photolysis experiments, it was found that the regioselectivity increased to ZE/EZ=8.88 in propionitrile (-80 °C).<sup>143</sup> But this regioselectivity is still small compared with that of cis-1-deuterio-1,3-pentadiene (ZE/EZ  $\geq$  25 in ether at 0 °C).<sup>4,74, 5,6</sup>

To further examine the effect of electron withdrawing groups and their charge stabilizing effects in solvents of different polarity, we studied the 1,1,1-trifluoro-2,4-hexadiene (TFHD), which was synthesized as described below.

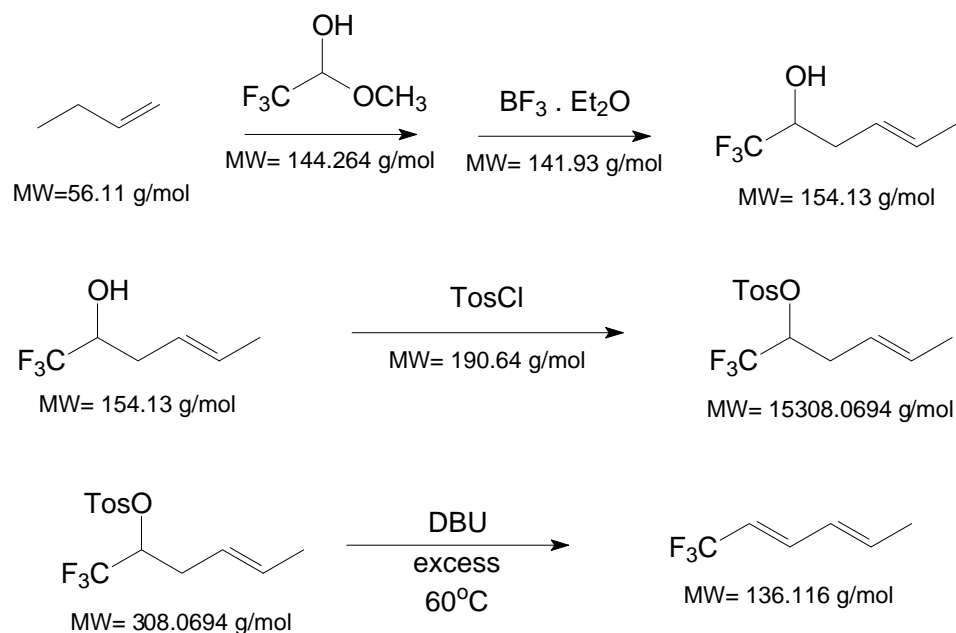


**Figure 1.79** Synthesis path for the preparation of 1,1,1-trifluoro-2,4-hexadiene

For the synthesis of TFHD we chose a tosylate elimination. Initially 1,1,1-trifluoro-4-hexene-2-ol was prepared from a Lewis acid catalyzed ene reaction involving trifluoroacetaldehyde prepared in situ from its hemiacetal and 1-butene. The alcohol was added to a dry pyridine-TosCl solution to form deep purple tosylate. The extraction of this specific tosylate proved to be very challenging as it formed very persistent emulsions. This greatly affected the overall yield of the final product as we never recovered more than 76% of the tosylate. However, the ease of this reaction path for obtaining the TFHD justified its application. The tosylate was eliminated by heating in DBU and the resulting isomeric mixture of TFHD was trapped.

To increase the initial concentration of the EE isomer, we equilibrated the crude solution with iodine (**Table 1.8**). To separate pure EE-TFHD needed for our photolysis experiments, we had to use an elaborate sequence of purification steps using preparative GC (**Figure 1.80**).

**Table 1.8:** Relative percentages of all TFHD isomers before and after I<sub>2</sub> equilibration

Type of sample	EE-TFHD %	EZ-TFHD %	ZE-TFHD %	ZZ-TFHD %
crude	72.001	19.21	6.77	2.02
I <sub>2</sub> equilibrated	86.78	11.55	3.09	0.38

On a GOW-MAC series 580 or 350 GC we first eliminated the ZZ isomer, remaining solvents, by-products and other impurities, by employing a 30'x1/4" 30% OV-17 on Chromosorb P 100/120 mesh column. In order to purify enough EE-TFHD for a photolysis sample, we “prepped” four 45 µL injections of the crude material. All four fractions collected from the OV-17 column contained the ZE, EZ and EE isomers.

To further purify the EE, as well as EZ, the sample was then injected through a 20'x1/4" 20% OV-210 on Chromosorb P NAW 80/100 mesh, which after one run would give us ~98% pure EE. In order to get the necessary 99.5%, or better purity, we had to pass the almost pure sample through the OV-210 column again.

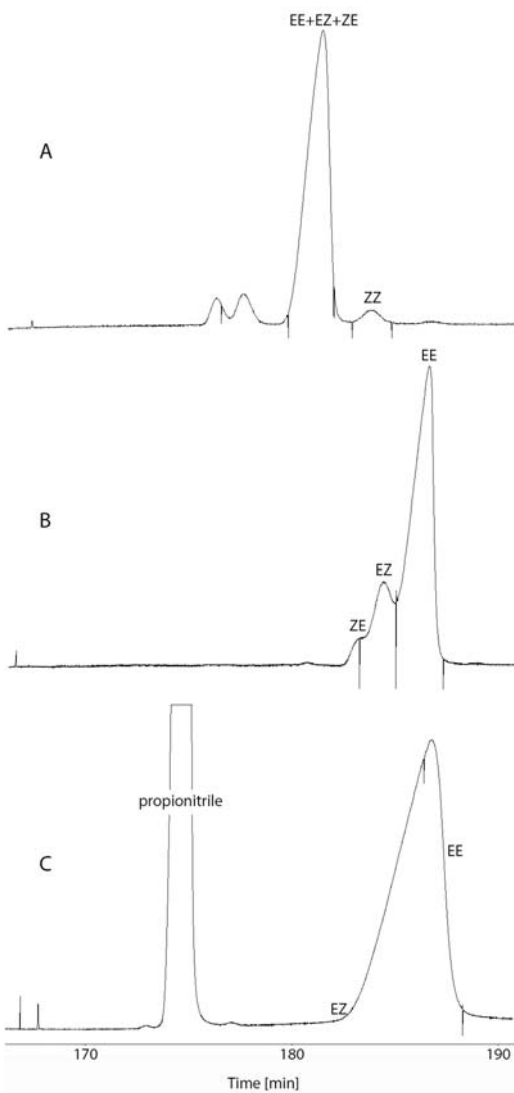


**Figure 1.80** Preparative GC of 1,1,1-trifluoro-2,4-hexadiene: (A) removing ZZ and impurities; (B) separation of EE from EZ and ZZ; (C) purification of B washed in propionitrile.

**Table 1.8:**  $^1\text{H}$  NMR,  $^{13}\text{C}$  NMR and coupling constants of the four isomers of 1,1,1-trifluoro-2,4-hexadiene (TFHD).

EE-TFHD			EZ-TFHD			ZE-TFHD			ZZ-TFHD		
ppm	Hz	Asgn	ppm	Hz	Asgn	ppm	Hz	Asgn	ppm	Hz	Asgn
6.82	$J_{3,\text{F}}=2.07$ $J_{3,4}=9.93$ $J_{2,3}=15.51$	H3	7.20	$J_{3,5}=1.17$ $J_{3,\text{F}}=2.20$ $J_{3,4}=11.19$ $J_{2,3}=15.49$	H3	6.53	$J_{2,3}=10.79$ $J_{3,4}=11.73$	H3	6.94	$J_{3,5}=1.20$ $J_{2,3}=11.67$ $J_{3,4}=12.24$	H3
6.19	$J_{3,4}=9.93$ $J_{4,5}=15.48$	H4	6.12	$J_{4,5}=10.81$ $J_{3,4}=11.19$	H4	6.49	$J_{3,4}=11.73$ $J_{4,5}=14.11$	H4	6.43	$J_{2,4}=1.14$ $J_{4,6}=1.94$ $J_{4,5}=10.96$ $J_{3,4}=12.24$	H4
6.13	$J_{5,6}=6.46$ $J_{4,5}=15.48$	H5	5.94	$J_{2,5}=0.85$ $J_{3,5}=1.17$ $J_{5,6}=7.22$ $J_{4,5}=10.81$	H5	6.15	$J_{5,6}=6.89$ $J_{4,5}=14.11$	H5	6.01	$J_{4,5}=10.96$ $J_{5,6}=7.25$	H5
5.73	$J_{2,\text{F}}=7.17$ $J_{2,3}=15.51$	H2	5.84	$J_{2,6}=0.64$ $J_{2,5}=0.85$ $J_{2,4}=1.09$ $J_{2,\text{F}}=7.19$ $J_{2,3}=15.49$	H2	5.48	$J_{2,\text{F}}=9.28$ $J_{2,3}=10.79$	H2	5.61	$J_{2,\text{F}}=9.28$	H2
1.81	$J_{5,6}=6.46$	H6	1.83	$J_{5,6}=7.22$	H6	1.84	$J_{5,6}=6.89$	H6	1.82		H6
139.67		C5	136.16		C5	141.30		C5	137.068		C5
139.440		C3	133.92		C3	140.48		C3	134.585		C3
129.160		C4	126.81		C4	126.44		C4	123.397		C4
125.160		C1	125.12		C1	124.90		C1			C1
116.410		C2	118.56		C2	114.29		C2	116.33		C2
18.610		C6	13.94		C6	18.70		C6	13.522		C6

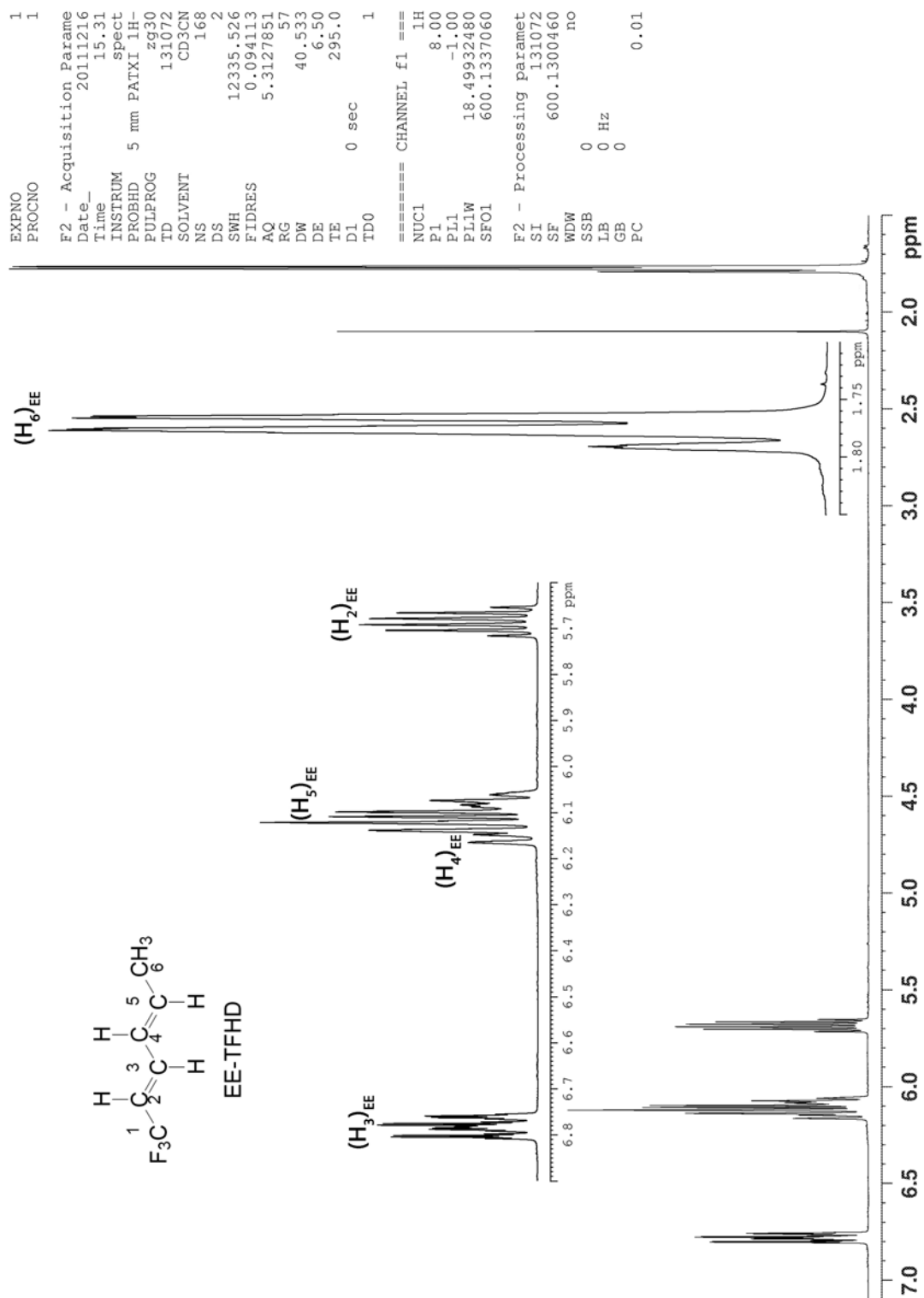


Figure 1.81  $^1\text{H}$  NMR spectrum of EE-TFHD.



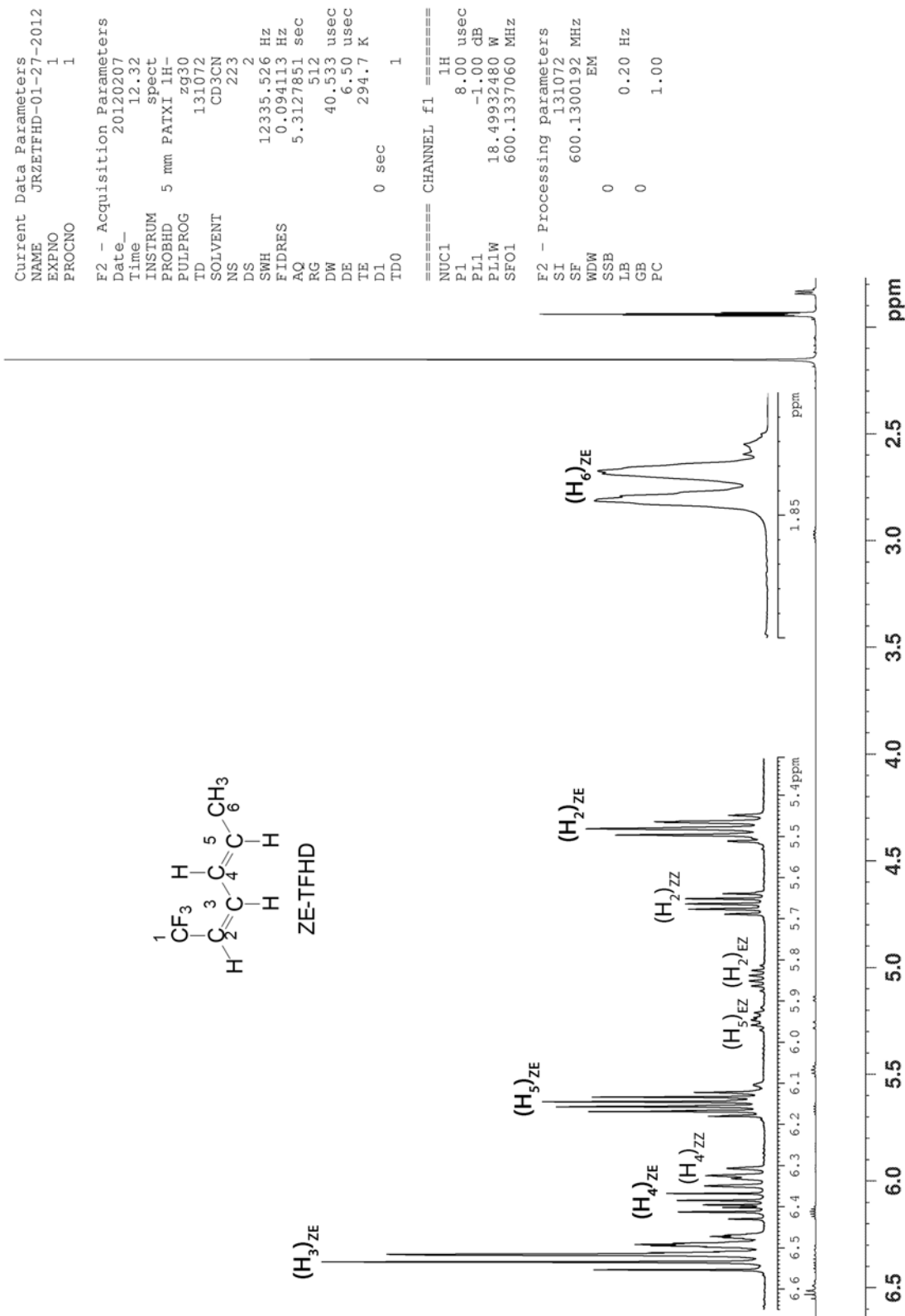
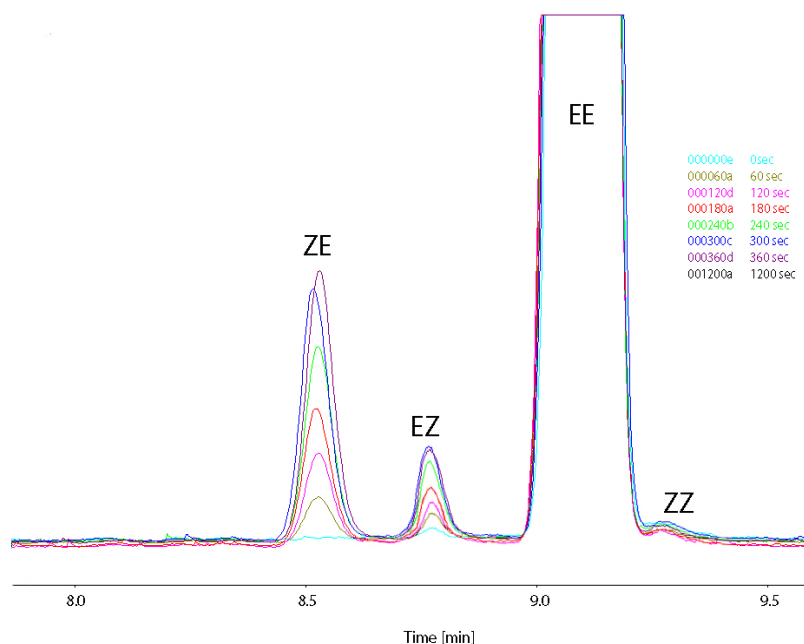


Figure 1.82 <sup>1</sup>H NMR spectrum of ZE-TFHD.

The final collection of pure EE-TFHD (99.5% or better) was 5-8  $\mu\text{L}$  in volume. Even though this procedure allowed us to collect very small amounts of the desired isomers, the quantities were sufficient for microscale photolysis and subsequent analysis.

For the photolysis experiments, 99.9% isomerically pure EE-TFHD is diluted with 100  $\mu\text{L}$  of pure hexane, or in a hexane solution with different concentrations of propionitrile. A 100% propionitrile sample was made as well. Decane ( $\sim 5 \mu\text{L}/\text{sample}$ ) is used as a reference again. The solution is mixed in the same “golf tee shaped” quartz tube (**Figure 1.69**). Three or four 0.5  $\mu\text{L}$  samples are removed via a microliter syringe and examined via analytical GC for each time interval.

We were able to separate all TFHD isomers fairly well on a 30 m x .25mm column, coated with 0.25 $\mu\text{m}$  film of DB-210 (50% - Trifluoropropyl) methyl polysiloxane (**Figure 1.83**).



**Figure 1.83** Analytical GC of the photolysis of 1,1,1-trifluoro-2,4-hexadiene

The photolysis of pure EE-TFHD dissolved in propionitrile until photo equilibrium is reached is shown in **Figure 1.84**.

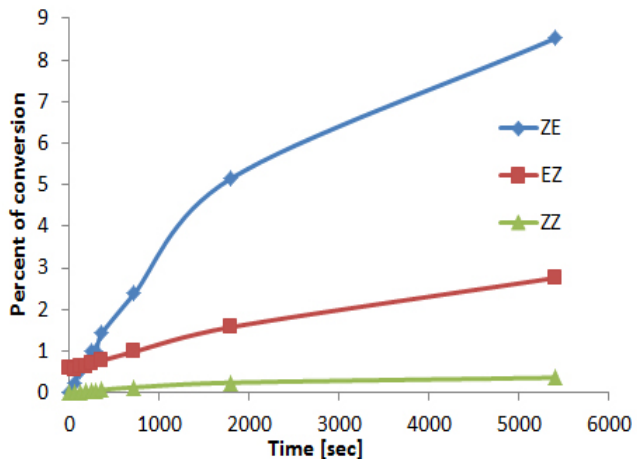


**Figure 1.84** Photoisomerization of EE-TFHD to ZE, EZ and ZZ isomers until photostationary state.

**Figure 1.85** shows the increase of ZE and EZ-TFHD versus photolysis time (in seconds) of a 100% hexane solution of pure EE-TFHD. At the observed small conversions (less than

5%) neither back photolysis nor cyclization occurs. The ratio between the ZE and EZ indicates that the double bond substituted with the heavier trifluoro substituent rotates 3.5 (**Figure 1.86**) times more often compared to the double bond bearing the lighter methyl group.

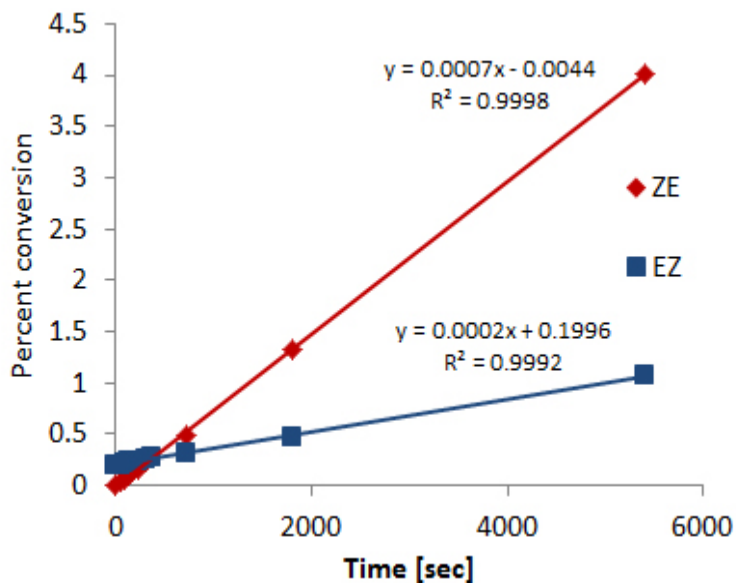


**Figure 1.85** Less than 5% conversion of EE-TFHD to ZE and EZ isomers (hexane; 254nm; 0°)

This result indicates charge stabilization must be playing a large role in determining the regiospecificity of double bond rotation of TFHD.

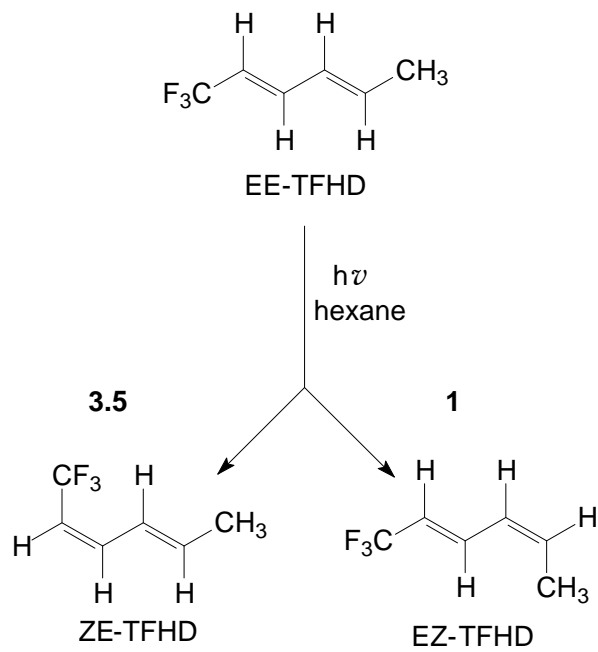


**Figure 1.86** Photoisomerization of pure EE-TFHD in 100% hexane solution.

To ensure that our results were representing aspects of the singlet excited state pathway we examined the triplet state photochemistry. A 100  $\mu$ L hexane solution of 99.525%

EE-TFHD and benzophenone as triplet

sensitizer was prepared. The results of the photolysis are plotted in **Figure 1.87**. Unlike the results of the direct photolysis (**Figure 1.84**), the ZZ isomer's formation shows no delay in its formation, i.e. it is now a primary photoproduct. It is interesting to point out that in this experiment the lighter double bond with methyl group exhibits 1.61 times higher preference of rotation rather than that with the trifluoro substituent. Considering the results from this experiment, it is safe to say that the reversed photoisomerization preferences, as well as the quantum yield of ZZ are characteristics distinguishing singlet from triplet photochemistry.

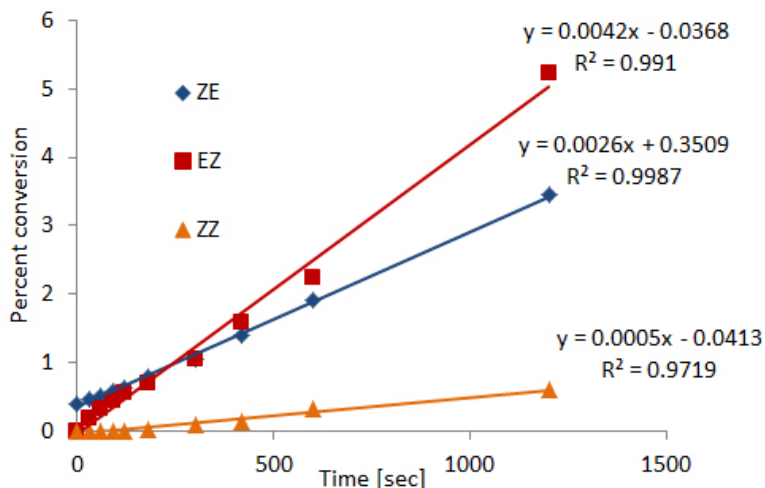


**Figure 1.87** Triplet photochemistry of EE-TFHD to ZE, EZ and ZZ (hexane; 254 nm; 0° C)

The triplet state of a 1,3-diene is considered to be either a 1,4-biradical<sup>152,153</sup> or an

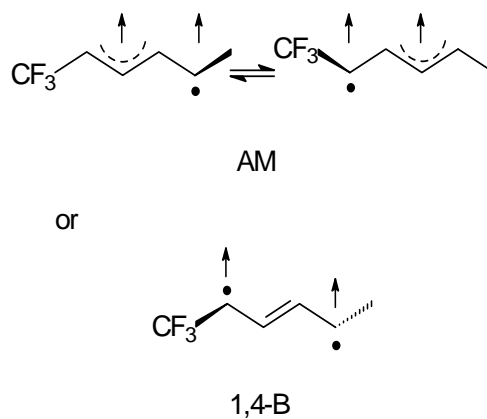


**Figure 1.88** Possible TFHD triplet states

equilibrating pair of allylmethylene biradicals<sup>154</sup> (Figure 1.88). The reversed regioselectivity in triplet photochemistry could be ascribed to the relatively high freedom of bond rotation in these species. However, this will only be true if the triplet lifetime is shorter than the rotation rate of the two double bonds. With longer triplet lifetimes the regioselectivity

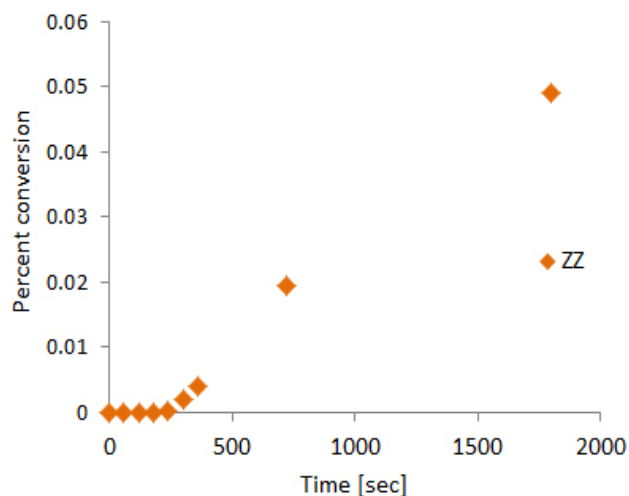


**Figure 1.89** Initial delay of ZZ-TFHD formation from EE-TFHD in degassed and sensitizer-free solution (100% hexane; 254 nm; 0° C).

will be determined by the ratio of conformers established by the triplet state.

The role of a charge stabilizing effect dominating the photoregioselectivity was further examined by performing the direct photolysis in the very polar solvent, propionitrile (Figure 1.90). In this solvent, the

data showed that the double bond substituted with the heavier, but highly electronegative, trifluoromethyl substituent photoisomerizes 4.75 times more often than the double bond with the lighter methyl substituent (Figure 1.91), a 36% increase in

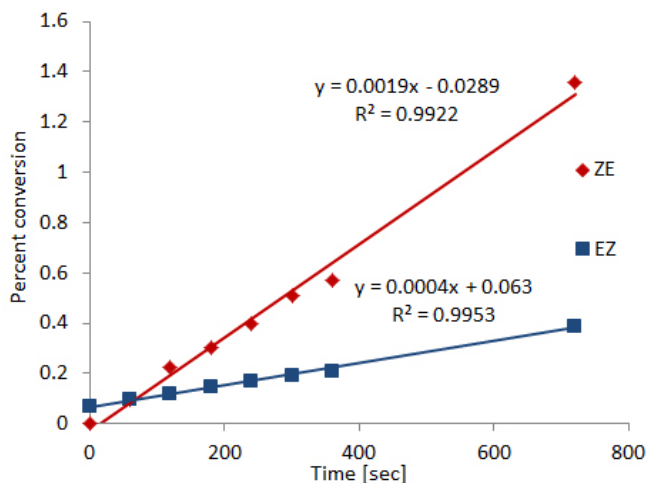


**Figure 1.90** Less than 2% conversion of EE-TFHD to ZE and EZ isomers (propionitrile; 254 nm; 0°).

the regiospecificity as compared to that found using hexane as the solvent. This solvent effect on the photoregioselectivity shows again that the excited state pathways include charge separation.

To further establish that this change in photoregioselectivity is caused by a change in polarity of the solvent, we investigated the effect of gradually changing solvent polarity on the photoregioselectivity of EE-TFHD.

We used  $E_t^{155,156}$  as a measure of the polarity of hexane/propionitrile mixtures. The  $E_t$  value is based on the absorption maxima of Reichardt's dye which can be determined very rapidly in the hexane/propionitrile solvents. Upon photochemical excitation the dye converts from neutral to zwitterionic species, which means that polar solvent will stabilize the absorption maximum when charge is developed. In **Table 1.9**<sup>157</sup> are presented the  $E_t$  values in kcal/mol and  $\lambda_{\max}$  for the hexane/propionitrile solvents with variable concentrations of propionitrile. The  $E_t$  values indicate that the polarity of the system increases very rapidly at low levels of propionitrile. When the concentration of the polar solvent reaches

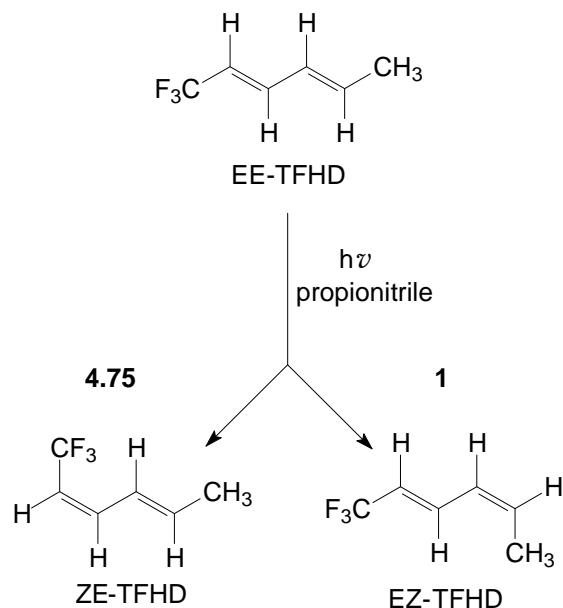


**Figure 1.91** Photoisomerization of EE-TFHD in propionitrile

**Table 1.9:** Determination of solvent polarity of propionitrile-hexane system using Reichardt's dye at RT.

conc. (%)	Wavelength (nm)	$E_t$ (kcal/mol)
0	922	30.9
3	762	37.4
5	724	39.4
10	704	40.5
20	686	41.6
40	672	42.4
70	662	43.1
100	650	43.9

20% or higher, the polarity of the solution changes very little and reaches a plateau of  $E_t$  values between 41 and 42 kcal/mol. The photoregioselectivity of EE-TFHD increases in exactly the same fashion (**Figure 1.93**). The fact that the photoregioselectivity of EE-TFHD mimics this change in solvent polarity, indicates that electrostatic effects must play a significant role in the regioselectivity of the photoisomerization of TFHD.

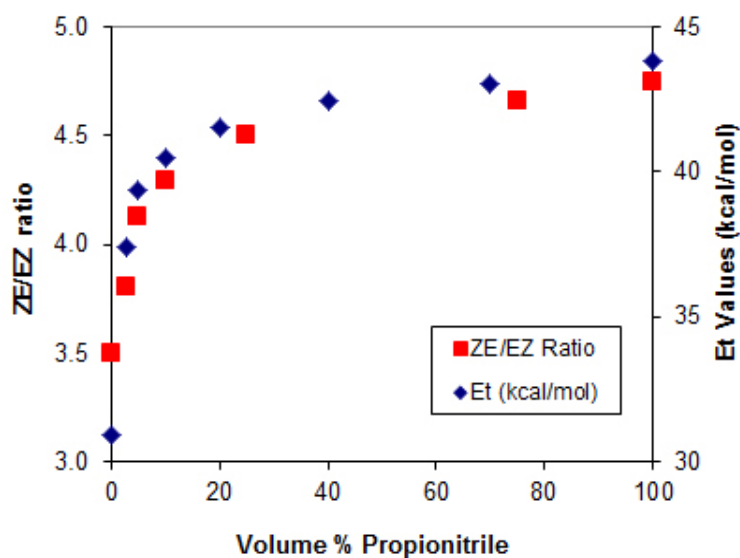


**Figure 1.92** Photoregioselectivity of EE-TFHD (254nm; 0° C) and  $E_t$  value of a mixed propionitrile-hexane solvent system.



#### 1.4. Conclusions

As mentioned earlier, the two lowest excited states of 1,3-dienes are considered to be  $1^1B_u$  and  $2^1A_g$ , where the  $1^1B_u$  is lower in energy.<sup>36,37,38,39,40,41,42,43,44</sup> After a photochemical excitation, the diene will be brought to the Franck-Condon region (FC) of the photochemically allowed  $1^1B_u$  state. From there, two possible pathways must lead to one of two possible conical intersections, i.e. isomerization about one or the other double bond will occur. Thus a major part of the selectivity of this isomerization occurs on the  $1^1B_u$  surface and it is here that the photoregioselectivity is determined.

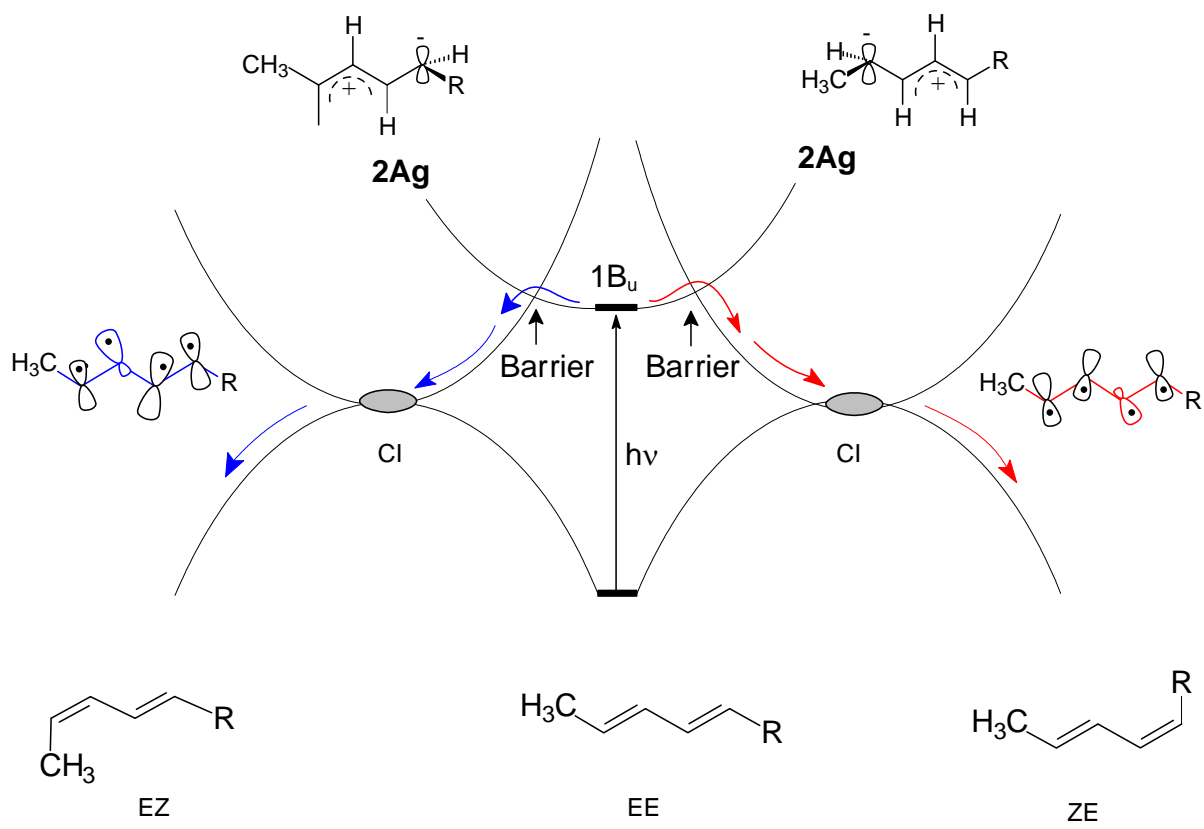
The results for EE-DMH indicate that there is no significant regioselectivity of the photoisomerization of the double bond bearing the lighter methyl group. This experimental result suggests that the mass related momentum of the substituent cannot be considered as a deciding factor in the regioselectivity of rotation, though the slight preference for rotation about the double bond substituted with the methyl group may be attributed to this mass effect. The small regioselectivity observed may also depend on the ability of the methyl group to stabilize charge better than a t-butyl group, though the lack of solvent effects on the photoregioselectivity argues against this as an explanation.

The results for the photochemistry of EE-ND are very similar to those observed for EE-DMH. However, a slightly higher preference for photoisomerization about the double bond substituted with the lighter methyl group is observed. Just like with EE-DMH, the photoregioselectivity was not affected by polarity changes of the solvent. These results again point to the mass of the substituent playing an insignificant role in determining the photoregioselectivity of the isomerization. The slight increase in the preference for rotation

about the methyl substituted double bond, compared to EE-DMH, along with the absence of a change in the photoregioselectivity when the solvent polarity is changed, suggests that charge stabilizing effects are not responsible for the small selectivity in either EE-DMH or EE-ND. Differences in charge stabilizing effects of the two substituents should be smaller in ND than in DMH, and would have led to a decrease in selectivity rather than the slight increase observed. We believe that the slightly larger photoselectivity in EE-ND came from viscosity effect, caused by the extended geometry of the n-butyl group.

The fact that EZ isomer of DMH displays only a 3-fold preference for photoisomerization of the t-butyl substituted bond while the ZE isomer of ND shows almost no preference suggests that steric effects do not have an overwhelming degree of control over the regioselective photoisomerization of a polyene. These results raise serious questions about the role of the C-12 methyl group of retinal.

A representation of these possible routes for the formation of the EZ and ZE isomers from EE-DMH and EE-ND, with the slightly lower barrier leading to EZ, is shown in **Figure 1.93**.



Where R=n-Bu; t-Bu

**Figure 1.93** Possible routes of photochemical isomerization of EE-DMH and EE-ND

Unlike DMH and ND, TFHD, with the introduction of the  $\text{CF}_3$  group at one terminus of a 1,3-diene system, shows a substantial photoregioselectivity. Just like with the DMH and ND, the two possible pathways from the Franck-Condon point of the  $1^1\text{B}_u$  surface would lead to distinct CI's. However, in the case of TFHD the charge stabilization effects of the substituents dominate which pathway is traversed. The pathway leading to the formation of ZE-TFHD is expected to be more polarized than that leading to the EZ isomer because of the match between the developing charge and the charge stabilizing effects of the substituents. This polarity difference explains the observed photoregioselectivity, but also the observed increase in the photoregioselectivity when solvent polarity is increased. This introduction of a polar solvent will stabilize the more polarized pathway preferentially and lead to a higher photoregioselectivity.

A representation of the possible route for the formation of EZ and ZE isomers from EE-TFHD, with the lower barrier leading to ZE, is shown in **Figure 1.94**.

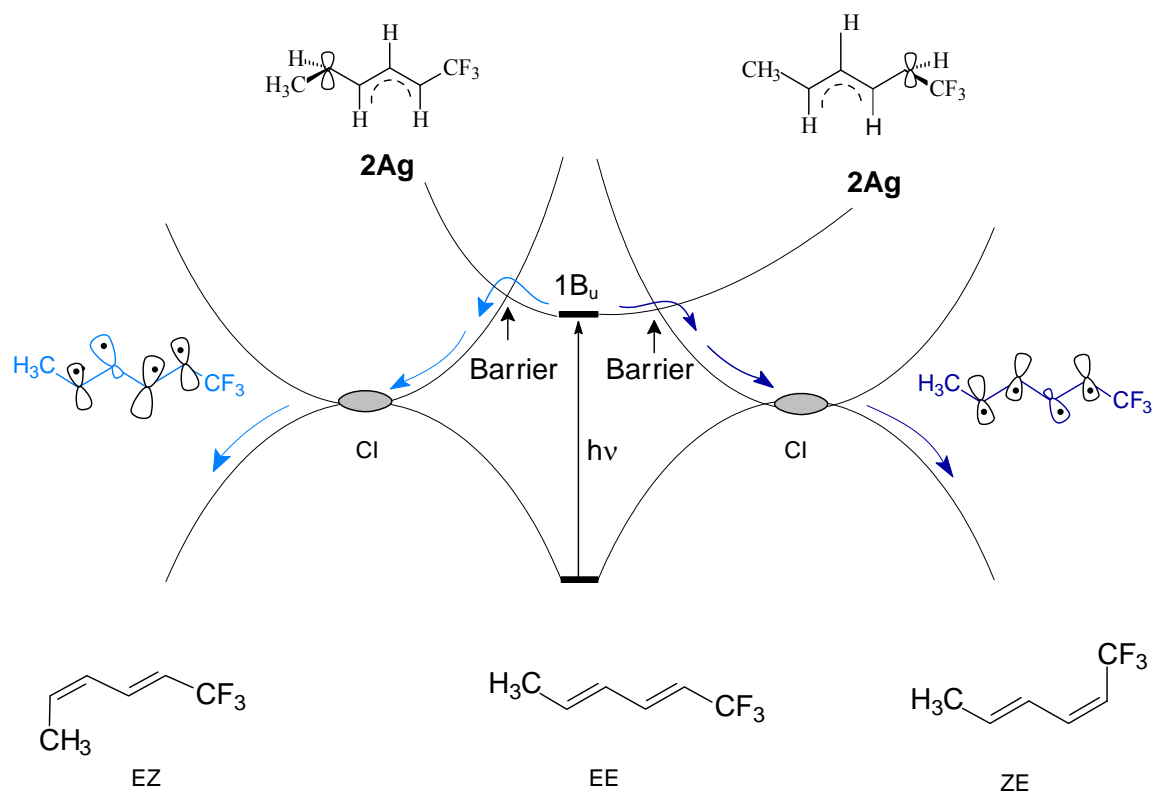


**Figure 1.94** Possible route for the photoisomerization of EE-TFHD

## 1.5. Future research

When initially investigated the mono-deutero substituted diene exhibited a ~20:1 preferential ratio of rotation around the double bond bearing the D atom, as shown in **Figure 1.95**.

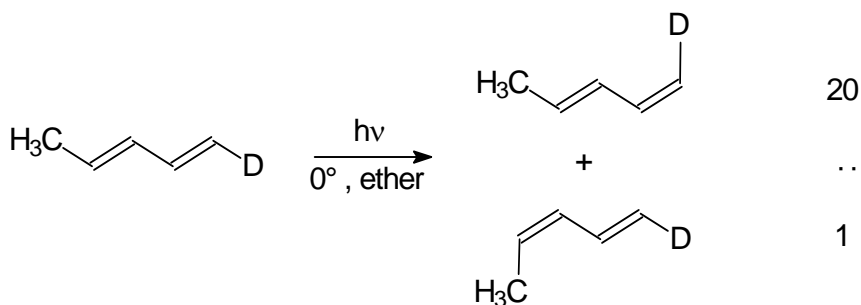


**Figure 1.95** Photoregioselectivity of 1-deutero-1,3-pentadiene in low temperature conditions.

To achieve even greater photoregioselectivity, we introduced the trifluoromethyl group.

The assumption was that with the introduction of negative charge stabilizing substituent, the energy gap between the formed zwitterions would increase (as shown in **Figure 1.96** right), and so TFHD was expected to show an increase in the photoregioselectivity. However, our experimental results showed a decrease! Thus the origin of the remarkable photoregioselectivity of

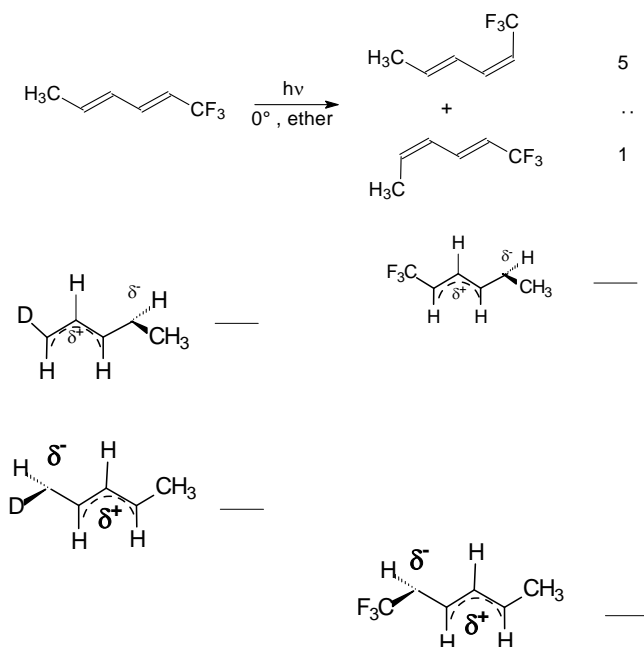


**Figure 1.96** Expected charge stabilizing effect on the energy gap between  $Z_{1B}$  and  $Z_{2B}$ .

the pentadiene system is yet to be explained. In particular it must be established if there is a solvent polarity effect on this system. If so, then the large regioselectivity of the photochemistry of the pentadiene system would have to be explained by an increase in the developing charge along the pathways leading from the Franck-Condon state. If solvent polarity has no effect on the rotational preference then it is likely that mass effects are playing a role in this system.

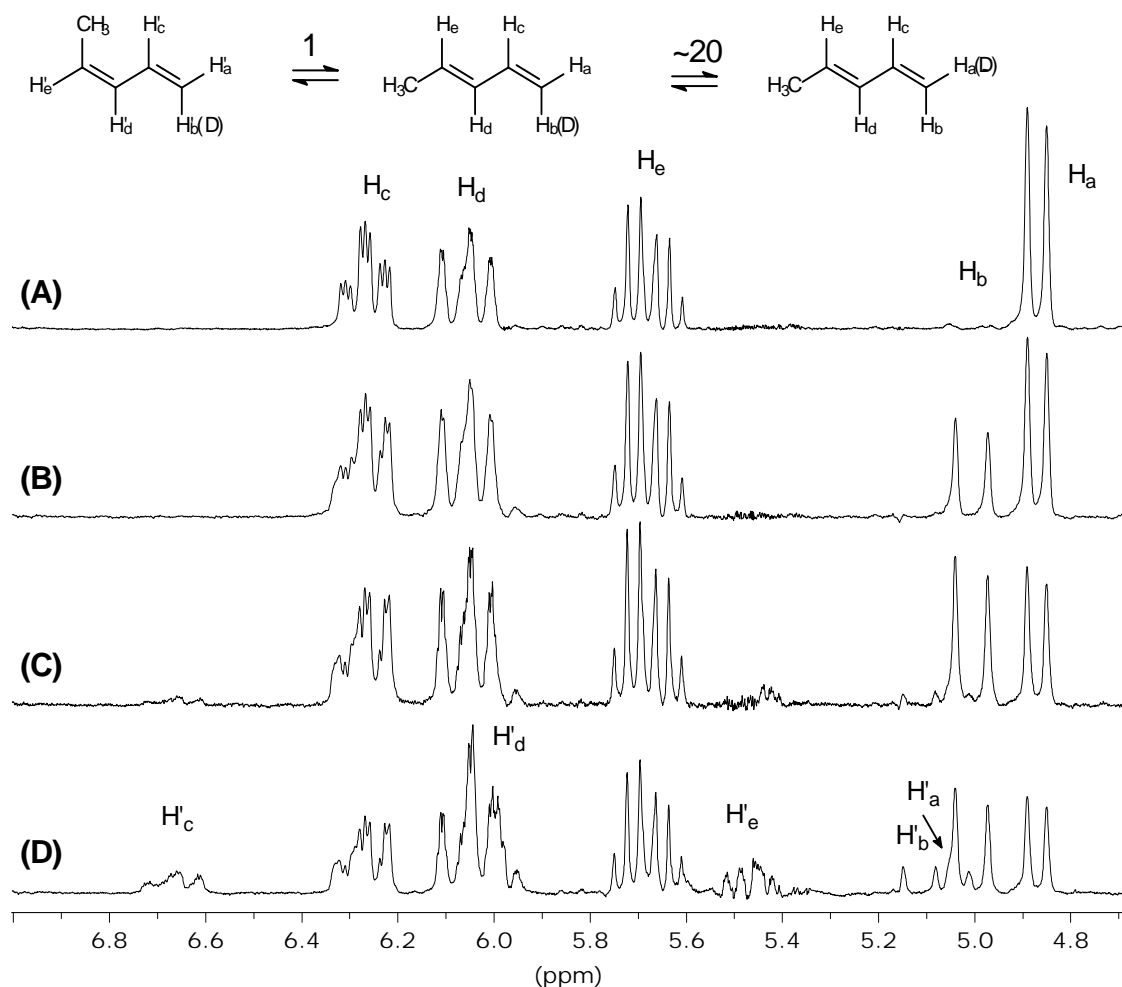


**Figure 1.97** 250-MHz  $^1\text{H}$  NMR of a 1% solution in diethylether of (A) *cis*-1-deutero-*trans*-1,3-pentadiene; (B) after 2 min of photolysis with a 1000W Hg(Xe) arc lamp at  $0^\circ\text{C}$ ; (C) after 30 min and (D) after 8 h of photolysis.

As described in section **1.1.6.**, Squillacote and Semple<sup>158</sup> investigated the photochemistry of *cis*-1-deuterio-*trans*-1,3-pentadiene (**Figure 1.33** diene A). After 2 minutes of irradiation time, about 25% of the deuterium substituted double bond has isomerized (**Figure 1.97** spectrum B), while the double bond bearing the methyl group does not show any signs of rotation, i.e. lack of H'<sub>c</sub> peak formation. Given the signal to noise ratio of this spectrum, they estimated an approximately 20 times higher preferential photoisomerization of the deuterium substituted double bond. However, they could not obtain an accurate integration due to the overlap of H<sub>b</sub> peak of *trans*-1,3-pentadiene with the H'<sub>a</sub> peak of *cis*-1,3-pentadiene. To obtain more accurate integration data and repeat the experimental photoregioselectivity, we need to eliminate the overlap between the peaks of H<sub>b</sub> in *trans*-1,3-pentadiene and peak H'<sub>a</sub> in *cis*-1,3-pentadiene. This could be accomplished by collapsing the terminal vinyl hydrogen doublets by having a deuterium at the H<sub>c</sub> position, i.e. by synthesizing *cis*-1,2-dideutero-*trans*-1,3-pentadiene (DDPD).

As higher signal to noise spectrum could be achieved with longer sample scans, the synthesis of the DDPD proved to be very challenging.

After multiple attempts, it came apparent that there were three major flaws of the route described in **1.2.7.3.**: (1) it gave very low yields; (2) because the tosyl-hydrazide is not very soluble in water, simply exchanging the hydrogens in a D<sub>2</sub>O slurry proved to be very difficult, leading to partially protonated pentadiene molecules and (3) there was partial isomerization of the double bond bearing the two deuterium atoms, i.e. producing *trans*-1,2-dideuterio product instead of *cis*-1,2-dideuterio product. Also, after GC purification and separation of the different fractions, we noticed a large increase in the



*trans*-1,2-dideutero-*trans* pentadiene, a problem which we later found to originate from the acid washed Alltech OV-17 packed column used to prep the sample.

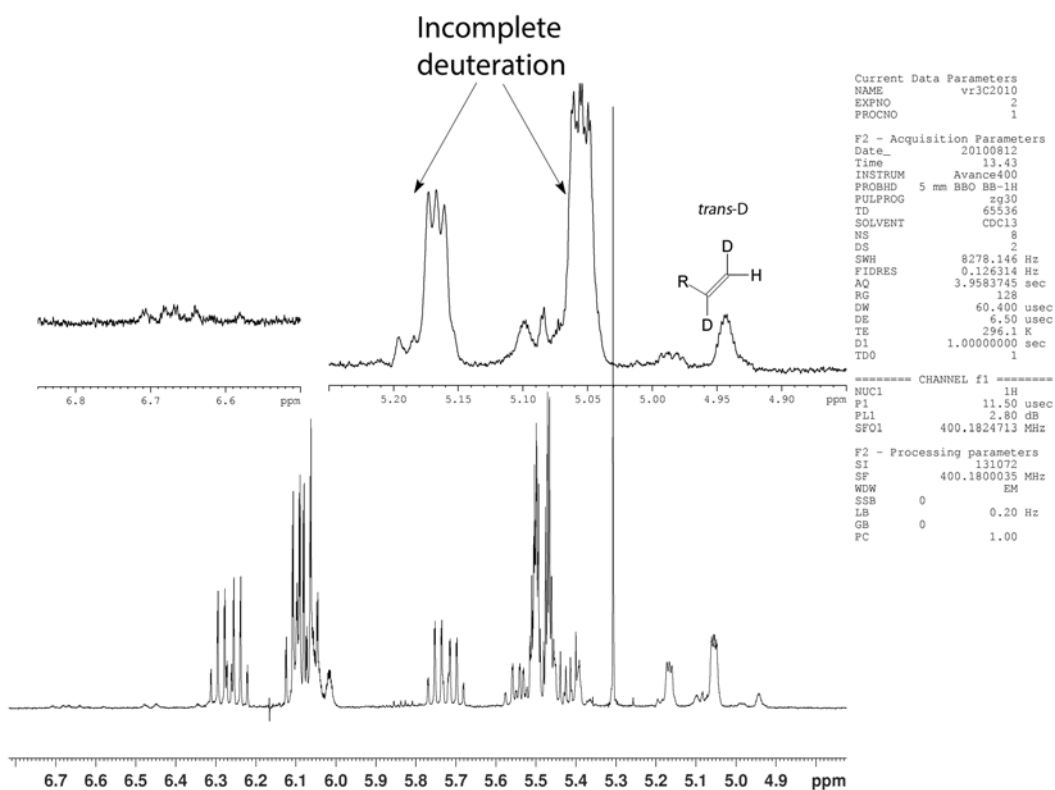


**Figure 1.98** Incomplete deuteration of the hydrazine leads to partially protonated product. Also the presence of *trans*-deuteration is detected.

After locating the source of the isomerization during purification, we tried to address the problem of low yields by changing the molar ratio of ene-yne to tosylhydrazide from 1:1.1 to 1:3 and 1:5. However, but there was no improvement of the yield in any of these attempts.

The incomplete exchanges persisted through all molar ratio-varied synthesis as well. To eliminate this problem we tried to diminish the presence of H by taking several precautionary measures, i.e. all glassware was flame-dried prior use, the NaAc was exchanged with D<sub>2</sub>O prior to every use. Unfortunately, the problem persisted and the deuterium exchanges remained incomplete. As a result, we increased both the volumes of D<sub>2</sub>O used in each wash as well as the temperature so as to dissolve the tosylhydrazide more. These modifications however, did not help as the incomplete exchanges persisted.

We felt that the low solubility in tosylhydrazide in water was the reason we got poor exchange so we investigated to use of solvents for the exchange. The criteria for these solvents were: a large solubility of the tosylhydrazide, the solvent needed to be immiscible with water but also needed to be able to dissolve substantial quantities of water to engender the exchange and finally boil high enough to be easily separable from the pentadiene product.

In **Figure 1.99** is shown the <sup>1</sup>H NMR vinyl region of the commercially available 1,3-pentadiene (Sigma Aldrich; magenta spectrum) and DDPD (green, red and blue) synthesized at various conditions and synthesis procedures we tried.

In the green spectrum is shown the <sup>1</sup>H NMR of poorly exchanged 1,2-dideutero-1,3-pentadiene synthesized using procedure **1.2.7.3**. The poor exchange is evident by the presence of H<sub>c</sub>' and H<sub>c</sub>' peaks at 6.7 and 6.3 ppm respectively. At ~4.9 ppm some isomerization of the dideutero substituted double bond is seen as well.

The red spectrum shows the <sup>1</sup>H NMR of DDPD, synthesized in quinoline solution. The synthesis was carried out following procedure **1.2.7.4**. When using quinoline as the reaction

solvent, the deuterium exchange was very good, as evident by the absence of the  $H'_c$  and  $H_c$  peaks, however substantial isomerization persisted as a problem. This isomerization was probably induced by the quinoline, because it was used not only as the solvent for the deuterio-exchanges, but also acted as the base in the elimination of the tosylate group to produce the diimide. It may be that some electron transfer mechanism involving the quinoline is causing isomerization, but we are not certain.

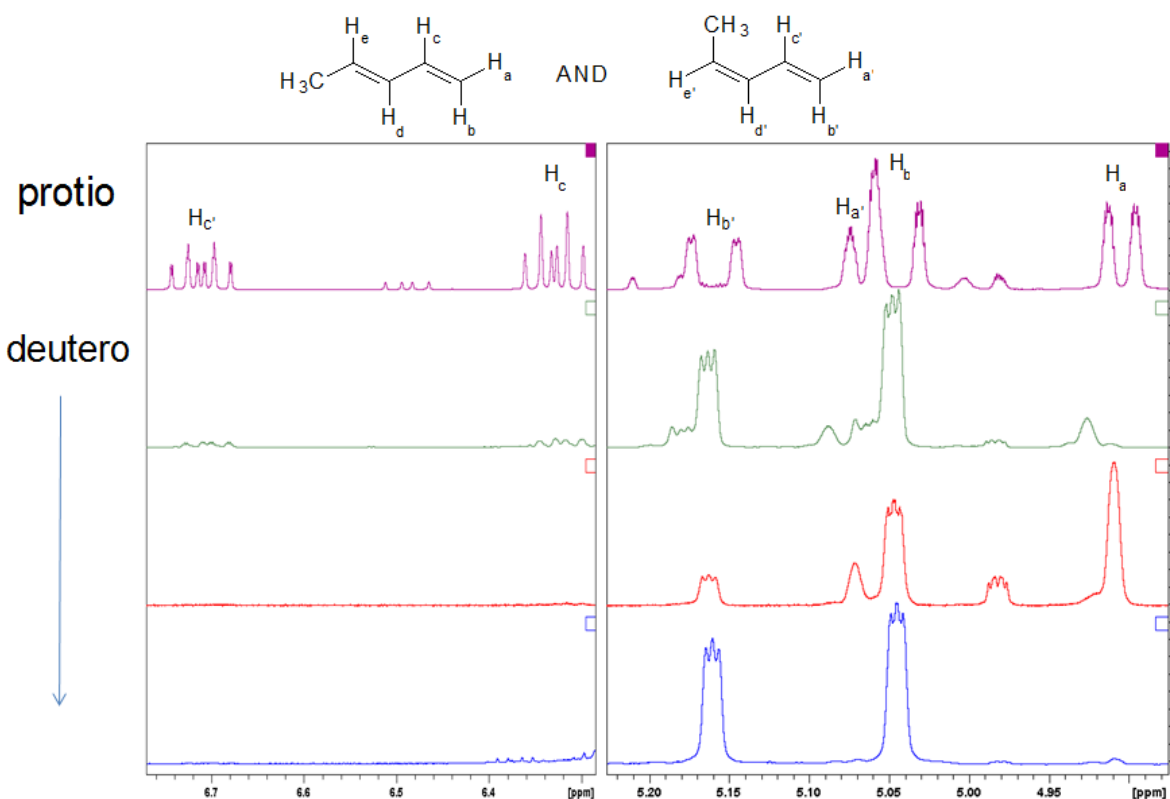


**Figure 1.99** Deuterium exchange and isomerization problems in the synthesis of 1,2-dideutero-1,3-pentadiene.

The blue spectrum shows the  $^1H$  NMR of DDPD synthesized in propionitrile solution. The synthesis was carried out following procedure 1.2.7.7. In this reaction we did not use

an external base, but rather left the TosNDND<sub>2</sub> itself to act as the base necessary to eliminate the Tos group. Our preliminary results indicate that the propionitrile is excellent environment not only for the deuterium exchanges, since no visible protons are observed for H<sub>c</sub> and H<sub>c'</sub>, but also for the stereospecific deuteration since there is very little H<sub>a</sub> present. Purification and photoisomerization in hexane and propionitrile of this diene will allow us to determine if charge effects is an important factor in this molecule's photochemistry.



## CHAPTER II

### STABLE TRANS CYCLOHEPTENES

#### 2. Stable trans cycloheptenes

##### 2.1. Introduction

The discovery of isomers and their different categories has repeatedly led to a greater understanding of chemistry. The realization of constitutional isomers by Wöhler, Liebig and Berzelius led to the structural theory of chemistry, i.e. that molecules were constructed of atoms bonded together in certain patterns. The discovery of stereoisomers by Pasteur and the possibility of rotating plane of polarized light, led van't Hoff and Pauling to the idea of the tetrahedral nature of the carbon atom.<sup>158</sup>

##### 2.1.1. Double bonds History

In the 19th century, scientists recognized that they needed to explain the linkage of atoms involving more than one bond.<sup>159,160,161</sup> It was again J. H. van't Hoff<sup>162</sup> who suggested the idea of connecting two carbon atoms in a double bond by linking two of the valencies of each tetrahedral atom (**Figure 2.1**). The stereochemistry shown, leaves the remaining four



**Figure 2.1** Double bond formation between two carbons, following Van't Hoff's idea of connecting two tetrahedral valencies of each atom, all laying in the plane of the paper.

available valences in the same plane with the carbon atoms. The proposed structure suggests

that rotation between the carbon atoms with respect to one another would be difficult, as a such rotation (twisting) would diminish the contact of the valances and break the double bond. Van't Hoff's proposal was one of the very first attempts to explain the double bond's nature. In the late 1920's, when the wave function for the hydrogen molecule was developed<sup>163,164,165</sup> a new picture of the double bond emerged.

### 2.1.2. Trying to understand character of double bond

In 1930 Hückel<sup>166</sup> proposed  $\sigma$ - $\pi$  model of the carbon-carbon double bond, inspired by his work on quantum theoretical treatment of molecular oxygen  $O_2$ .<sup>167</sup>

Because of Hückel's idea of trigonal C atoms and his later explanation of "the benzene problem",<sup>168</sup> he is considered the

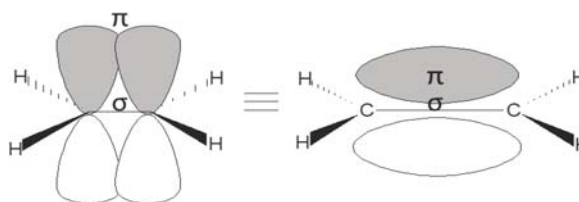


**Figure 2.2** Hückel's trigonal representation of double bond formation between two carbon atoms in the molecule of ethylene. The unhybridized  $p_z$  orbitals of both carbons overlap above and below the single sigma bond.

creator of what became the standard model of the double bond's structure (**Figure 2.2**).<sup>169</sup>

One year later Pauling<sup>170</sup> and Slater<sup>171</sup> developed a quantum mechanical description of the ethylene molecule as well. They represented the two C-C bonds as overlapping, and equal in nature, i.e.  $sp^3$  hybridized orbitals. In essence their quantum mechanical description was very

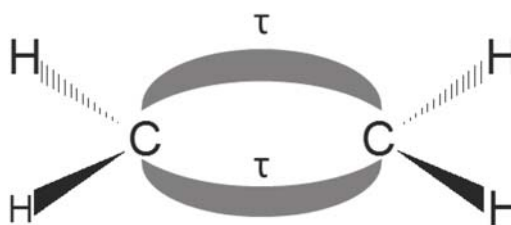


**Figure 2.3** Pauling's bent bonds representation of the double bond, formed in the molecule of ethylene.

close to Van't Hoff's representation of the double bond. The  $sp^3$  orbitals used in their models, correspond to the tetrahedral carbon atom spacial configuration. The proposed

double bond is formed by two tetrahedra sharing an edge. The triple bond was explained as two tetrahedral atoms sharing a face. Later in the 20<sup>th</sup> century their model became known as the bent bond or banana description of a double bond (**Figure 2.3**).<sup>172</sup>

The introduction of these models, however, could explain another type of isomerism.<sup>173,174</sup> In 1874 van't Hoff proposed the structural formula of *cis*-maleic acid and *trans*-fumaric acid (**Figure 2.4**) as examples of

geometric isomerism. Indeed, geometric isomers were initially termed “maleoid” or “fumaroid” before these terms were dropped and the *cis*-*trans* terminology of Bayer was generally adopted.

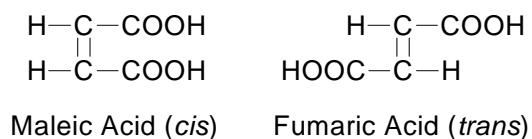


**Figure 2.4** Van't Hoff's structures of *cis*-Maleic and *trans*-Fumaric acids

### 2.1.3. Strain in double bonds

Introducing strain has added to our understanding of the bonding character of a double bond. A double bond can be strained in two ways - twisting and bending.<sup>175</sup> In **Figure 2.5A**, the twist angle is defined as the angle between the two planes made of C1R'R'' and C2R''R'''. The angle is easily apprehended as the free rotation around the axis of the double bond, i.e. misalignment of the p<sub>z</sub> orbitals



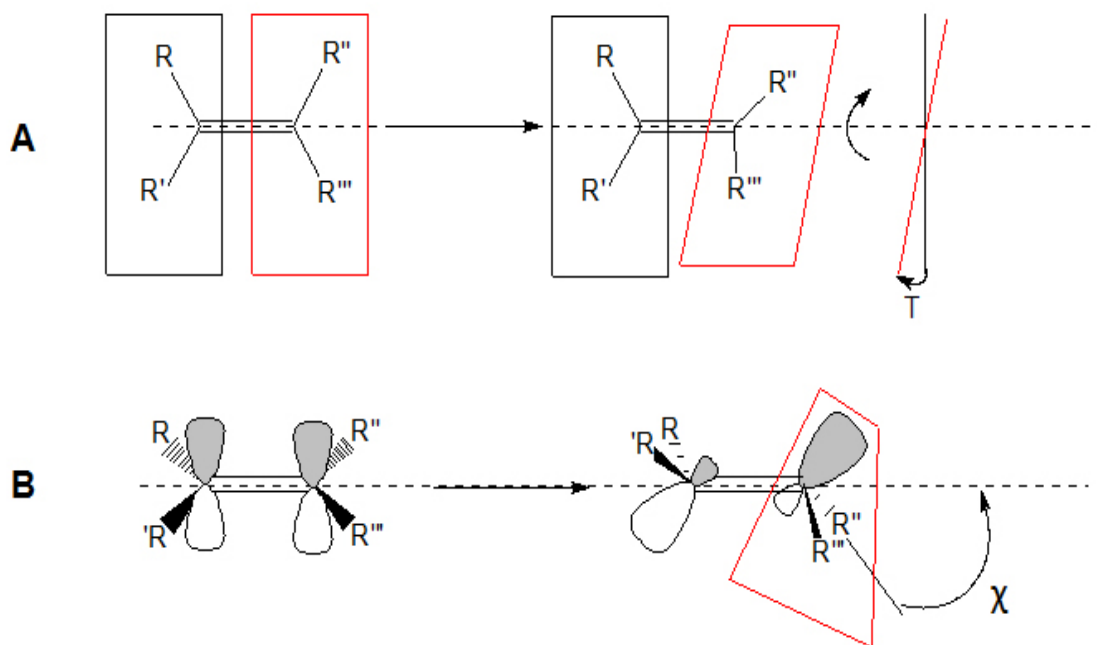


**Figure 2.5** Twisting (**A**) and bending (**B**) distortions in a double bond. With **T** is marked the angle of twisting; angle **P** denotes the angle of pyramidalization (bending).

**Figure 2.5B** shows a planar alkene which has a  $p_z$  orbital attributed to each carbon atom. When the molecule is distorted (in this case in an anti sense), the carbons of the double bond rehybridize and so pyramidalize. As discussed below  $\chi$  is considered to be the pyramidalization angle as defined by Borden. As long as the  $\chi$  angle does not exceed  $54^\circ$ , the system can still be identified as a double C=C bond.<sup>180</sup> Note, that a symmetric bending distortion will also result in pyramidalization.

## 2.2. Understanding the formation of strained geometries of cyclic alkenes

### 2.2.1. Pyramidalization angle

Pyramidalized alkenes are molecules containing C-C double bonds in which one or both of the doubly bonded carbons do not lie in the same planes as the three atoms attached to it. If, even at geometries where the doubly bonded carbons are constrained, the two faces of the

double bond are nonequivalent, the probability of the doubly bonded carbons being exactly planar at the equilibrium geometry is essentially zero. However, the degree of pyramidalization may be so slight as to be undetectable experimentally.

When defining a pyramidalization angle,  $\chi$ , there are two definitions to be considered:

#### 2.2.1.1. Borden's definition<sup>176</sup>

In **Figure 2.6**,  $\chi$  is the pyramidalization angle as defined by Borden. As shown  $\chi$  is the angle between the plane defined by the two R substituents bonded to one of

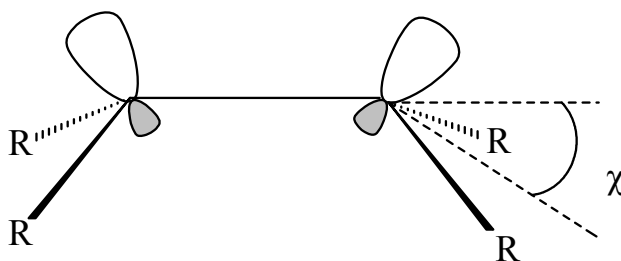


**Figure 2.6** Scheme representation of a pyramidalized alkene by Borden.

and the extended projection of the double bond itself. By applying the bond-angle values of R-C-R and R-C-C in the formula:

$$\cos \chi = -\cos(\text{R-C-C}) / [\cos 1/2(\text{R-C-R})]$$

one can easily calculate the pyramidalization angles,  $\chi$ . Borden's definition of pyramidalization angle is generally used in symmetrical alkenes.

#### 2.2.1.2. Winkler definition<sup>177</sup>

In **Figure 2.7** the pyramidalization angle  $\chi_B$  is defined by the ZBA plane and the dihedral angle with the YBA plane.

The Winkler definition of pyramidalization angle is used for distorted double bonds. This is why, for the planar  $sp^2$ - $sp^2$  double bond the pyramidalization angle's value is close

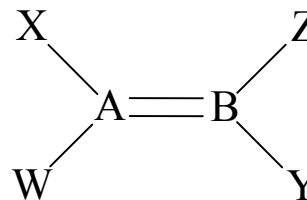


**Figure 2.7** Model to explain Winkler's definition of pyramidalization angle.

to zero. For an  $sp^3$  atom the  $\chi \approx 60^\circ$ . The p-orbital torsion angle  $\tau_{A-B}$  is calculated as the average value of the torsion angles between WABY and XABZ. If the  $\pi$ -orbital is not distorted, the p-orbital torsion angle  $\tau_{A-B}$  is zero.

### 2.2.2. Twisting and pyramidalization

In their careful examination, Wijsmams et. al.<sup>178</sup> examined trans-cycloalkenes, where the two ends of the “bridge” of atoms is connected in a trans fashion to the carbons of the double bond. Because this “bridge” connects two opposite ends of the bond strain will be present. In general the longer the atom chain, the less the strain. However, the intramolecular steric repulsion coming from the interaction between the methylene group at the middle of the carbon chain and the  $\pi$ -orbitals of the double bond will also contribute to the isomer’s strain.

A twisting action is the perfect example on how to break the symmetry of an alkene around the double bond (**Figure 2.8a**). If the two carbon atoms at the double bond still stay fully  $sp^2$  hybridized, the two  $p_z$ -orbitals forming the  $\pi$ -bond become misaligned, which makes the  $\pi$ -component of the double bond weaker. The angle between the two  $p_z$ -orbitals is defined as  $\tau$ . The dihedral angle between the *cis*-substituents is marked as  $\phi$ . If  $\tau = \phi$ , then

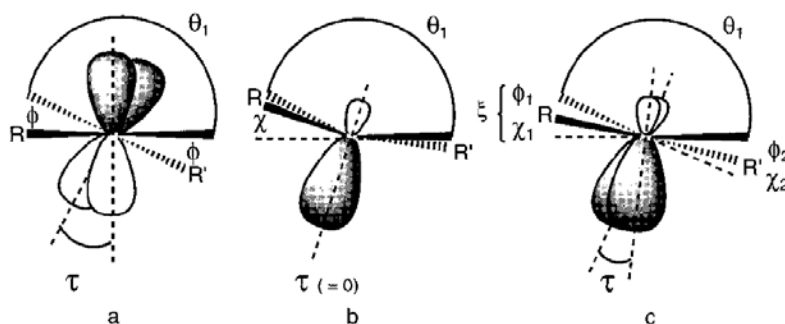


**Figure 2.8** Modes of distortion of strained alkenes.

the carbon atoms are planar and have pure  $sp^2$  hybridization.

If the carbon atoms involved in the double bond are rehybridized by adding more  $p$ -character to the initial  $sp^2$   $\sigma$ -bonds, this will make the geometry around the carbons more nonplanar. When the  $\pi$ -bond involves two  $p_z$ -orbitals mixed with some  $s$ -character, the alignment is still optimal, i.e.  $\tau = 0$ . This hybridization leads to increase of the distance between the bonding orbitals, and so a decrease of their net overlap. The pyramidalization angle  $\chi$  can be the same at both carbon centers or different (see also **Figure 2.9**).  $\chi$  is defined as the dihedral angle between the planes through  $C=C-R^1$  and  $C=C-R^2$ .

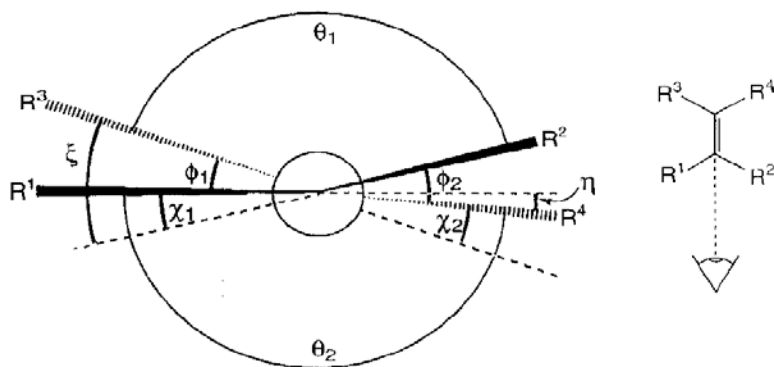


**Figure 2.9** Definition of angles around a distorted  $C=C$  bond.

There is another form of pyramidalization, where the  $sp^n$  orbitals involved in the  $\pi$  system are forced towards the opposite sides of the double bond. This type of twist is called asymmetric pyramidalization, but it does not play a significant role in the formation of trans-cycloalkenes.

When the double bond is found in a medium-sized cyclic molecule, ring strain destabilizes the trans isomers and only the cis isomers are observed. Currently the smallest cycloalkene molecule stable at room temperature is *trans*-cyclooctene, it has been fully

characterized, and is only 9 kcal/mole less stable than the cis isomer.

The distortion of the double bond in *trans*-cycloalkenes is a combination of twisting and pyramidalization (**Figure 2.8c**). The double bond may not be symmetric, so different pyramidalization angles at the two carbons,  $\chi_1$  and  $\chi_2$ , combined with the twisting angle  $\tau$  to describe the overall distortion of the double bond.

The angles  $\xi$  and  $\eta$  are used as measures of global strain of the double bond in *trans*-cycloalkenes and are defined by equations 1 and 2 below. They are derived from the mutual contributions of twisting ( $\tau$ ) and pyramidalization ( $\chi_{av}$ ) angles' values. The angle  $\eta$  value indicates the relative contribution of twisting  $\tau$  and pyramidalization  $\chi_{av}$  while  $\xi$  is a measure of the overall strain. These angle values will depend on the size of the ring as well as on the repulsion between the  $\pi$ -cloud and the bridge. In general, the backbone of the bridge and the substituents will not have a significant effect on the  $\xi$ 's values.

$$(1) \quad \xi = \tau + \chi_{av}$$

$$(2) \quad \eta = \tau - \chi_{av}$$

When  $\eta = 0$ , twisting and pyramidalization are equally important. When  $\eta = 0$  the angle between  $R^1$ ,  $R^4$  and  $\theta_2$  equal  $180^\circ$ . This is when the olefin is considered to be flat (**Figure 2.10a**). When  $\eta$  is positive, twisting dominates as the source of strain in the double bond, ( $\tau > \chi_{av}$ ). In this case the angle between  $R^1$  and  $R^4$   $\theta_2 < 180^\circ$  and the alkene is considered to look “concave” (**Figure 2.10b**). When  $\eta < 0$ , pyramidalization causes more strain than twisting ( $\chi_{av} > \tau$ ). In this case the alkene is considered to look “convex” (**Figure 2.10c**).

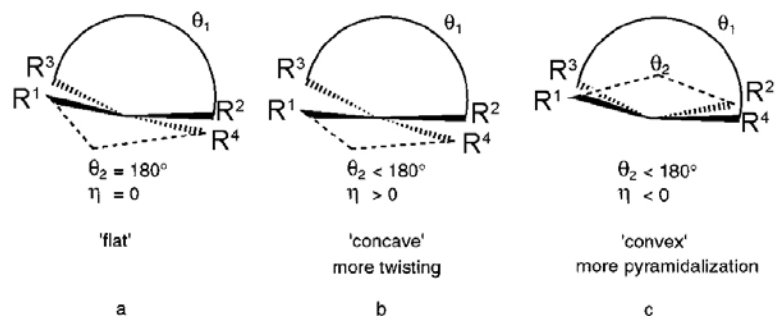


**Figure 2.10** Flat, concave and convex deformations of a strained alkene.

### 2.2.3. POAV analysis

In 1986 Haddon<sup>179</sup> published his work on  $\pi$ -orbital axis vector (POAV) analysis of alkene strain. He developed POAV theory to better describe the way  $\pi$ -bonding behaves when the strain increases in conjugated, non-planar organic molecules. In bridged annulenes and cycloalkenes, due to ring strain, the  $\sigma$ -system was assumed to change in such way, that helps the  $\pi$ -orbital's overlap to remain in its most favorable geometry. These changes of course, were proposed with the consequence of structural deviations from the pure  $sp^2$  hybridization state. Even in non-planar molecules, POAV treated the  $\sigma$  and  $\pi$  bonding separately assuming orthogonal orbital interactions. This means that the  $\sigma$  system is looked at as the sturdy backbone of the molecule. When the strain is increased and adjustment of the  $\sigma$  system occurs, only the  $\pi$ -electrons will be subject of bonding change.

Stabilization in polycyclic alkenes can come from both bending and twisting of the double bonds. In the case of the anthracene derivative<sup>180</sup> in **Figure 2.11a**, all substituents are

bent towards the same side of the ethylene backbone.

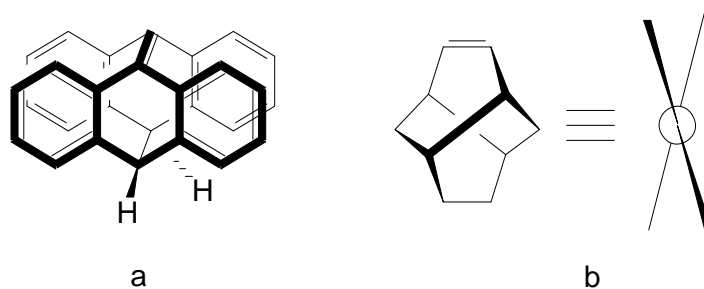


**Figure 2.11** a) Anthracene derivative with all substituents bent toward one side of the ethylene skeleton; b) Twisted double bonds in twistene

In twistene (**Figure 2.11b**) the angle of twist in the double bond was reported to be  $21^\circ$ .<sup>181</sup> This molecule was isolated in its optically active form. This high degree of double bond twisting, however, is not the highest reported. In a unsaturated steroid derivative, X-ray diffraction experiments determined approximately  $30^\circ$  of twist.<sup>182</sup>

In the beginning of the 20<sup>th</sup> century, J. Brecht studied the bicyclic camphene and pinene series. In the course of his work he found that a C=C double bond in “atomic-bridged-ring” bicyclic structures impairs the stability of the molecule, i.e. species with double bond at the bridgehead atom cannot exist. In later years<sup>183</sup> many examples violating Brecht’s rule were discovered (**Figure 2.12**).<sup>253</sup>

One of the ways to relieve the strain is to expand one of the rings. Species **b** from

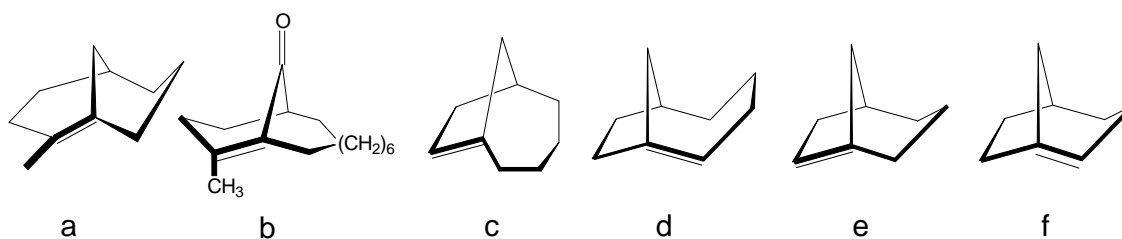


**Figure 2.12** Anti-Bredt's bridged trans-cyclo alkenes.

**Figure 2.12** is the perfect example, a ketone proposed by Prelog. The bi-cyclo [3.3.1] non-1-ene (**Fig 2.12a**) is found to be stable if no air, acids and other reagents are present. The rest of the examples are essentially bridged trans cyclooctenes or cycloheptenes.

#### 2.2.4. Early recognition of trans more stable than cis in acyclic vs. cyclic

Even from the early days, shortly after geometric isomerism was defined, organic chemists have noticed that in nature, in most cases, the acyclic unsaturated even



**Figure 2.13** Twisted cyclooctene

conjugated, carbo-hydrates were found to be more stable in their trans configuration. The “opposite” positioning of the substituents along the carbon chain, allows the molecules to have little steric strain. Unlike acyclic alkenes, *cis* cycloalkenes are in general the more stable isomer. As shown in the case of *trans*-1,2-dibromocyclooctene (**Figure 2.13**), the trans conformation of the double bond causes high strain on the ring. In the 1970's however, some trans cycloalkenes were found to be stable and exist under normal conditions.<sup>26</sup> Later examinations, both experimentally and theoretically, showed that “the magnitude of the energy difference between cis and trans becomes smaller and smaller as one moves to larger and larger ring size”<sup>184</sup> When 7-10 membered rings of trans-cycloalkenes were carefully examined, there were four geometric “deficiencies” determined, absent from their corresponding cis conformers: (1) twisted  $\pi$  bonds; (2) pyramidal “sp<sup>2</sup>”-hybridized carbon atoms; (3) changes from ideal sp<sup>3</sup> bond angles and (4) non optimal bond lengths.<sup>184,175</sup>



## 2.3. Conformations of strained cyclic alkenes

### 2.3.1. Geometry of *trans*-cyclooctene

*Trans*-cyclooctene is the smallest unsubstituted cycloalkene currently believed to be stable at room temperature. The chemical reactivity of its double bond is facilitated by its non-planar nature. In the past years, the geometry of the molecule (**Figure 2.14**) was studied in great detail both experimentally<sup>185</sup> and computationally.<sup>186</sup> A derived projection from these studies (**Figure 2.14 b**), shows that

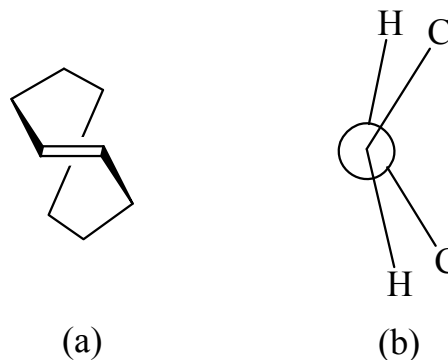


**Figure 2.14** (a) Conformation of *trans*-cyclooctene; (b) Projection of cyclooctene structure along the C=C bond.

the two faces of the  $\pi$  electron system are asymmetrical, i.e. that pyramidalization is occurring.

While investigating a platinum complex of *trans*-cyclooctene in X-ray, Shoemaker determined the dihedral angle of C-C=C-C to be  $136.5^\circ$ .<sup>187</sup> The X-ray investigations continued on two crystalline derivatives. In his examination of *trans*-2-cyclooctenyl 3',5'-dinitrobenzoate<sup>188</sup> Ermer measured the angles describing the trans double bond's strain forces induced by the six-membered carbon bridge, finding the values of:  $\tau = 18^\circ$ ,  $\chi_{av} = 24^\circ$ ,  $\xi = 42.3^\circ$  and  $\eta = -6$ . While researching the mono diazofluorene adduct of *trans*, *trans*-1,5-cyclooctadiene, Boeckh et al. obtained very similar values for the angles observed by Ermer:  $\tau = 17.7^\circ$ ,  $\chi_{av} = 26.1^\circ$ ,  $\xi = 43.7^\circ$ ,  $\eta = -8.4^\circ$ .<sup>189</sup> Though the large  $\xi$  values show that the two derivatives experience similar overall strain on the double bond, in both

cases the negative values for the difference between twisting and pyramidalization,  $\eta$ , suggest that pyramidalization plays a significant role in the relief of strain.

### 2.3.2. Geometry of *trans*-molsila-cycloheptene

X-ray analysis of the at room temperature stable sila derivative of *trans*-cycloheptene was conducted at  $-148^\circ\text{C}$  (**Figure 2.15**).<sup>251</sup>

It was found that the C-C=C-C *trans* dihedral angle was only  $130.97^\circ$  while the H-C=C-H ( $173.1^\circ$ ) and the C-C=C angles ( $121^\circ$ ) did not differ very much from normal values. Even though the strain on the double bond is significant, the length of the C=C double bond was within normal values, i.e.  $1.33 \text{ \AA}$ , while the Si-C2(C7) ( $1.91 \text{ \AA}$ ) and the C2-C3 (C6-C7) bonds ( $1.56 \text{ \AA}$ ) were found to be extended

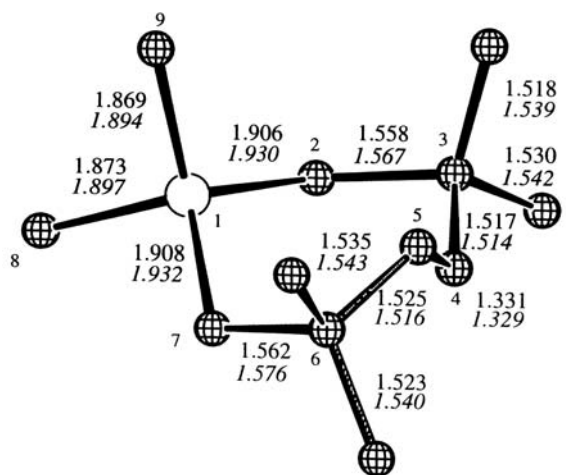


**Figure 2.15** X-ray structure of *trans*-1,1,3,3,6,6-hexamethyl-1-sila-4-cycloheptene with comparison to HF/6-31\*\* calculation (italics) bond lengths ( $\text{\AA}$ ). The hydrogens have been omitted.

considerably over “normal” values. To support the measured structural parameters an *ab initio* calculation at the HF/6-31\*\* level was performed, which agreed well with the experimental values.

Wijsman et. al.<sup>20</sup> provided the X-ray measured values for the “strain” angles:  $\tau = 23.12^\circ$ ,  $\chi_{\text{av}} = 26.08^\circ$ ,  $\xi = 49.19^\circ$ ,  $\eta = -2.96^\circ$ . The results from his work, confirm that the  $\xi$  value is close to the  $\xi$  values in *trans*-cyclooctenes, meaning that the longer C-Si bond reduces the overall strain in the ring.

### 2.3.3. Geometry of *trans*-trisilacycloheptene

In the early 90's Ando<sup>252</sup> synthesized and isolated *cis*-trisilacycloheptene. He then photolyzed it to produce its pure *trans*-trisilacycloheptene isomer (**Figure 2.16**). Just like the *trans*-1,1,3,3,6,6-hexamethyl-1-sila-4cycloheptene, the *trans*-trisilacycloheptene is stable under normal conditions because of the extended Si-Si bond lengths in the ring.

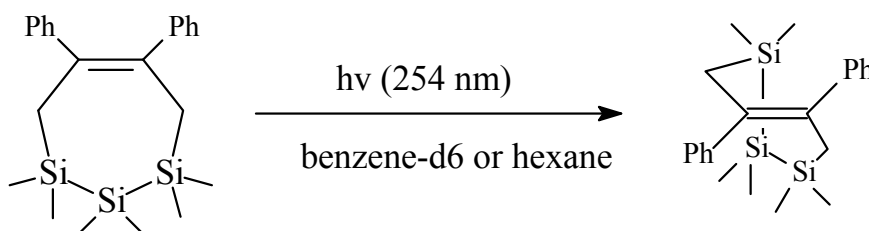


**Figure 2.16** Synthesis of trisilyl *trans*-cycloheptene.

Additionally, the X-ray structural analysis and strain angles measurements ( $\tau=19.6^\circ$ ,  $\chi_{av} = 13.2^\circ$ ,  $\xi=32.8^\circ$ ,  $\eta=6.4^\circ$ ) indicate that this species is significantly less strained than the previously discussed *trans*-cycloalkenes. The positive value of  $\eta$  suggests that the bonds between the Si atoms allow for twisting to be dominant in stabilizing the double bond. It has been suggested that this shift from pyramidalization stabilization to twist stabilization is facilitated by the steric interactions between the methyl and phenyl substituents.<sup>178</sup> Though they may also indicate a preference for  $sp^2$  hybridization of benzoyl carbons.

## 2.4. Thermal Isomerization of cycloalkenes

### 2.4.1. Determination of the isomerization barrier by Gano and Doering

In 1987 Gano<sup>253</sup> performed an experiment with (*Z*)-2,2,3,4,5,5-hexamethyl-3-hexene. He

prepared a carefully neutralized and degassed solution of the alkene. By measuring the thermal isomerization barrier of the sterically hindered alkene, he was able to determine the value of  $40.4 \pm 1.7$  kcal/mol for the *Z*→*E* rotational barrier and a preexponential factor, *A*, of  $3 \times 10^{14}$ . Gano proposed a method to calculate the effects of steric forces on alkene rotational barriers. He determined that when isomerizing, the transition state energy is the product of the lost  $\pi$  energy of the double bond combined with part of the *trans*-isomer's strain energy. Using his method, he calculated the isomerization barrier for (*Z*)-2,2,5,5-tetramethyl-3-hexene to be 53 kcal/mol, in agreement with the previously obtained barrier of  $54.4 \pm 0.7$  kcal/mol<sup>254</sup> in the gas phase.

By using known heats of hydrogenation and/or force-field calculations, in 1989 Doering<sup>254</sup> examined series of alkenes, and was able to determine the strain energies of the alkenes in their *trans* isomer forms. Using the MM2 forcefield to calculate the rotational transition state energies and taking the *trans* isomer strains into account, he found a constant value  $65.9 \pm 0.9$  kcal/mol for breaking the  $\pi$  bond during the *trans*-to-*cis* isomerization.

#### **2.4.2. Isomerization of *trans*-cyclooctene and cyclohexene**

It remained unclear whether the isomerization of *trans*-cyclooctene to *cis*-cyclooctene could occur by direct rotation about the double bond or another type of mechanism.<sup>255</sup> One example could be a radical-chain process involving a comparatively low-energy *trans*-cyclooctene-3-yl radical isomerization.<sup>256</sup> Another possibility is through a [1,3]antarafacial hydrogen shift, made possible by twist of the double bond.

To distinguish the simple rotation process from other processes, Baldwin<sup>257</sup> investigated the photoisomerization of 1,2-dideutero-*trans*-cyclooctene. The reaction demonstrated

reliable first-order kinetics showing that the trans to cis isomerization occurred via direct rotation of the double bond with a free energy of activation, of 47 kcal/mol. Doering et.al.<sup>254</sup> reported a  $49.3 \pm 0.8$  kcal/mol rotational barrier for the trans to cis isomerization of *trans*-cyclooctene, which fits well with the energy value obtained by Baldwin.<sup>257</sup>

Even though Jousot-Dubien *et al* reported the formation of 1-phenyl-*trans*-cyclohexene upon flash pyrolysis,<sup>258</sup> unambiguous proof for the existence of *trans*-cyclohexene is yet to be reported. Caldwell<sup>259</sup> conducted direct laser flash photolysis experiments with *cis*-1-phenylcyclohexene. He produced the trans isomer by direct irradiation of the cis alkene at 266 nm, as well as with thioanthon sensitizer at 355 nm. He measured the temperature dependence of the trans-to-cis isomerization rate constant between  $-20^\circ$  and  $+73^\circ$  for 1-phenylcyclohexene and obtained the activation parameters,  $\log A = 14.1 \pm 0.09$ ,  $E_a = 12.1$

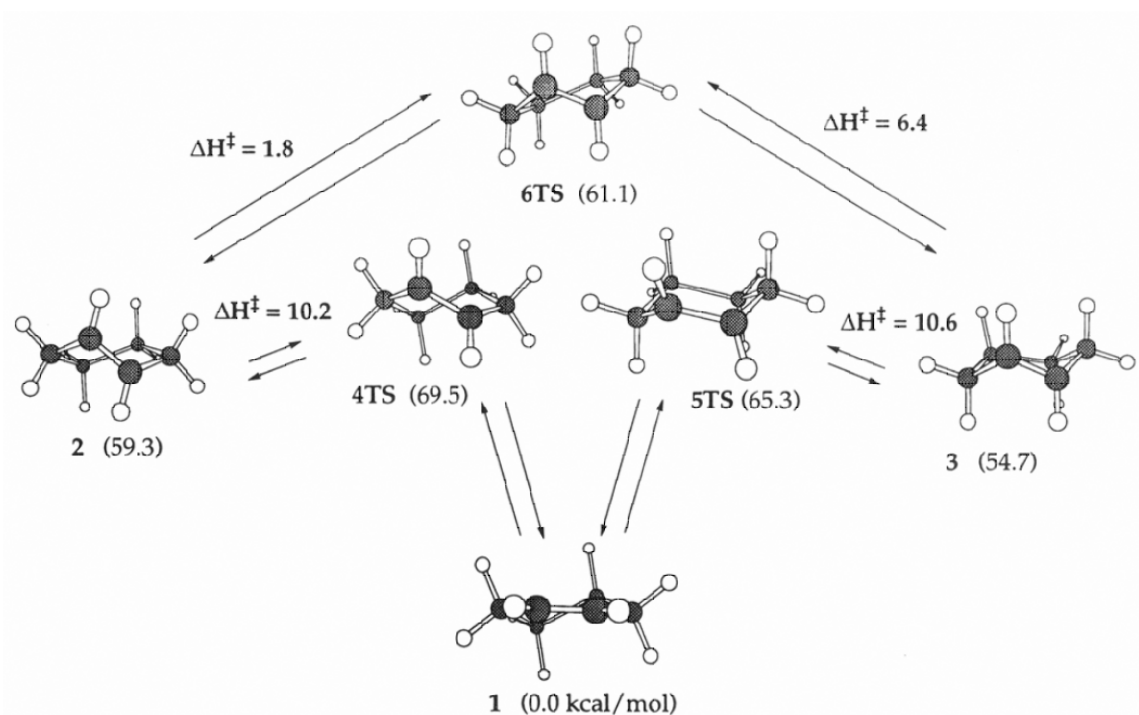


**Figure 2.17** Structures and relative energies (kcal/mol) for *trans*-cyclohexene conformers and transition states.

$\pm 0.12$  kcal/mol for this isomerization.

By employing *ab-initio* calculations at the TCSCF/6-31G\* level, Johnson<sup>260</sup> investigated the conformational properties of *trans*-cyclohexene (**Figure 2.17**). Structure **1** shows the half-chair conformation of *cis*-cyclohexene. Structures **2** and **3** represent the twist-boat and chair conformers for *trans*-cyclohexene respectively. The two transition states for  $\pi$  bond rotation to **1** are shown as **4TS** and **5TS**. The transition state for conformational interconversion between chair and twist-boat is shown as **6TS**. The *trans* isomer **3** can go through two reaction paths: (1) a  $\pi$  bond rotation to **1** with calculated barrier of 10.6 kcal/mol and (2) an interconversion to the twist-boat conformation with a calculated barrier of 6.4 kcal/mol. The twist-boat conformer **2** exhibited a 10.2 kcal/mol barrier for  $\pi$  bond rotation with only a 1.8 kcal/mol barrier for isomerization to **3**. Those results fit fairly well to the barrier for *trans*-1-phenyl cyclohexene found by Coldwell.

## 2.5. Excited states

### 2.5.1. The most simple cis-trans isomerization - Ethylene

The potential energy (PE) surfaces of the ground state ( $S_0$ ) and the first excited singlet ( $S_1$ ) and triplet ( $T_1$ ) states of ethylene are shown in **Figure 2.18**.<sup>261</sup> When, either by direct photoexcitation or by use of a sensitizing agent, an electron is promoted to the  $\pi^*$  orbital, it leads to either the first singlet excited state ( $S_1$ ) or the first triplet excited state ( $T_1$ ). The  $\pi^*$  antibonding interaction can be diminished if the molecule is twisted to an orthogonal configuration. This will lead to the formation of the minimum energy  $90^\circ$  twisted conformation. From this point the molecule will form addition products, or to go back to the  $S_0$  surface area via internal conversion. This transition, which occurs via the high vibrational

levels of the ground state's potential energy surface, gives, to a substituted ethylene molecule, the possibility of reaching a ground state energy minimum by either reverting to its original conformation or isomerizing to another geometric isomer.

### 2.5.2. Potential Energy Surfaces of cyclic alkenes

In general the above explained mechanism could be applied to any acyclic alkene. However, with cyclic, or "closed" alkenes, the potential energy surfaces are changed significantly when the double bond is twisted. The effect of the ring strain, induced in this twisting, becomes more dominant. General exceptions are the relatively large cyclic alkenes because of their relative freedom to adopt the orthogonal  $T_1$  or  $S_1$  geometries, which allows them to isomerize to their stable ground states as the trans isomer, even under normal conditions. When the ring size of the photolyzed alkene is decreased though, the stiffer geometry applies severe restrictions on the freedom to twist. In

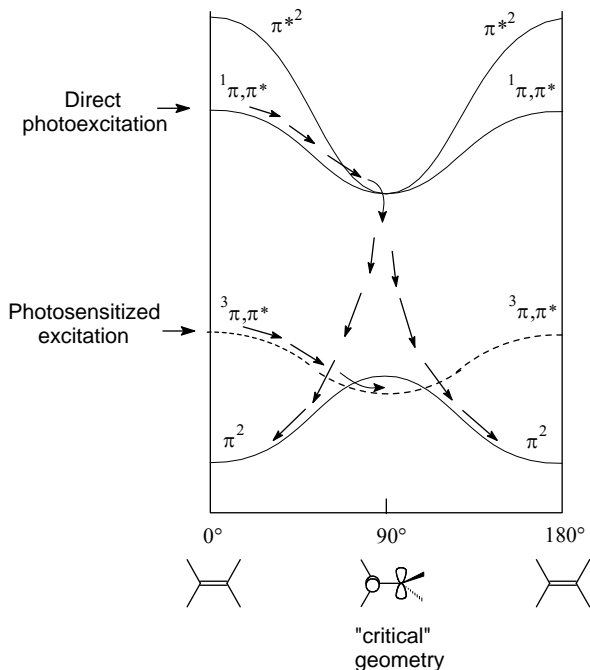


**Figure 2.18** Potential Energy surfaces of the ground and lower excited states of ethylene.

**Table 2.1:** Degree of twist available to cycloalkene  $\pi, \pi^*$  excited states as estimated from dreiding models.

Cycloalkene	Twist, deg
Cyclopentene	40
Cyclohexene	90
Cycloheptene	110
Cyclooctene	160

**Table 2.1**<sup>262</sup> is shown the examination of Dreiding models for the degrees of twist available to the  $\pi$ - $\pi^*$  excited states of small ring alkenes. The results suggest that six-membered cyclic alkenes and bigger, have a higher probability of orthogonal  $T_1$  and  $S_1$  geometry formation, compared to smaller cycloalkenes, such as cyclopentene. In such small entities, the ring strain becomes so big, that the full  $180^\circ$  twist to a trans double bond is no longer possible. This means that trans cyclic alkenes have geometries, where the twist around the double bond is more than  $90^\circ$  but may not be completely  $180^\circ$  at their minimum.<sup>263</sup> Essentially this will lead to non symmetric ground and excited state surfaces. The energy difference between the cis and trans becomes very distinct, which lowers the energy barrier between them and creates nondegeneracy. Subsequently this leads to different shapes of their excited states' surfaces, compared to those of ethylene. Thus the transition, from excited state to ground state may not produce a 1:1 cis : trans ratio.<sup>264</sup>

The possibility of making trans isomer vs. the ring size by photoexcitation was given by Turro:<sup>265</sup>

- 1) trans- 3 or 4 carbon rings is considered impossible to make
- 2) trans- cyclopentenes are considered difficult, while producing reactive cycloalkenes
- 3) trans- cyclohexenes and cycloheptenes might be easy to make, while producing reactive cycloalkenes, which can be detected at low temperatures<sup>266</sup>
- 4) trans-cyclooctenes and bigger are also considered facile, while producing stable cycloalkenes.

During the first step of any photochemical synthesis, a higher energy state is reached. In general, there are three ways to excite an alkene to a higher electronic excited state ( $S_1$  or  $T_1$ ),



direct absorption, sensitization by a donor in a triplet or singlet state, or exciplex formation and decomposition.

#### **2.5.2.1. Absorption - direct photolysis**

Direct photolysis is in effect when with a photon absorption, a direct vertical transition of an electron from the ground state's zero point energy level reaches the zero point energy level, or a higher vibrational level, of an excited singlet state. For the excitation of the single  $\pi$  bond chromophore, energies of 200 nm or more are required. The disadvantage of this method of photolysis is the risk of producing not only the needed trans alkene, but also a large variety of side products.<sup>267</sup>

Sometimes on the excited state surface there could be a barrier to twisting, as is known in stilbene.<sup>268</sup> These barriers increase transitions like fluorescence or surface crossing, which could form vibrationally high ground state, followed by subsequent reactions. Such a barrier to twisting on the excited state's surface could also inhibit the cis-trans isomerization.

#### **2.5.2.2. Energy transfer excitation**

If the  $S_D$  and  $S_A$ , or  $T_D$  and  $T_A$  (**A** for acceptor and **D** for donor), are "ordered correctly" then energy transfer can be an efficient method to induce cis- to trans- alkene conversion. It is worth mentioning though, that the higher singlet energy transfer could lead to the formation of products similar to those from direct excitation.

Triplet photosensitization is the photochemical process used most in photochemistry. When a photosensitizer is used, a  $T_1$  state can be produce rather easily because the transition from the sensitizer to the alkene will be transition between two energy levels of the same multiplicity. For one to be considered a good sensitizer one must exhibit:

- Fast rate of  $T_1$  formation, i.e. inter system crossing, over other competing photochemical events
- The  $T_1$  of the alkene, i.e. acceptor, must be lower in energy
- Long  $T_1$  lifetime assuring enough time for the excitation transfer which is near diffusion controlled
- Good absorption at wavelengths where the acceptor does not absorb well (or at all)
- Low chemical reactivity so that it does not get involved in photochemical reactions with the acceptor

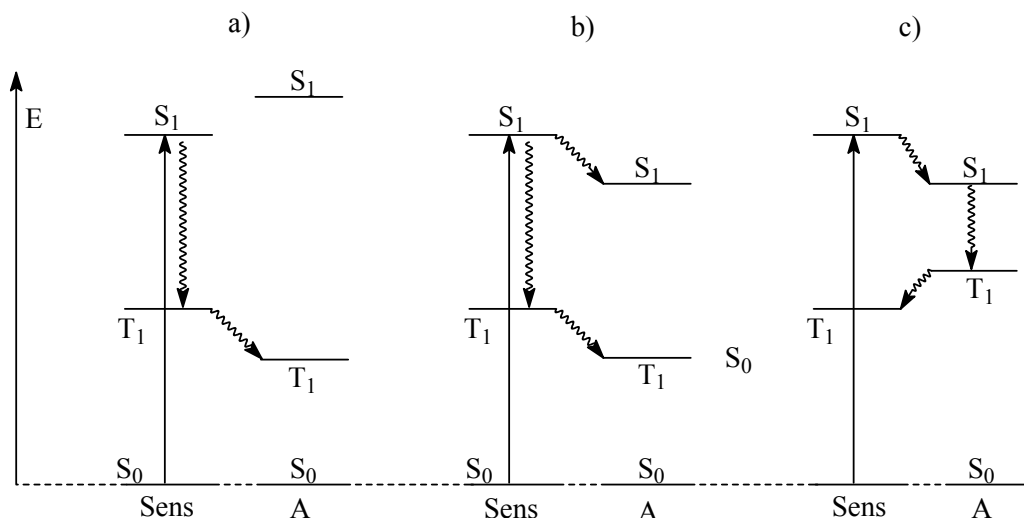


**Figure 2.19** Three possible situations for energy transfer between sensitizer (Sens) and Acceptor (A)

Considering all parameters for ideal sensitizer, one can assume that the most important parameter in the selection of a triplet sensitizer for a particular alkene's photoisomerization, would be the energy gap between  $D_T^*$  and  $A_T^*$ . The ideal correlation between the energy levels of both the sensitizer D and the acceptor A is shown in **Figure 2.19a**. There one can see that when absorption produces  $D_{S_1}$ , intersystem crossing from  $D_{S_1}$  to  $D_{T_1}$ , occurs, while

the  $A_{S1}$  is not produced because it is higher in energy than  $S_{A1}$ , and singlet energy transfer will not occur. However, the  $A_{T1}$  energy level is lower than that of  $D_{T1}$  which favors the transition between D and A. If the energy levels have the relationship shown in **Figure 2.19b**, singlet-singlet and triplet-triplet energy transfer are both possible. If the energy levels are related one to another as shown in **Figure 2.19c**, it allows singlet-singlet energy transfer from the donor's first excited state to the acceptor's first singlet excited state, followed by internal conversion and triplet-triplet energy transfer from the alkene back to sensitizer.<sup>269</sup>

When the triplet energy of the acceptor is about 3.5 kcal/mol or more below that of the sensitizer, triplet-triplet energy transfer is generally diffusion controlled. When both triplet energies are the same, then only the 0-0 bands overlap and the energy transfer constant is smaller by a factor of  $10^2$ ; it decreases even further with increasing triplet energy of the acceptor.

In cis-trans sensitized isomerization, the last step is the  $T_1 \rightarrow S_0$  intersystem crossing transition. The rate of this final step is very important. This rate is determined by the energy gap between the excited triplet state and the ground singlet state, as well as the spin orbital coupling term (SOC).<sup>270</sup> As mentioned before, for ethylene the energy is minimum at the perpendicular twisted geometry. For other alkenes the minima is assumed to occur near that angle, if structural constraints do not inhibit it.<sup>271</sup> After conducting a series of calculations on SOC matrix elements, Caldwell<sup>272</sup> found that the SOC was highly dependent on the twist angles around the C=C double bond, being zero at the  $90^\circ$  geometry and maximal at  $45^\circ$  and  $135^\circ$ . He also determined that pyramidalization at one of the trigonal centers increased spin orbital coupling.

Good sensitizers for the photoisomerization of alkenes include both benzene derivative triplets (Table 2.2)<sup>273</sup> and ketone triplets.<sup>274</sup> However, because of the sensitizer's different chemistries, the mechanisms of

**Table 2.2:** Some benzene derivatives triplet energies.

Sensitizer	Triplet energy (kcal/mol)
Benzene	84.4
Toluene	82.9±0.2
p-Xylene	81.7±0.2
Mesitylene	80.5±0.4

the electron transfer are most probably different as well. The triplet energy of benzene is higher than that of 2-butene by about 4 kcal/mol (84 kcal/mol vs. 80 kcal/mol). This small difference in favor of the sensitizer means that a triplet energy transfer from benzene to the butene is likely to occur. There are sensitizers, like the benzophenone for example, with a triplet energy of 70 kcal/mol or less, but still exhibit the capability of isomerizing 2-butene, by forming an exciplex (Figure 2.20). This is the so called Schenck mechanism (see below).

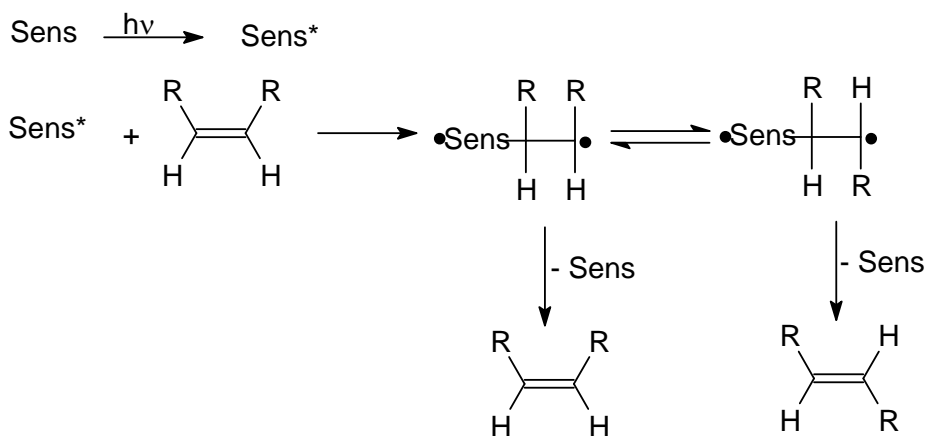


**Figure 2.20** Sensitization by Schenck mechanism

An exciplex is formed when two species combine - the donor D\*, i.e. sensitizer, in its excited triplet state, and the acceptor A, i.e. alkene, in its ground state:



At its minimum energy the exciplex may adopt a twisted alkene geometry.<sup>275</sup> When it degrades, the exciplex may produce a vibrationally hot newly orthogonal alkene. This can then decay down to the ground state of either cis or trans isomers. Unlike direct excitation or energy transfer process, during the formation of exciplex species, an excited state entity with the geometry of the cis-alkene is not necessarily formed.

### 2.5.3. Strained Cycloheptenes produced photochemically

The strain in the small cyclic system *trans*-cycloheptene is unique because it is caused by a severe twisting force rather than a bending force on the double bond, as is the case with cis double bonds constrained in very small ring systems.<sup>276,277</sup> The change of the geometry of the double bond and the thermal stability of the *trans*-cycloheptene systems are therefore of great interest in determining the limits of the bonding in a carbon-carbon double bond.

Photochemically generated *trans*-cycloheptene was probably produced for the first time by Kropp<sup>278</sup> in 1969. In his experiment, he photolyzed the cis isomer in the presence of xylene as sensitizer. The solvent was deuterated acidic methanol. As a result he got methoxycycloheptane-d<sub>1</sub>, as a major protonation product via the *trans* addition of methanol across the double bond.

However, Kropp encountered a problem - he could not determine with certainty whether a T<sub>1</sub> excited state of the cis- or a reactive S<sub>0</sub> state of the *trans*-cycloheptene was the precursor of the methoxycycloheptane.

Almost a decade later, Inoue<sup>279</sup> proved the presence of ground state *trans*-cycloheptene. He used Kropp's technique for trapping<sup>278</sup> the methoxycycloheptane in acidic methanol. In his experiment he irradiated a 0.01M solution of *cis*-cycloheptene in pentane with 184.9 nm light. To prove that the intermediates of the reaction were not species in their excited state, Inoue stored the irradiated solution in dark and cold (-78 °C) for twenty hours. He then added the acidic methanol and observed a yield of methoxycycloheptane, about 80% of that which occurred when photolysis was carried out directly in acidic methanol. This result confirmed that the *trans*-cycloheptene was present in the ground state, and relatively stable at -78° C.

Inoue conducted series of decay studies as well. In those experiments, he warmed up a freshly photolyzed sample for a certain amount of time and then cooled it down again to -78 °C. He then added acidic methanol to it and determined that the *trans*-cycloheptene's lifetime at -10 °C is 23 minutes, which corresponds to a  $\Delta G^\ddagger = 17$  kcal/mol

During his experiment he used 185 nm light source. When trapped, he identified not only the presence of methoxycycloheptane, but also methylenecyclohexane and bicyclo[4.1.0]heptane. He explained that the side-products in his direct photolysis experiment, as well as the trapped *trans* isomer, were produced through an excited singlet state or the  $\pi, R(3s)$  Rydberg excited state. He speculated that the *cis*-*trans* isomerization was interfered with by the involvement of the competing rearrangements to 4 and 5 (**Figure 2.21**), *via* the carbene intermediate produced by the [1,2] shift of an allylic C-C bond of the excited cycloalkene.

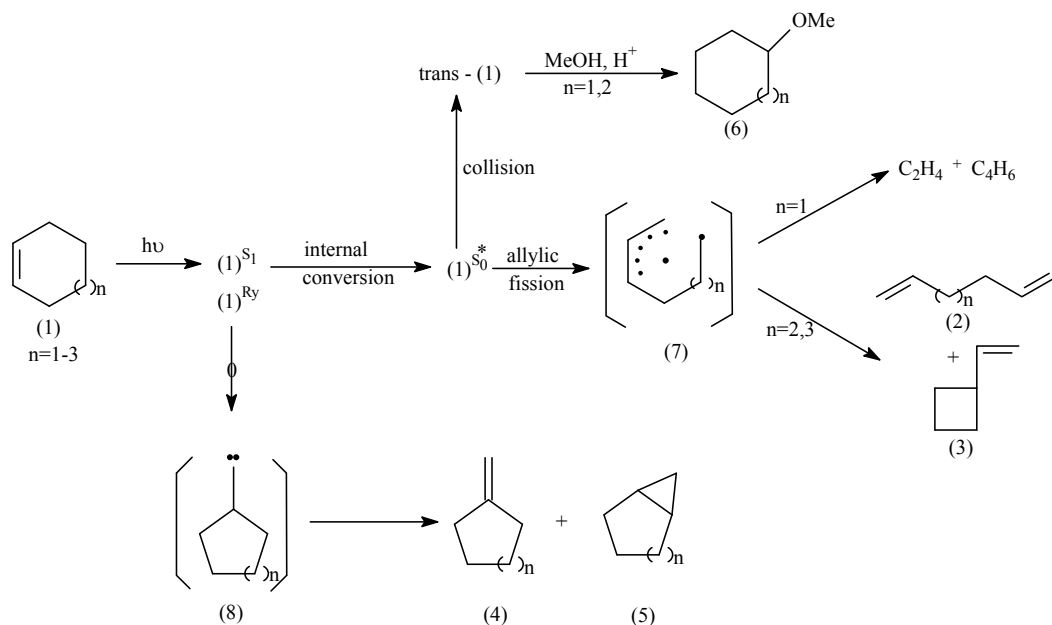


**Figure 2.21** Proposed direct photolysis mechanism for CHP.

Inspired by the results of his early work with the *cis-trans* isomerization of *cis*-cyclooctene<sup>280</sup>, Inoue<sup>281,282</sup> modified the *cis*-cycloheptene photoisomerization experiment by employing a singlet sensitizer, i.e. methyl benzoate (**Figure 2.22**).

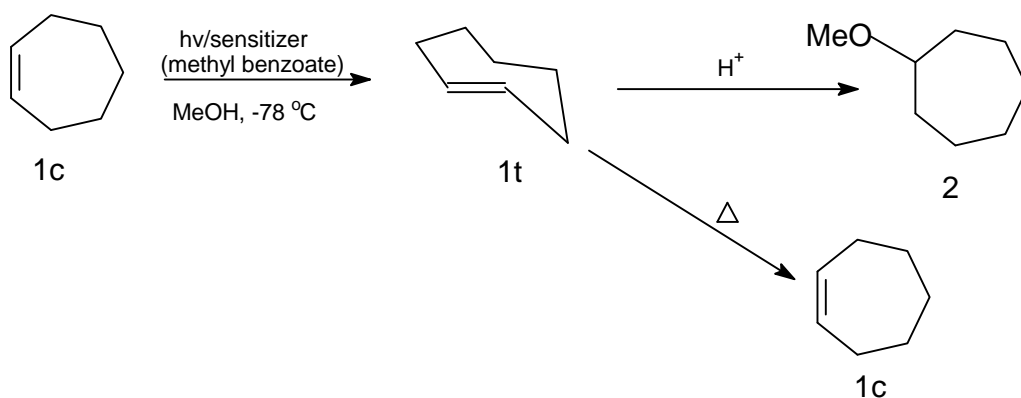
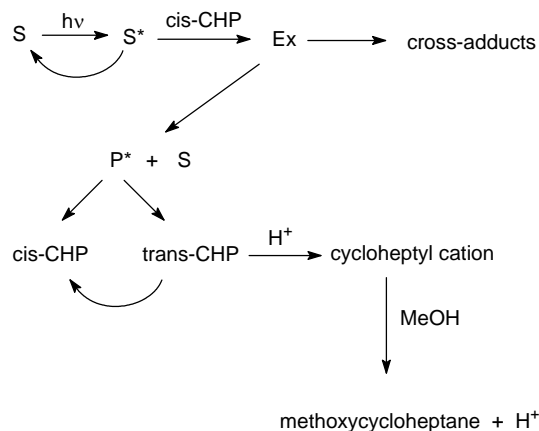


**Figure 2.22** *Cis-trans* photosensitization of CHP.

Using this method a higher yield of methanol trapping product was seen suggesting a higher trans to cis ratio, as compared to those obtained via direct photolysis. This method also proved to be cleaner since it produced less side products. His mechanism for making *trans*-cycloheptene via singlet exciplex is shown in



S = singlet sensitizer, methyl benzoate, Ex = exciplex  
P\* = intermediate, CHP = cycloheptene

**Figure 2.23** (an asterisk denotes electronic excitation). Utilizing G.L.C.-M.S, small amounts of cross-adducts were also detected. His observations confirmed the stability of *trans*-cycloheptene at  $-78^{\circ}\text{C}$ .<sup>282</sup>

**Figure 2.23** Inoue's mechanism for production of *trans*-CHP via a singlet exciplex.

In 1999, Inoue<sup>283</sup> was able to obtain optically active *trans*-cycloheptene for the first time using enantio-differentiating photoisomerization of *cis*-cycloheptene. The sensitizers used were chiral aromatic esters. The isomerization was conducted in the temperature range of  $-40$  to  $-80^{\circ}\text{C}$ . The resulting *trans*-cycloheptene was trapped later using two methods: (1) Diels-Alder reaction with 1,3-diphenyl-isobenzofuran or (2) oxidation with  $\text{OsO}_4$ .

Using Inoue's trapping method, Squillacote et. al. were able to produce a species, whose NMR spectrum showed a *trans* vinyl coupling constant and which upon warming to  $-30^{\circ}\text{C}$  quickly decayed with a concomitant increase in the *cis*-cycloheptene's resonances. Based on these observations, they concluded the observed species was in fact *trans*-cycloheptene.<sup>286</sup> Using 2D NMR techniques and *ab-initio* calculations of the carbon chemical shifts at the



MP2/6-31+G(2d,p)//B3LYP/6-31G(d) level, they were able to identify and assign all  $^1\text{H}$  chemical shifts, as well as to confirm the  $^{13}\text{C}$  chemical shifts for *trans*-cycloheptene, reported by Michl (**Table 2.3**).<sup>285</sup>

**Table 2.3:** Characterization of *trans*-cycloheptene via  $^{13}\text{C}$  NMR and force field simulations.

Carbon	c-CHP		t-CHP	
	Exp <sup>a</sup>	Calc <sup>b</sup>	Exp <sup>a</sup>	Calc <sup>b</sup>
1	130.2	130.6	135.5	134.8
2	130.2	130.6	131.8	130.6
3	29.4	28.5	36.2	35.2
4	29.4	28.5	25.3	23.8
5	27.9	27.0	31.7	30.6
6	27.9	27.0	33.9	32.6
7	33.4	32.8	26.2	24.8

Force field calculations suggested that the *trans* isomer is

a. observed  $^{13}\text{C}$  chemical shifts in acetone- $\text{d}_6$ .  
 b. Method used was MP2/6-311+G(2d,p)//B3LYP/6-31G(d).

unsymmetrical and will exhibit a dynamic NMR caused by the ring flip between the two unsymmetrical conformers. Squillacote et al. were able to observe the dynamic NMR and to simulate it so as to obtain a barrier for the ring flip of *trans*-cycloheptene (**Figure 2.24**). They found a barrier of 10.0 kcal/mol for this pseudorotation. In addition, decay studies were performed which, assuming a simple rotation of the double bond, gave a *trans* to *cis* barrier of 15.6 kcal/mol.<sup>308</sup>

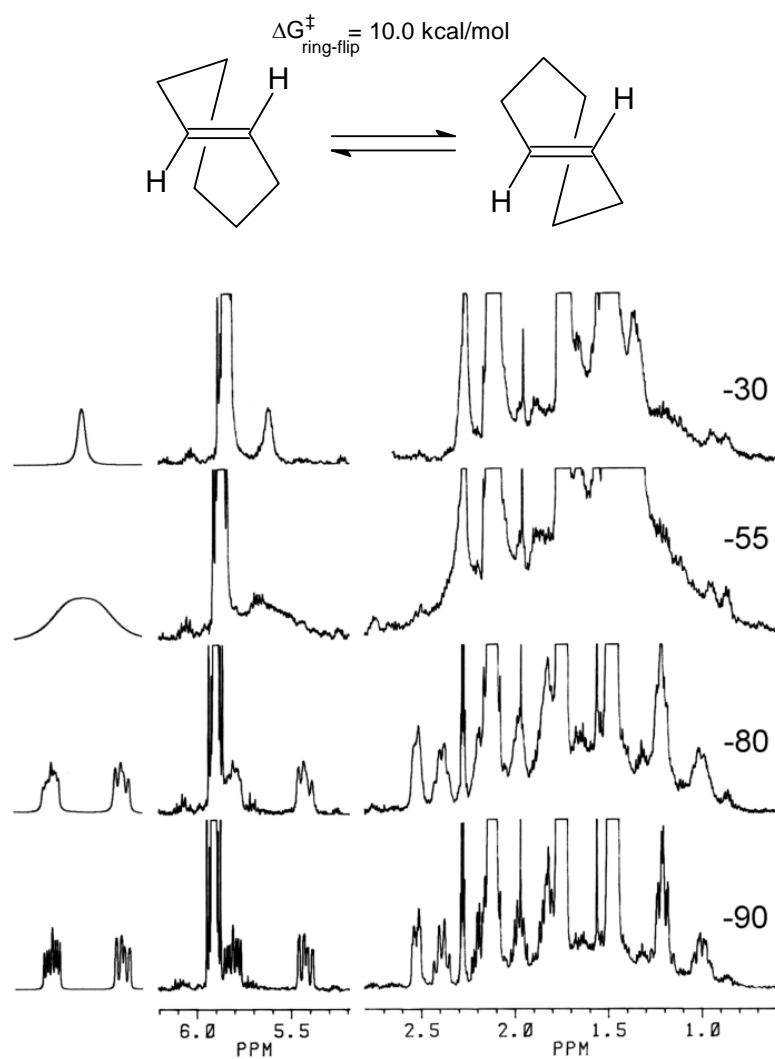


**Figure 2.24** Characterization of trans-cycloheptene via experimental (right) and simulated (left) dynamic  $^1\text{H}$  NMR.

### 2.5.3.1. Barrier of trans to cis transition determination in cycloheptenes

In the early 1990's Caldwell<sup>284</sup> calculated the energy barrier of cis/trans isomerization for several cycloalkenes, including cycloheptene. In their studies they found that the semiempirical calculation using the PM3 parameter set gave the best matching values. Low level *ab initio* approximation provided similar results (**Table 2.4**) Just like the results of Allinger's,<sup>263</sup> Michl's<sup>285</sup> and our group,<sup>286</sup> Caldwell's results showed ~30kcal/mol

**Table 2.4:** Calculated *trans-cis* cycloheptene energy differences.

Calculation Method	Cycloheptene $\Delta H_{c \rightarrow t}$ (kcal/mol)
PCMODEL 4.0	33.19
MM2	20.24
MM3	22.16
MNDO	34.97
MINDO/3	36.95
AM1	30.9
PM3	30.17
SAM1	31.69
HF/3-21G	44.6

more strain in the trans vs cis isomer. Using a value of 65 kcal/mol for the  $\pi$  portion of the double bond, and this 30 kcal/mol cis/trans energy difference, **Figure 2.25** shows that even

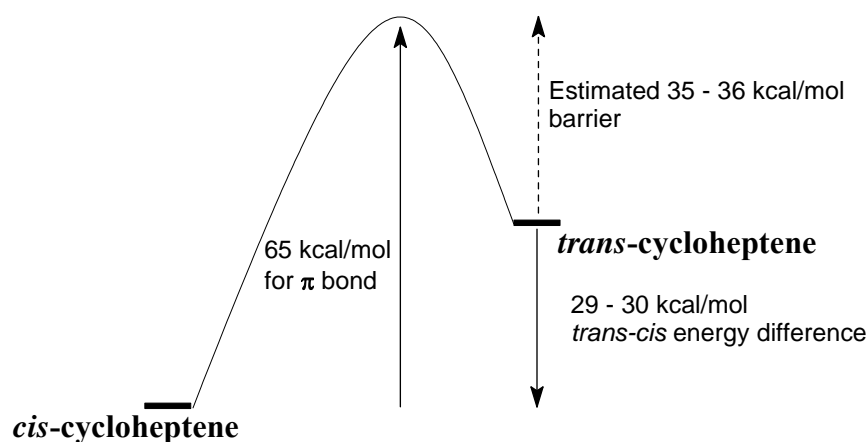


**Figure 2.25** Calculated transition energies for cis to trans cycloheptene's transition

if all ring strain was relieved in the transition state, an energy barrier of at least 35 kcal/mol would be expected. This leads to the conclusion that trans-cycloheptene is expected to be stable at temperatures well above the room temperature. Inoue's<sup>283</sup>, as well as our initial experimental results<sup>286</sup>, however, show that trans-cycloheptene is unstable at normal conditions and isomerizes back its more stable cis form at low temperatures.

#### **2.5.4. Previous computational investigations and results**

To investigate this seeming incompatibility between our experiments and Caldwell's computational results, we examined the cis-trans cycloheptene system in more detail computationally by carrying out *ab-initio* calculations. They were done using the Gaussian 98 or Gaussian 03 programs<sup>287</sup> and visualized with PCMODEL version 7.0.<sup>288</sup>

The *cis*- and *trans*-CHP geometries used were optimized using the MMX forcefield of the PCMODEL program as input geometries for the *ab-initio* calculations. They were optimized with a 6-31G(d) basis set at different electron correlation levels, such as HF, CASSCF, and CASSCF with dynamic electron correlation introduced at the MP2 level.

By changing the dihedral angle of the double bond in small increments, combined with energy minimization after each change, the potential energy profiles were calculated for the trans-cis conversion of CHP employing CASSCF and CASSCF with MP2 correction. Every stationary structure was calculated as a minimum, i.e. no imaginary frequency, or as a transition state, i.e. one imaginary frequency, following harmonic vibrational frequency analysis. The pseudo rotation of *trans*-cycloheptene was also determined. It resulted in a transition state found to have a C<sub>2</sub> axis of symmetry and a force constant matrix with the requisite single negative frequency.

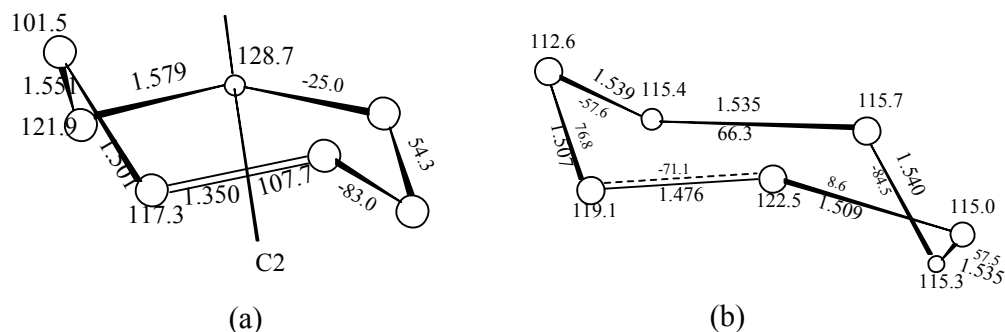


**Figure 2.26** Geometries optimized by CASSCF/6-31G(d) (a) pseudorotation transition state of *trans*-CHP. (b) *trans*-to-*cis* transition state of CHP (bond lengths in Å, torsion angles given for each C-C bond and CCC valence angle for each C atom).

The calculations showed a barrier to ring flip of 10.6 kcal/mol (CASSCF) and 10.74 kcal/mol (CASSCF MP2) (**Figure 2.27**) in good agreement with our value determined from dynamic NMR of 10.0 kcal/mol.

In **Table 2.5** are listed the determined the energy differences between the *cis*- and *trans*-cycloheptene species, calculated at different computational levels. From the results, one sees an additional 30 kcal/mol strain added to the *trans*-cycloheptene compared to *cis*. This results are in good agreement with Michl's<sup>285</sup> and Caldwell's<sup>284</sup> computations. To further test the efficacy of using this type of computation for the *trans*-

**Table 2.5:** Experimental and calculated <sup>13</sup>C chemical shifts of *cis* and *trans*-CHP.

Carbo n	<i>cis</i> -CHP		<i>trans</i> -CHP	
	Exp <sup>a</sup>	Calc <sup>b</sup>	Exp <sup>a</sup>	Calc <sup>b</sup>
1	130.2	130.6	135.5	134.8
2	130.2	130.6	131.8	130.6
3	29.4	28.5	36.2	35.2
4	29.4	28.5	25.3	23.8
5	27.9	27	31.7	30.6
6	27.9	27	33.9	32.6
7	33.4	32.8	26.2	24.8

<sup>a</sup> Observed <sup>13</sup>C chemical shifts in acetone-d<sub>6</sub>.

<sup>b</sup> MP2/6-311+G(2d,p)//B3LYP/6-31G(d) level.

cycloheptene system, the  $^{13}\text{C}$  chemical shifts for the *cis*- and *trans*-cycloheptene were calculated. The geometries were determined by geometry optimizations at the B3LYP3/6-31G(d) level, while establishing that the calculated geometries were energy minima using vibrational frequency analysis. Employing GIAO approach at MP2 level with a 6-311+G(2d,p) basis set, the  $^{13}\text{C}$  NMR isotropic magnetic shielding tensors were calculated and compared to that of tetramethylsilane calculated at the same level. The chemical shifts thus obtained, along with the experimental values, are reported in **Table 2.6**. The excellent fit between the experimental and computed chemical shifts shows again that calculations at this *ab initio* level accurately reflect the real system. However, as seen in the calculated torsional potential energy profile shown in **Figure 2.27**, the calculations also determined a 33.83 kcal/mol (CASSCF), or 35.74 kcal/mol (CASSCF MP2), energy barrier for the double bond rotation of the *trans* to *cis* isomer conversion, widely divergent from the experimental values. So the question arises how can these high-level calculations produce very good fits to the ring-flip barrier and  $^{13}\text{C}$  NMR spectrum, but do such a poor job at the *trans*-to-*cis* barrier? To further examine the efficiency of the computation a closer look at the calculated *trans* geometry was undertaken.

**Table 2.6:** Calculated *cis* - *trans* CHP energy difference at various levels. All *ab initio* energies are corrected for zero-point energy.

Methods	$\Delta H_{\text{c}=\text{t}}$ (kcal/mol)
PCMODEL (MMX)	33.2
AM1	30.9
HF/6-31G(d)	34.9
B3LYP/6-31G(d)	29.4
CASSCF(2,2)/6-31(G)d	30.8
CASSCF(2,2)/6-31G(d) MP2	29.8

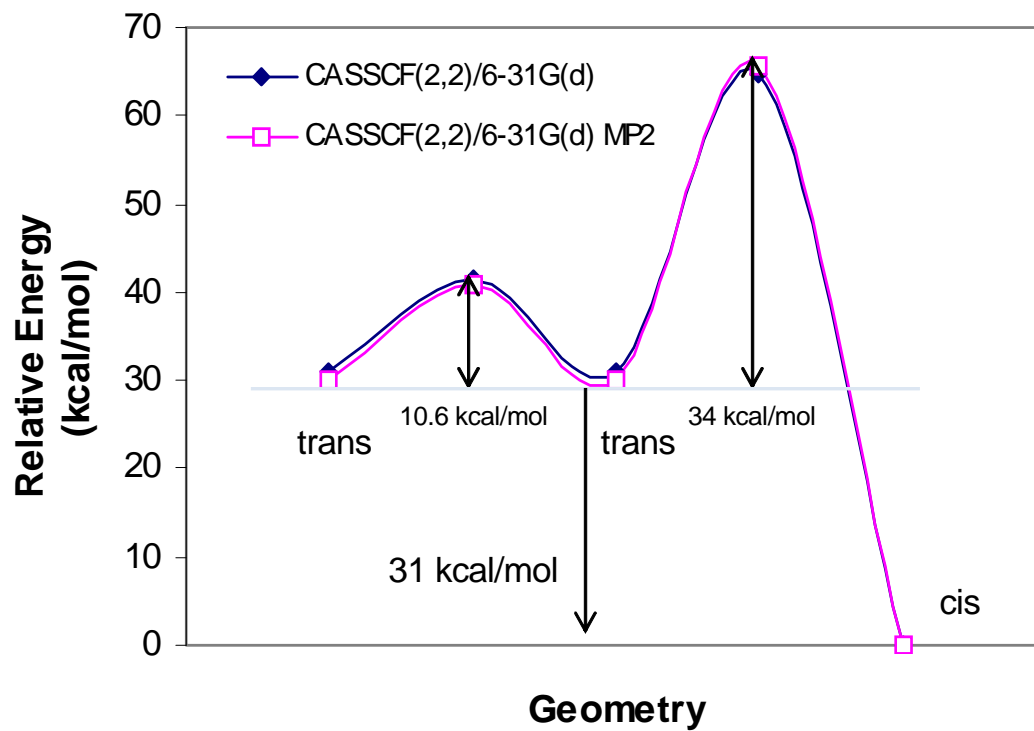


Figure 2.27 The double bond torsional potential energy profile of CHP.

### 2.5.5. Winkler and POAV analysis of *trans*-CHP

When optimized at CASSCF(2,2)/6-31G(d), the geometry of *trans*-cycloheptene showed that the pyramidalization angles for both vinyl carbon atoms are very close with  $\chi_1 = 37.0^\circ$  and  $\chi_2 = 35.4^\circ$ . It was also found that the p-orbital twist angle ( $\tau$ ) is  $30.1^\circ$ . The resulting negative value of  $\eta$  implies that

*trans*-cycloheptene's strain was relieved predominantly by pyramidalization, i.e.

bond bending. For comparison, in

**Table 2.7** are reported the optimized values for *trans*-cycloheptene, the

*trans*-cyclooctene<sup>188</sup> (**1**) a mono<sup>289</sup> (**2**) and

a trisila<sup>290</sup> (**3**) *trans*-cycloheptene (**Figure 2.28**).

**Table 2.7:** Distortion Angles (deg) of some *trans*-cycloalkenes.

	<i>trans</i> -CHP	1	2	3
$\tau$	30.03	18	23.12	19.6
$\chi_{av}$	36.2	24	26.08	13.2
$\xi$	66.23	42.3	49.19	32.8
$\eta$	-6.17	-6	-2.96	6.4

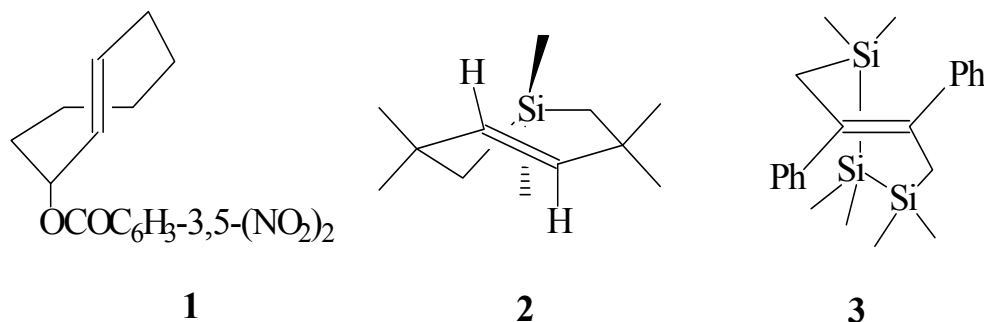


**Figure 2.28** Some *trans*-cycloalkenes

Note that the large  $\xi$  value of 66.2 for *trans*-CHP suggests that there is much more strain in *trans*-CHP than the molecules shown in **Figure 2.28**. This is explained by either larger ring sizes, or the longer Si-C and Si-Si bond lengths. However, except for **3**, the  $\eta$  values



were found to be all negative, which meant that the strain in all of those trans cyclic alkenes was diminished mostly by bond bending, i.e. pyramidalization, rather than by twisting.

The results from the performed POV analysis on *trans*-cycloheptene and on the molecules of **Figure 2.28** are shown in **Table 2.8** and **2.9**. The rehybridizations, i.e. the p-character changes of the  $\sigma$ -orbitals ( $sp^n$ ) and the s-character changes of the  $\pi$ -orbitals ( $s^{mp}$ ) in *trans*-cycloheptene, are more significant compared to those of the **1**, **2** and **3**. These results confirm the above-discussed higher strain in *trans*-cycloheptene and the preferability of pyramidalization, over twisting, in its effort of relieve it.

**Table 2.8:** POAV1/3D-HMO analysis of some strained cyclic alkenes.

	C=C length (Å)	Torsional angle (°)	overlap integral				$\rho^B$	
			s,s	s,p $_{\sigma}$	p $_{\sigma}$ ,p $_{\sigma}$	p $_{\pi}$ ,p $_{\pi}$		total
<i>Trans</i> -CHP	1.352	30.1	0.0307	-0.0409	0.0104	0.2054	0.2056	0.837
<b>1</b>	1.329	18.2	0.0126	-0.0171	0.0044	0.2496	0.2494	1.015
<b>2</b>	1.344	19.2	0.0035	-0.0049	0.0013	0.2500	0.2499	1.017
<b>3</b>	1.330	21.7	0.0150	-0.0204	0.0052	0.2412	0.2411	0.981

**Table 2.9:** POAV2/3D-HMO analysis of some strained cyclic alkenes.

	C=C length (Å)	Torsional angle (°)	overlap integrals				$\rho^B$	
			s,s	s,p $_{\sigma}$	p $_{\sigma}$ ,p $_{\sigma}$	p $_{\pi}$ ,p $_{\pi}$		total
<i>Trans</i> -CHP	1.352	30.1	0.0306	-0.0433	0.0117	0.2045	0.2035	0.828
<b>1</b>	1.329	18.1	0.0125	-0.0183	0.0050	0.2491	0.2483	1.010
<b>2</b>	1.344	18.9	0.0035	-0.0056	0.0017	0.2501	0.2497	1.016
<b>3</b>	1.330	20.1	0.0148	-0.0208	0.0055	0.2431	0.2426	0.987

The mismatch of the calculated trans to cis barrier compared to the accuracy shown by the *ab initio* calculations for both the ring-flip barrier and the  $^{13}\text{C}$  chemical shifts for *trans*-cycloheptene prompted a closer look at the experimentally determined barrier. Many control experiments were carried out showing that acidic impurities in solution or on the glass walls of the NMR tube were not responsible for the low barrier. However, when precise measurements were made of the rates of decay of *trans*-cycloheptene with different starting concentrations, it was found that the trans to cis decay occurred via a second order mechanism, i.e. that the decay process was bimolecular. A possible bimolecular decay process could involve two *trans*-cycloheptene molecules combining to form a 1,4-biradical which then cleaves to give two *cis*-cycloheptene molecules (Figure 2.29).

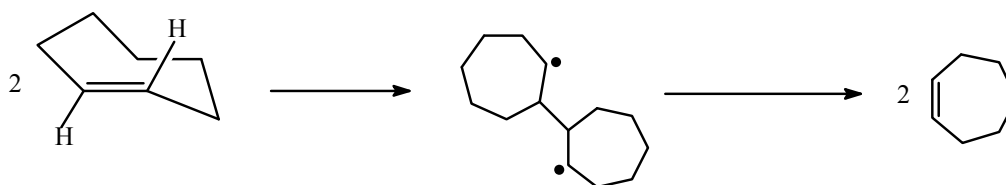


**Figure 2.29** 1,4-biradical mechanism of *trans*-CHP isomerization.

### 2.5.6. Biradical mechanism for *trans* to *cis* decay

What is known about the fragmentation of 1,4-biradicals? Figure 2.30 shows the formation of a tetramethylene biradical where bond rotation followed by fragmentation is the proposed path for *cis*

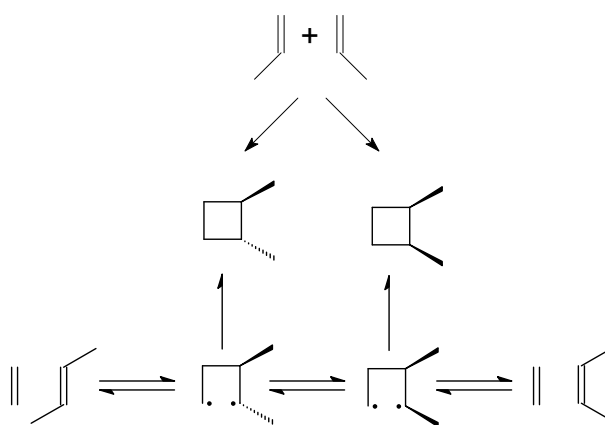


**Figure 2.30** Reaction scheme of tetramethylene biradical.

and *trans*-2-butene formation from the thermal cycloaddition of propene.<sup>291</sup> The mechanism of formation of this 1,4-biradical intermediate was also applied to explain the thermal decomposition of 3,4-dimethyl-3,4,5,6-tetrahydropyridazines.<sup>292</sup>

Hoffmann conducted an extended Hückel calculation<sup>293</sup> for the energy surface found between cyclobutane and two molecules of ethylene, and found a nearly flat hypersurface. Later Segal<sup>294</sup> derived two well-defined potential energy minima for the gauche and trans conformations of tetramethylene

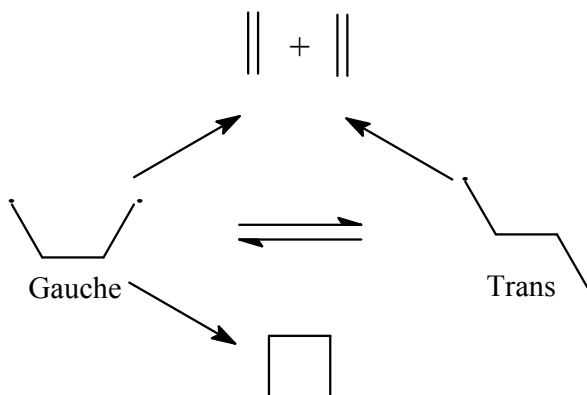


**Figure 2.31** Reaction scheme of tetramethylene biradical.

(**Figure 2.31**) by utilizing STO-3G level *ab-initio* calculations.

In his work delineating the reaction paths of tetramethylene, Zewail<sup>295</sup> employed the spin-unrestricted DFT method at the B3LYP/6-31G(d) level. He found that the gauche conformer was less stable than *trans*-tetramethylene by a small amount, and he calculated a 3.0 kcal/mol barrier, around the central bond for the *trans*→*gauche* isomerization. His barriers of fragmentation for the *trans* and *gauche* conformations to a pair of ethylene molecules were 1.2 and 2.0 kcal/mol, respectively. Calculations at another levels of theory found similar numbers with deviations no more than few kcal/mol.<sup>296</sup> Thus, the calculated energies for rotation, cleavage and closure in the parent 1,4-biradical were calculated to be nearly barrierless.<sup>297</sup> The calculated values were also found to be in excellent fit with the observed lifetime.<sup>298</sup>

In 1984 Michl<sup>299</sup> synthesized in the gas phase ethylene and cyclobutane from the reaction of sodium vapor and diiodobutene and found a preponderance of cleavage over closure of his presumed intermediate. The proposed intermediate for his reaction was a 1,4-biradical, formed in the *trans* geometry (**Figure 2.32**). Comparing Zewal's 3.0 kcal/mol energy barrier for *trans*-to-*gauche* transition in tetramethylene, to the 1.2 kcal/mol fragmentation energy barrier found by Michl, shows that a 1,4-biradical can preferentially cleave rather than close.

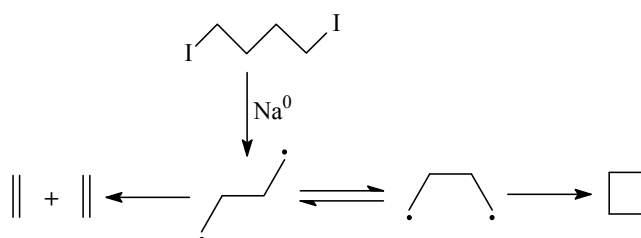


**Figure 2.32** Michl's proposed formation of *trans* tetramethylene to explain high ratio between cleavage and closure.

Another case of favored cleavage over ring-formation in a *trans*-1,4-biradical is shown in **Figure 2.33**, describing the photodecarbonylation of 2,3,4,5-tetraphenylcyclopentanone.<sup>300</sup> Here the ratio of stilbenes to cyclobutanes was equal to 20:1. Again cleavage is preferred even though in this case the 1,4-biradical is initially produced in a *gauche* conformation.

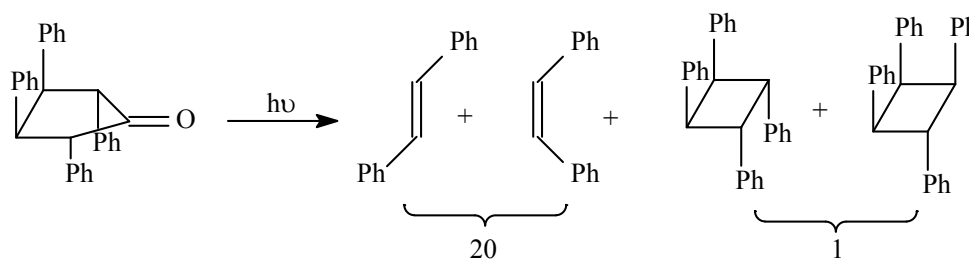


**Figure 2.33** Photolysis of 2,3,4,5-tetraphenylcyclopentanone.

The unequivocal existence of 1,4-biradical intermediates, formed in the isomerization reactions in strained cyclic alkenes, could explain the second order isomerization of *trans*-cycloheptene (Figure 2.34). Indeed, other double bond isomerizations involving 1,4-biradicals have been proposed.<sup>301,302,303,302c,304,305,306</sup>

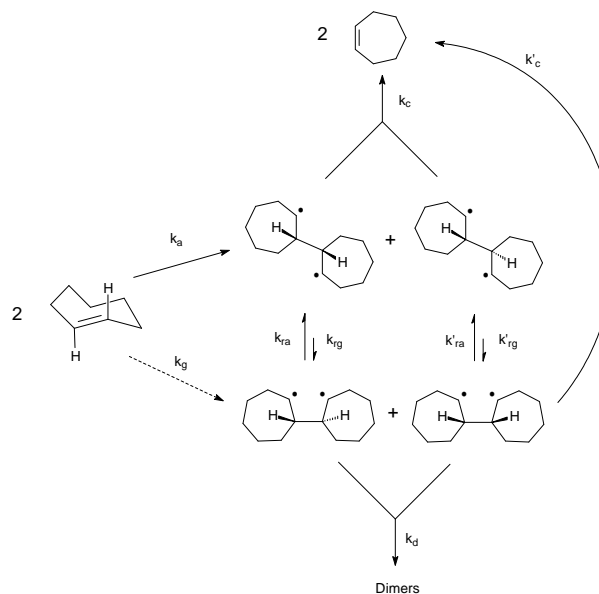


**Figure 2.34** Bimolecular mechanism for *trans* to *cis* isomerization of CHP,  $k_a \gg k_g$ ,  $k_c \gg k_{rg}$ .

In the figure two *trans*-cycloheptene molecules join to form a 1,4-biradical intermediate which can have a *gauche* but more probably a *transoid* form.<sup>307</sup> The two rings, no longer constrained by the double bonds, will flip into more stable geometries, i.e. a *twist-chair* or *chair*. At this point the 1,4 biradical cleaves into two *cis*-cycloheptene entities.

Support for this mechanism comes from GC/MS experiments which suggest about 1% cycloheptene dimer formation. Further support comes from computational methods. Due to the complexity of the system (Figure 2.35), *ab-initio* calculations on all maximum and minimum on the potential energy surface on all 35 biradical conformations, found by using the GMMX conformation searching routine in PCMODEL, would be an extremely comprehensive and daunting task. However, some of those values were obtained employing the UB3LYP/6-31G(d) level. At this level, it was found that the energy barriers for cleaving *gauche* and *transoid* biradicals were 2.6 kcal/mol and 1.2 kcal/mol respectively. However,

the interconversion of those biradicals would take approximately 4 kcal/mol. Thus, again with the bicycloheptyl 1,4-biradical, cleavage would be favored over rotation and closure.

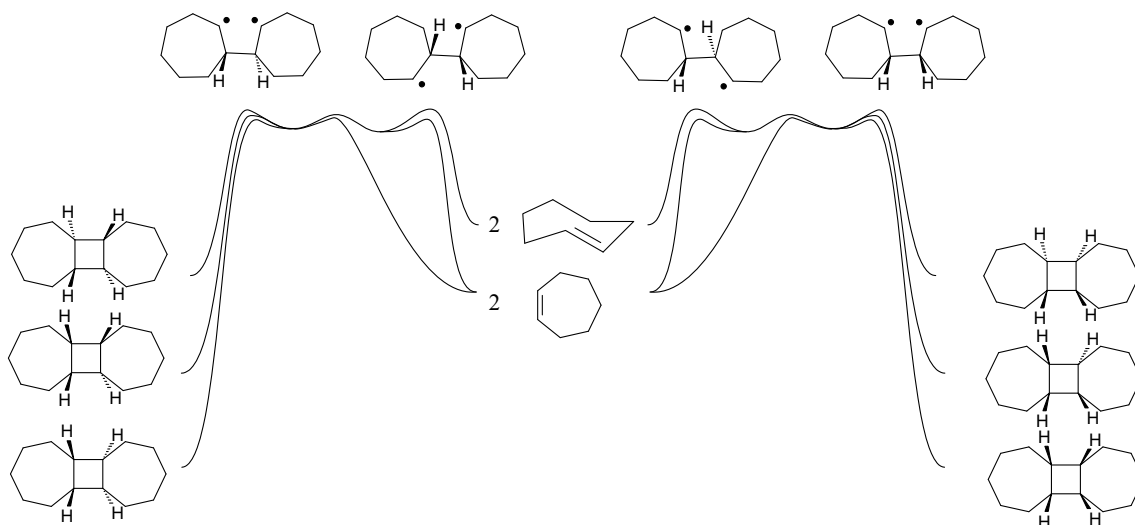


**Figure 2.35** CHP dimerization. The cleavage of gauche biradicals to two *trans*-CHP as well as the cleavage of all biradicals to *trans*- and *cis*-CHP are not depicted.

The barrier to the formation of the 1,4-biradical was also calculated. The anti and syn approach geometries of two *trans*-cycloheptenes were calculated at the UB3LYP/6-31G(d) level. The computational results gave 11.3 kcal/mol and 9.5 kcal/mol for pathways leading towards the syn transoid biradical and anti transoid biradical formation respectively. These results were in good agreement with the experimental energy of activation for the bimolecular reaction of 13.8 kcal/mol found in our group. Further if the constraint approaches were eliminated in the calculations, both the syn gauche and the anti gauche geometries twisted to the transoid approach geometry. Those results indicate that the steric interactions between the seven membered rings will preferably push the two *trans*-cycloheptenes into transoid biradical formation rather than towards a gauche biradical,

again favoring cleavage.<sup>272</sup>

Thus, the initial disagreement between the experimentally determined and calculated stability of *trans*-cycloheptene, was solved by explaining that the observed decay of *trans*- to *cis*-cycloheptene does not occur via “direct twisting” about the double bond. Instead, it was determined that the process was a second order dimerization. The 1,4-biradical formed during the dimerization of two *trans*-cycloheptenes quickly changed to a more stable geometry. This geometrically relaxed biradical quickly cleaves and forms two *cis*-cycloheptene molecules. If this bimolecular mechanism could be inhibited sterically, there is a possibility that one could produce room temperature stable *trans*-cycloheptenes. To test this possibility, we look at the stability of substituted *trans*-cycloheptenes. Initially, *trans*-1-methyl cycloheptene was produced, but a methyl group in this position proved ineffective in blocking the  $\pi$ -portion of the double bond and bimolecular decay still occurs.<sup>308</sup> In this work we chose to examine the stability of three allylically substituted *trans*-cycloheptenes, the 3,3,7,7-tetramethyl (TMCHP) and the *syn* and *anti* 3,7-di-*t*-butyl (DTBCHP) *trans*-cycloheptenes (**Figure 2.36**).

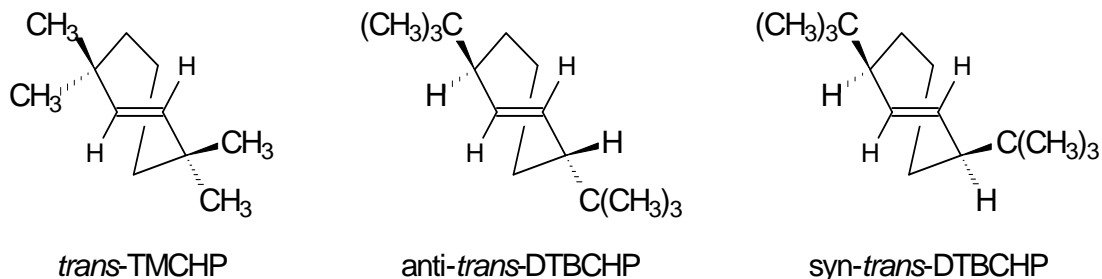


**Figure 2.36** Sterically blocked substituted *trans*-cycloheptenes of interest.

## **2.6. Experimental**

### **2.6.1. Equipment and techniques used**

#### **2.6.1.1. Materials**

All reagents and solvents were purchased from Sigma Aldrich, Fisher Scientific and Cambridge Isotope Labs. All chemicals were used without any further purification except otherwise specified. Toluene-d<sub>8</sub> was distilled over CaH<sub>2</sub> under nitrogen atmosphere and stored over 3Å molecular sieves.

#### **2.6.1.2. Analytical data collection**

All data was collected using a Bruker Avance 250-NMR and Bruker Avance 400-NMR standard bore spectrometers. All chemical shifts from <sup>1</sup>H and <sup>13</sup>C NMR spectra were collected and reported in reference to the solvent's characteristic chemical shift(s).

#### **2.6.1.3. Sample purification**

Both the TMCHP and DTBCH were purified using preparatory vapor gas chromatography with a GowMac 580 equipped with 30'x1/4" 30% OV-17 on Chromosorb P 100/120 mesh column. All injection port inserts, collection vials and ampules were base washed as described in procedure 2.6.1.4. Due to the high temperature conditions, the injectors were equipped with silicon based septa with one teflon side.

#### **2.6.1.4. Glassware and equipment**

All glassware, NMR tubes, capillary tubes, storing ampules and syringes were base washed. These were soaked in a base bath for 2 hours and then thoroughly washed with deionized water. The syringes were subsequently rinsed with methanol prior to every use.



### 2.6.1.5. Photolysis equipment

The photolysis was carried out at low temperature using the apparatus pictured in **Figure 2.37**. The flow of the cooling nitrogen was controlled by a pressure gauge and traveled through a copper coil submerged in a dewar filled with liquid nitrogen.

Once the cooled nitrogen gas left the coil, it was conveyed through a short tube wrapped with a heating element, which allowed us to control the temperature of the cooling gas. The chilled gas would evacuate past the 25mm quartz tube holding a pentane cooling bath in which the quartz NMR tube containing the sample was immersed. A hose punctured with small holes was fastened near the bottom of the dewar and a continuous flow of room temperature of nitrogen was used to prevent any clouding to the outside surface.

A home-made Rayonet reactor assembled in two hemi-cylindrical parts was used as the light source. Each part is equipped with six 25W Hg<sub>2</sub> vapor bulbs GE-G2578 emitting light at 254 nm.

### 2.6.1.6. Purification of substituted cycloheptenes.

TMCHP was GC purified by collecting multiple 30  $\mu$ L injections using 65 ml/min flow of UHP300 He gas carrier with the following settings: Injector = 190°C; Column = 150°C; Detector = 190°C. The fraction collected had a retention time of 58 minutes. <sup>1</sup>H NMR: (250 MHz, CDCl<sub>3</sub>)  $\delta$  1.02 (s, 12H), 1.54 (m, 4H), 1.66 (m, 2H), 5.14 (s, 2H); <sup>13</sup>C NMR: (400 MHz, CDCl<sub>3</sub>)  $\delta$  137.54, 43.13, 37.19, 31.11, 21.46.

DTBCH was GC purified by multiple 40  $\mu$ L injections with a 60 ml/min flow of UHP300 He gas carrier and the following settings: Injector = 190°C; Column = 170°C; Detector = 190°C. The syn and anti DTBCHP fractions could be collected separately and

had retention times of 182 and 187 minutes, respectively.

Chemical shifts of first peak DTBCHP with retention time of 182 min:  $^1\text{H}$  NMR: (400 MHz,  $\text{CDCl}_3$ )  $\delta$  1.07 (s, 9H), 1.18 (m, 2H) 1.84 (m, 4H), 2.27 (m, 2H), 5.95 (s, 2H);  $^{13}\text{C}$  NMR: (400 MHz,  $\text{CDCl}_3$ )  $\delta$  134.39, 50.06, 33.3, 32.9, 28.55, 27.68.

Chemical shifts of second peak DTBCHP with retention time of 187 min:  $^1\text{H}$  NMR: (400 MHz,  $\text{CDCl}_3$ )  $\delta$  0.89(s, 9H), 1.62 (m, 2H), 1.43 (m, 4H), 2.09 (m, 2H), 5.52 (s, 2H);  $^{13}\text{C}$  NMR: (400 MHz,  $\text{CDCl}_3$ )  $\delta$  130.31, 48.54, 34.05, 28.02, 25.78, 24.05.

#### **2.6.1.7. Bromination to assign *syn* and *anti* DTBCHP isomers**

In order to distinguish *syn*-DTBCHP from *anti*-DTBCHP, we made the 1,2-dibromo adduct of each of the isomers. Prior to the  $\text{Br}_2$  addition, the sample was prepped as described in **2.6.1.6.** and then passed through  $\text{CaH}_2$  to eliminate any acidic residues and water. Using a 50  $\mu\text{L}$  air-tight syringe,  $\text{Br}_2$  was added to an NMR sample one drop at a time and then shaken vigorously on vortex mixer. The addition was continued until no more discoloration occurred, i.e. the  $\text{Br}_2$  was in slight excess. The samples were then analyzed with NMR:

*Syn*-1,2-dibromo-3,7-di-*t*-butyl cycloheptene  $^{13}\text{C}$  NMR: (400 MHz,  $\text{CDCl}_3$ )  $\delta$  61.27, 60.02, 60.308, 48.94, 34.71, 34.08, 0.35, 28.89, 28.47, 26.97, 26.3.

*Anti*-1,2-dibromo-3,7-di-*t*-butyl cycloheptene's two diastereoisomers  $^{13}\text{C}$  NMR: (400 MHz,  $\text{CDCl}_3$ )  $\delta$  63.12, 45.51, 34.14, 28.52, 27.97, 23.42 and  $^{13}\text{C}$  NMR: (400 MHz,  $\text{CDCl}_3$ )  $\delta$  57.45, 57.39, 34.4, 31.74, 25.19, 24.64

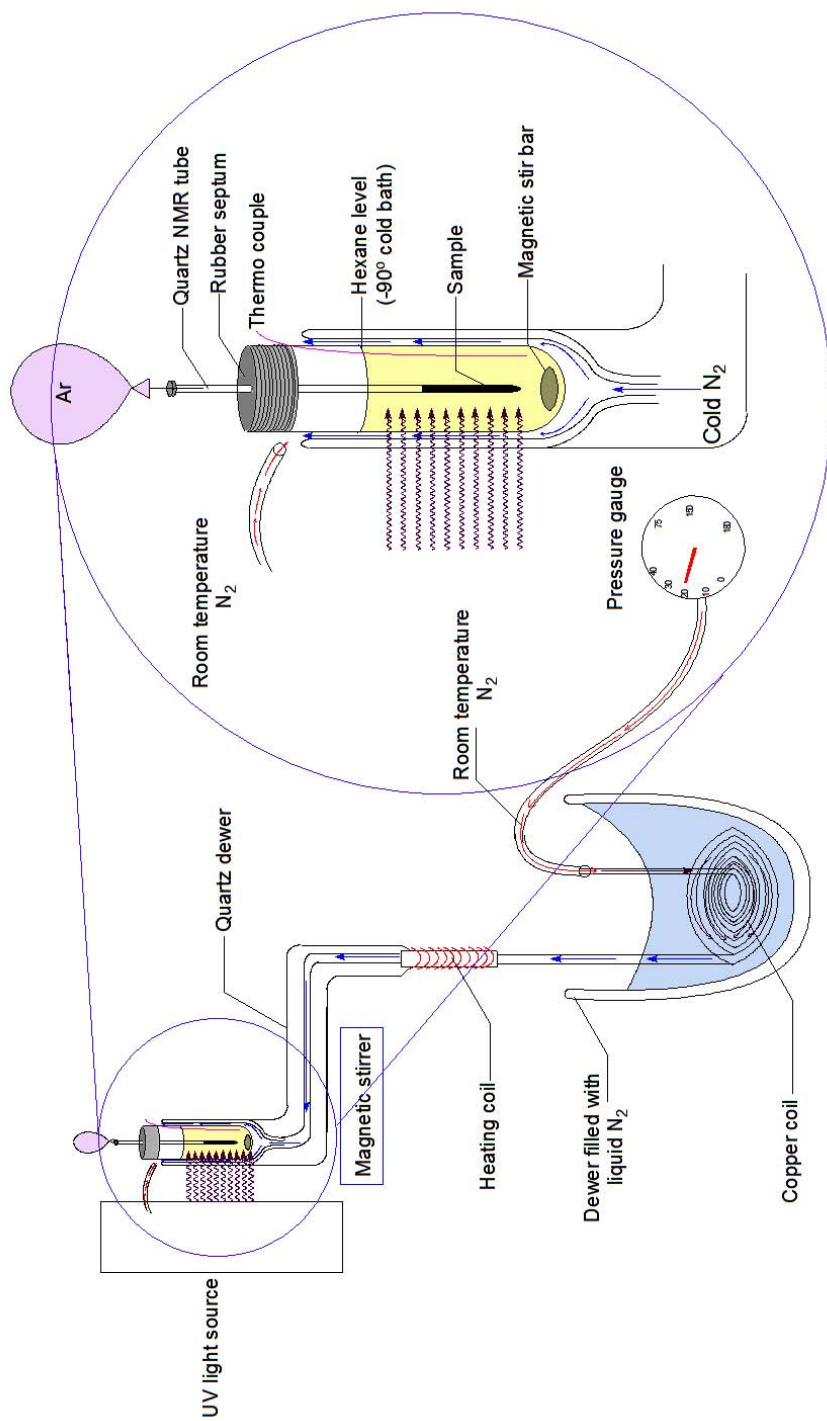


**Figure 2.37** Modified low temperature photolysis apparatus.

### 2.6.3. Low temperature photolysis experiments - sample preparation and conditions

The GC purified syn-DTBCHP was dissolved in tol- $d_8$  and to eliminate any acidic residues and water this solution was passed through a CaH<sub>2</sub> pipette filter and then collected into a base washed quartz NMR tube, sealed with a rubber septum. The sample was then degassed by purging it with Ar through a teflon cannula for 20 minutes. After degassing, the cannula was pulled out and replaced with an Ar balloon sealed to a needle (closeup **Figure 2.37**), which penetrated the septum and maintained a positive pressure of Ar during photolysis. The Ar used was purchased from Airgas as UHP300. The sample was then put in a pentane bath contained in a 25mm quartz tube and cooled by using the apparatus shown in **Figure 2.37**. Before the photolysis began, the homemade arc reactor was turned on and warmed up for 20-30 minutes. After reaching steady temperature the sample was photolyzed for 60 minutes at -85° C.

After the photolysis was complete the sample was moved to a dry ice/acetone slurry and maintained at low temperature until the sample is transferred to a precooled NMR tube held at -90°C. The probe was purged with nitrogen and cooled via a flow of cool nitrogen gas passed through a stainless steel coil, dipped in a liquid nitrogen dewar.

### 2.6.4. TMCHP room temperature decay experiments

Tol- $d_8$  was passed through CaH<sub>2</sub> pipette filter to eliminate any acidic residues and water. The sample was then prepared in two different solution concentrations with 6.25  $\mu$ L and 12.5  $\mu$ L of GC purified TMCHP. The samples were placed into a base washed, quartz NMR tube and capped with rubber septum. The samples were then degassed by purging with Ar through a teflon cannula for 20-30 minutes. Once the degassing was complete, the

cannula was pulled out and replaced with balloon sealed with a needle and filled with Ar (closeup **Figure 2.37**). The samples were then cooled and photolyzed in a hexane bath as previously.

After the photolysis was complete the sample was removed and allowed to warm up to room temperature. Multiple NMR's were taken within the next several hours and decay studies were performed by using the integrated values obtained from the NMR spectra.

#### **2.6.5. Computational experiments - methods and basis sets**

All NMR shifts were calculated on Alabama Super Computer using Gaussian03 at MP2/6-311+(2d,p)//MP2/6-31G(d) level. These calculations used the GIAO method and the isotropic magnetic shift tensors were compared to that of tetramethylsilane to obtain the chemical shifts.

## 2.7. Results and discussion

### 2.7.1. Dynamic NMR

TMCHP and both DTBCHP's were previously synthesized by the route below.

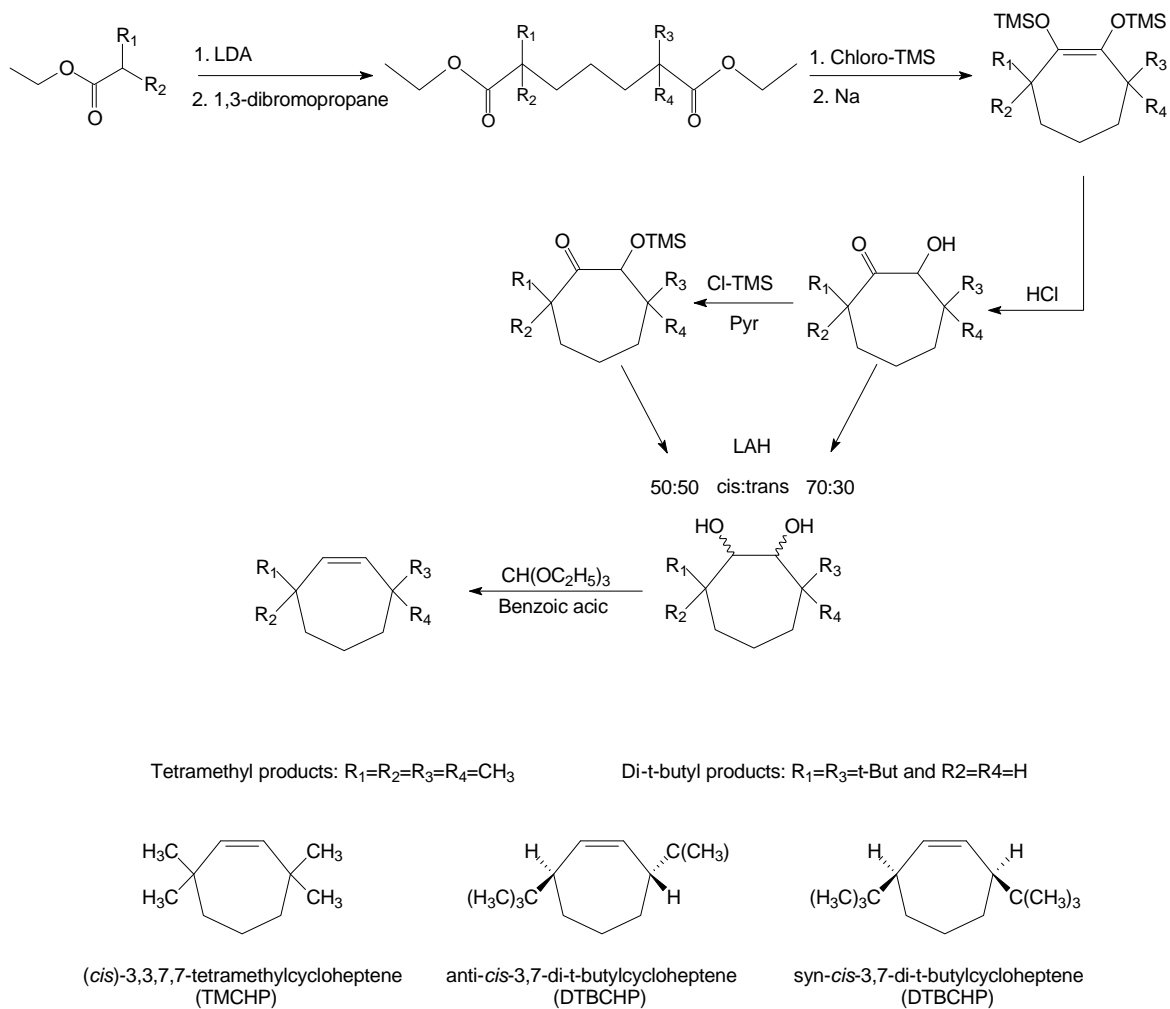


**Figure 2.38** Synthesis of substituted cycloheptenes.

However, the syn and anti isomers of DTBCHP had not been previously identified. Using preparatory GC we were able to separate the syn and anti isomers and then brominate them as described in 2.6.2.3. The trans bromination of the syn isomer results in a pair of

enantiomers and 11 carbon NMR signals would be expected (**Figure 2.39**). On the other hand, bromination of the anti isomer would give a pair of diastereomers and two sets of six chemical shifts would result. The bromination of the isomer with retention time of 182 minutes gave 11 carbon peaks, and so was identified as the syn isomer while the DTBCHP with a retention time of 187 minutes upon bromination showed two sets of 6 carbon shifts in about a 2:1 ratio and so was identified as the anti isomer.

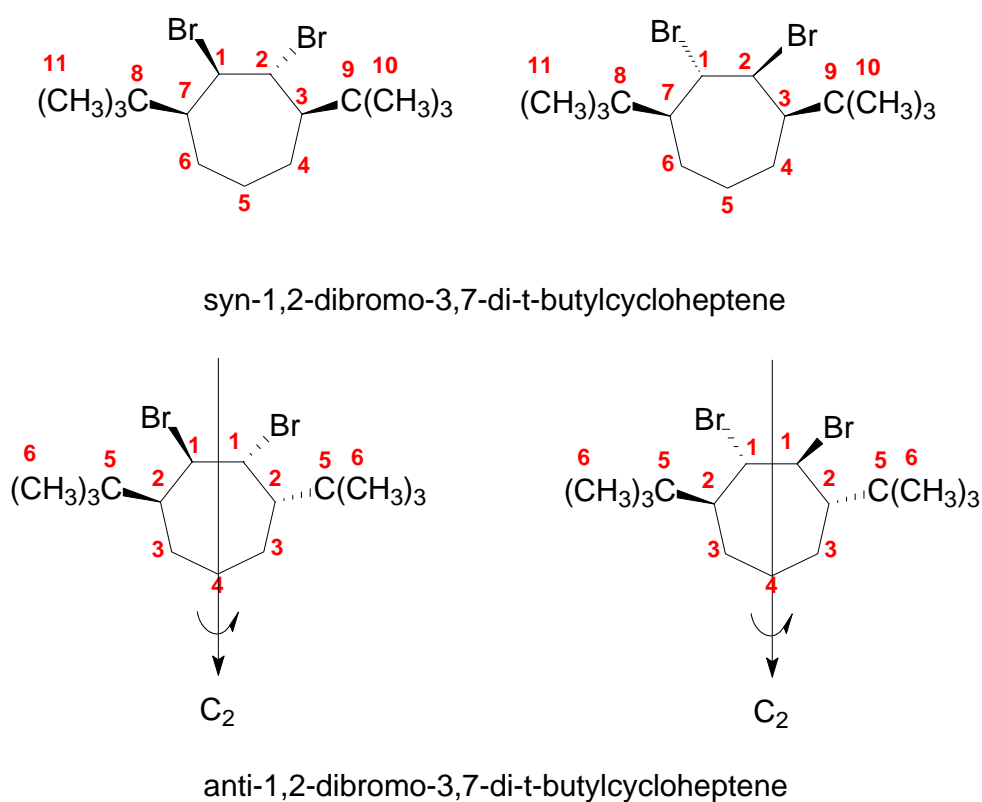


**Figure 2.39** Identification of substituted cycloheptenes through bromination.

The cis isomers of the now identified syn- and anti-DTBCHP's, as well as TMCHP, were photolyzed using triplet sensitization via the toluene- $d_8$  solvent. Species, later identified as the trans isomer, were produced but in smaller concentrations as compared to the parent

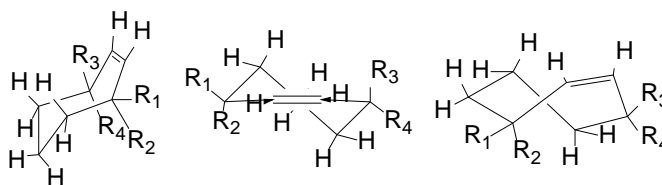
cycloheptene. Syn-DTBCHP, anti-DTBCHP and TMCHP gave 5%, 6% and 1.3% maximum conversions of the trans isomer. To identify these species as the trans isomers a series of spectroscopic and computational studies were undertaken.

To determine the minimum energy conformations of *cis*- and *trans*-TMCHP, as well as those of syn- and anti-DTBCHP, force field calculations using the MMX parameter set of PCModel v.9.10 were performed (**Figure 2.39**). From the MMX results one can see that the parent trans-cycloheptene shows the expected unsymmetrical geometry. The flip of this ring, occurring through a transition state with a  $C_2$  axis was shown to have a barrier of 10.0 kcal/mol and is responsible for the observed dynamic NMR.<sup>286</sup> The substituted trans-cycloheptenes who adopt this unsymmetrical structure will therefore also experience this ring flip.

Our approach to identify the species produced photochemically from *cis*-TMCHP and *cis*-syn- and *cis*-anti-DTBCHP was three fold. First, did the species show a trans coupling constant between the two vinyl hydrogens? Second, was the expected dynamic NMR caused by the ring flip of a trans isomer observed and finally was there a good correlation between the experimentally observed  $^{13}\text{C}$  NMR shifts and those computed at a level which had been shown to give excellent agreement to the experimental shifts of the parent compound?



## Cis



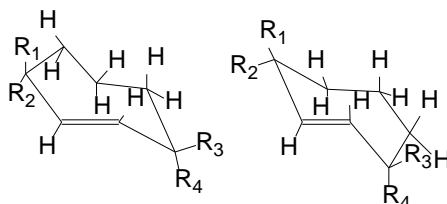
Chair

C<sub>2</sub>

Twist-boat

R <sub>1</sub> = R <sub>2</sub> = H R <sub>3</sub> = R <sub>4</sub> = H	0.00	0.73	2.41
R <sub>1</sub> = R <sub>2</sub> = CH <sub>3</sub> R <sub>3</sub> = R <sub>4</sub> = CH <sub>3</sub>	0.00	0.76	2.93
R <sub>1</sub> = R <sub>4</sub> = C(CH <sub>3</sub> ) <sub>3</sub> R <sub>2</sub> = R <sub>3</sub> = H (anti)	2.97	3.30	0.00
R <sub>1</sub> = R <sub>3</sub> = C(CH <sub>3</sub> ) <sub>3</sub> R <sub>2</sub> = R <sub>4</sub> = H (syn)	0.00	4.65	2.76

## TRANS



Trans-1

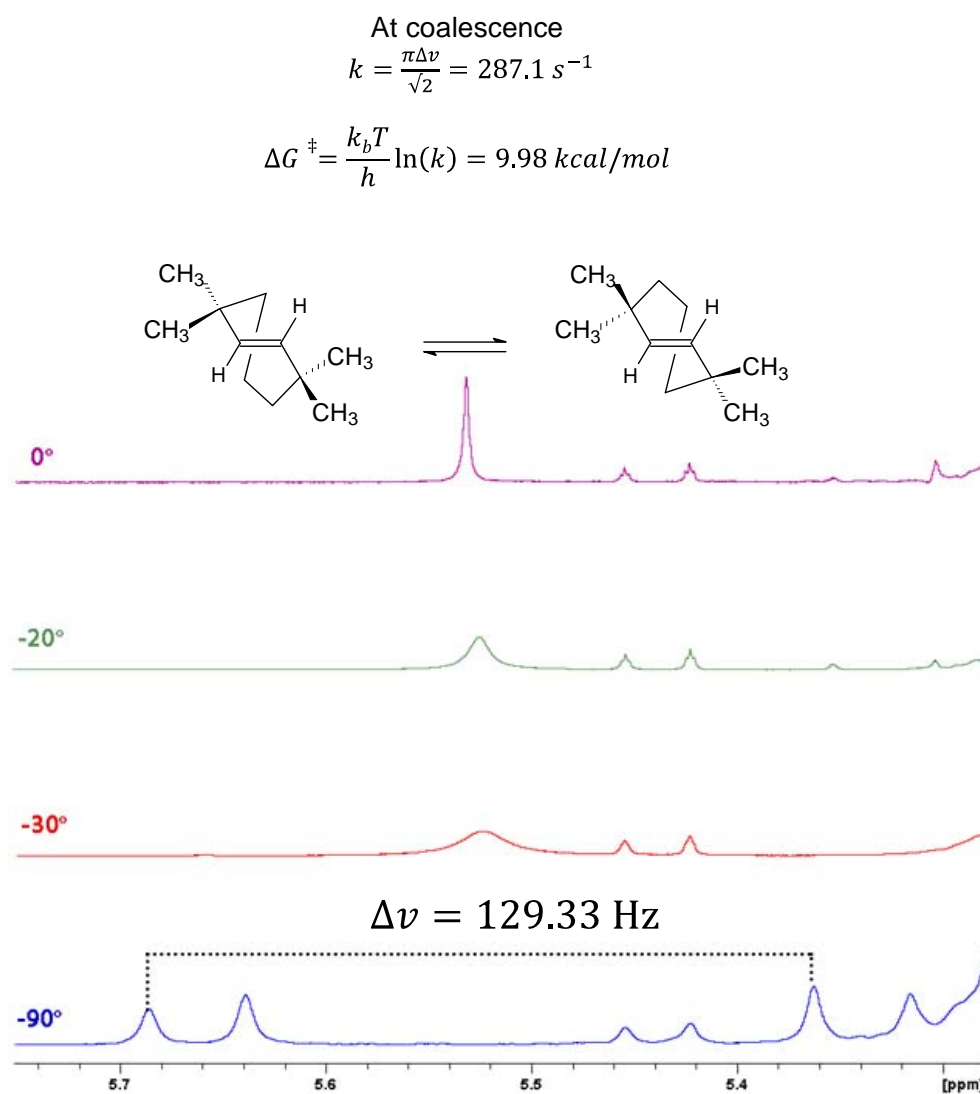
Trans-2

R <sub>1</sub> = R <sub>2</sub> = H R <sub>3</sub> = R <sub>4</sub> = H	31.83	
R <sub>1</sub> = R <sub>2</sub> = CH <sub>3</sub> R <sub>3</sub> = R <sub>4</sub> = CH <sub>3</sub>	28.68	28.68
R <sub>1</sub> = R <sub>4</sub> = C(CH <sub>3</sub> ) <sub>3</sub> R <sub>2</sub> = R <sub>3</sub> = H (anti)	34.07	34.07
R <sub>1</sub> = R <sub>3</sub> = C(CH <sub>3</sub> ) <sub>3</sub> R <sub>2</sub> = R <sub>4</sub> = H (syn)	29.69	33.51

**Figure 2.40** Conformational MMX calculations of minimum energies (kcal/mol) of different cis and trans substituted cycloheptenes.

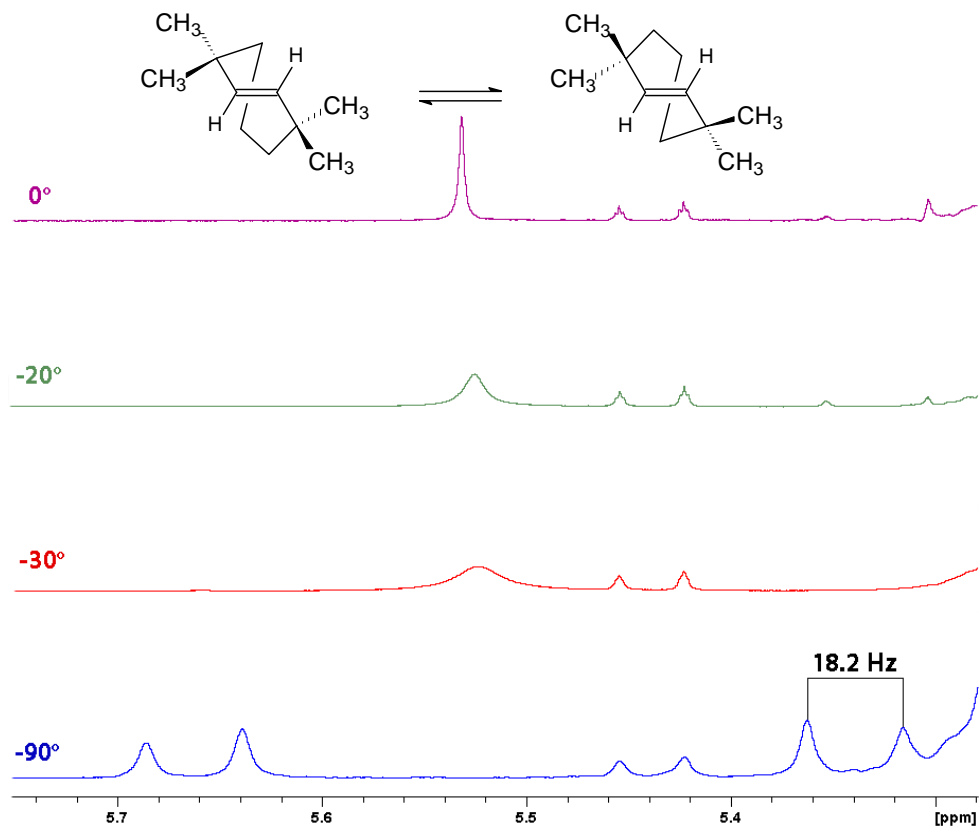
### 2.7.2. *Trans*-TMCHP

As seen in **Figure 2.39** *trans*-TMCHP has two degenerate ring geometries and thus will be expected to show a dynamic NMR when the ring flip occurs. Indeed, as seen in **Figure 2.40** dynamic NMR is observed. The experimentally obtained dynamic NMR shows a coalescence temperature of about  $-30^{\circ}\text{C}$  which given the low temperature shift difference of 129.33 Hz corresponds to a  $\Delta G = 9.98$  kcal/mol.



**Figure 2.41** Ring flip barrier for *trans*-TMCHP

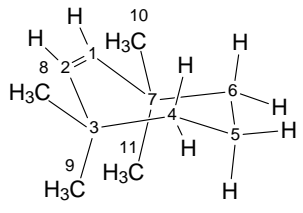
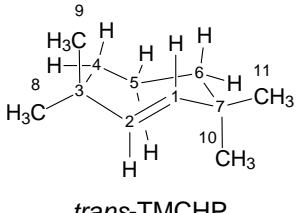
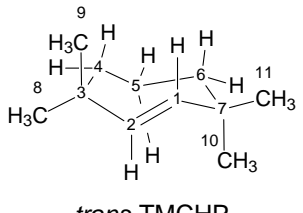
This barrier is almost identical to the parent compound's ring flip barrier. Additionally, the low temperature spectrum shows a *trans*- vinyl coupling of 18.2 Hz due to the *trans*-TMCHP's vinyl hydrogens (**Figure 2.42**).



**Figure 2.42** Identification of *trans*-TMCHP through dynamic  $^1\text{H}$  NMR and coupling constant.

The calculated chemical shifts for this species fit the experimentally observed (**Table 2.10**) very closely. Thus, the observation of dynamic NMR, the presence of a *trans* vinyl coupling and the excellent match of calculated and experimental  $^{13}\text{C}$  chemical shifts proves that the species produced by the photolysis of *cis*-TMCHP in toluene- $d_8$  is indeed *trans*-TMCHP.

**Table 2.10:** Identification of *trans*-TMCHP via experimental vs. calculated  $^{13}\text{C}$  NMR shifts.

 <i>cis</i> -TMCHP			 <i>trans</i> -TMCHP (high-temp)			 <i>trans</i> -TMCHP (low-temp)		
Carbon	Exp <sup>a</sup>	Calc <sup>b</sup>	Carbon	Exp <sup>a</sup>	Calc <sup>b</sup>	Carbon	Exp <sup>a</sup>	Calc <sup>b</sup>
1,2	137.54	141.06	1,2	140.41	143.96	1	143.46	148.3
3,7	37.19	40.46	3,7	38.96	42.4	2	136.65	139.63
4,6	43.12	47.60	4,6	48.97	52.2	3	34.59	37.47
5	21.45	24.43	5	23.14	25.82	4	50.33	54.64
8,9,10,11	31.10	33.61	8,11	22.4	26.44	5	22.59	25.82
			9,10	29.56	29.68	6	45.82	49.75
						7	43.22	47.33
						8	24.91	31.49
						9	29.11	27.49
						10	19.47	21.39
						11	29.45	31.88

a. Observed  $^{13}\text{C}$  chemical shifts in  $\text{tol-d}_8$   
 b. Method used was MP2/6-311+G(d,p)//MP2/6-31G(d)

### 2.7.3. *Trans*-anti-DTBCHP

As seen in **Figure 2.39** *trans*-anti-DTBCHP also has two ring-flip conformers of equal energy. As such it is also expected to show dynamic NMR. As seen in **Figure 2.43** dynamic NMR is indeed observed. Here the doublet of doublets of the averaged vinyl hydrogens, showing the two allylic couplings, broadens and shows a coalescence temperature of  $\sim -45^\circ\text{C}$ . Low temperature NMR spectra show two vinyl hydrogens with a 211.5 Hz shift difference. From this and the coalescence temperature a ring-flip barrier of 10.5 kcal/mol can

be determined. This barrier matches the barrier of the parent compound very well. Unfortunately the down-field vinyl hydrogen has the same shift as the  $^{13}\text{C}$  satellite of the peak of the vinyl hydrogen of the *cis* isomer which obscures the coupling of this down-field hydrogen (Figure 2.44). Nevertheless a *trans* coupling of 16.2 Hz is observable in the up-field vinyl hydrogen.

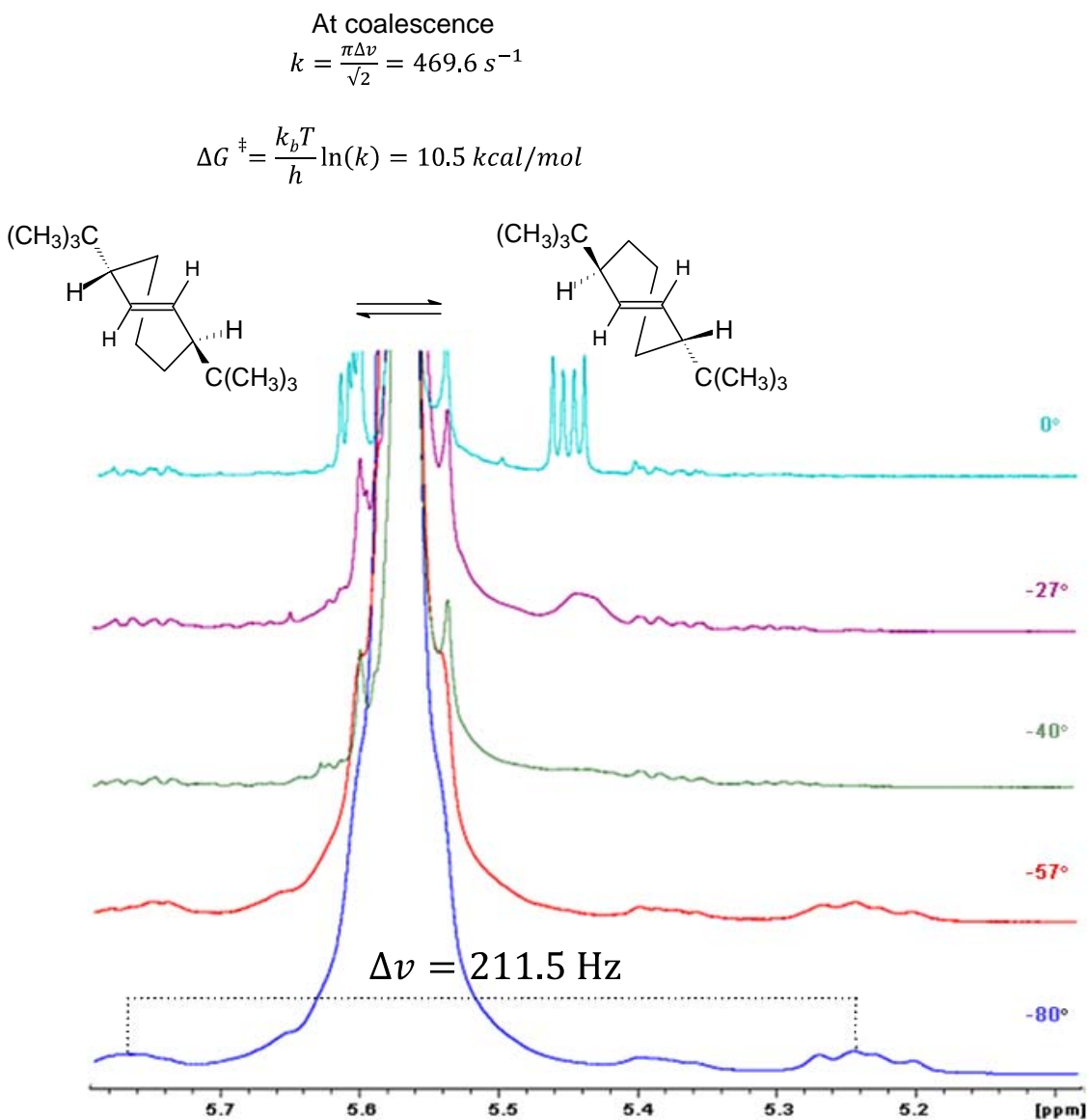


**Figure 2.43** Ring flip barrier calculation for *trans-anti-DTBCHP*

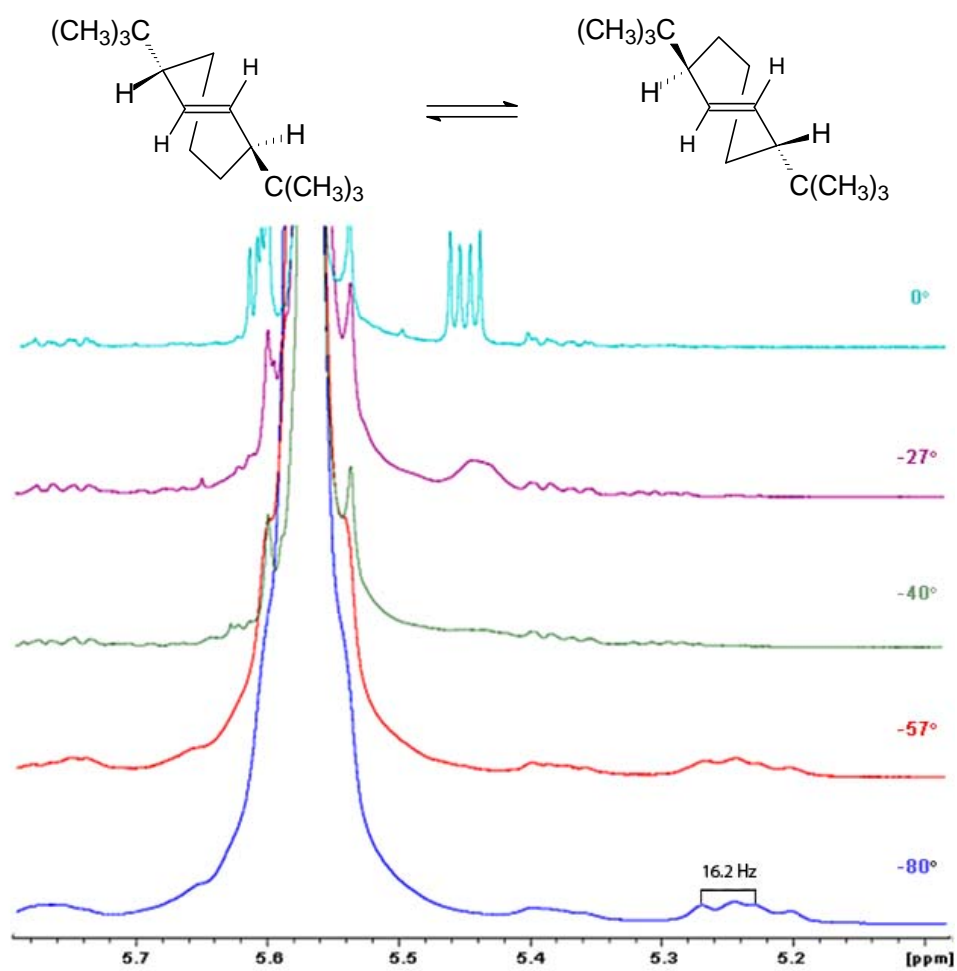
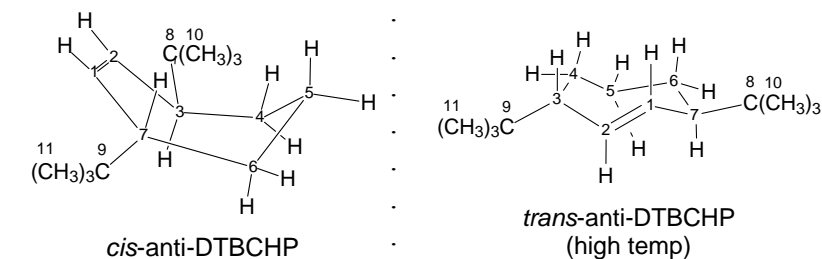


**Figure 2.44** Identification of *trans-anti*-DTBCHP through dynamic  $^1\text{H}$  NMR

Again, the calculated NMR shifts are in good agreement with those experimentally observed (**Table 2.11**), though in this case the lower solubility and additional low temperature broadening of the NMR spectra made it impossible to obtain a static  $^{13}\text{C}$  spectrum at low temperature.

However, again here the presence of dynamic NMR, a trans vinyl coupling constant and an excellent fit between calculated and experimental chemical shifts confirms the presence of *trans*-anti-DTBCHP.

**Table 2.11:** Identification of *trans*-anti-DTBCHP via experimental vs. calculated  $^{13}\text{C}$  NMR chemical shifts.



Carbon	Exp <sup>a</sup>	Calc <sup>b</sup>	Carbon	Exp <sup>a</sup>	Calc <sup>b</sup>
1,2	130.94	132.90	1,2	135.68	138.92
3,7	48.34	52.25	3,7	54.73	59.52
4,6	25.51	27.89	4,6	32.84	36.53
5	23.72	25.37	5	26.34	29.44
8,9	33.60	36.60	8,9	32.03	34.7
10,11	27.52	29.02	10,11	27.86	29.35

a. Observed  $^{13}\text{C}$  chemical shifts in  $\text{tol-d}_8$

b. Method used was MP2/6-311+G(d,p)//MP2/6-31G(d)

#### 2.7.4. *Trans*-syn-DTBCHP

In the case of *trans*-syn-DTBCHP the two conformations of the trans-CHP ring are substantially different in energy so the equilibrium of the trans isomer will be dominated by

one conformer. In a case such as this dynamic NMR will not be observed. As expected, the room temperature NMR shows two H's in the vinyl region with a trans coupling of 18.63 Hz (**Figure 2.45**). It should be noted that the second vinyl hydrogen atom overlaps partially with the cis-isomer's vinyl peak. This overlap prevents measurement of the coupling constants for the down-field trans vinyl hydrogen atoms. However, the up-field peak clearly shows an 18.6 Hz trans coupling and 8.2 Hz allylic coupling. An interesting side point observable in the spectra of Figure 2.45 is the complicated pattern of coupling in the  $^{13}\text{C}$  satellite peaks of the cis vinyl hydrogens. Because the presence of a  $^{13}\text{C}$  at one of the vinyl position breaks the symmetry of the molecule, the normally unobservable cis coupling of 10.98 Hz can be determined (**Figure 2.45**).

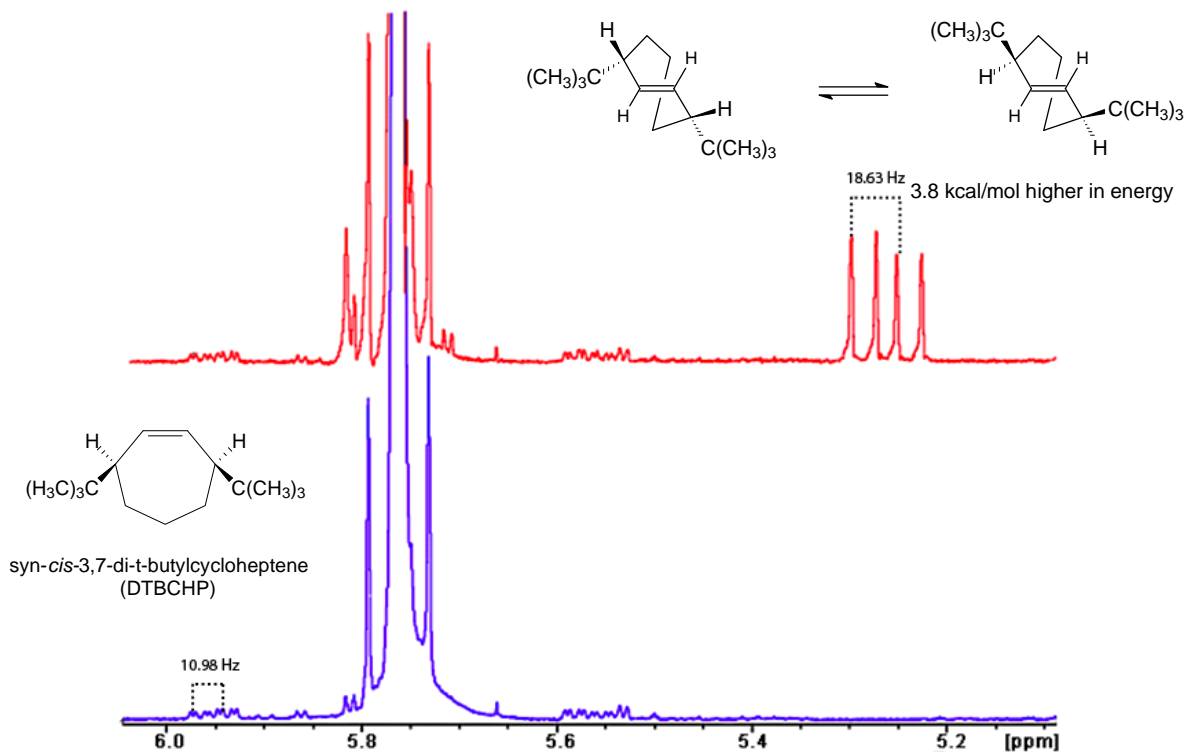
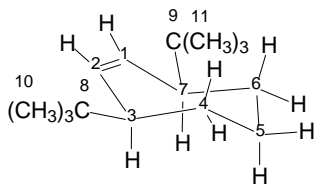


**Figure 2.45** Room temperature  $^1\text{H}$  NMR spectra of *cis*- and *trans*-syn-DTBCHP.

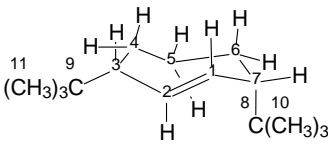


With this unsymmetrical trans isomer, all chemical shifts are identified. As seen from **Table 2.12** there is an excellent fit between the observed and calculated  $^{13}\text{C}$  NMR chemical shifts. This result combined with the observed trans coupling constant shows that again photolysis of the *cis*-syn-DTBCHP successfully produces its trans isomer.

**Table 2.12:** Identification of *trans*-syn-DTBCHP via experimental vs. calculated  $^{13}\text{C}$  NMR chemical shifts.



*cis*-syn-DTBCHP



*trans*-syn-DTBCHP

Carbon	Exp <sup>a</sup>	Calc <sup>b</sup>	Carbon	Exp <sup>a</sup>	Calc <sup>b</sup>
1,2	134.06	137.34	1	143.69	142.74
3,7	49.72	53.17	2	136.23	135.98
4,6	28.24	31.80	3	50.22	53.32
5	32.96	37.63	4	36.52	39.41
8,9	32.64	35.17	5	27.59	29.17
10,11	27.35	28.63	6	32.14	36.16
			7	62.93	58.51
			8	33.49	35.09
			9	31.69	23.89
			10	28.33	33.25
			11	28.13	32.06

a. Observed  $^{13}\text{C}$  chemical shifts in  $\text{tol-d}_8$

b. Method used was MP2/6-311+G(d,p)//MP2/6-31G(d)

### 2.7.5. Stability

Unlike the parent compound, the *trans*-TMCHP was found to be stable at room temperature. While its lifetime in solution was several days, the calculated barrier of ~34 kcal/mol for the parent compound would suggest a much longer lifetime. As a result, we investigated the decay rate of this molecule at room temperature by preparing two samples with different concentrations. In 500  $\mu\text{L}$  toluene- $d_8$  we photolyzed 6.25  $\mu\text{L}$  and 12.5  $\mu\text{L}$  *cis*-TMCHP. The photochemical conversion was approximately the same for both samples ~1.3%. The samples were then left at room temperature and proton NMR's were taken periodically to monitor the decay. The results of the studies are plotted in **Figure 2.46**.

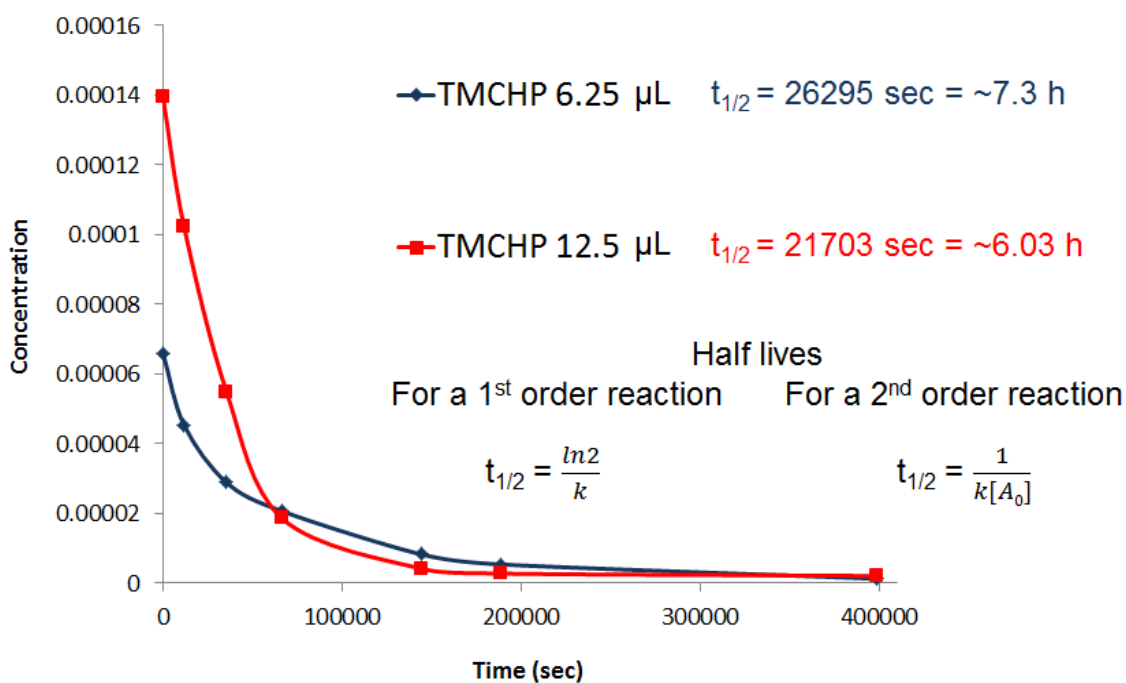


**Figure 2.46** Room temperature decay studies of *trans*-TMCHP.

The results from our studies show that the half lives of the two samples differ. So we do not have a pure 1<sup>st</sup> order decay of *trans*-TMCHP. On the other hand the initial concentrations of *trans*-TMCHP differed by a factor of two, so the 6.25  $\mu$ L sample would show twice the half-life of the more concentrated sample if the reaction is purely bimolecular. These results suggest, that for this molecule the kinetics are a mix of uni- and bimolecular decay and that the methyl groups are not sterically large enough to block bimolecular formation of a 1,4-biradical.

As shown in **Figure 2.47** and **2.48**, unlike the TMCHP, both of the *trans* isomers of both *syn* and *anti*-DTBCHP are stable at room temperature for extended periods of time. Both show pure uni-molecular kinetics from which can be obtained *trans* $\rightarrow$ *cis* barriers very close to the calculated barrier of 34 kcal/mol (**Table 2.13**).

**Table 2.13:** Results of DTBCHP rate studies.

	Syn- <i>trans</i> -DTBCHP	Anti- <i>trans</i> -DTBCHP
$\Delta G^\ddagger_{\text{trans} \rightarrow \text{cis}}$	32.9 kcal/mol	32.3 kcal/mol

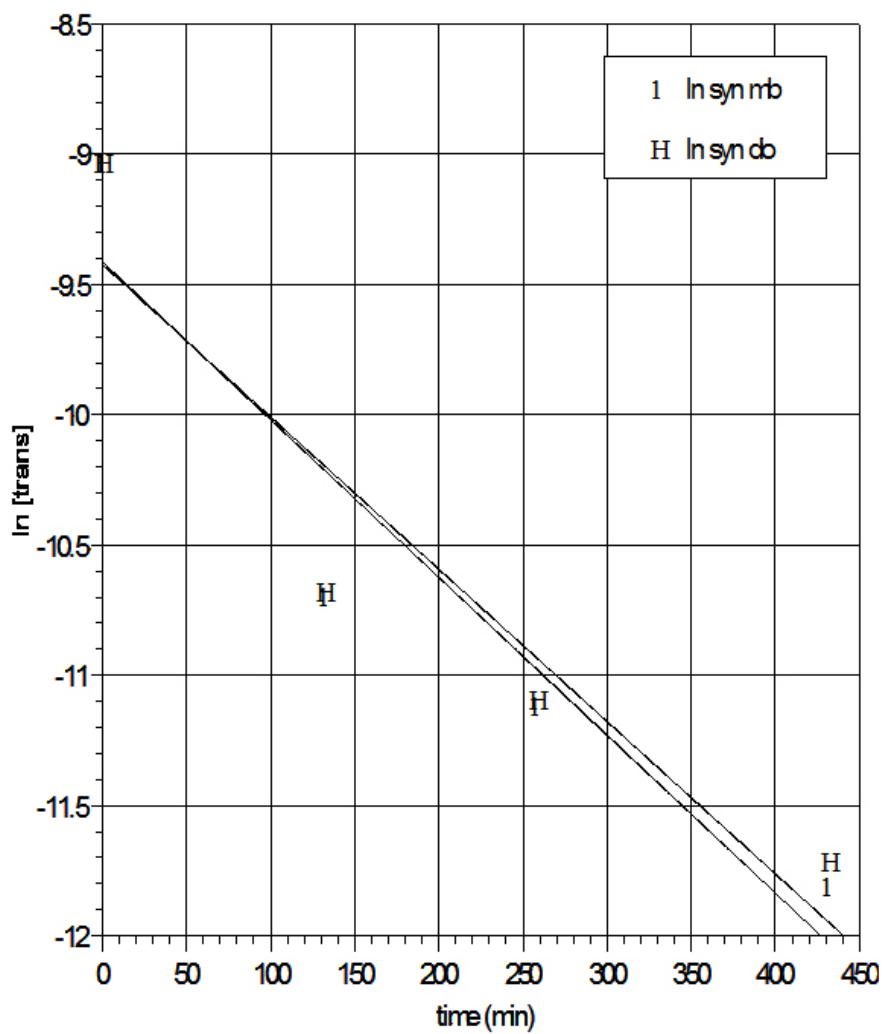


**Figure 2.47** Plot of the thermal decay at 133 °C for *trans*-anti-DTBCHP using methyl benzoate and dodecane standards.

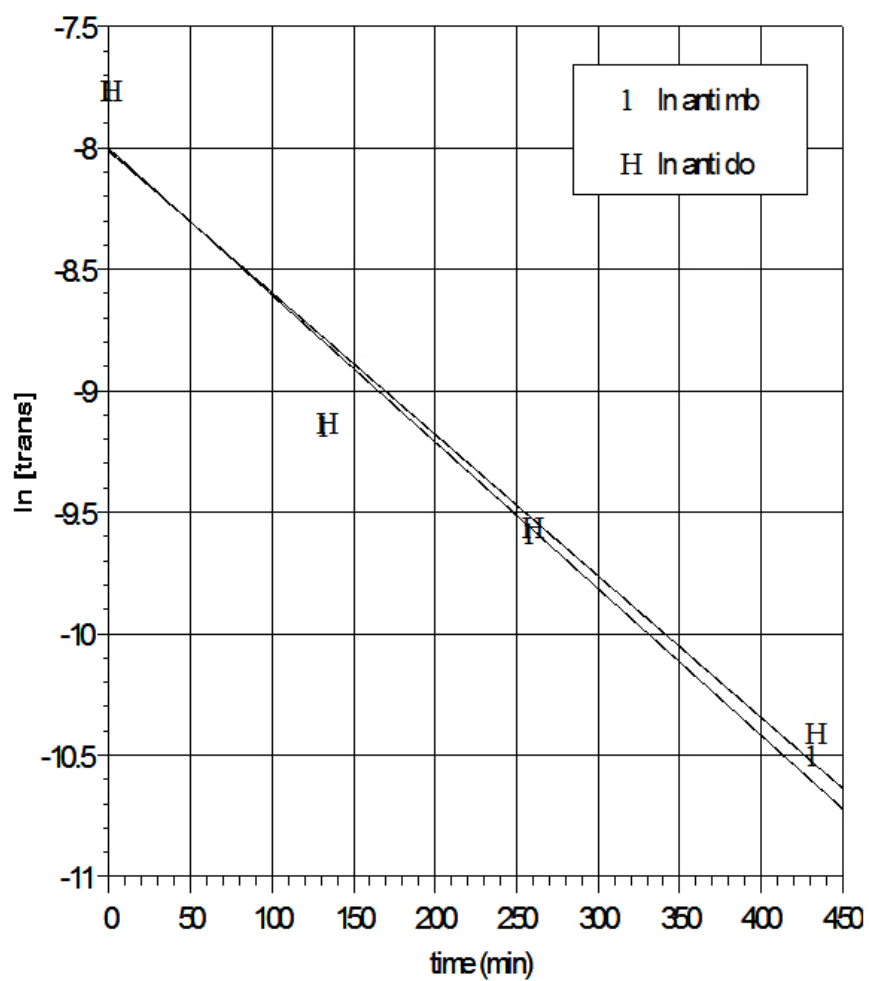


**Figure 2.48** Plot of the thermal decay at 133°C for *trans*-syn-DTBCHP using methyl benzoate and dodecane standards.

## 2.8 Conclusions

We have successfully shown that one can produce room temperature stable trans-cycloheptenes, and in doing so have shown the limits of a double bond subjected to a twisting strain.

“In practice, the smallest trans cycloalkene stable at room temperature is *trans*-cyclooctene. Even here, the trans isomer is 11.4 kcal/mol less stable than its cis counterpart” - Jones, J., *Organic Chemistry*, p 120.

“The smallest isolated simple trans cycloalkene is *trans*-cyclooctene. It is 9.2 kcal/mol less stable than cis isomer and has a highly twisted structure”  
- Vollhardt, P. K., *Organic Chemistry*, p 460

“*Trans*-cyclooctene has been isolated, however. Here the ring is large enough to accommodate the geometry required by a trans double bond and still be stable at room temperature...

*Trans*-cycloheptene has been observed with instruments called spectrometers, but it is a substance with a very short lifetime and has not been isolated”  
- Solomons, T. W., *Organic Chemistry*, p 316.

So contrary to what the preceding quotes from current Organic Chemistry textbooks suggest, the 8-membered ring is not the smallest ring that allows a room temperature stable trans isomer. That honor now goes to the 7-membered ring trans-cycloheptenes we have discussed here.



## REFERENCES

1. Schapiro, I., Ryazantsev, M., Ding, W., Huntress, M., Melaccio, F., Olivucci, T., *Aus. J. Chem.* **3** **2010** 413.
2. Weingart, O., *J. Am. Chem. Soc.* **2007**, 129, 10618.
3. Wald., G., *Science.* **1962**, 62, 230-239.
4. Ramamurthy, V., M. Denny; R. Liu. *Tetrahedron Lett.*; **1981**, 22, 2463-2466.
5. Breek, A., Muradin, M., Courtin, J., Lugtenburg., J., *Recl. Trav. Chim. Pays-Bas.*; **1983**, 102, 46.
6. W. Waddell; D. Hopkins; M. Uemura; J. West. *J. Am. Chem. Soc.*; **1978**, 100, 1970.
7. Trabanino, R. J.; Vaidehi, N. Goddard, W. A. III *J. Phys. Chem. B* **2006**, 110, 17230.
8. R. Mathies; C. Cruz; W. Pollard; C. Shank. *Science.* **1988**, 240, 777.
9. Altoe, P.; Cembran, A.; Olivucci, M.; Garavelli, M.; *Proc. Natl. Acad. Sci USA.* **47** **2010** 20172.
10. Liu, Y.; Edens, G.; Grzymiski, J, Mauzerall, D.; *Biochem*, **2008**, 47, 7752.
11. Birge, R. R., Cooper, T. M., Lawrence, A. G., Masthay, M. B., Zhang, C., and Zidovetzki, R. (1991) Revised assignment of energy storage in the primary photochemical event in bacteriorhodopsin. *J. Am. Chem. Soc.* 113, 4327.
12. Godvindjee, R., Balashov, S. P., and Ebrey, T. G. (1990) Quantum efficiency of the photochemical cycle of bacteriorhodopsin. *Biophys. J.* 53, 597.
13. Logunov, S. L., Song, L, and El-Sayed, M. A. (1994) pH dependence of the rate and quantum yield of the retinal photoisomerization in bacteriorhodopsin. *J. Phys. Chem.* 98, 10674.
14. Logunov, S. L., and El-Sayed, M. A. (1997) Determination of quantum yield of photoisomerization and energy content in the K-intermediate of bacteriorhodopsin photocycle and its mutants by the photoacoustic technique. *J. Phys. Chem. B.* 101, 6629.
15. R. S. H. Liu; A. E. Asato. *Proc. Natl. Acad. Sci. USA.*; **1985**, 82, 259.



16. R. S. H. Liu.; D. T. Browne., *Acc. Chem. Res.*; **1986**, 19, 42.
17. A. Warshel. *Nature (London)* **1976** 260, 5553, 679.
18. W. G. Dauben; J. S. Ritscher. *J. Am. Chem. Soc.*; **1970**, 92, 2925.
19. F. Bernardi; M. Olivucci; M. A. Robb. *Chem. Soc. Rev.*; **1996**, 25, 321.
20. B. S. Hudson; B. E. Kohler. *Chem. Phys. Lett.*; **1972**, 14, 299.
21. J. Michl.; V. Bonacic-Koutecky.; *Electronic Aspects of organic photochemistry*. John Wiley & Sons, New York, **1990**.
22. M. Garavelli; F. Bernardi; M. Olivucci; M. J. Bearpark; S. Klein; M. Z. Robb. *J. Phys. Chem. A*. **2001**, 105, 11496.
23. B. S. Hudson; B. E. Kohler. *Chem. Phys. Lett.*; **1972**, 14, 299.
24. Michl.; V. Bonacic-Koutecky.; *Electronic Aspects of organic photochemistry*. John Wiley and Songs, New York, **1990**.
25. M. Garavelli; F. Bernardi; M. Olivucci; M. J. Bearparks: S. Klein; M.Z. Robb. *J. Phys. Chem. A*. **2001**, 105, 11496.
26. K. Schulten; I. Ohmine; M. Karplus. *J. Chem. Phys.*; **1976**, 64, 4422.
27. P. Tavan; M. Karplus. *J. Chem. Phys.*; **1979**, 70, 5407.
28. A. C. Lasaga; R. J. Aerni; M. Karplus. *J. Chem. Phys.*; **1980**, 7, 5230.
29. F.M. F. Granville; G. R. Holtom; B. E. Kohler. *J. Chem. Phys.*; **1980**, 72, 4671.
30. R. M. Gavin; C. Weisman; J. K. McVey; S. A. Rice. *J. Chem. Phys.*; **1978**, 68,522.
31. P. Tavan; K. Schulten. *J. Chem. Phys.*; **1979**, 70, 5407.
32. M. Girard; E. Arvidson; R. Christensen. *J. Chem. Phys.*; **1984**,80, 2265.
33. J. H. Simpson; L. Mc Laughlin; D. S. Smith; R. L. Christensen. *J. Chem. Phys.*; **1987**, 87, 3360.
34. B. E. Kohler; C. S. Spangler; C. S. Westerfield. *J. Chem. Phys.*; **1988**, 89, 5422.
35. G. Orlandi; F. Zerbetto; M. Z. Zgierski; *Chem. Rev.*; **1991**, 91, 867.
36. O. Kitao; H. Nakatsuji. *Chem. Phys. Lett.*; **1988**, 143, 528.

37. K. Nakayama; H. Nakano; K. Hirao. *Int. J. Quant. Chem.*; **1998**, 66, 157.
38. R. J. Cave; E. R. Davidson. *J. Phys, Chem.*; **1987**, 91, 4481.
39. R. J. Cave; E. R. Davidson. *Chem. Phys. Lett.*; **1988**, 148, 190.
40. R. J. Graham; K. Freed. *J. Chem. Phys.*; **1992**, 96, 1304.
41. L. Serrano-Andres; J. Sanchez- Marin; I. Nebot-Gil. *J. Chem. Phys.*; **1992**, 97, 7499.
42. J. P. Malrieu; I. Nebot-Gil; J. Sanchez-Marín. *Pure & Appl. Chem.*; **1984**, 56, 1241.
43. L. Serrano-Andres; M. Merchan; I. Nebot-Gil; R. Lindh; B. O. Roos. *J. Chem. Phys.*; **1993**, 98, 3151.
44. M. A. Nascimento; W. A. Goddard III. *Chem. Phys.* **1980**, 53, 251.
45. R. McDiarmid. *Chem. Phys. Lett.*; **1992**, 188, 423.
46. M. E. Squillacote; R. S. Sheridan; O. L. Chapman; A. L. Anet. *J. Am. Chem. Soc.*; **1979**, 101, 3657.
47. S. Boue; R. Srinivasan. *J. Am. Chem. Soc.*; **1970**, 92, 3226.
48. J. Sateil; L. Metts; M. Wrighton. *J. Am. Chem. Soc.*; **1970**, 92, 3227.
49. M. Squillacote; T. C. Semple. *J. Am. Chem. Soc.*; **1987**, 109, 892.
50. M. Squillacote; T. C. Semple. *J. Am. Chem. Soc.*; **1990**, 112, 5546.
51. R. Srinivasan; S. Boue. *Tetrahedron lett.*; **1970**, 203.
52. R. Srinivisan. *J. Am. Chem. Soc.*; **1968**, 90, 4498.
53. R. S. H. Liu; G. S. Hammond. *Proc. Natl. Acsd. Sci. USA.*; **2000**, 97, 11153.
54. R. S. H. Liu. *Acc. Chem. Res.*; **2001**, 34, 555.
55. R. S. H. Liu; G. S. Hammond. *Chem. . Eur. J.*; **2001**, 7, 4536.
56. U. K. Genick; S. M. Soltis; P. Kuhn; I. L. Canestrelli; E. D. Getzoff. *Nature*, **1998**, 392, 206.
57. M. E. Squillacote; T. C. Semple; P. W. Mui. *J. Am. Chem. Soc.*; **1985**, 107, 6842.

58. A. E. Asato; M. Denny; R. S. H. Liu. *J. Am. Chem. Soc.*; **1986**, 108, 5032.
59. M. Sheves; A. Albeck; M. Ottaleni; P. H. M. Bovee-Geurts; W. J. De Grip; C. M. Einterz; J. M. Lewis; L. E. Schaechter; D. S. Kliger. *J. Am. Chem. Soc.*; **1986**, 108, 6440.
60. M. Ishiguro. *J. Am. Chem. Soc.*; **2000**, 122, 444.
61. A. M. Muller; S. Lochbrunner; W. E. Schmid; W. Fub. *Angew. Chem. Int. Ed.*; **1998**, 37, 505.
62. J. R. Akerman; S. A. Forman; M. Hossain; B. Kohler. *J. Chem. Phys.*; **1984**, 80, 39.
63. M. Garavelli; P. Celani; N. Yamamoto; F. Bernardi; M. A. Robb; M. Olivucci. *J. Am. Chem. Soc.*; **1996**, 118, 11656.
64. M. Garavelli; P. Celani; F. Bernardi; M. A. Robb; M. Olivucci.; *J. Am. Chem. Soc.*; **1997**, 119, 6891.
65. Altoe, P.; Cembran, A.; Olivucci, M.; Garavelli, M.; *Proc. Natl. Acad. Sci USA*. 47 **2010** 20172.
66. W. G. Dauben; J. S. Ritscher. *J. Am. Chem. Soc.*; **1970**, 92, 2925.
67. W. G. Dauben; M. S. Kellogg; J. I. Seeman; N. D. Wietmeyer; P. H. Wendschuh. *Pure. Appl. Chem.*; **1973**, 33, 197.
68. A. Padwa; L. Brodsky; S. Clough; *J. Am. Chem. Soc.*; **1972**, 94, 6767.
69. C. E. Wulfman; S. Kumei. *Science*; **1971**, 172, 1061.
70. L. Salem; C. Rowland. *Angew. Chem.*; **1972**, 84, 86.
71. L. Salem; C. Rowland; *Angew. Chem. Internat. Edit.*; **1972**, 11, 92.
72. L. Salem. *Pure. Appl. Chem.*; **1973**, 33, 317.
73. L. Salem. *Science.*; **1976**, 191, 822.
74. V. Bonacic-Koutecky; P. Brukman; P. Hiberty; J. Koutecky; C. Leforestier; L. Salem. *Angew. Chem. Int. Ed. Engl.*; **1975**, 14, 575.
75. L. Pogliani; N. Niccolai; C. Rossi. *Chem. Phys. Lett.*; **1984**, 108, 597.

76. V. Bonacic-Koutecky; M. Persico; D. Dohnert; A. Sevin. *J. Am. Chem. Soc.*; **1982**, 104, 6900.
77. P. Bruckmann; L. Salem. *J. Am. Chem. Soc.*; **1976**, 98, 5037.
78. D. J. Patel; D. I. Schuster. *J. Am. Chem. Soc.*; **1968**, 90, 5137.
79. D. I. Schuster; D. J. Patel. *J. Am. Chem. Soc.*; **1968**, 90, 5145.
80. D. I. Schuster; A. C. Brisimitzakis. *J. Org. Chem.*; **1987**, 52, 3644.
81. F. G. West; P. V. Fisher; C. A. Willoughby. *J. Org. Chem.*; **1990**, 55, 5936.
82. M. F. Semmelhack; S. Kunkes; C. S. Lee. *Chem. Comm.*; **1971**, 698.
83. J. Kagan; P. Y. Juang; B. E. Firth; J. P. Przybytek; S. P. Singh. *Tetrahedron Lett.*; **1977**, 49, 4289.
84. M. W. Klett; R. P. Johnson. *Tetrahedron Lett.*; **1983**, 24, 1107.
85. P. J. Baldry. *J. Chem. Soc., Perkin Trans. I.*; **1975**, 19, 1913.
86. P. J. Baldry. *J. Chem. Soc. Perkin Trans II.*; **1980**, 5, 809.
87. J. Woning; A. Oudenampsen; W. H. Llaarhoven; *J. Chem. Soc. Perkin. Trans II*, **1989**, 2147.
88. J. Woning; A. T. F. Lijten; W. H. Laarhoven; *J. Org. Chem.*; **1991**, 56, 2427.
89. J.A. Baltrop; H. E. Browing; *J. Am. Chem. Soc.*; **1968**, 1481.
90. W. G. Dauben; J. H. Smith; J. Saltiel. *J. Org. Chem.*; **1969**, 34, 261.
91. W. Th. A. M. van der Lugt; L. J. Oosterhoff. *J. Am. Chem. Soc.*; **1969**, 91, 6043.
92. R. B. Woodward; R. Hoffmann. *J. Am. Chem. Soc.*; **1965**, 87, 395, 2046.
93. R. B. Woodward; R. Hoffmann. *Angew. Chem., Int. Ed. Engl.*; **1969**, 781.
94. W. Th. A. M. van der Lugt; L. J. Oosterhoff. *J. Am. Chem. Soc.*; **1969**, 91, 6043.
95. M. Desouter-Lecomte; J. C. Lorquet. *J. Chem. Phys.*; **1977**, 71, 4391, 3661.
96. E. E. NiKitin. In: *Chemische Elementarprozesse*; Hartman, H. Ed.; Springer-Verlag; Berlin, 1968, P43.

97. V. Bonacic-Koutecky; J. Koutecky; J. Michl. *Angew. Chem. Int. Ed. Engl.*; **1987**, 26, 170.
98. M. Klessinger; J. Michl. *Excited States and Photochemistry of Organic Molecules*; VCH publishers, Inc.; New York.; 1995.
99. M. Klessinger. *Pure & Appl. Chem.*; **1997**, 69, 773.
100. F. Bernardi; M. Olivucci; M. A. Robb. *Chem. Soc. Rev.*; **1996**, 25, 321.
101. M. Klessinger. *Angew. Chem. Int. Ed. Engl.*; **1995**, 34, 549.
102. V. Vaida. *Acc. Chem. Res.* **1986**, 19, 114.
103. B. E. Kohler. *Chem. Rev.*; **1993**, 93, 41.
104. H. Petek; A. J. Bell; Y. S. Choi; K. Yoshihara; B. A. Tounge; R. L. Christensen. *J. Chem. Phys.*; **1993**, 98, 3771.
105. R. M. Gavin Jr; S. Risemberg; S. A. Rice. *J. Chem. Phys.*; **1973**, 58, 3160.
106. M. O. Trulson; R. A. Mathies. *J. Phys. Chem.*; **1990**, 94, 5741.
107. P. J. Reid; S. J. Doig; S. D. Wickham; R. A. Mathies. *J. Am. Chem. Soc.*; **1993**, 115, 4574.
108. S. Pullen; L. A. Walker II; B. Donovan; R. J. Sension. *Chem. Phys. Lett.*; **1995**, 242, 415.
109. D. R. Cyr; C. C. Hayden. *J. Chem. Phys.*; **1996**, 104, 771.
110. F. Farmanara; V. Stert; W. Radloff. *Chem. Phys. Lett.*; **1998**, 288, 512.
111. W. Fuß; W. E. Schmid; S. A. Truskin. *Chem. Phys. Lett.*; **2001**, 343, 91.
112. R. P. Krawczyk; K. Malsch; G. Hohlneicher; R. C. Gillen; W. Domcke; *Chem. Phys. Lett.*; **2000**, 320, 535.
113. D. G. Leopold; R. D. Pendley; J. L. Roebber; R. J. Hemley; V. Vaida. *J. Chem. Phys.*; **1984**, 81, 4281.
114. F. Zerbetto; M. Z. Zgierski. *Chem. Phys. Lett.*; **1989**, 157, 515.
115. M. A. Robb; M. Olivucci. *J. Photochem & Photobiol.*; **2001**, 144, 237.
116. H. C. Longuet-Higgins. *Proc. R. Soc. Lond. A.*; **1975**, 344, 147.

117. Y. Haas; S. Zilberg. *J. Photochem & Photobio A.*; **2001**, 144, 221.
118. S. Zilberg; Y. Haas. *Chem. Eur. J.*; **1999**, 5, 1755.
119. W. Gerhartz; R. Poshusta. J. Michl. *J. Am. Chem. Soc.*; **1977**, 99, 4263.
120. M. Olivucci; I. Ragazos; F. Bernardi; M. Robb. *J. Am. Chem. Soc.*; **1993**, 115, 3710.
121. M. Olivucci; F. Bernardi; P. Celani; I. Ragazos; M. A. Robb. *J. Am. Chem. Soc.*; **1994**, 116, 1077.
122. F. Bernardi; M. Olivucci; M. Robb. *J. Photochem & Photobio. A.* **1997**, 105, 365.
123. F. Bernardi; M. Olivucci; I. Ragazos; M. Robb. *J. Am. Chem. Soc.*; **1992**, 114, 2752.
124. F. Bernardi; S. De; M. Olivucci; M. Robb. *J. Am. Chem. Soc.*; **1990**, 112, 1737.
125. F. Bernardi; M. Olivucci; M. Robb. *Isr. J. Chem.*; **1993**, 33, 265.
126. F. Bernardi; M. Olivucci; M. Robb; G. Tonachini. *J. Am. Chem. Soc.*; **1992**, 114, 5805.
127. S. Zilberg; Y. Haas. *Chem. Phys.*; **2000**, 259, 249.
128. H. E. Zimmerman. *Acct. Chem. Res.*; **1971**, 4, 272.
129. H. E. Zimmerman.; *J. Am. Chem. Soc.*; **1966**, 88, 1564.
130. H. E. Zimmerman. *J. Am. Chem. Soc.*; **1966**, 88, 1566.
131. E. Heilbronner. *Tetrahedron Lett.*; **1964**, 1923.
132. S. Zilberg; Y. Haas. *J. Phys. Chem. A.*; **1999**, 103, 2364.
133. M. Garavelli; T. Vreven; P. Celani; F. Bernardi; M. A. Robb; M. Olivucci.; *J. Am. Chem. Soc.*; **1998**, 120, 1285.
134. M. Garavelli; P. Celani; F. Bernardi; M. A. Robb; M. Olivucci.; *J. Am. Chem. Soc.*; **1997**, 119, 11487.
135. P. Celani; F. Bernardi; M. Olivucci. *J. Chem. Phys.*; **1995**, 102, 5733.
136. A. H. Zewail. *J. Phys. Chem.*; **1996**, 100, 12701.

137. P. Celani; S. Ottani; M. Olivucci; F. Bernardi; M. A. Robb. *J. Am. Chem. Soc.*; **1994**, 116, 10141.
138. M. Squillacote; T. C. Semple. *J. Am. Chem. Soc.*; **1987**, 109, 892.
139. J. Chen. *Doctoral Dissertation.*; Auburn university, **2000**.
140. M. Aoyagi; Y. Osamura. *J. Am. Chem. Soc.*; **1989**, 111, 470.
141. Vreven, T.; Bernardi, F.; Garavelli, M.; Olivucci, M.; Robb, M. A.; Schlegel, H. B. *J. Am. Chem. Soc.*, **1997**, 119, 12687.
142. Fuß, W.; Lochbrunner, S.; Muller, A. M.; Schikarski, T.; Schmid, W. E.; Trushin, S. A. *Chem. Phys.*, **1998**, 232, 161.
143. D. D. Perrin; W. L. F. Amarego; D. R. Perrin. *Purification of Laboratory Chemicals*, 2<sup>nd</sup> ED, Pergamon Press Inc. NY. **1980**.
144. Walter and Ramaly, *Analytical Chemistry.*; **1973**, 45, 165.
145. Burfield, D., Lee, K., Smithers, R. *J. Org. Chem.*, Vol. 42, No. 18, 1977.
146. D. Seyferth, G. Singh *J. Am. Chem. Soc* **1965**, 02139.
147. B. A. Reith, J. Strating, A. M. Can Leusen., *J. Org. Chem.* **1974** 39, 18.
148. Wittig, G. ; Schoellkopf, U. *Ber.*, **1954**, 87, 1318.
149. Hepperle, S. S.; Li, Q.; East, A. L. *J Phys Chem A*. **2005**, 48, 10975.
150. a) Baker, J. W. "Hyperconjugation", Oxford University Press, London, **1952**. b) Dewar, M. J. S. "Hyperconjugation", Ronald Press, New York, N.Y., **1962**. c) Arnett, E. M.; Abboud, J. L. M. *J. Am. Chem. Soc.*, **1975**, 97, 3865. d) Olah, G. A.; Donovan, D. J. *J. Am. Chem. Soc.*, **1977**, 99, 5026.
151. Wald, G. *Science*, **1968**, 162, 230
152. J. Saltiel; L. Metts; M. Wrighton. *J. Am. Chem. Soc.* **1969**, 24, 5684.
153. J. Saltiel; D. E. Townsend; A. Sykes. *J. Am. Chem. Soc.*; **1973**, 95, 5968.
154. J. Saltiel; J. D'Agostino; E. D. Megarity; L. Metts; K. Neuberger; M. Wrighton; O. C. Zafiriou. *Org. Photochem.*; **1973**, 3, 1-113.
155. (a) Kosower, E. M. *J. Am. Chem. Soc.* 1958, 80, 3253-3271. (b) Dimroth, K.; Reichardt, C; Siepmann, T.; Bohlmann, F. *Liebigs Ann. Chem.* **1963**, 661, 37.

156. (a) Reichardt, C. *Angew. Chem. Int. Ed.* **1965**, 4, 29-40, (b) Reichardt, C. Liebigs, *Ann. Chem.* **1971**, 752, 64.
157. (a) Squillacote, M., Wang, J., Chen, J. *J. Am. Chem. Soc.* **2004**, 126, 1940-1941; (b) Jiwei Chen *Dissertation Auburn University* **2000**.
158. M. Squillacote; T. C. Semple. *J. Am. Chem. Soc.*; **1987**, 109, 892.
159. Bone, W. A. *J. Chem. Soc.*, **1906**, 89, 660.
160. Linebarger, C. E., *J. Am. Chem. Soc.* **1895**, 17(5), 354.
161. Dodge, F. D., *J. Am. Chem. Soc.* **1902**, 24(7), 649.
162. van't Hoff, J. H., *The Arrangement of Atoms in Space*, 2<sup>nd</sup> ed. **1898**.
163. Heitler, W.; London, F. *Z. Physik* **1927**, 44, 455.
164. Sugiura, Y., *Ibid.* **1927**, 45, 484.
165. Wang, S. C., *Phys. Rev.* **1928**, 31, 579.
166. Hückel, E. Z., *Phys.* **1930**, 60, 423; *Z. Electrochem. Angew. Phys. Chem.* **1930**, 36, 641.
167. Berson, J., A., *Angew. Chem. Int. Ed. Engl.* **1996**, 35, 2750.
168. Kikuchi, S. *J. Chem. Ed.* **1997**, 74(2), 194.
169. Ingold, C. K., *Structure and Mechanism in Organic Chemistry*, Cornell University Press, Ithaca, **1969**, 2<sup>nd</sup> ed, 26
170. Pauling, L. *J. Am. Chem. Soc.*, **1931**, 53, 1367, 3225.
171. Slater, J. S., *Phys. Rev.* **1931**, 37,481; *ibid*, **1931**, 38,1109.
172. Pauling, L.; Hayward, R., *The Architecture of Molecules*, **1964**, 26.
173. Ihde, A., *J. Chem. Educ.* **1959**, 36(7), 330.
174. Kauffman, G. B., *J. Chem. Educ.* **1982**, 59(9), 745.
175. Barrows, S. E.; Eberlein., T. H., *J. Chem. Educ.*, **2005**, 82(9), 1329
176. Borden, W. T. *Chem. Rev.* **1989**, 89, 1095.
177. Winkler, F. K.; Dunitz, J. D. *J. Mol. Biol.* **1971**, 59, 169.



178. Wijsman, G. W.; Iglesias, G. A.; Beekman, M. C.; de Wolf, W. H.; Bickelhaupt, F.; Kooijman, H.; Spek, A. L. *J. Org. Chem.* **2001**, *66*, 1216.
179. (a) Haddon, R. C. *Chem. Phys. Lett.* **1986**, *125*, 231. (b) Haddon, R. C. *J. Am. Chem. Soc.* **1986**, *108*, 2837.
180. Trinquier, G.; Malrieu, J.-P., *J. Phys. Chem.*, **1990**, *94*, 6184.
181. Tichy, M.; Sicher, J., *Tetrahedron Lett.*, **1969**, 4609.
182. (a) Brecht, J. et al. *J. Liebigs Ann. Chem.*, **1924**, 437; (b) Brecht, J. *Ann. Acad. Sci. Fenn.*, **1972**, *29A*, 3.
183. Werner, P. *Chem. Rev.*, **1989**, *89*, 1067.
184. Barrows, S. E.; Eberlein, T. H., *J. Chem. Educ.*, **2005**, *82(9)*, 1334.
185. (a) Traetteberg, M. *Acta Chem. Scand.* **1975**, *29*, 29. (b) Ermer, O.; Mason, S. A. *Acta Cryst.* **1982**, *B38*, 2200.
186. Leong, M. K.; Mastryukov, V. S.; Boggs, J. E. *J. Mol. Struct.* **1998**, *445*, 149.
187. Manor, P. C.; Shoemaker, D. P.; Parkes, A. S. *J. Am. Chem. Soc.* **1970**, *92*, 5260.
188. Ermer, O. *Angew. Chem.* **1974**, *86*, 672.
189. Boeckh, D.; Huisgen, R.; Noeth, H. *J. Am. Chem. Soc.* **1987**, *109*, 1248.
251. Block, E. *Organic Reactions* **1984**, *30*, 457.
252. Shimizu, T.; Shimizu, K.; Ando, W. *J. Am. Chem. Soc.* **1991**, *113*, 354.
253. Gano, J. E.; Lenoir, D.; Park, B. S.; Roesner, R. A. *J. Org. Chem.* **1987**, *52*, 5636.
254. Doering, W. V. E.; Roth, W. R.; Bauer, F.; Breuckmann, R.; Ebbrecht, T.; Herbold, M.; Schmidt, R.; Lennartz, H.-W.; Lenoir, D.; Boese, R. *Chem. Ber.* **1989**, *122*, 1263.
255. Dugave, C.; Demange, L. *Chem. Rev.* **2003**, *103*, 2475.
256. Korth, H.-G.; Trill, H.; Sustmann, R. *J. Am. Chem. Soc.* **1981**, *103*, 4483.
257. Andrews, U. H.; Baldwin, J. E.; Grayston, M. W. *J. Org. Chem.* **1982**, *47*, 287.
258. Bonneau, R.; Jousset-Dubien, J.; Salem, L., L.; Yarwood, A. J. *J. Am. Chem. Soc.* **1976**, *98*, 4329.

259. Caldwell, R. A.; Misawa, H. *J. Am. Chem. Soc.* **1987**, *109*, 6869.
260. Johnson, R. P.; DiRico, K. J. *J. Org. Chem.* **1995**, *60*, 1074.
261. Turro, N. J. *Modern Molecular Photochemistry*, Benjamin Cummings Publishing, Menlo Park, 1978.
262. Kropp, P. J.; Krauss, H. J. *J. Am. Chem. Soc.* **1967**, *89*, 5199.
263. (1) Verbeek, J.; Lenthe, J. H. *J. Org. Chem.* **1987**, *52*, 2955. (2) Johnson, R. P.; DiRico, K. J. *J. Org. Chem.* **1995**, *60*, 1074. (3) Allinger, N. L.; Sprague, J. T. *J. Am. Chem. Soc.* **1972**, *94*, 5734.
264. Cope, A. C.; Moore, P. T.; Moore, W. R. *J. Am. Chem. Soc.* **1960**, *82*, 1744.
265. Turro, N. J. *Modern Molecular Photochemistry*, Benjamin Cummings Publishing: Menlo Park, **1978**.
266. Bonneau, R.; Jousot-Dubien, J.; Salem, L.; Yarwood, A. J. *J. Am. Chem. Soc.* **1976**, *98*, 4329.
267. Yamazaki, H.; Cvetanovic, R. J. *J. Am. Chem. Soc.*, **1969**, *91*, 5404.
268. Cowan, D. O.; Drisko, R. L. *Elements of Organic Photochemistry*. Plenum press: New York, **1976**.
269. Klessinger, M.; Michl, J. *Excited States and Photochemistry of Organic Molecules*, VCH Publishing: New York, **1995**.
270. Garcia-Exposito, E.; Gonzalez-Moreno, R.; Martin-Vila, M.; Muray, E.; Rife, J.; Bourdelande, J. L.; Branchadell, V.; Ortuno, R. M. *J. Org. Chem.* **2000**, *65*, 6958.
271. Gorner, H.; Schulte-Frohlinde, D. *J. Phys. Chem.* **1981**, *85*, 1835.
272. Caldwell, R. A.; Carlacci, L.; Doubleday, C. E. Jr.; Furlani, T. R.; King, H. F.; McIver, J. W. Jr. *J. Am. Chem. Soc.* **1988**, *110*, 6901.
273. Hirokami, S.-I.; Sato, S. *Can. J. Chem.*, **1967**, *45*, 3181.
274. Carless, H. A. J., *J. Chem. Soc. Perkin II*, **1974**, 834.
275. Turro, N. J.; Daltin, J. C.; Weiss, D. S. *Organic Photochemistry*, ed. Chapman, O. L., **1969**, *1*, 2.

278. Kropp, P. J. *J. Am. Chem. Soc.* **1969**, *91*, 5783.
279. Inoue, Y.; Takamuku, S.; Sakurai, H. *J. Chem. Soc. Perkins II* **1977**, *9*, 1635.
280. Inoue, Y.; Takamuku, S.; Kunitomi, Y.; Sakurai, H. *J. Chem. Soc. Perkins II* **1980**, *9*, 1672.
281. Inoue, Y.; Ueoka, T.; Hakushi, T. *J. Chem. Soc. Perkins II* **1984**, *10*, 2053.
282. Inoue, Y.; Ueoka, T.; Kuroda, T.; Hakushi, T. *J. Chem. Soc. Perkin II*, **1981**, *5*, 1031.
283. Hoffmann, R.; Inoue, Y. *J. Am. Chem. Soc.* **1999**, *121*, 10702.
284. Strickland, A. D.; Caldwell, R. A. *J. Phys. Chem.*, **1993**, *97*, 13394.
285. Wallraff, G. M.; Boyd, R. H.; Michl, J. *J. Am. Chem. Soc.* **1983**, *105*, 4550.
286. Squillacote, M.; Bergman, A.; DeFelippis, J. *Tetrahedron Lett.* **1989**, *30*, 6805.
287. Frisch, M. J.; Trucks, G. W.; Schlegel, H. B.; Scuseria, G. E.; Robb, M. A.; Cheeseman, J. R.; Zakrzewski, V. G.; Montgomery, J. A., Jr.; Stratmann, R. E.; Burant, J. C.; Dapprich, S.; Millam, J. M.; Daniels, A. D.; Kudin, K. N.; Strain, M. C.; Farkas, O.; Tomasi, J.; Barone, V.; Cossi, M.; Cammi, R.; Mennucci, B.; Pomelli, C.; Adamo, C.; Clifford, S.; Ochterski, J.; Petersson, G. A.; Ayala, P. Y.; Cui, Q.; Morokuma, K.; Malick, D. K.; Rabuck, A. D.; Raghavachari, K.; Foresman, J. B.; Cioslowski, J.; Ortiz, J. V.; Stefanov, B. B.; Liu, G.; Liashenko, A.; Piskorz, P.; Komaromi, I.; Gomperts, R.; Martin, R. L.; Fox, D. J.; Keith, T.; Al-Laham, M. A.; Peng, C. Y.; Nanayakkara, A.; Gonzalez, C.; Challacombe, M.; Gill, P. M. W.; Johnson, B. G.; Chen, W.; Wong, M. W.; Andres, J. L.; Head-Gordon, M.; Replogle, E. S.; Pople, J. A. *Gaussian 98*, revision A.7; Gaussian, Inc.: Pittsburgh, PA, **1998**.
288. PCMODEL v6.00 Serena Software: Bloomington, IN.
289. Shimizu, T.; Shimizu, K.; Ando, W. *J. Am. Chem. Soc.* **1991**, *113*, 354.
290. Krebs, A.; Pforr, K. I.; Raffay, W.; Tholke, B.; Konig, W. A.; Hardt, I.; Boese, R.; *Angew. Chem., Int. Ed.* **1997**, *36*, 159.
291. Scacchi, G.; Richard, C.; Bach, M. H. *Int. J. Chem. Kinet.* **1977**, *9*, 525.
292. Dervan, P. B.; Uyehara, T.; Santilli, D. S. *J. Am. Chem. Soc.* **1979**, *101*, 2069.

293. Hoffmann, R.; Swaminathan, S.; Odell, B. G.; Gleiter, R. *J. Am. Chem. Soc.* **1970**, *92*, 7091.
294. Segal, G. A. *J. Am. Chem. Soc.* **1974**, *96*, 7892.
295. Feyter, S. D.; Diau, E. W.; Scala, A.; Zewail, A. *Chem. Phys. Lett.* **1999**, *303*, 249.
296. (a) Houk, K. N.; Beno, B. R.; Nendel, M.; Black, K.; Yoo, H. Y.; Wi;sey, S.; Lee, J. K.; *J. Mol. Struct.* **1997**, *398-399*, 169. (b) Doubleday, C. *Chem. Phys. Chem.* **1996**, *100*, 15083. (c) Moriarty, N. W., Lindh, R., Karlstrom, G. *Chem. Phys. Lett.* **1998**, *289*, 442. (d) Dervan, P. B.; Santilli, D. S. *J. Am. Chem. Soc.* **1980**, *102*, 3863. (e) Bernardi, F.; Bottoni, A.; Celani, P.; Olivucci, M.; Robb, M. A.; Venturini, A. *Chem. Phys. Lett.* **1992**, *192*, 229.
297. (a) Doubleday, Jr., C. *J. Am. Chem. Soc.* **1993**, *115*, 11968. (b) Doubleday, Jr., C. *Chem. Phys. Lett.* **1995**, *233*, 509. (c) Doubleday, Jr., C. *J. Phys. Chem.* **1996**, *100*, 15083. (d) Moriarty, N. W.; Lindh, R.; Karlström, G. *Chem. Phys. Lett.* **1998**, *289*, 442.
298. (a) Pedersen, S.; Herek, J. L.; Zewail, A. H. *Science* **1994**, *266*, 1359. (b) De Feyter, S.; Diau, E. W.-G.; Scala, A. A.; Zewail, A. H. *Chem. Phys. Lett.* **1999**, *303*, 249.
299. Otteson, D.; Michl, J. *J. Org. Chem.* **1984**, *49*, 866.
300. Lewis, F. D.; Field, T. L.; Sabat, M. J. *Photochem. Photobio.* **1990**, 277.
301. (a) Leitich, J. *Int. J. Chem. Kinet.* **1979**, *11*, 1249. (b) Martin, H-D.; Eisenmann, E. *Tetrahedron Lett.* **1979**, *20*, 3069. (c) Rencken, I; Orchard, S. W. *S. Afr. J. Chem.* **1988**, *41*, 22.
302. (a) Shumate, K. M.; Neuman, P. M.; Fonken, G. J.; *J. Am. Chem. Soc.* **1965**, *87*, 3996. (b) McConaghy, J. S.; Bloomfield, J. J. *Tetrahedron Lett.* **1969**, *10*, 3719. (c) Bloomfield, J. J; McMonaghy, J. S; Hortmann, A. G. *Tetrahedron Lett.* **1969**, *10*, 3723.
303. (a) Padwa, A.; Koehn, W.; Masaracchia, J.; Osborn, C. L.; Trecker, D. J. *J. Am. Chem. Soc.* **1971**, *93*, 3633. (b) Leitich, J.; Heise, I.; Angermund, K.; Rust, J. *Eur. J. Org. Chem.* **2002**, *11*, 1803.
304. Baldwain, J. E.; Gallagher, S. S.; Leber, P. A.; Raghavan, A. *Org. Lett.* **2004**, *6*, 1457.

305. Andrews, U. H.; Baldwin, J. E.; Grayston, M. W. *J. Org. Chem.* **1982**, *47*, 287.
306. Leitich, J. *Tetrahedron*, **1982**, *38*, 1303.
307. (a) Berson, J. A. *Science* **1994**, *266*, 1338. (b) Dervan, P. B.; Uyehara, T; Santilli, D. S. *J. Amer. Chem. Soc.* **1979**, *101*, 2069. (c) Dervan, P. B.; Santilli, D. S. *J. Amer. Chem. Soc.* **1980**, *102*, 3863.
308. DeFelippis, J. *Dissertation Auburn University* **1990**.